UNIVERSITA' DEGLI STUDI DI PADOVA

Sede amministrativa: Università degli Studi di Padova

Dipartimento Territorio e Sistemi Agro-Forestali

DOTTORATO DI RICERCA IN GESTIONE AMBIENTALE DEI BACINI IDROGRAFICI E TECNICHE DI RAPPRESENTAZIONE DEL TERRITORIO

CICLO XVI

LOCAL SCOURING IN NATURAL AND ARTIFICIAL STEP POOL SYSTEMS

(EROSIONE LOCALIZZATA IN STRUTTURE A GRADINATA NATURALI ED ARTIFICIALI)

Coordinatore: Ch.mo Prof. Mario Aristide Lenzi

Supervisore: Ch.mo Prof. Mario Aristide Lenzi

Co-supervisore: Ing. Andrea Marion

Dottorando: Francesco Comiti

31 Ottobre 2003

RIASSUNTO

I torrenti montani a forte pendenza (>3-5 %) presentano spesso una morfologia naturale a gradinata, detta a *step pool*. Del resto, la sistemazione di tali torrenti mediante opere trasversali di consolidamento quali briglie e soglie di fondo determina la formazione di una analoga sequenza di salti e pozze rendendo in tal modo a gradinata il profilo longitudinale del corso d'acqua. L'attività di ricerca ha coinvolto prove sperimentali di laboratorio e rilievi di campo al fine sia di valutare la dimensione delle buche di scavo in base alle variabili idrauliche, sedimentologiche e geometriche, che di comprendere se l'analogia fra strutture a gradinata naturali ed artificiali sia statisticamente significativa, in tal caso permettendo di trarre indicazioni riguardo la dinamica formativa e la geometria delle sequenze naturali.

Vent'otto prove sperimentali sono state condotte utilizzando una canaletta inclinabile senza alcuna alimentazione solida da monte. Si e' utilizzata una miscela granulometrica composta da ghiaia pressoché uniforme e si sono testati quattro valori di pendenza iniziale: 0.03, 0.045, 0.062, 0.08. Tale intervallo aveva lo scopo di estendere verso il basso l'intervallo di pendenze già sperimentato presso HR Wallingford (UK). Tre sono le distanze tra soglie sperimentate: 1.5 m, 0.75 m e 0.5 m. La combinazione di diverse portate liquide con le varie pendenze ed i vari interassi ha condotto ad avere 112 buche di scavo le cui dimensioni (i.e. profondità, lunghezza e volume) e forma sono state correlate con le rispettive variabili idrauliche e geometriche. Per quanto riguarda le misurazioni in campo, complessivamente sono state rilevate le caratteristiche principali di 73 scavi a valle di briglie e soglie e di 37 pozze a valle di gradini naturali, in 10 torrenti delle Alpi Italiane Orientali con pendenze comprese tra 0.02 e 0.16. Inoltre, in due torrenti sistemati con briglie e soglie si è effettuato un rilievo granulometrico di dettaglio per poter analizzare la distribuzione longitudinale delle varie classi diametriche.

I dati di laboratorio e di campo hanno permesso di ottenere diverse formulazioni empiriche e semi-empiriche per la previsione della massima profondità di scavo, della lunghezza di scavo e del volume eroso, introducendo il nuovo concetto di energia teorica del getto e della relativa efficienza di scavo. E' stato inoltre descritto e modellato un fenomeno di interferenza geometrica tra opere poste a distanze ravvicinate su pendenze elevate, ed uno di interferenza morfodinamica nel caso si formino onde stazionarie su pendenze minori. L'analogia geometrica ed idraulica tra strutture a gradinata naturali ed artificiali è stata infine verificata statisticamente, fornendo così un nuovo modello geometrico-idraulico per spiegare la geometria complessiva delle sequenze a *step pool* naturali.

SUMMARY

High-gradient (>3-5%) streams often present a step pool structure, featuring an apparent geometric regularity and a peculiar tumbling flow pattern. A close analogy can be found in the sequences of grade-control structures such as check-dams and bed sills placed in alluvial mountain rivers in order to stabilize these channels by preventing bed incision and by reducing their longitudinal slope. The purpose of this thesis is to elucidate the physics behind natural step pool geometry and to provide engineers and technicians with predictive tools for designing safe and effective control work schemes for the stabilization of steep channels.

This research has involved both laboratory and field activities. Two flume data sets on clear-water scouring at artificial step are used herein: the first comprises 26 tests carried out in 1999 using a mobile-bed physical model set up at HR Wallingford Ltd (UK), the second set (28 runs) was obtained in 2002 at the Hydraulic Labs of University of Padova, Italy. Uniform and heterogeneous sediments have been tested, along with wide ranges of sills spacing (0.5 – 1.5 m) and initial slope (0.03 – 0.148). As to field measurements, 73 scour holes below grade-control structures and 37 pools in 10 mountain rivers in the Eastern Italian Alps were surveyed. Their mean longitudinal gradients range between 0.02 and 0.16. Two rivers trained with boulder structures were object of detailed investigations and thus represent case-studies as well. Furthermore, two channels were chosen to look at surface grain size sorting occurring along an artificial step pool sequence.

Flume and field data allowed to derive empirical and semi-empirical formulations for long-term maximum scour depth, scour length and scour volume, introducing the new concept of jet energy and the relative scouring efficiency. Also, flume results led to the first description of the "geometric interference" phenomenon causing reduction of scour dimensions in steep gradients, and of the "morphodynamic interference" caused by standing waves on milder slopes. The first quantitative evaluation in the field of the longitudinal grain size sorting showed the mean diameter at pool bottom to range between the D_{80} and D_{87} of the surface grain size distribution found on the equilibrium slope bed. A statistically significant similarity between dimensionless characteristics and geometry of pools formed downstream of grade-control structures and below natural steps has been found, and the explanation of step formation in terms of depositional berms in a upstream-forced cascade model is put forward. Finally, an analytical derivation of the observed trend linking step pool overall geometry (relative steepness factor c) to the mean channel slope is presented, starting from the evidence that pool geometry can be considered approximately invariant.

1. INTRODUCTION

Uniform flow establishes along an open channel when cross-section area and mean velocity do not vary longitudinally. The assumption that a uniform flow is present at a certain point along a channel is widely made to calculate shear stresses at the boundary, sediment entrainment, sediment transport, and so on. In most natural rivers, however, uniform flow does exist only if short distances are considered. Channel sinuosity, bedforms and bars contribute to render non-uniform the flow along alluvial channels, because they induce flow acceleration and deceleration at different cross-sections and in some cases even at a same cross-section.

The uniform flow assumption appears to be far too gross when attempting to analyze morphological processes, such as erosion, deposition and sediment transport, particularly in boulder-bed streams, whose gradient is typically above 3-5%. These high-gradient streams may show either a step pool or cascade morphology, according to the definitions by Montgomery and Buffington (1997, Fig. 1.1).

Probably because the cascade type does not present any regularity in their bed configuration and represent channels where the hydraulic processes are not able to shape considerably a very resistant boundary, so far they have not stimulated any modeling attempt as to their dynamics and characteristics. Instead, step pool torrents have been under active research for two decades now, both for their apparent geometric regularity which stimulates hypothesis about its origin, and for the peculiar tumbling flow pattern (Peterson and Mohanty, 1960, Fig. 1.2) they present, which leads to dissipate energy in a different and more effective manner compared to that accounted for by traditional flow resistance formula (Wohl and Thompson, 2000; Lee and Ferguson, 2002).

Stepped spillways or cascade drops are used to dissipate high-energy flows from dams, and at a first sight they might be considered at as step pool systems. However, in this case the bed is fixed being of concrete, the tread is horizontal, no erosion takes place (or at least should not) and therefore pools are not present here. A hydraulic analogy (Chanson, 1996) between stepped spillways and step pool streams might be misleading and erroneous because flow patterns and hydraulic jumps are very different as to their characteristics of submergence, bottom roughness and jet diffusion geometry.

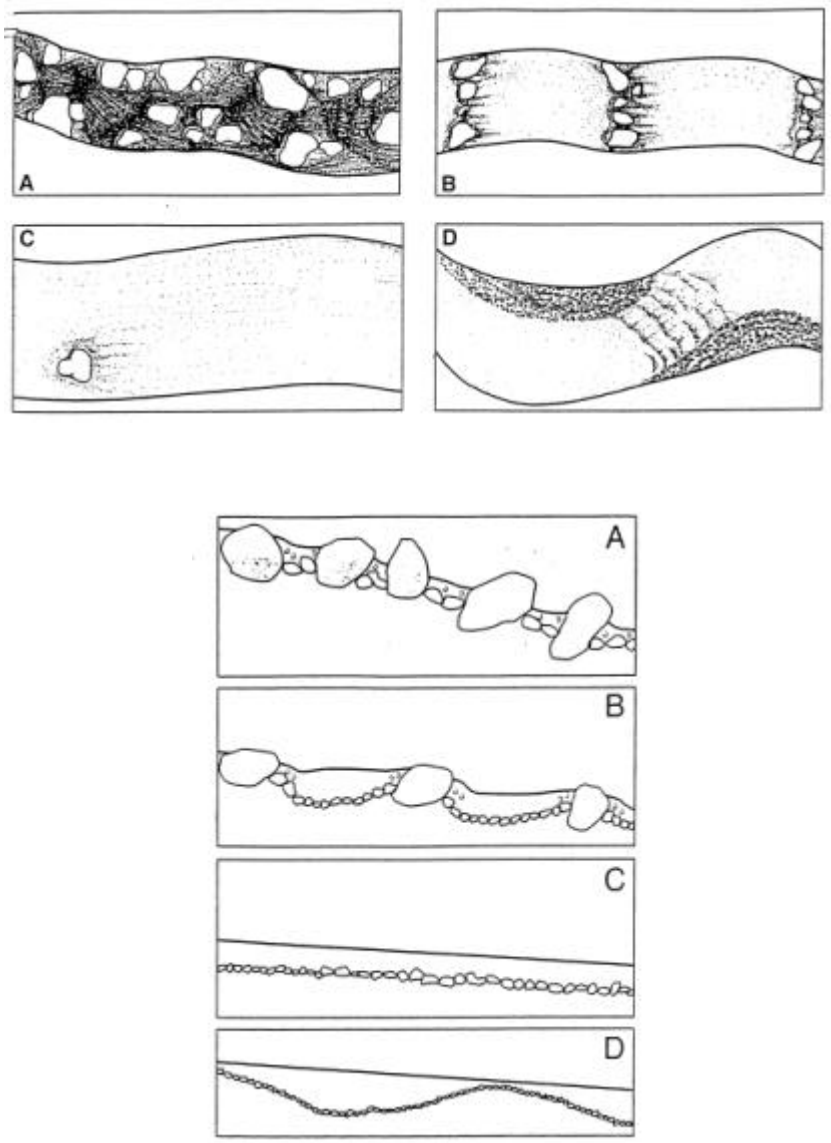

Figure 1.1 – Plan (above) and lateral (below) view of the four categories of mountain rivers' bed morphology as defined by Montgomery and Buffington (1997). *A* refers to cascade streams, *B* to step pool streams, *C* and *D* to plane bed and riffle-pool respectively.

Figure 1.2 – Step pool in the Rio Cordon creek, Dolomiti, Italy.

A more suited analogy can be found in the sequences of grade-control structures such as check-dams and bed sills placed in alluvial mountain rivers in order to stabilize these channels by preventing bed incision and by reducing their longitudinal slope (Fig. 1.3). The river beds of such trained channels show a stair-like profile, but for lower gradients a positive bed slope – a downward sloping tread – called either ultimate, compensation or equilibrium slope (Ferro, 2002) is usually achieved between two drops, because their spacing is large enough to allow the flow to establish a sort of "uniform" regime downstream of the scour pool. However, for steep streams, short spacings are usually assigned, so that the next drop structure locates just at the end of the upstream pool, thus making the profile very similar to a natural step pool sequence (Fig. 1.4).

What gives step pool systems its peculiarity is the hydraulic regime which is featured, that is the above mentioned tumbling flow. It alternates gravity-driven jets just below steps and jet diffusion in pools, in a more or less rhythmic way with critical flow conditions occurring somewhere before the step lips. The passage between supercritical ($Fr>1$) falling nappes and subcritical ($Fr<1$) pools is made through a hydraulic jump, where the jet diffuses generating a great deal of turbulence. Therefore flow resistance in step pool systems is dominated by turbulent mixing energy dissipation analogous to that of hydraulic jumps more than by grain or form drag, even though the latter may be significant if steps are very rough (Knighton, 1998). However, if a positive bed slope downstream of the pools is present, also "continuous" energy expenditures take place, but given the macroroughness characteristics of

steep boulder beds no supercritical flow is generally established along this span even if it might be present for very short distances (Jarrett, 1984; Trieste, 1994; Grant, 1997; Tinkler, 1997; Wohl, 2000_a). Therefore at the next downstream step the flow can achieve again critical (Fr˜1) conditions, thus allowing to treat each step and its related pool identically from a hydraulic standpoint notwithstanding different upstream bed slopes, albeit this procedure might neglect the effect of different jet issuance angles and different jet turbulence characteristics.

Figure 1.3 – Grade-control structures in the Cordevole di Visdende River, Italy.

A scour hole – the pool – will be shaped by the diffusing jet (or by the hydraulic jump depending on how one decides to look at the phenomenon) if the bed material can be entrained and removed by the flow. It is obvious that a pool due its existence to the upstream step, less straightforward is how the variables of the system are interrelated and how they determine the ultimate system geometry. In particular, it is still poorly understood the relative importance between downstream versus upstream boundary conditions, between sediment properties and jet characteristics, and finally what are the physical processes involved in the origin and disruption of natural step pool sequences.

Figure 1.4 – Closely-spaced concrete check dams in the Pramper River, Dolomiti, Italy.

To date, morphological studies on step pool streams have all neglected to shed light on scouring process leading to pool formation, apart from the early works by Whittaker (1987_a, 1987_b) and the more recent ones by Thomas (1999) and Zimmermann and Church (2001). Instead, pool dimensions have been extensively investigated for almost a century now in connection to drop structures, but mostly for single works (i.e. not forming a sequence) in non-sloping beds with well-sorted gravel mixtures. However, results from these numerous studies are difficult to export into step pool systems – both natural and artificial as the case of grade-control works in steep channels – because hydraulic and sedimentological boundary conditions are there much different. Therefore a deeper understanding and a sound quantitative modeling of local scouring dynamics and dimensions in step pool systems are of great interest both from a geomorphological and an engineering perspective.

The purpose of this thesis is twofold: it aims at attempting to clarify the physics behind natural step pool geometry but it also intends to provide engineers and technicians with predictive tools (i.e. equations on maximum scour depth, scour length, scour shape and volume) for designing safe and effective control work schemes for the stabilization of steep channels. The comparison between natural and artificial step pool systems will also serve as a strong basis for morphologically-oriented stream restoration project in high-gradient channels.

2. NATURAL STEP POOL SYSTEMS

2.1 General description

Steep (gradient larger than 1-3 %) mountain streams differ from lowland rivers for many aspects. They are strongly coupled to hillslopes which represent their most important source of sediment supply, and linked to this, large particles with diameters on the same order of channel depth and sometimes width are present on the streambed. Sediment transport occurs episodically, and it is mostly controlled by the availability of sediment from a limited number of sites, i.e. steep channels are usually supply-limited systems (Whittaker, 1987_a; Knighton, 1998). All these factors have been identified to be critical to the formation and persistence of a stepped-bed morphology (Grant et al., 1990).

Natural step pool channels are characterized by a more or less regular alternation between steps composed of clasts, large woody debris and/or bedrock, and plunge pools that form at the base of each step. Steps and pools having a stair-like appearance are typical of streams on slopes greater than 3-5 % (Chin, 1989; Montgomery and Buffington, 1997; Knighton, 1998; Wohl, 2000_a). Immediately under this values, plane bed and riffle pools morphologies usually occur, whereas for slopes larger than 15-25 % a more chaotic structure takes place – named cascade by Montgomery and Buffington (1997) – where cobbles, boulders and small, poorly formed pools not spanning the entire channel width make up the streambed. However, a weakly or totally disorganized structure may be present for channel slopes within the range of step pool systems as well (Zimmermann and Church, 2001).

In step pool channels, step risers are composed of several large boulders that act as a framework against which smaller clasts are imbricated, creating a tightly interlocking structure Keystones are therefore needed in order to create a well-defined and stable stepped structure (Fig. 2.1), and this implies a strong control of local conditions, both by hillslopes and by channel processes (Knighton, 1998). Even more strongly influenced by non-fluvial processes appear to be steps in bedrock channels (Fig. 2.2, Hayward, 1980; Wohl and Grodeck, 1994; Duckson and Duckson, 1995, 2001; Wohl, 2000_b), and those formed by large woody debris accumulations (Fig. 2.3, Keller and Swanson, 1979; Wohl et al., 1997; Faustini and Jones, 2003).

Fig. 2.1 – Step pool in the Rio Cordon creek (Italy): large keystones (some are likely immobile at all flows) are crucial for step formation in steep streams.

Fig. 2.2 – Bedrock step pool sequences in the Dry Meadow Creek (California, USA); note the kayaker in the circle for scale.

Figure 2.3 – Log step in a monsoon-dominated creek in Nepal. The diameter of the log is approximately 0.8 m.

Step pool sequences have been reported from a wide range of humid and arid environments (Wohl, 2000_a), on supraglacial streams (Knighton, 1981), and from a similarly vast vertical scale range, i.e. from the orders of few centimeters, as in rills (Fig. 2.4) to some meters (boulder-bed channels, Fig. 2.5). The Author has observed step pool sequences also in small channels formed by wave run-up on beaches where shells act as boulders and form steps. However, it might be possible that different processes are responsible for the stepped structure at different scales, as observed for meanders (Knighton, 1998, p. 225).

Figure 2.4 – Step pool sequences in a 7-cm-wide rill (Rio Cordon basin, Italy).

Figure 2.5 – Digon River (Italian Alps): steps are roughly three meters high.

2.2 Hydraulics of step pool streams

No matter the scale or the type of material composing the channel, the hydraulics of step pool system present a typical and peculiar pattern, called tumbling flow (Peterson and Mohanty, 1960), characterized by pseudo-cyclic acceleration and deceleration, with supercritical flow (Fr > 1) from the step lip to the impingment point and subcritical (Fr<1) conditions thereafter in the pool, the change occurring via a hydraulic jump. However, the extent to which this alternation persists at high to extreme flows has not been ascertained yet, since smaller steps could eventually become completely drowned out and a faster skimming flow may onset, as argued by Lee and Ferguson (2002) and Weichert et al. (2003).

Very little is known about the hydraulics of these channels. It has long been recognized that the presence of steps and pools is a major additional source of macroroughness, with spill resistance due to the hydraulic jumps dominating the energy losses along a reach (Hayward, 1980). Indeed, this channel morphology is very complex to analyze from an analytical point of view due to the overwhelming control on its hydrodynamics exerted by hydraulic jumps. In fact, these phenomena still lack a comprehensive understanding and modeling for boundary conditions more complex than those investigated for decades by engineers in laboratory

flumes (Vallé and Pasternak, 2002). To the author's knowledge, only few studies have been carried out to determine hydrodynamic characteristics of step pool streams.

Stüve (1990) found energy losses and roughness at low flows much variable along a step pool reach in Bavaria; a more uniform energy expenditure between cross sections was observed for higher flow rates.

Egashira and Ashida (1991) made an attempt to develop analytically a resistance formula for step pool channels, where relative wave height and length, wall roughness and the head loss due to the hydraulic jump are the independent variables. Unfortunately, their formula was proved – by flume experiments – to work out only when steps were completely drowned out (profile *B* in Fig. 2.6) and no jumps occurred, so that the last variable – unknown – could be ruled out. When hydraulic jumps were present (i.e. what they called chutes and pools flow, profile *C*) the friction factor *f* was found to be two to three times greater than that predicted by their equation.

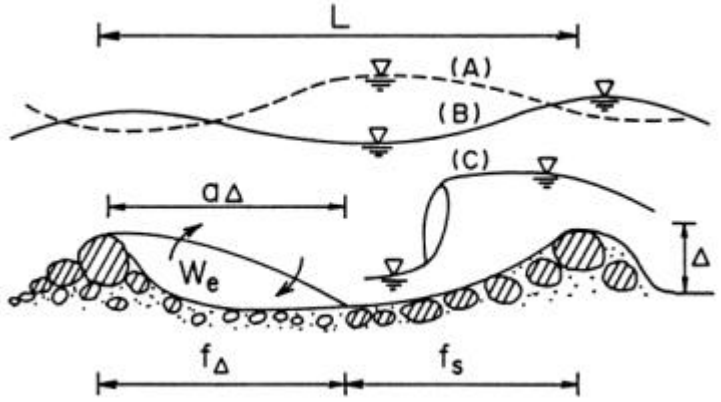

Figure 2.6 – Flow patterns on a stepped bed profile as in Egashira and Ashida (1991). Their resistance formula strongly underestimates resistance occurring for a water profile like (C), i.e. chute and pools, where hydraulic jumps are formed.

O'Connor (1994_a, 1994_b) computed grain resistance in steep, low-order streams in the Olympic Mountains of Washington and found that grain resistance accounted for only about 25% of the total flow resistance, but did not separate the remaining resistance into different components.

Wohl and Thompson (2000) measured velocity profiles and fluctuations over steps and pools. Flow became more turbulent as stage increased, as well as when gradient and bed roughness augmented. Pools had wake turbulence from mid-profile shear layers generated by jet diffusion, whereas just upstreams from steps, at step lips and in runs bed-generated turbulence prevailed. The wake-generated turbulence is responsible for the higher energy

dissipation occurring along step pool reaches relative to more uniform-gradient channels (Wohl, 2000_a).

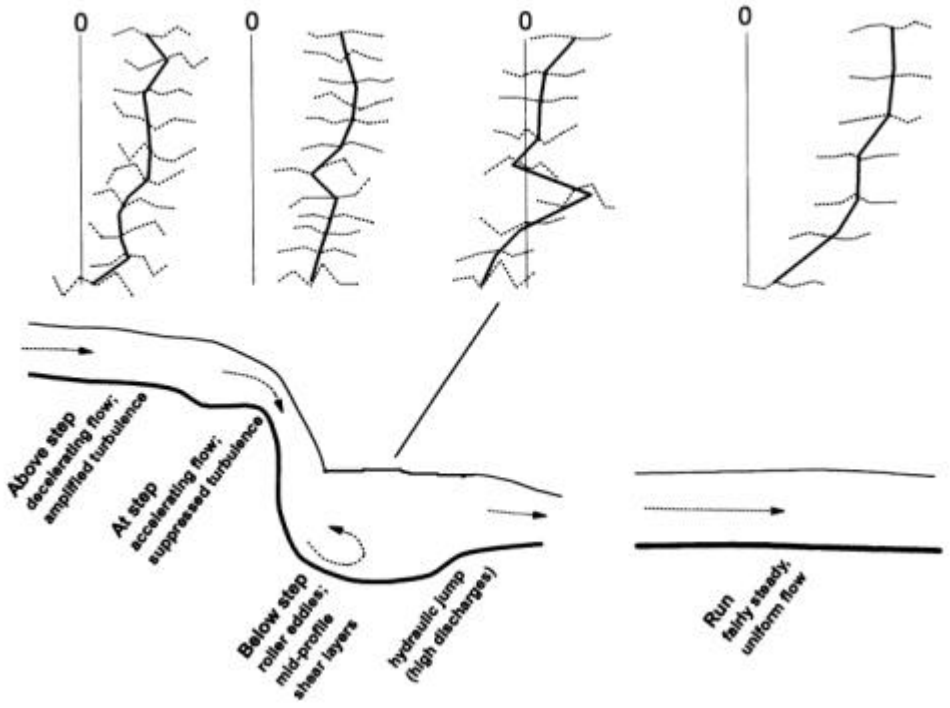

Figure 2.7 – Schematic illustration of flow characteristics along a step-pool sequence and a run. The upper figures are vertical velocity profiles, with vertical axis of 0 m s^{-1}. The dotted lines represent the magnitude of velocity fluctuations. The lower portion illustrates the dominant flow features at different cross sections (Wohl and Thompson, 2000, modified).

Lee and Ferguson (2002) performed measurements of mean velocity by using salt-dilution methods in 6 step pool creeks (channel slope S = 3-18 %) and in a laboratory flume (S = 6.7 %). All the data showed a rapid increase in velocity as flow rate increased, with a correspondingly strong reduction of flow resistance. Further, the increase in velocity was always faster than that in depth, on the contrary of what happens in lower gradient rivers, implying that the resisting force – i.e. the energy losses – becomes larger less rapidly than the driving force. Onset of skimming flow when smaller steps get drowned out likely leads to a reduction of resistance bigger than any increase of spill resistance possibly occurring at large hydraulic jumps for larger discharges (Lee and Ferguson, 2002). They also found that the Keulegan-type resistance formula proposed by Thompson and Campbell (1979) for stepped spillways was the most appropriate to use without any calibration. The equation is the following:

$$\left(\frac{1}{f}\right)^{0.5} = 2.03\log\left(\frac{12.2R}{k_s}\right)\left(1-\frac{0.1k_s}{R}\right) \qquad (2.1)$$

where f is Darcy-Weisbach friction factor, R is the hydraulic radius and k_s is a roughness height, usually estimated as some multiple of the D_{84}. The second factor in Equation 2.1 increases markedly the resistance for shallow flows, aiming at simulating the "blocking" effect – i.e. the reduction of the available cross sectional area – induced by large bed elements. Step D_{50} was found to be the most consistent estimate of the roughness height k_s, but good results were also obtained by using step-pool amplitude and the K3 index introduced by Ergenzinger (1992).

Wilcox et al. (2002), in order to partition total resistance and to quantify variations in total resistance caused by changes in large woody debris (LWD) configurations, discharge, and slope, changed variables contributing to flow resistance in step-pool channels through over 200 flume runs. For each test, total resistance was calculated based on measurement of reach-averaged velocity in a flume configured to resemble a step-pool channel. They tested the effect of discharge, slope (0.10, 0.14 m/m), presence/absence of steps and grains, and LWD density, orientation, piece length, and arrangement. They state that "calculations of resistance partitioning indicated that spill resistance and debris resistance were responsible for the largest components of total resistance, and that grain roughness was a small component of total resistance when steps and/or debris were present. Discharge had the largest effect on resistance of all variables tested, and the effect of LWD configuration on roughness tended to be drowned out at high discharges. Debris density, debris orientation, and slope also had highly significant effects on total friction factor" (Wilcox et al., 2002).

Curran and Wohl (2003) made the first attempt to partition the total resistance in real step pool streams. Based on the analyses of channel geometry and low-flow hydraulics (by salt-dilution methods) along 20 step-pool reaches in the Washington Cascade Range, they observed friction factors (f) ranging from 5 to 380 during low flows. These values are high in comparison to gravel-bed streams with gradients smaller than 0.05, where reported values of f range from 0.06 to 5.5 (Jarrett, 1984; Bathurst, 1985; Thorne and Zevenbergen, 1985). The authors argue that such high values of f arise from energy losses at hydraulic jumps, flow separations, vertical falls, extreme turbulence, and channel expansions and contractions. Dividing the flow resistance into grain resistance, form resistance from large woody debris, and spill resistance from steps showed that a large proportion of the total flow resistance was

generated at steps. Grain and form resistance accounted for less than 10% of the total flow resistance in all but two of the study reaches. These figures indicate the dominance of spill resistance, which is on the order of 90% of total flow resistance. They also noted that large woody debris exerted a marked indirect control on spill resistance by accentuating step height, and that cumulative water surface drop associated with steps may be used as a first-order approximation of energy loss related to steps.

Finally, Wilcox and Wohl (2003) collected three-dimensional measurements of time-averaged and turbulent velocity components using a SonTek FlowTracker Handheld Acoustic Doppler Velocimeter (ADV) on a 40-m reach of a step-pool channel (slope $S = 0.11$) in the Colorado Rockies. Their data "indicate that bedform type significantly affected mean downstream and cross-stream velocities; downstream velocities were higher at locations upstream of steps and at step lips than in pools downstream of steps". And also, "downstream velocities also decreased significantly with decreasing discharge, although discharge effects on cross-stream and vertical velocities were not significant. Discharge and bedform type also significantly affected turbulence intensities for all flow components, with the greatest turbulence intensities occurring in pools and at high discharges" (Wilcox and Wohl, 2003).

2.3 Step pool geometry

Compared to investigations on step pool hydraulics, studies on geometrical characteristics of these channels are more abundant in the literature. Given the predominant stream-wise characteristic of step pool morphology, this has been mostly investigated and analyzed in terms of step wavelength *L* measured parallel to the mean bed slope, and of step height *H*, measured as the difference in elevation between step crest and pool bottom (Fig. 2.8).

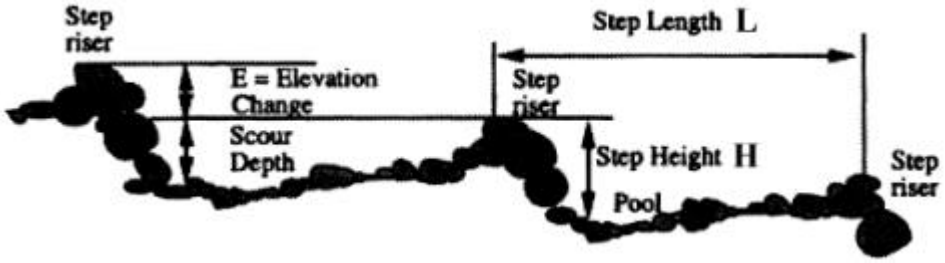

Figure 2.8 – Sketch of main step pool morphological variables (after Chartrand and Whiting, 2000, modified).

As for riffle-pool units, a relation between spacing *L* and channel size (i.e. width) has been sought, but with poorer results, since values range between 0.6 (Chartrand and Whiting, 2000), to 1.4 (Bowman, 1977) and 1.9 (Chin, 1989) up to 2.7 channel width (Whittaker, 1987_a). However, step geometry appears more well-defined and more regular on steeper gradients (Hayward, 1980; Wohl and Grodek, 1994). Since the earliest investigations on this topic, a negative correlation between step spacing and channel slope has been identified (Judd and Peterson, 1969; Hayward, 1980; Whittaker, 1987_a; Grant et al., 1990; Chin, 1999_a; Chartrand and Whiting, 2000; Weichert et al., 2003) but the parameters of the best-fit power law equation differ considerably among the authors. Rickenmann and Dupasquier (1995) did not even find any significant correlation between step wavelength and channel slope in the Erlenbach stream (Switzerland).

As to step height, Wohl et al. (1997) and Chin (1999_a) found a strong positive correlation between step height and mean particle size on the step riser, with average values between 1 and 1.2. Chartrand and Whiting (2000) observed a weaker yet significant correlation with the step median particle size D_{50}, with $H/D_{50} = 1 - 1.5$. It has then been argued that step height is largely controlled by the rocks comprising the step, and because particle size generally decreases downstream, a similar trend is to be expected for step height, providing the rationale for the observation that steps are smaller in lower gradient reaches

(Chin, 1999_a). Furthermore, Wohl et al. (1997) found that no significant difference existed between log and clast steps with regard to step spacing and height in 32 streams in Montana.

All the other possible correlations among dimensional geometrical variables, i.e. step wavelength and height, and external factors as discharge, slope and sediment size have been examined and can be found in Wohl et al. (1997), Chin (1999_a) and Chartrand and Whiting (2000). However, a marked improvement towards the understanding of variations in step pool geometry has been achieved by the adoption of a non-dimensional approach focusing on the so-called steepness *H/L* – analogous to a relative wave amplitude – and its normalization by the channel slope, to give the relative steepness factor (Abrahams et al., 1995):

$$c = \frac{H / L}{S} \qquad (2.2).$$

It is notable to point out that the ratio height-to-spacing *H/L* resembles a loss of head per unit of channel length, thus bearing energetic implications (Knighton, 1998). The innovative yet controversial experimental work by Abrahams et al. (1995) has demonstrated by flume tests that maximum flow resistance occurs with evenly-spaced steps and within the range:

$$1 < \frac{H / L}{S} < 2 \qquad (2.3).$$

Such conditions had been found by the same authors to describe rather well real step pool streams, where on average was c = 1.5. Geometrically, this result shows the lack of significant down-sloping streambed lengths in a step pool reach, i.e. downstream of pools – where bed slope is reversed – only a short, roughly flat zone is generally present before the next step. From an energetic perspective this means that the elevation loss due to steps approximates the total elevation loss along a reach, confirming the role of step-induced spill resistance on the overall energy budget in step pool channels.

Subsequent field investigations (Wohl et al., 1997; Chartrand and Whiting, 2000; Zimmermann and Church, 2001) has somewhat narrowed the extent to which Abrahams et al.'s slope-normalized geometry is valid in real streams, because they have observed for channel slopes below 5-7% ratios *c* usually larger than 2, and a negative correlation with channel slope (Fig. 2.9). Moreover, data from step pool channels in the Italian Alps (Lenzi

and D'Agostino, 1998, 2000; Lenzi, 2001) confirm its suitability only for streams which have experienced several "ordinary" floods after the step-forming one, otherwise the ratio *c* tends to be below the unity. Therefore they argued that Eq. 2.3 might represent a geometrical equilibrium condition requiring processes of bed armoring and localized erosion to occur, in order to scour fine sediment from pools and thus attain a reverse bed-slope between steps. In fact, following an extraordinary flood with unlimited sediment supply, the steepness factor can suddenly decrease as a result of sediment trapped in the pools and a lengthening of step spacing.

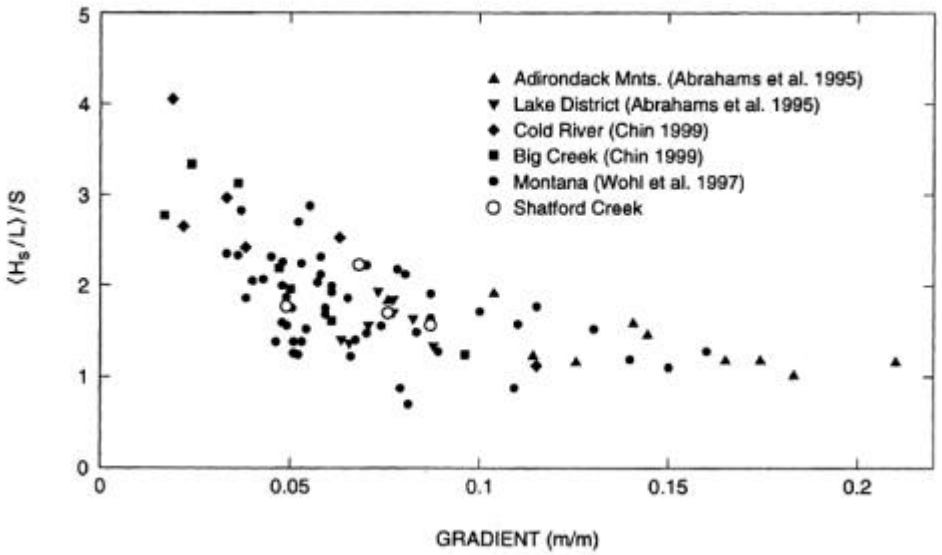

Figure 2.9 – Plot of the parameter *c* vs mean channel slope (after Zimmermann and Church, 2001). Shatford Creek points refer to this paper.

2.4 Formation of step pool sequences

Unfortunately, flow conditions under which steps form are too infrequent to allow statistically significant field-based investigation of step-forming processes. Beside of this, most factors affecting step formation, such as discharge, slope, grain size, channel width and flow depth, present a high degree of covariance, making the discern of the actual cause-effect linkage a real challenge. Is a downstream increase in step spacing due to a smaller sediment size, to a larger discharge, to a milder slope or to a "mix" of them ? To date, general agreement has yet to come on such questions (Crowe, 2002).

In fluvial hydraulics and fluvial geomorphology, but it could be generalized for science in general, two different approaches and perspectives exist: one is local, reductionistic, the other is system-oriented, holistic. Where the former pays more attention to small-scale processes and then attempt to extend them to a larger scale, the latter follows the opposite way, starting from the physical system as a whole, often applying concepts of non-equilibrium thermodynamics. A strong debate on which one is "superior" is still active among scientists, but it seems reasonable to conceive them as two different ways to look at the same processes, each applicable at its proper scale. For theories on step pool formation, a similar distinction can be drawn.

The systemic approach was first adopted for step pools with the contribution of Abrahams et al. (1995), even though some hints can be found in previous papers (Yang, 1971; Yang and Song, 1979), where the extremal theory invoking the minimization of the energy dissipation rate is used to provide the rationale basis for riffle pool units and meanders formation. As mentioned above in section 2.3, Abrahams et al. (1995) carried several flume experiments and found that step pool sequences not only increase flow resistance but maximize it, thus proving the validity of the extremal general theory by Davies and Sutherland (1980) proposed for all kinds of channels with deformable boundaries (in turn such a theory has been demonstrated by Yang (1987) to derive from that regarding the minimum rate of energy dissipation). Abrahams et al. (1995) then concluded that step pool streams geometry adjusts towards this friction maximization (Eq. 2.3) because this implies maximum bed stability against erosion. As reported before, Lenzi (2001) argued based on field evidences that this extremal theory is applicable only for the evolution over time (i.e. scale of years), not for explaining mechanisms of step formation during a single flood event. Indeed, the inherent teleoscopic nature of Abrahams et al.'s theory prevents it to adhere to actual "snapshots" of step pool geometry (i.e. spacing and height) as observable at random times in the field.

Few years later, Grant (1997) put forward that the critical condition, i.e. flow Froude number $Fr \tilde{} 1$, constrains flow hydraulics and bed morphology of steep streams, based on measurements in sand-bed channels and on widespread evidences of the rarity of supercritical flows even in very steep alluvial channels. It is pointed not only the thermodynamic validity of this hypothesis, being consistent with the minimization of the energy dissipation rate, but also its mechanical rationale due "to the close coupling of the flow hydraulics with bed deformation and sediment transport. (…) Critical conditions represents an energy threshold beyond which flow instabilities – i.e. hydraulic jumps – results in rapid energy dissipation and

in turn in morphological change counteracting flow acceleration" (Grant, 1997). The adjustments to such a threshold is attained dynamically, through bed-water profile feedbacks which cause the Froude number to oscillate around the unity (Fig. 2.10). In sand-bed streams these oscillations occur both in time and space, whereas in coarse-grained channels – i.e. step pool channels – the spatial dimension dominates, due to the lower bed load rate, more chaotic bed structure and importance of particles interactions (Grant, 1997). Compared to Abrahams et al. (1995) theory, Grant's has the merit of trying to put together a thermodynamic rationale and a detailed hydraulic reasoning, invoking well-documented processes as standing waves and hydraulic jumps.

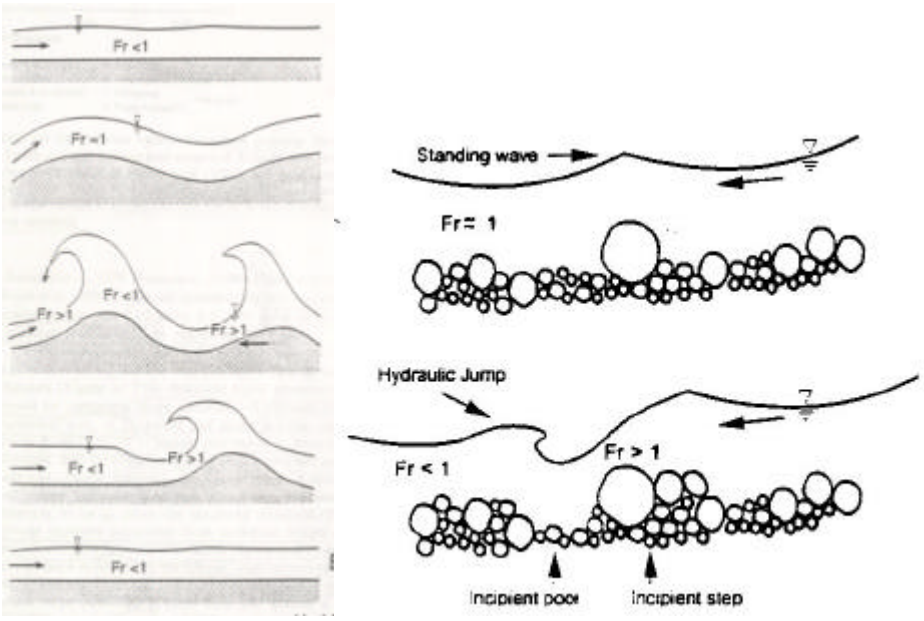

Figure 2.10 – After Grant (1997), the mechanisms responsible for the oscillation around the critical conditions (i.e. *Fr*=1) in sand-bed channels (left) and in coarse-grained streams (right). Standing waves and hydraulic jumps are the link between hydraulics and morphodynamics.

As to the purely mechanistic models, several of them have been proposed over the years, mainly to explain step formation and to predict step wavelength. All of these recognize steps as being depositional features, and pools as scour-driven elements, occurring in channels having well-graded sediment mixture with immobile clasts at most flows, low sediment supply, low width-to-depth ratio (Grant et al., 1990; Knighton, 1998). Naden and Brayshaw (1987) proposed also for step pool sequences – after meanders and riffle pools – the kinematic wave theory where inter-particles reactions alone are able to produce longitudinal sorting. However, what the models disagree about are the actual hydraulic phenomena taking place and shaping the bed. Crowe (2002) presented a detailed summary of them. Basically,

antidunes – or more generally standing waves – and hydraulic jumps are the controlling hydraulic processes considered by all the investigators.

Judd (1963) and Judd and Peterson (1969) proposed an upstream-forced model where a large immobile clast promotes the formation of a particle cluster around it, up to create a channel-spanning step, the initial one. This bed irregularity generates a train of standing waves downstream of it, with large particles settling down in correspondence with wave crests, thereby building up a series of steps. Pools then originate from local scouring below each step. This model – inferred by field observations – is the first to hypothesize that step wavelength is set by standing waves characteristics, but requires the random formation of an intial step.

Instead, Whittaker and Jaeggi (1982) in their flume tests noted that a step pool structure arose from antidunes developing from a plane bed in concomitance with bed degradation and consequent bed armoring. A single, large clast would deposit on the upstream side of each antidune, anchoring it in place. Further deposition at the antidunes crest would increase their elevation, thus transforming them into steps. At decreasing flow rates, pools would result from scouring at each step's toe. Since steps derive from an antidune train, their spacing must be roughly equal to the antidune wavelength and should be also in accordance with the stability field defined by Kennedy (1963) for these bed forms function of the wave number and the mean Froude number. According to Kennedy's analysis, a stable antidune wavelength is given by (with V = mean flow velocity in m s^{-1} and g acceleration due to gravity in m s^{-2}):

$$L = \frac{2\pi V^2}{g} \qquad (2.4)$$

which for Froude numbers near 1.0 approximates (with h = mean flow depth in m):

$$L = 2\pi h \approx 6.3h \qquad (2.5).$$

Step formation mechanisms due to antidunes – and with a decisive role played by bed armoring – have been later observed in the laboratory by other researchers, lending support to such a theory (Ashida et al., 1984; Grant and Mizuyama, 1991; Grant, 1994; Rosport and Dittrich, 1995). Some investigations claim to have established the applicability of the antidune model to step pool sequences measured in real channels, having found good

agreement with the antidune's stability field (Figs. 2.11 and 2.12) and with Eqs. 2.4-2.5 (Chin, 1999_b; Chartrand and Whiting, 2000; Lenzi, 2001); but Chin herself noted that "…true antidunes as specified by Kennedy (1963) may be difficult to maintain in the steep headwaters where large and less mobile roughness elements may disturb the regularity of the process."

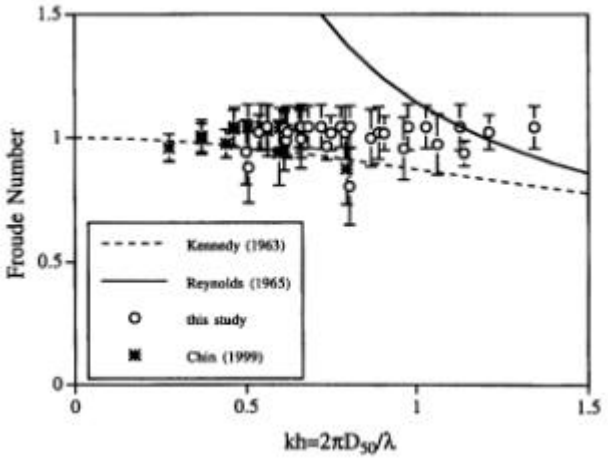

Figure 2.11 – Stability field of antidunes and field data from step pool channels in the U.S. (after Chartrand and Whiting, 2000, modified).

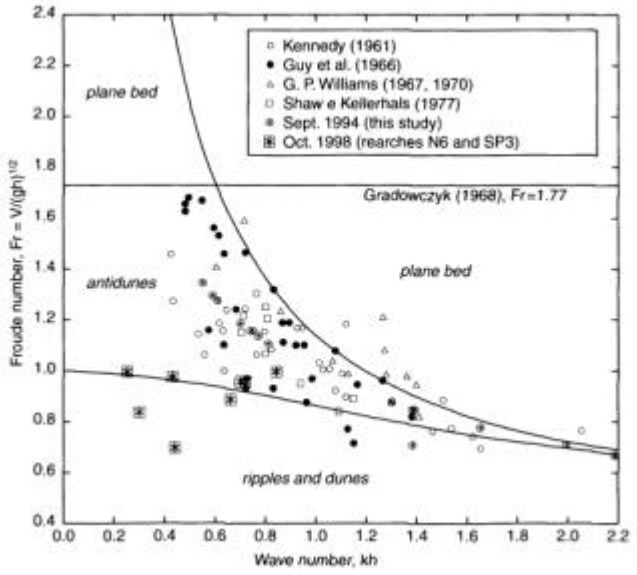

Figure 2.12 – Stability field of antidunes and data of step pool in the Rio Cordon creek (Italian Alps) for two step-forming flood events, Sept 1994 and Oct 1998 (after Lenzi, 2001).

As demonstrated by the number of papers regarding the antidune-step pool link, such a theory has exerted a great deal of enthusiasm among fluvial geomorphologists and river engineers; previously, however, other hydraulic models had been proposed originally for the genesis of those small steps found in braided streams called transverse ribs (Allen, 1982).

McDonald and Day (1978) were the first to pose the accent on hydraulic jumps' role. They conducted several flume experiments and observed that transverse ribs (i.e. small steps) are formed by a self-repeating process controlled by downstream conditions in which a hydraulic jump migrates rapidly upstream. Pebbles would accumulate just downstream of the hydraulic jump during the intervals when it is stationary. An empirical equation was developed for step wavelength L:

$$L = h(5.7Fr - 2.2) \tag{2.6}$$

where h is the flow depth (m). For critical conditions (i.e. for Fr = 1) Eq. 2.6 gives:

$$L = 3.5h \tag{2.7}$$

thus predicting much shorter step spacings compared to Eq. 2.5 derived from the antidune analogy. However, no field evidences of this process nor its validation have been documented yet.

Allen (1982, 1983) developed a cascade model invoking a self-repeating process of deposition where – differently from McDonald and Day (1978) – an upstream commencement and control is hypothesized. The Author envisages "train of ribs spreading downstream from an initial rib located where perhaps an unusually large clast had come to rest" (Allen, 1982, p. 394). As in the particle cluster model by Judd (1963), it is stressed the importance of random large elements to start the formation of a sequence. The difference between Judd's and Allen's models lies in the actual hydraulic phenomena taking place downstream of each step. The former assumes standing waves to occur, whereas the latter suggests that hydraulic jumps are responsible for the deposition of large particles which will become the next step. An exclusion zone exists within which another step cannot be formed, given by the length for the onset of a supercritical flow, required to have a jump. To evaluate the length of this zone, representing a minimum spacing for step pool sequences, Allen (1982) proposed to use the following equation (Peterson and Mohanty, 1960) developed for regularly spaced baffles:

$$L \geq 0.15\frac{h_c}{S} \tag{2.8},$$

where h_c is the flow depth at step crest equal to the critical depth, and S is the bed slope.

It is interesting to note that for S = 0.05 (i.e. close to the lower limit for existence of step pool) Eq. 2.8 gives:

$$L \geq 3h_c \qquad (2.9),$$

very similar to the empirical Equation 2.7 by McDonald and Day (1978) for near critical conditions. For steeper slopes, the coefficient in Eq. 2.9 decreases, e.g. for S=0.15 equals 1.

Arguing that the coarsest step-forming grain size D is in the order of h_c, and accounting for the effect of grain packing by introducing the parameter a, Allen (1983) modified Eq. 2.8:

$$L \geq 0.15\frac{aD}{S} \qquad (2.10),$$

with a ranging linearly from 1 for S=0.05 to 2 for S=0.20. Chartrand and Whiting (2000) applied Eq. 2.9 to their measured step wavelengths assuming a=1, and found that measured spacings were mostly larger than the lower boundary given by the inequality, thus satisfying it. However, the plot (Fig. 10 of their paper) shows a rather poor correlation between measured and predicted values.

All the deterministic models presented above start from one basic assumption: step spacing is determined by only one hydraulic phenomenon. The reconnaissance – in the writer's opinion revolutionary indeed – that steps might originate from different processes and a large variability in their spacing is then to be expected was first acknowledged in the work by Zimmermann and Church (2001), where a random distribution of step spacing was mainly attributed to the influence of bed and bank irregularities. But the first study attempting to identify and quantify the relative importance of various formative processes is represented by the live-bed flume runs (slope S ranging from 0.035 to 0.052) carried out and discussed by Crowe (2002).

Crowe analyzed the formation of 374 steps, described four mechanisms and determined the occurrence frequency. She named them obstacle, re-emergent, knick-point, and mound. The first (50.0 % of total formed steps) happens when a "step-forming grain lodges against an obstacle on the rough bed surface. (…) sediments blocked from traveling downstream deposit around the step forming grain." Re-emergent (4.8 %) refers to steps once buried that become again exposed due to surface erosion, affecting spacing distribution. A knick-point (19.5 %) mechanism occurs when "an existing step breaks-up, a knick-point can form and migrate upstream until it encounters either the pool of an upstream step or a large,

immobile grain in the bed. The large grain arrests the knick-point, and a new step develops around the newly exposed grain". Finally, the mound process (25.7 %) corresponds to the already mentioned action of a series of standing waves – generated by an existing step – causing deposition at their crests downstream from the initial step. From these figures, it can be summarized that 75 % of step locations were obtained without any influence of the water surface, since in the first three mechanisms the deposition of the step-forming grains is controlled by the bed surface, whereas only in the mound process there is a direct influence of the hydraulic conditions, i.e. wavelength of standing waves. An exponential distribution was found to fit the step spacing distribution for all types of formative processes separately, but it does not adequately adhere to small values of step spacing, thus prompting a modification to model the existence of an exclusion zone downstream of a step. A simple probabilistic model built from the assumption of equally probable deposition was then developed and found to generate an exponential curve, modified for the presence of the exclusion zone where deposition is less likely.

Crowe argued that the fact of finding an exponential distribution to fit step spacing indicates that deposition of step-forming clast is equally likely at any location along the bed, apart from the exclusion zone. No preferred locations thus exist for step formation, which would lead to different spacing frequency distribution and "step spacing does not follow a regular pattern, because it is not established through a systematic process forcing the deposition of step-forming grains at specific locations on the bed..." (Crowe, 2002). The influence of step formation mechanism (obstacle, mound, ...) is limited to the extent of the exclusion zone, this being shorter for the mound process. However, in the tests where many steps formed through such a mechanism (i.e. those with lowest flow depths and/or highest transport rates), it was observed that the distribution tended to become bimodal, because of their shorter average spacing compared to the other three processes.

Finally, Crowe points out how the mound mechanism might seem consistent with the antidune model, but actually a "complete sequence of steps did not form from a train of antidunes", because once the first crest of the train becomes a step, the "remainder of the antidune washes out" (Crowe, 2002). Beside of this, the pairs of Froude and wave numbers from her tests plot out of the stability field for antidunes proposed by Kennedy (1963), in particular all the runs were characterized by subcritical conditions (Fig. 2.13). Nevertheless, none of the previously discussed models for step pool (or transverse ribs) formation gives neither a satisfactorily prediction of the observed step spacings, nor a complete description of formation processes.

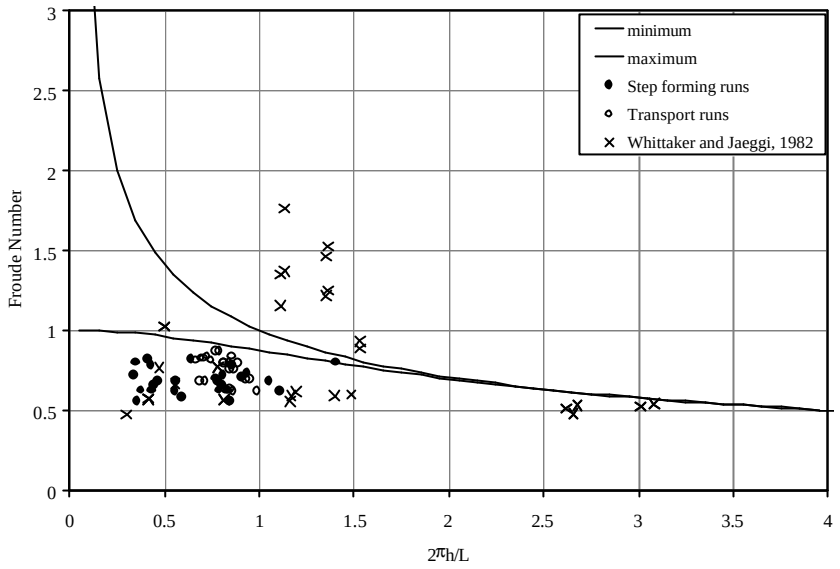

Figure 2.13 – Crowe's tests lie below the lower limit of the antidune stability field (after Crowe, 2002)

2.5 Step stability

Compared to formative processes, much less attention has been devoted to investigate the destruction of steps, which is nonetheless required for a whole new sequence to establish. The large dimensions and the tight interlocking of clasts forming a step provide them with a strong stability which only extreme floods can disturb, suggesting that step pools can be viewed as an equilibrium form, considering also their role in satisfying the condition of flow resistance maximization (Knighton, 1998; Lenzi, 2001).

Hayward (1980) described major and minor steps, where the former – composed of bedrock outcrops, immobile rocks and large boulders – control the large-scale channel morphology and are stable for periods not shorter than 50-100 years. In between these control points, minor steps were instead observed to break down every 2-5 years and their unstable pattern was superimposed on the more permanent one given by the major steps.

Chin (1998) supported this "relative stability" idea – i.e. it depends on step particle size – by applying an incipient motion calculation on step forming particles, using Costa's (1983) critical velocity formula. This analysis indicated that step pools are active channel features with a very wide range of permanence, from 5 to 100 years; it presents nevertheless a large limitation due to the assumption that step destruction occurs via a "Shields-like" mobilization, whereas particles forming steps can hardly be considered isolated boulders immersed in the flow.

On the other hand, Whittaker (1987_a) first addressed the problem of step stability by studying local scouring at their toe, thus acknowledging the importance of destabilization by undermining. His experimental work has inspired the present research, stimulating to investigate in detail local scouring phenomena taking place below steps. In fact, both field (Lenzi, 2001) and laboratory observations (Giacometti, 2000; Weichert et al., 2003) have showed step failure by toe over-scouring to be the most frequent cause of step destabilization. However, the destruction of a single step causes rearrangements on the bed structure which overall stability can be either enhanced or decreased, thus posing the need for a definition of the scale at which stability has to be considered (Weichert et al., 2003).

As for formative models, the experimental work by Crowe (2002) provides valuable insights into the complexity of destructive phenomena that may actually occur in a step pool sequence. She identified four types of step "elimination", three of which involve step break-up (i.e. tumble, slump and impact) whereas one – burial – refers to deposition occurring in the pool until the step pool form is lost in the profile, and accounted for 13.4 % of all the processes. Impact happens when large moving grains dislodge the step-forming particles, causing the step to break-up and the other grains previously part of the structure to be eroded. Its frequency of occurrence was the lowest, with only 10.1%. Therefore it becomes apparent that as much as 76.6% of all step cancellations are due to mechanisms – tumble and slump – involving scouring in the pool, destabilizing the base of the step (Fig. 2.14).

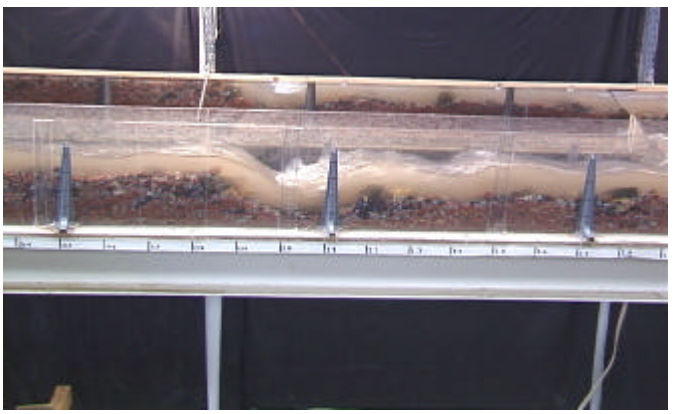

Figure 2.14 – Photo depicting a large step and the relative pool in one of the runs carried out by Crowe (2002).

In the former process (39.1%), the top of the step tumbles first, then other grains fall into the pool and are not transported downstream. In the slump mechanism (37.5%), particles from the bottom of the step move first into the pool, subsequently the upper part slides down intact, breaks-up in the pool and then clasts are entrained by the flow.

3. LOCAL SCOURING AT GRADE-CONTROL STRUCTURES

3.1 Control works in steep incising channels

High-gradient mountain streams are often prone to channel incision. Its prevention in mountain rivers through sequences of grade-control works has been implemented for a century in the Alps. Human settlements in this region have always been subject to the hazards of flood events characterized by intense sediment transport. Steep, high-energy streams are usually sediment supply-limited and therefore tend to erode their boundary in alluvium when – a few times a year – the water discharge rises above the motion threshold. Vertical incision and lateral erosion must be controlled in order to stabilize these streams for at least two reasons: first they may trigger landslides, secondly huge amounts of solid material might be delivered to downstream reaches at milder slopes, thereby leading to aggradation with possible subsequent overflooding. Such gentle-sloped reaches typically characterise alluvial fan areas, which are the most densely urbanized zones throughout the Alpine region.

Grade-control works in steep rivers are built in staircase-like sequences. Incision is controlled both by fixing the bed height at several points and by reducing stream transport capacity through the lowering of the initial longitudinal channel slope S to a lower value S_{eq} (ultimate or equilibrium slope). Grade-control structures are generally called check-dams when they are 1.5-2 m high above the original bed level and sills if less. Check-dams are generally preferred when the height of the river bed is to be somewhat raised, for example in order to reduce instability of the valley sides (Fig. 3.1).

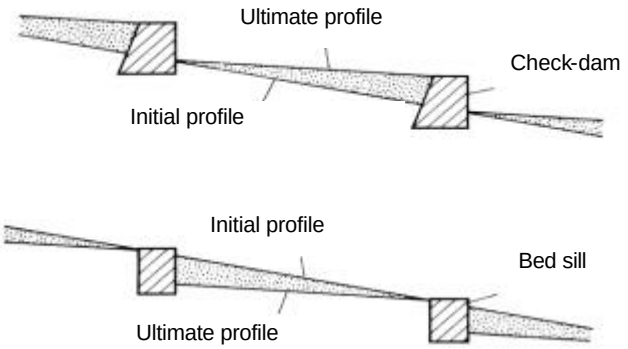

Figure 3.1 – Sketch illustrating differences between check-dams and bed sills

.

Even though their initial dynamics are different – prevailing sedimentation for check-dams and erosion for bed sills – once check-dams become filled-up with material the overall hydraulic functioning tends to the same pattern: plunging jets issued from structures' crests diffuse their energy in turbulent rollers inside the pools below. Further downstream, uniform flow can be attained if the river bed presents an equilibrium slope for a significant length. This condition is satisfied when the distance between the works is sufficiently large. Flow over work crests features critical conditions ($Fr \tilde{} 1$), as shown by previous laboratory tests (Comiti, 1999). At the edge of the sill, flow becomes supercritical, being accelerated by gravity as an overfall jet.

As mentioned above, the principle governing the prevention of channel erosion through bed sills or check-dams is to reduce the actual longitudinal channel slope S to a lower value S_{eq} (equilibrium slope) which should represent a dynamic equilibrium between bed scouring and aggradation. Different methods have been proposed for the evaluation of such an ultimate bed slope S_{eq} (Ferro, 2002). They can be grouped into empirical relationships (Ferrel, 1958; Heede, 1960; Woolhiser and Lenz, 1965; Falciai et al., 1977; Della Lucia and Fattorelli, 1981) and analytical approaches based on incipient motion criterion (Gessler, 1970; Ferro and Giordano, 1988; Julien and Wargadalam, 1995; Porto and Gessler, 1999; Gaudio et al., 2000). The equilibium slope is needed in order to evaluate the structure or drop height – without considering foundations – once the spacing L between the works is chosen (Gaudio et al., 2000):

$$a_1 = (S - S_{eq})L \tag{3.1}.$$

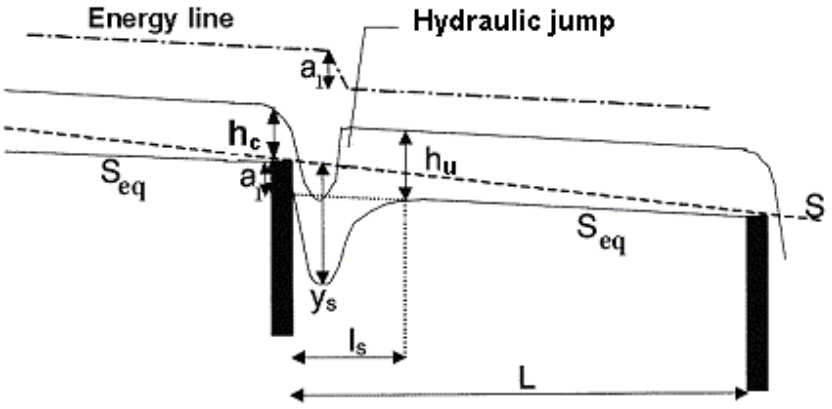

Figure 3.2 – Main geometrical and hydraulic variables involved in the analysis of the behaviour of grade-control structures. The spacing *L* is actually measured along the "equilibrium" bed profile.

Assuming at the equilibrium a steady and quasi-uniform flow along the staircase-like system (i.e. where the uniformity is at a macro-scale with flow specific energy equal at each sill), the product:

$$Z = SL \tag{3.2}$$

represents the stream potential energy which must be dissipated along the distance L between two sills. The height a_1 (hereafter called morphological jump as in Gaudio et al., 2000) is roughly the drop energy associated to the free jet impinging into the pool tailwater. Approximately, drop energy a_1 is locally dissipated in the scour hole whereas the remaining Z-a_1 potential energy is dissipated downstream as the water flows past the sloping bed (see energy line in Fig.3.2). If this regular bed span is long enough, the water-level slope attains the value S_{eq}, indicating that steady, uniform flow is then established. The passage between the complex hydrodynamics inside the scour hole and the uniform flow is rather smooth and a transition zone is observed where flow convergence occurs and the bed gradually reaches the downstream final slope (Fig. 3.3).

Figure 3.3 – Pool area at intermediate flows below a bed sill in the Maè River (Forno di Zoldo, Belluno, Italian Alps). It can be noted the "upwelling" due to the hydraulic jump's roller and the downstream transition zone before the "equilibrium" slope, at the left border of the picture.

Structure stability is heavily conditioned by the spacing L, because local scouring produced by the impinging nappe may lead to toe failure (Fig. 3.4). In practice, foundations size is generally assigned to equal the maximum scour depth y_s (Benini, 1990; Ferro, 2002). In fact, the gravity-accelerated jet (Figs. 3.5 - 3.8) – free or partially submerged depending on the drop characteristics – causes a scour hole which can be so deep as to undermine the foundations of the works, leading to collapse of the structure. A reliable prediction of the maximum scour depth is therefore needed to design safe foundations of control works, usually for flood events having return periods of around 50-100 years. In some cases (e.g. when the drop height is large), smaller secondary transversal structures (Fig. 3.7) and/or aprons (Fig. 3.8) are placed downstream of these works in order to limit scouring or to avoid it altogether, respectively. Technical guidelines for designing grade-control structures can be found in Goitom and Zeller (1989), Benini (1990), Mendrop and Little (1997), Biedenharn and Smith (1997) and Ferro (2002).

Figure 3.4 – Boulder bed sill in the Plima River (Val Martello, Bolzano, Italian Alps). Initially, the bed profile was level with the bed sill's crest. After few years the difference in elevation between the crest and the pool bottom has become as large as 4.1 m.

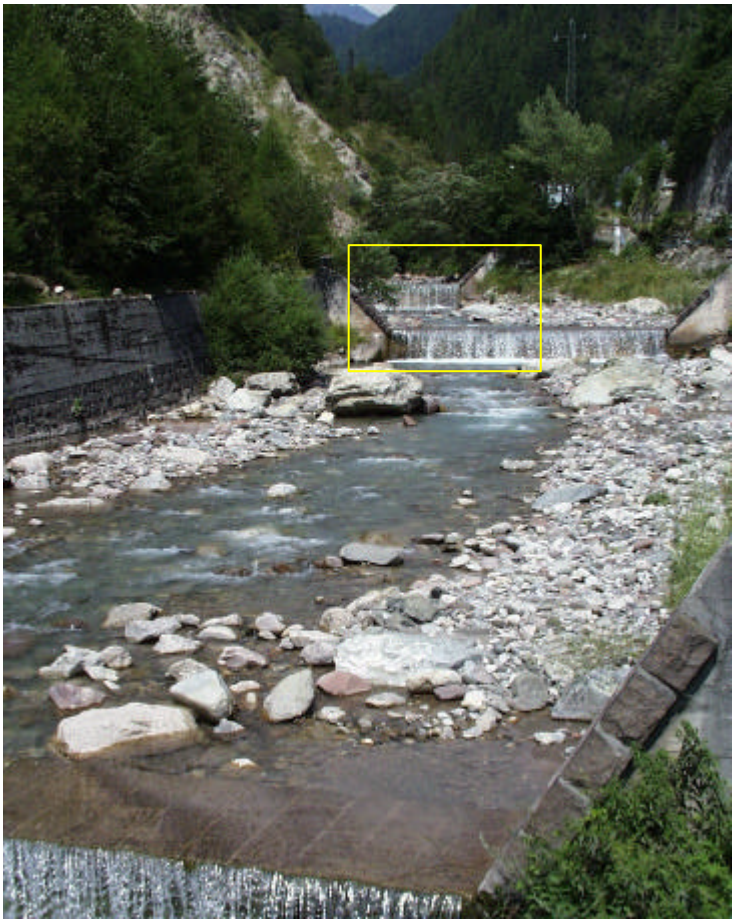

Figure 3.5 – Check-dams in the Biois River (Cencenighe Agordino, Belluno, Italian Alps): above, during summer's low flow; the area inside the frame is shown during the November 2002 flood (below).

Figure 3.6 – Side view of the falling nappe and the hydraulic jump below a check-dam in the Biois River (Cencenighe Agordino, Belluno, Italian Alps) during the November 2002 flood.

Figure 3.7 – At low flows, check-dam (right) and its subsidiary structure (left) in the Biois River (Cencenighe Agordino, Belluno, Italian Alps). A plunge pool is present between them.

Figure 3.8 – Tall check-dams with secondary structures at their toes (Cordevole River, Belluno, Italian Alps): above just after the completion of the works, below during the Novembre 2002 flood. Aprons composed of large boulders are present between the two structures, causing the jet to disintegrate without forming hydraulic jumps. Energy dissipation occurs via air resistance, as in ski-jump spillways.

3.2 Flow and scour at single drop structures

3.2.1 Jets and hydraulic jumps

The problem of local scouring downstream of drops is intimately tied up to jets' dynamical properties, because the falling nappe from a structure's crest represents a high-velocity current with massive erosive power that diffuses its momentum in a slower ambient, generating very intense turbulent fluctuations. This phenomenon can be viewed and studied either from the perspective of jet diffusion and/or considering it as a hydraulic jump, where the jet is a supercritical flow turning into subcritical conditions in the pool below.

During the last sixty years, many studies have been conducted to investigate the velocity field of jets, pressures and shear stresses developed along a surface being impinged by a jet (Fig. 3.9), and the mechanics of jet erosion. Different types of jets have been studied and include submerged and impinging jets, as well as circular and rectangular jets. In most cases, small-scale models were used for both hydrodynamic and scour dimensions measurements.

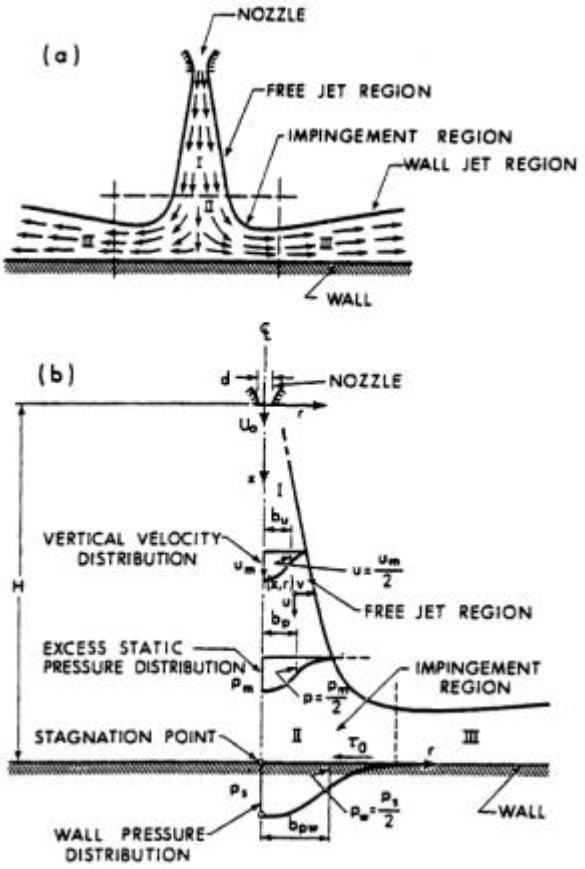

Figure 3.9 – Jet velocity and pressure distribution near a wall (after Beltaos and Rajaratnam, 1974).

For a comprehensive presentation of the abundant literature about hydrodynamic characteristics of air-surrounded and diffusing jets (impact velocity, air entrainment and concentration, jet disintegration, pressure distribution, velocity decay, etc..), see Breusers and Raudkivi (1991), Vischer and Hager (1995), Schleiss and Bollaert (2002). However, the main results relevant to scouring can be summarized as:

- impact velocity is directly proportional to the issuance velocity and to the square root of the drop height, but a corrective – reducing – factor accounting for aerodynamic drag should be used for large heights when disintegration occurs (Bohrer and Abt, 1996);
- jet centerline velocity decreases as the jet transfers energy to the surrounding fluid by shearing, and is inversely proportional to the square root of the diffusing distance and is directly proportional to the square root of jet original thickness (Kuroiwa, 1999);
- hydrodynamic pressures – and also their fluctuations – on a plate impinged by a jet diminish as the tailwater level increases (Lencastre, 1961; Fiorotto and Rinaldo, 1992) but only up to a certain depth (Ursino et al., 2003);
- the angle of impingement affects the velocity decay rate, this being faster when the angle is different from the vertical (Hom-ma, 1953);
- the energy loss occurring at a drop with fixed bottom and no tailwater is mainly due to mixing of the jet with the pool behind, correlates with the circulating discharge in the pool and is a function of the drop ratio, given by critical flow depth/drop height (Rajaratnam and Chamani, 1995).
- jet aeration reduces the available pressures at the bottom (Ervine et al., 1997) because its total energy is expanded into a larger area before impingement (Fig. 3.10); also, the air concentration of the jet at the tailwater surface influences the centerline velocity decay (Bohrer and Abt, 1996).

Recently, Vallé and Pasternak (2002) tested for the first time in the field the application of the Time Domain Reflectometry (TDR) to evaluate the air content in natural hydraulic jumps, where other laboratory techniques fail to work reliably.

A less explored yet very important aspect of jets released from drop structures is the type of hydraulic jump they generate downstream. After the early works on hydraulics of rectangular drops by Moore (1943) and Rand (1955), Little and Murphey (1982) had

described the transition between a direct jump (the so called B-jump) to an undular jump at low grade-control structures when the drop ratio z/h_c (drop height over critical flow depth) became approximately smaller than one.

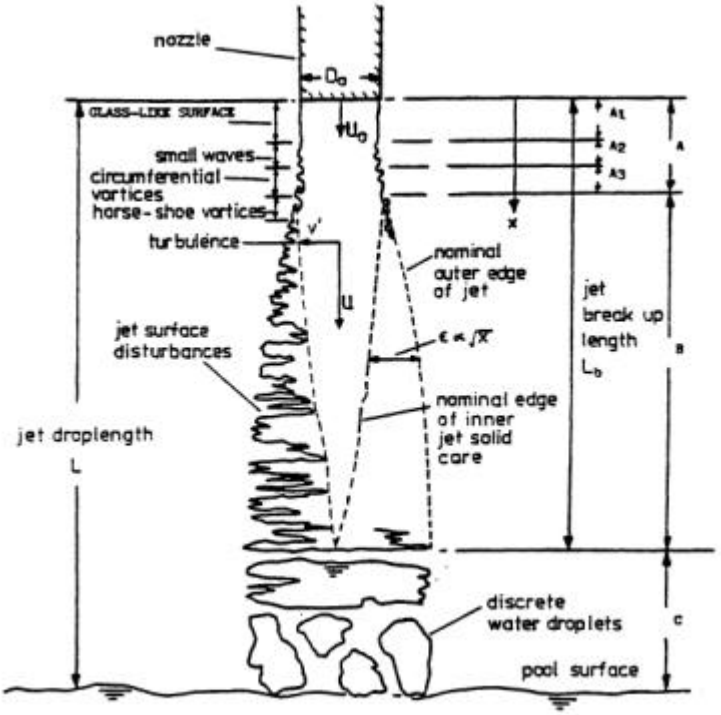

Figure 3.10 – Definition of zones in an impinging jet related to aeration effects (after Ervine et al., 1997).

Leutheusser and Birk (1991) and Ohtsu and Yasuda (1997) schematized different conditions that can occur below a weir, depending on the tailwater level. For low tailwater depths, a free hydraulic jump forms, where the jet impinges onto the bottom (B-min jump). An increase in the tailwater depth pushes the jump against the weir and the nappe plunges into the water cushion, the jump becoming submerged with the onset of strong vortexes with horizontal axis (B-jump). A further raise of the downstream level leads to the disappearance of the surface roller, the nappe stays on the surface forming standing waves, as in an undular jump.

Later, Wu and Rajaratnam (1996, 1998) defined two "jet regimes" below sharp- and broad-crested weirs based on flow patterns: the impinging jet and the surface flow regimes. In turn, the latter comprises three sub-regimes, named breaking wave, surface wave and surface jet, in order of increasing submergence conditions (Fig. 3.11). The approaching flow was always subcritical.

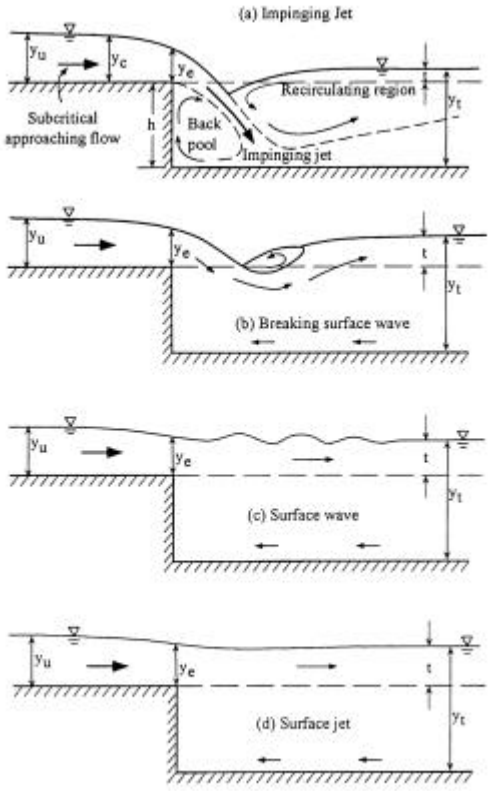

Figure 3.11 - The four jet (sub-) regimes at drops according to Wu and Rajaratnam (1998).

They introduced the parameter ?, defined as:

$$I = \frac{\sqrt{g(y_c - t)}}{q / y_t} \tag{3.3}$$

where the symbols are shown in Fig. 3.11. This parameter is proportional to the ratio between two characteristic velocities, namely the initial velocity of the surface flow (the upstream boundary) and the mean velocity in the downstream channel (the downstream boundary). The existence field of the two regimes resulted to be function of the drop ratio t/y_c and of the parameter ? (Fig. 3.12), but it was also noted a marked hysteresis effect depending on whether the tailwater level was being lowered or raised. These results indicate the important influence of downstream flow conditions, which are usually not taken into account for the transition between undular and classical hydraulic jump on a flat bottom (e.g., Chanson and Montes, 1995; Reinauer and Hager, 1995; Ohtsu et al., 2001).

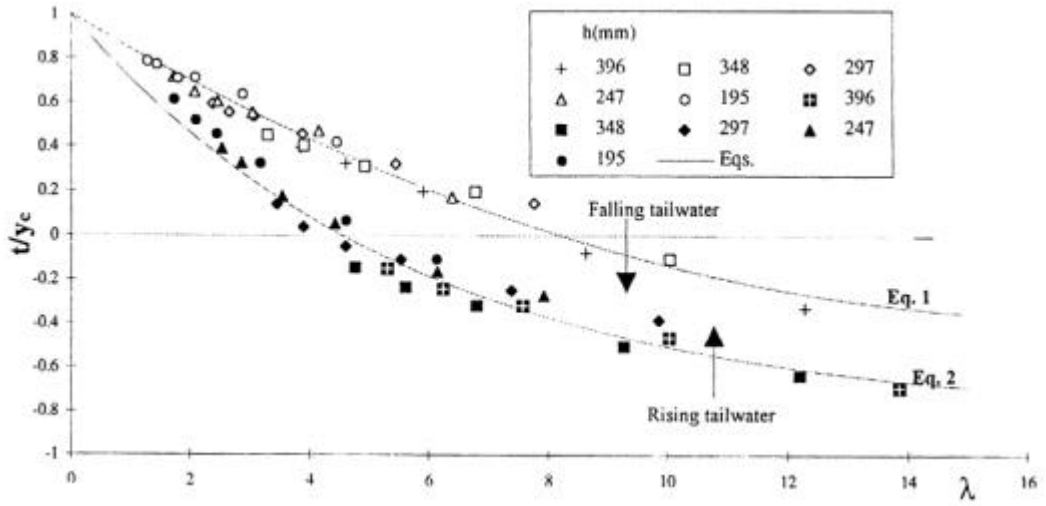

Figure 3.12 – Boundaries of impinging jet (below the lower curve) and surface flow (above the upper curve) regimes for drops. In between, a transition zone exists, where the regime depends on the initial tailwater state (after Wu and Rajaratnam, 1998).

.

Recently, more complex classifications of hydraulic jumps at drops have been proposed by other authors who studied supercritical approaching flows (Mossa et al., 2002; Ferreri and Nasello, 2002). However, to the writer's knowledge, no investigations have been so far performed on hydraulic jumps at drops in deformable beds.

3.2.2 Scour pool formation

Three distinct phases or zones can be observed when an impinging jet scours an erodible bed (Kuroiwa, 1999). At first (Zone 1), the jet is issued above the tailwater depth. Gravitational acceleration transforms potential into kinetic energy, and the jet impinges with a certain angle with respect to the vertical at a higher velocity than the initial, unless it disintegrates. This happen if the trajectory path is large in comparison to the disintegration length, which depends on unit discharge and turbulence level at issuance (McKeogh and Elsawy, 1980; Ervine et al., 1997). If the jet disintegrates, its velocity might be less than that at issuance. In the Zone 2, the jet dissipates energy after it impinges on the tailwater, and its velocity undergoes decay due to momentum transfer to the surrounding slower fluid. Therefore jet residual velocity hitting the bed depends on the length of this diffusion path. In Zone 3, if the residual power of the jet is sufficient to entrain and transport bed particles a scour hole forms. Because the forces available at the beginning on the bed surface are higher

than those acting afterwards when the scour depth increase lengthens the dissipating path in the tailwater, the temporal rate of scour decreases as time passes (Breusers and Raudkivi, 1991; Stein and Julien, 1994; Balachandar and Kells, 1997; Gaudio and Marion, 2003). However, jet diffusion inside the scour hole can be expected to be different from that occurring above in the tailwater cushion, where the flow is less restricted.

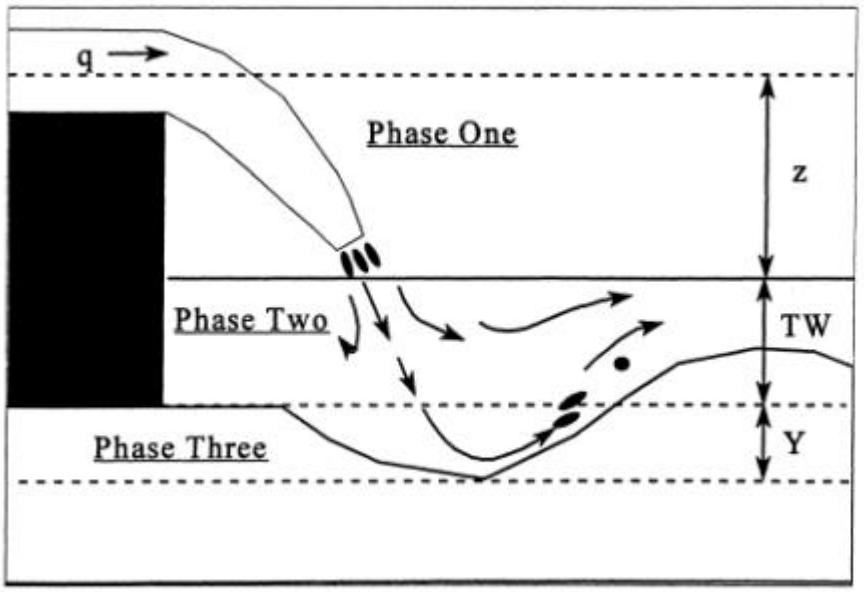

Figure 3.13 – The three zones or phases for an impinging jet scouring an erodible bed (after Kuroiwa, 1999); *z* is the drop height, *TW* is the tailwater depth, *Y* is the scour depth.

As the scour hole starts to form, deposition occurs downstream of it. Depending on the tailwater depth (D'Agostino, 1994; Kuroiwa, 1999), material will either deposit immediately downstream of the hole (relative deep tailwater) or will be carried away (shallow tailwater). In the first case, a typical mound or dune – analogous to a flow separation berm (Carling, 1995) – will buildup, whose presence strongly influences scouring processes and dimensions (D'Agostino, 1994). During the process of approaching the equilibrium dimensions, lighter (i.e. smaller) particles are transported away whilst heavier (i.e. coarser) remain at the bottom of the scour hole, determining armoring of its surface. If the downstream channel width is approximately the same as the width of the jet, downstream flow streamlines will be straight and no recirculation (i.e. backflows) will occur. If recirculation takes place, the scour hole will appear three-dimensional, with the presence of side slopes along with longitudinal ones, and the maximum scour depth will be smaller (D'Agostino, 1994). Side and longitudinal slopes' gradient and roughness will affect scouring by inducing different energy losses.

The typical flow pattern in a two-dimensional scour hole formed by an impinging jet is shown in Fig 3.14, with the expanding decelerating jet and the two horizontal counter-flowing rollers. Basically different is the pattern existing when surface regime establishes at the drop (Fig. 3.15).

Figure 3.14 – Flow pattern in a scour hole formed by an impinging jet.

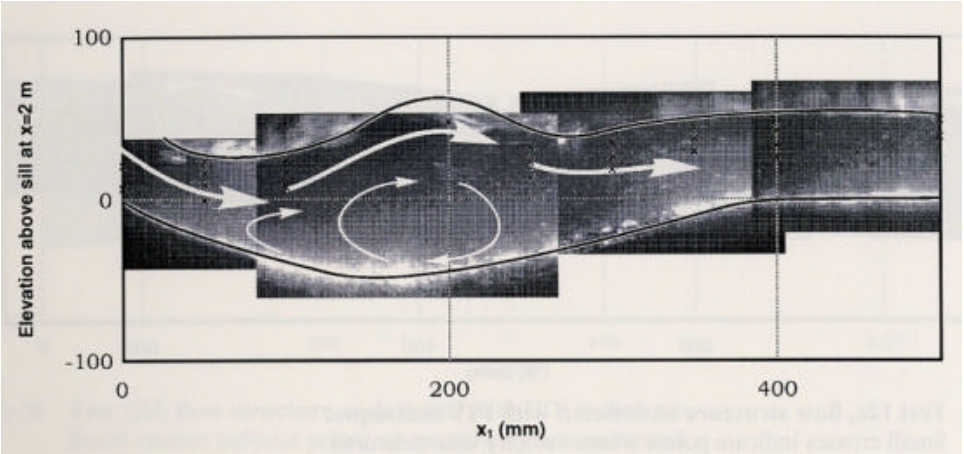

Figure 3.15 – Flow pattern in a scour hole formed in surface wave regime (after Gaudio and Marion, 2000)

Ideally, equilibrium dimensions of a scour hole can be studied and predicted from a strongly deterministic mechanical perspective. In fact, sediment particles will be entrained and then moved up from the downstream side of the scour hole as long as the hydrodynamic

moments applied overcome the resisting moments of the weight both parallel and perpendicular to the slope (Fig. 3.16).

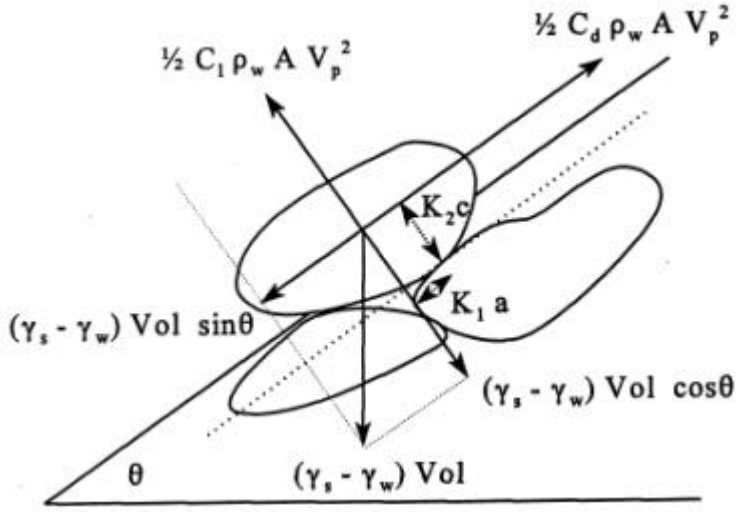

Figure 3.16 – Moments acting on a particle located on the downstream slope of the scour hole (after Kuroiwa, 1999).

Taking into account all the three zones described above, an equation to predict scour dimensions (i.e. maximum depth and length) must include terms which consider the jet travel in the air (acceleration, aerodynamic drag and jet aeration, impinging angle), the effect of energy dissipation in the tailwater depth (deceleration, turbulence generation, pressure fluctuations), and the resistance of the bed to jet scouring (sediment relative density, characteristic diameter, interlocking factor).

Since most of the phenomena and factors cited above are so closely linked to each other, some complications arise when attempting to generalize and simplify. For example, keeping fixed the other conditions, the higher the drop the deeper the scour, but only to a certain value when aeration and disintegration decelerate the jet (Ervine et al., 1997); or, the deeper the tailwater the smaller the scour depth, but only above a threshold under which an increase of tailwater level leads to deeper holes (Thomas, 1953; Hallmark, 1955; Lencastre, 1961; D'Agostino, 1994; Balachandar et al., 2000); or again, the more vertical the jet, the steeper the downstream side of the scour hole (Rajaratnam, 1981; Bormann and Julien, 1991) only up to a given jet angle (Kuroiwa, 1999, around 18 degrees to the vertical, corresponding to a scour slope of 26 degrees to the horizontal), and the deeper the scour hole (Mossa, 1998) but again up to a certain jet inclination only (Mirtskhulava et al., 1967, around 15 degrees to the vertical).

As to the characteristic sediment diameter, no general agreement has been reached yet. Given the armoring processes taking place in the scour hole, the majority of the authors use D_{90}, but in some cases D_{50} was chosen. Hallmark (1955) found that the material constituting the bottom surface of scour holes was approximately D_{85}. Kuroiwa (1999) reported median grain size at the bottom ranging from D_{77} to D_{85}, and selected D_{85} to be used in his maximum scour depth equation. Therefore the effect of sediment gradation has been so far reduced to the selection of a coarse armoring size, neglecting other possible effects on scour shape and dimensions. Only Ghodsian and Faradonbeh (2001) proposed a formula taking explicitly into consideration the degree of sorting of the mixture.

3.2.3 Models predicting scour dimensions at equilibrium

The complexity of factors and the highly turbulent hydrodynamics determining scour dimensions have inhibited for long time analytical approaches for the derivation of predictive formulae. Numerical modeling of local scouring processes is far from being robust and reliable, and laboratory experiments and – very few – field data have been and are still mostly used for its investigation. The great majority of equations regard the maximum depth of scour, given its obvious relevance for structures stability (Breusers and Raudkivi, 1991; Hoffmans and Verheij, 1997). Only few investigations have addressed scour length too, and commonly this has been expressed simply as a multiple of scour depth, thus acknowledging the self-similaraty of scour profiles.

Historically, different types of predictive equations have been developed for single drop structures. Here only a general summary will be presented, since they will not be addressed in the present research.

The first category of equations can be named empirical formulae, where variables are not organized in non-dimensional groups. Most variables are defined as in Fig. 3.17. The most common general form of these equations can be generalized as:

$$s + h = a \frac{H^a q^b h^g}{D_x^{\ l}} \qquad (3.4),$$

where s = maximum scour depth (m), h = tailwater depth (m), H = drop height (m), q = unit water discharge (m^2s^{-1}) and D = characteristic – of percentile x - sediment size (m); coefficient a and exponents a, ß, γ, λ are to be determined empirically.

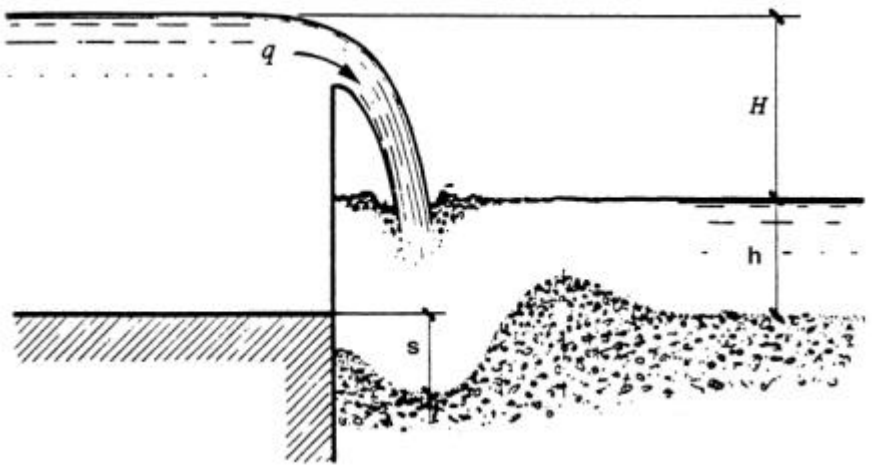

Figure 3.17 – Defining sketch for local scouring below a single drop structure (after Breuesers and Raudkivi, 1991)

The following wide ranges have been reported by the different authors: a = 3.27-12.4, α = 0.05-0.5; β = 0.54-0.64, γ = 0-0.15, λ = 0.10-0.42. Examples of these formula are numerous (among others, Schoklitsch, 1932; Veronese, 1937; Jaeger, 1939; Eggenberger and Müller, 1944; see also Breusers and Raudkivi, 1991). Very similar are Falciai and Giacomin's (1978) – derived from field data – and Mason e Arumugam's (1985) formulae which do not contain the tailwater depth at the left side of the equation. A different type (Bisaz and Tschopp, 1972) of dimensional equation was used by D'Agostino (1994), who introduced a factor accounting for three-dimensional jet geometry and obtained:

$$s = (0.7K_r + 0.58)(0.94q^{2/3} - 1.6D_{90}) \qquad (3.5),$$

where K_r is the ratio between crest width and downstream channel width.

A second group of equations can be identified as semi-empirical, because they derive from a dimensional analysis carried out by applying the Buckingham's Pi-Theorem to the variables involved in the phenomenon. Non-dimensional groups are thus obtained, and then experiments follow to allow the determination of coefficients and exponents of the dimensionless expression.

For example, D'Agostino (1996), for scour length defined as the distance L_b between the weir and the mound crest, obtained the following equation neglecting sediment size:

$$\frac{L_b}{z} = 8.4\left(\frac{h_c}{z}\right) + 0.55 \qquad (3.6),$$

where z is the elevation difference between the weir crest and the bed downstream, and h_c is the critical flow depth.

Kuroiwa (1999), studying scours by rectangular jets, proposed the following dimensionless relationship, where the scour depth s is function of Froude number of the jet at the impingement, Fr, of the dimensionless diffusion path in the tailwater, of the dimensionless particle fall velocity, and of the interlocking factor of particles on the downstream slope of the scour hole, IF:

$$\frac{s}{h_c} = f\left(Fr, \frac{h/\cos d}{h_1}, \frac{w}{\sqrt{gh_1}}, IF\right) \qquad (3.7)$$

with h_c = critical flow depth Fr = Froude number of the jet at the impingement, h_1 = jet thickness at the impingement, h = tailwater depth, d = jet inclination at the impingement, w = particle fall velocity.

Another type of function has been proposed by Ghodsian and Faradonbeh (2001) and by Ghodsian and Najafi (2003) for scour depth due to impinging rectangular and circular jets respectively:

$$\frac{s}{z} = f\left(Fr_d, \frac{h}{d}, \frac{z}{d}\right) \qquad (3.8)$$

where z = drop height, h = tailwater depth, d = outflow jet thickness, and Fr_d is the densimetric Froude number (V = outflow initial velocity, g = acceleration due to gravity, r_s = sediment density, r = water density) given by:

$$Fr_d = \frac{V}{\sqrt{gD_{50}\left(\frac{r_s - r}{r}\right)}} \qquad (3.9).$$

Ghodsian and Faradonbeh (2001) evaluated also the armoring effect deriving from sediment gradation, and incorporated a scour-reducing parameter in Eq. 3.8.

Some attempts to derive scour dimension formulae by a purely analytical approach have also been made, thus these equations should be grouped into a third category. Stein and Julien (1994), extending and modifying the analysis based on jet diffusion and incipient motion by Bormann and Julien (1991), developed the following equation for the equilibrium scour depth *s* below overfalls:

$$s = \frac{C_d{}^2 C_f \, r V_1{}^2 h_1}{t_c} \sin c \qquad (3.10),$$

where C_d = diffusion coefficient, C_f = friction coefficient, r = water density, V_1= jet velocity at the impingement, h_1 = jet thickness at the impingement, t_c = critical shear stress for the sediment, c = jet inclination with respect to the horizontal at the impingement.

Hoffman (1998) applied Newton's second law of motion and derived:

$$s + h = C_{2v} \sqrt{\frac{q V_1 \sin(90 - d)}{g}} \qquad (3.11),$$

where the new symbol C_{2v} is a coefficient constant and equal to 2.9 for D_{90} < 0.0125 m, whereas for coarser sediment is a function of the D_{90}.

Chen and Hong (2001) presented a complex geometrical analysis of the shape of scour holes formed below check-dams that provided equations for scour dimensions and volume, then validated by experimental tests with uniform and graded sediment.

Finally, Jia et al. (2001) simulated computationally the scouring process in a plunge pool with uniform bed material due to a two-dimensional plane impinging jet. A finite-element-based unsteady three-dimensional model with k-epsilon turbulence closure was employed to solve the flow field. The Authors considered the effects of both shear stress and lift force on sediment particles due to pressure fluctuations. The latter was taken into account by using empirical relationships. Both of these effects were incorporated in a non-equilibrium sediment transport model consisting of sediment pickup rate and step length adopted for the jet scour problem.

3.3 Flow and scour at sequences of drop structures

3.3.1 Fixed-bottom drop sequences: stepped spillways

Given the relevance for dams' safety, much attention has been devoted to study the dissipation effect of stepped spillways, which constitute a rigid boundary analogy to sequences of grade-control structures in alluvial (i.e. deformable) channels. In a stepped spillway, the spillway face is provided with a series of steps, from near the crest to the toe. The energy dissipation caused by the steps reduces the size of the dissipator, generally present at the toe of the spillway. Most of the following description of stepped channels hydraulics comes from Dr. H. Chanson's website (http://www.uq.edu.au/~e2hchans/index.html).

Stepped channels may be characterized by two types of flow: nappe flow and skimming flow (Fig. 3.18). At low flow rates and for relatively large step height, the water bounces from one step onto another as a succession of free-falling nappes (i.e. nappe flow). Dominant flow features include, at each drop, an enclosed air cavity, a free-falling jet and nappe impact on the downstream step. Most energy dissipation takes place by nappe impact and in the downstream hydraulic jump At larger flow rates, the flow skims over the step edges with formation of re-circulating vortices between the main stream and the step corners. Most energy is dissipated in maintaining the recirculation in the step cavities. The transition between nappe and skimming flow is related to the flow rate, chute slope, step geometry and local flow properties at each step.

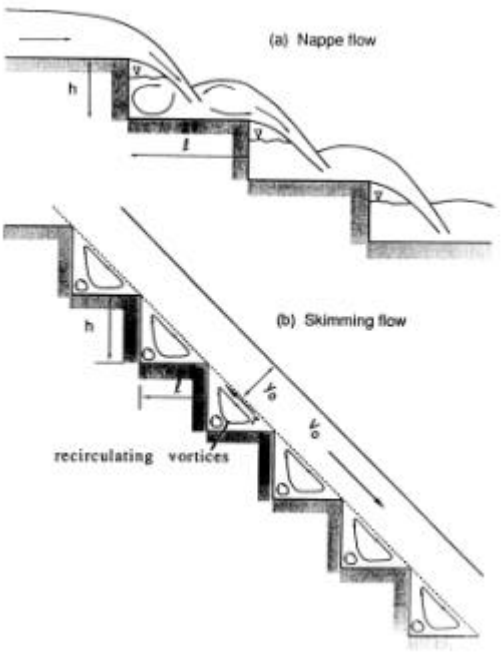

Figure 3.18 – Sketch of nappe and skimming flow on a stepped channel (after Rajaratnam, 1990).

In the nappe regime, the flow at each step consists of the free-falling nappe, nappe impact followed by a fully-developed hydraulic jump (NA1 type). The kinetic energy of the flow is dissipated at nappe impact and in the hydraulic jump, and the head loss at each step equals the step height. This flow pattern occurs for (Chanson, 1994):

$$\frac{h_c}{h} < 0.09 \left(\frac{h}{l} \right)^{-1/3} \tag{3.12}$$

with h_c = critical flow depth, h = step height, l = step distance (Fig. 3.18).

For a given chute geometry, the drop length of the nappe increases with increasing flow rate and the hydraulic jump flow interferes with the downstream overfall (nappe flow with partially-developed hydraulic jump, NA2). A nappe flow without hydraulic jump might occur also for relatively large discharges before the apparition of skimming flow. Three-dimensional flow patterns in a nappe flow without hydraulic jump (NA3) has also been described At each step the nappe impact induces significant water splashing and jet deflection, followed by the propagation of oblique shock waves (i.e. cross-waves) intersecting further downstream on the channel centreline. More sidewall standing waves are observed at the impact of the nappe along the sidewalls. The maximum height of the wall standing waves might be as large as the step height. The flow properties of nappe flow regimes NA2 and NA3 are not well understood yet.

The transition between nappe and skimming flow is related to the flow rate, chute slope, step geometry and local flow properties at each step. In uniform equilibrium flows down prismatic rectangular channels, a limiting condition for skimming flow is (Chanson, web site cited above):

$$\frac{h_c}{h} = 1.1 - 0.4 \frac{h}{l} \tag{3.13}.$$

Equation (3.13) is limited to flat horizontal steps for h/l ranging from 0.2 to 1.4, it characterizes the onset of skimming flow for uniform or quasi-uniform equilibrium flows and its accuracy is within +/- 30%. For more details about stepped spillways, see Chanson (1995_a), and for interesting results on their energy dissipation efficiency see Chamani and Rajaratnam (1994) and Vischer and Hager (1995). However, it must be pointed out that no systematic study has been conducted with pooled steps, inclined steps or non-rectangular cross-section channels. Therefore the application of Eqs. 3.12-3.13 (e.g. in Chanson, 1996) to step pool systems cannot be made reliably.

3.3.2 Pool formation, tumbling flow and flow instability

Let's consider a sloping alluvial channel where new transversal grade-control structures are placed, and where a water discharge capable of eroding the bed happens to flow some time after the completion of the works. Ideally, local scour initial formation will differ depending on the initial geometry, i.e. whether structures are check-dams or bed sills. In fact, in the case of check-dams a certain considerable drop height already exists at the time of the eroding flow occurrence, whereas if bed sills are concerned a step is not present or is very small (Fig. 3.1), and its formation is required first in order to have a jet causing local scouring at the structure's toe . For the formation of such a drop, the bed slope must become lower than the initial value (Fig. 3.2, Eq. 3.1), thus implying that bed stability conditions for a certain flow and bedload rate must be different from the initial ones, otherwise – only virtually – no scour would occur downstream of a bed sill. Below check-dams, a scour hole will definitely form because of the initial drop, and only subsequently the bed slope changes will affect its height. In practice the flow field disturbed by the presence of a bed sill will likely lead to the formation of a localized erosion anyway, except for aggrading conditions.

Two bed evolutionary process occurring simultaneously can be analyzed separately: one is the general bed slope adjustment between two structures – depending on the relationship among sediment characteristics, water discharge and incoming bedload rate – whereas the second refers to local scouring phenomena immediately downstream of each work. The first gives rise to the rotation of the bed profile between two transversal works, where each downstream structure acts as a pivoting point. The determination of the equilibrium or ultimate slope (see also section 3.1) presents many uncertainties, but such a topic will be not addressed here for sake of brevity. The reader can found up-to-date analysis and discussions in Mussetter (1982), Martin Vide et al. (1998), Martin-Vide and Bateman (1999), Porto and Gessler (1999), Bateman et al. (2000), Ferro (2002, pp. 293-315). It is worth to mention, however, that Martin-Vide and Andreatta (2003) found equilibrium slopes between sills considerably milder than the correspondent ones without sills, and the shorter the spacing the greater the slope reduction.

As to the local bed evolution induced by a drop structure, the case of check-dams (i.e. large drop heights) is easier because from the beginning of the erosive process an oblique impinging jet scours the bed. Instead for bed sills level with the bed the evolutionary complexity is much greater, mainly due to the transition over time between different type of hydraulic jumps/jet regimes.

Bateman et al. (2000) described in detail the different phases characterizing scouring development at bed sills (Fig. 3.19).

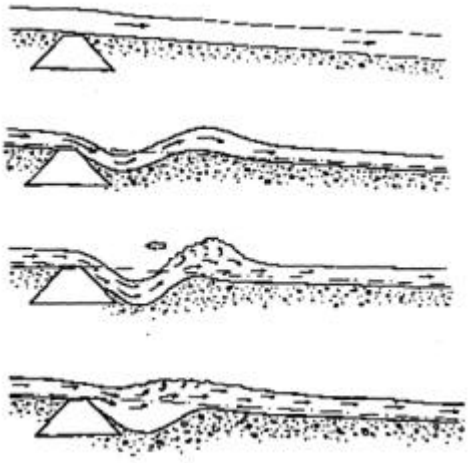

Figure 3.19 – Different phases during scour formation below bed sills starting from a level bed (after Bateman et al., 2000, modified).

At the beginning of the process, a standing wave establishes when acceleration is experienced by the flow at sill crest as soon as a difference in elevation appears. The jet shapes the bed scouring a trough and depositing a mound downstream, below the wave crest. The mound grows up until the wave breaks when its characteristics achieve the critical threshold for wave stability (Fig. 3.20).

Figure 3.20 – First stages of scour formation: on the left the standing wave has just formed, on the right the mound has become higher and the wave is close to breaking; the flow is from right to left, and no recirculation vortex is present yet, as in a surface jet regime (Padova tests, this research).

According to Bateman et al. (2000), this stage is the most effective as to the erosive action. After the breaking wave stage onsets, the scouring action decreases and eventually the roller is pushed upstream towards the sill, drowning the hydraulic jump and thus altering the flow pattern inside the scour hole (Fig. 3.21a). Scouring proceeds, but at slower pace due to the higher energy dissipation due to turbulent mixing.

However, in some cases a flow instability is observed (Fig. 3.21), characterized by a regular periodical shift between a standing wave (surface wave regime) and a drowned roller (impinging jet regime). Bateman et al. (2000) attributed this phenomenon to the propagation of a small sediment accumulation in the scour hole, noted also by Gaudio and Marion (2003). However, purely hydrodynamic cyclic instabilities in hydraulic jumps are known as well (Mossa, 1999).

Figure 3.21 – Equilibrium stages of scour formation: on the left (a), a submerged hydraulic jump is present, as in the impinging jet regime; on the right (b), the cyclic appearance of a standing wave as in the surface wave regime with an analogous superficial fast current (Padova tests, this research).

A detailed study on the temporal evolution of scour holes at bed sills has been carried out by Gaudio and Marion (2003). Scour formation showed to develop rapidly and conditions close to equilibrium were achieved in a short time. The introduction of a morphological time permitted the non-dimensional description of the development of scour depth over time through a unique exponential decreasing curve for different sediment and flow conditions. In this curve a short- and a long-term local scour regions were differentiated.

Once pools are scoured below the structures, a regular pattern of supercritical-subcritical flow transition forms, analogous to the so-called tumbling flow in natural step pool systems (see section 2). In the case of sequences of grade-control structures, the assigned spacing between the works will give more or less hydrodynamic and energetic relevance to

such an analogy. In fact, if the distance between two drop structures is large enough – as is usually the case for relatively low gradients – a fairly long stretch of the stream bed will achieve an equilibrium slope ideally presenting uniform flow conditions, generally subcritical to critical, rarely supercritical (see Introduction). However, in steep streams short spacings are usually assigned, so that the next drop structure locates just at the end of the upstream pool, thus making the profile very similar to a natural step pool sequence with a typical tumbling flow pattern.

Two types of tumbling flow have been reported by Whittaker (1987_a). He carried out several flume tests to study the formation of pools below steps, and observed that the "(…) the scour hole develops as flow rate increases (for a given slope) only up to a certain point. After this the downstream step begins to limit the scour development, distorting the scour process. As flow rate is increased beyond this point, the flow attains an instability limit and slug waves form." Whittaker called this regime unstable tumbling flow, to differentiate it from the stable tumbling flow occurring before the instability is reached (Fig. 3.22). The same pool deformation process was previously described by Volkart (1972). Whittaker also noted that in natural channels this unstable flow has not been observed yet, because "(..) scour holes between steps in step pool systems rarely become so large in extent that the scour process is distorted by the next step downstream."

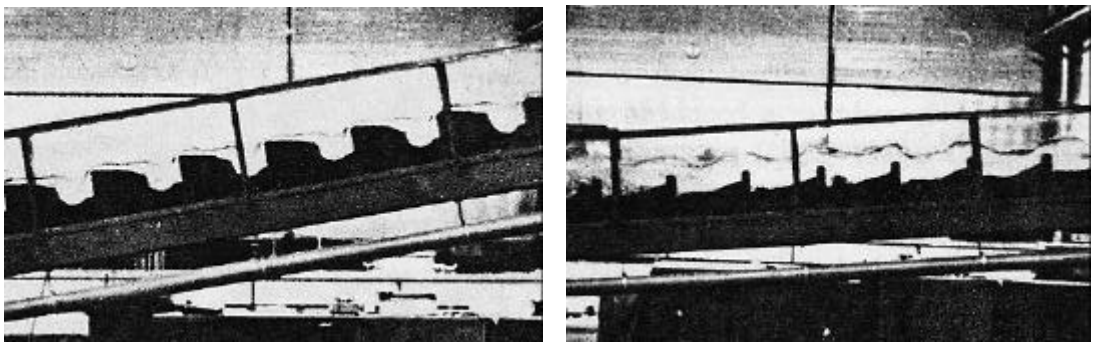

Figure 3.22 – Stable (left) and unstable (right) tumbling flow (after Whittaker, 1987_a, modif.).

In a previous paper (Whittaker and Davies, 1982) Whittaker had also shown and discussed the formation of water and sediment unsteadiness in similar experiments on tumbling flow characteristics. He reported the occurrence of roll waves, attributing their formation when "(…) the discharge coefficient for flow over a baffle increased due to the water surface in the pool upstream of the baffle rising beyond a certain level. This increase in discharge resulted in washing out of the hydraulic jump immediately upstream of the baffle into the pool downstream. The water level in the upstream pool thus fell, while that in the

inundated pool rose. The same process subsequently occurred with greater amplitude at the next baffle downstream(…).” Again, he highlighted that roll waves have never been observed in natural step pool channels, arguing that the irregularity of natural steps might damp out these waves, preventing their amplification.

Recently, field evidences of instability phenomena both in a natural step pool stream and in a mountain river trained with check-dams have instead been reported and subsequently investigated in the laboratory (Ganz, 2003; Ganz and Schöberl, 2003). Wave properties and flow stability fields have been determined, even though the exact nature of these wave trains is not totally clear yet. Finally, some preliminary results about velocity profiles and bed profiles in scour holes for different sill spacings can be found in Wu et al. (2002).

3.3.3 Models predicting scour dimensions at equilibrium

To the writer’s knowledge, the work by Volkart (1972) and Volkart et al. (1973) represent the first investigations providing a formula for scour dimensions at bed sills forming a sequence in a sloping channel. After a dimensional analysis and several clear-water flume tests, the equation for the maximum scour depth y_s with reference to the sill crest – corresponding to the initial bed level – was proposed as (Volkart, 1972):

$$y_s = 1.25 \frac{q^{1/2} S^{1/2} L^{2/3}}{D_{90}^{5/12}} \frac{g_w}{g_s g^{1/4}} \qquad (3.14),$$

where q = unit water discharge, S = initial slope, L = sill spacing, D_{90} = grain size for which 90% of the sediments are finer, γ_w = specific weight of water, γ_s = specific weight of sediment, g = acceleration due to gravity. The slope range was $0.0075 < S < 0.07$.

As already mentioned, Whittaker (1987_a) performed laboratory runs in order to study flow characteristics and scouring below fixed steps. He investigated three initial slopes, 0.098, 0.172 and 0.248, using three different quasi-uniform gravelly mixtures (D_{90} = 0.0049, 0.0055 and 0.012 m). For the maximum scour depth with clear-water and a stable tumbling flow, he considered the residual value s defined as in Fig. 3.23, and obtained:

$$s = 0.9121 \frac{(q - q_{cr})^{0.4526} h^{0.5877}}{D_{90}^{0.2666}} \quad (3.15),$$

with, beside the usual symbols, q_{cr}= incipient motion specific discharge (m^2s^{-1}) and h = drop height (m, Fig. 3.23). For the water depth at the point of maximum scour, the equation reads:

$$s_0 = 1.4115 \frac{(q - q_{cr})^{0.5034} h^{0.476}}{D_{90}^{0.2311}} \quad (3.16),$$

or, in dimensionless terms, as:

$$\frac{s_0}{l_2} = 0.3404 S^{0.7} \left(\frac{L}{D_{90}} \right)^{0.399} \quad (3.17),$$

where l_s is the scour length. Finally, for the scour area A', the empiric formula is:

$$A' = 2.385 \frac{(q - q_{cr})^{1.1552} h^{0.618}}{D_{90}^{0.3508}} \quad (3.18)$$

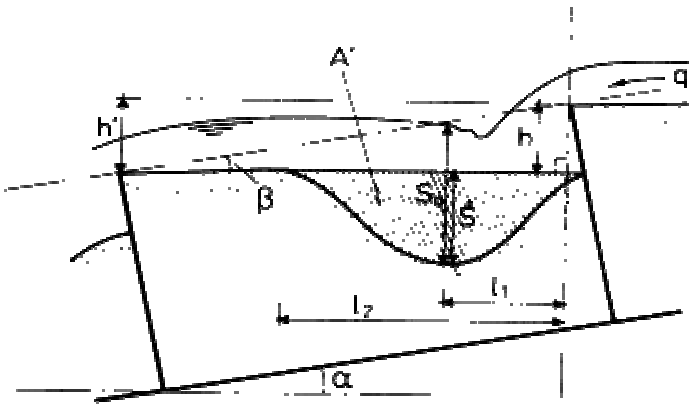

Figure 3.23 – Definition sketch of variables in Eqs. 3.15 – 3.18 (after Whittaker, 1987_a).

Whittaker (1987_a) presented also the first evaluation of the reducing effect brought about by a certain bed load rate, q_s, coming from upstream; this time, he considered the scour depth with reference to the sill crest, y_s. The ratio between the maximum scour depth for live-bed conditions ($y_{s\,qs}$) and the correspondent clear-water case (y_s) is given by:

$$\frac{y_{sq_s}}{y_s} = \ln\left(\frac{0.8662 S^{0.1097} q^{0.2164}}{D_{90}^{0.0579} q_s^{0.1778}}\right) \qquad (3.19).$$

More recently (Gaudio et al., 2000) the problem of local scouring at bed sills has been actively investigated for lower gradient channels ($S < 0.015$) and large sill spacings. A new dimensionless approach has been used. Considering the system sketch in Fig. 3.24, the function for the maximum clear-water, long-term scour depth has been written as:

$$y_s = f(g, \nu, \rho_w, \rho_s', q, h_u, D, a_1) \qquad (3.20)$$

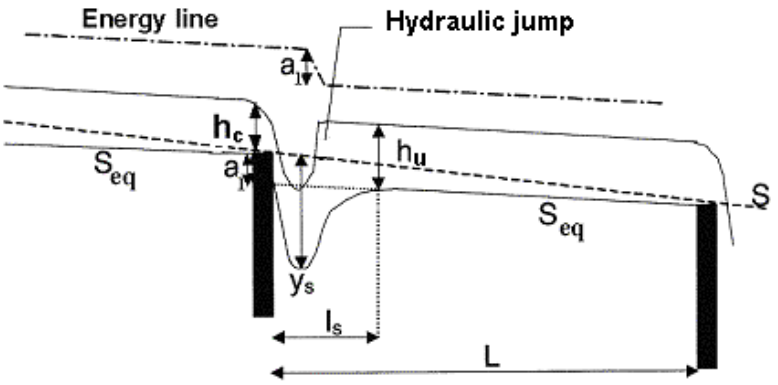

Figure 3.24 – Definition sketch for the model proposed by Gaudio et al. (2000) and Ferro (2002).

where g is the gravity acceleration, ν is the kinematic viscosity of water, r_w is the density of water, r_s' is the submerged density of sediments, q is the water discharge per unit width, h_u is the water depth of uniform flow condition, D is a characteristic grain size and a_1 is the "morphological jump", defined as:

$$a_1 = (S - S_{eq})L \qquad (3.21)$$

where S is the initial longitudinal bed slope, S_{eq} is the equilibrium bed slope and L is the distance between sills. According to Gaudio et al. (2000), the equilibrium slope for clear-water can be addressed by the Shields' condition for threshold of motion for fully developed turbulent flows:

$$q_c = \frac{h_u S_{eq}}{\Delta D} = \text{constant} \tag{3.22}$$

where q_c is the critical dimensionless shear stress and $\Delta=\rho_s'/\rho_w$ is the relative submerged density of sediments. Therefore:

$$S_{eq} = \frac{\theta_c \Delta D}{h_u} \tag{3.23}.$$

Coupling Eq. (3.23) and a resistance formula like the Manning's equation for wide channels (with *n* roughness coefficient):

$$q = \frac{h_u^{5/3} S_{eq}^{1/2}}{n} \tag{3.24},$$

the uniform flow depth and the equilibrium slope can be expressed as:

$$h_u = \frac{(nq)^{6/7}}{(\theta_c \Delta D)^{3/7}} \tag{3.25}$$

$$S_{eq} = \frac{(\theta_c \Delta D)^{10/7}}{(nq)^{6/7}} \tag{3.26}$$

Eq. (3.25) expresses the dependence of the uniform flow depth from other physical parameters. This allows h_u to be dropped from Eq. (3.20).

Introducing the critical specific energy on the sills:

$$H_s = 1.5 \cdot \sqrt[3]{q^2/g} \tag{3.27},$$

the application of the Buckingham's Π theorem to Eq. (3.20) without h_u and choosing g, r_w and q as fundamental variables led to:

$$\frac{y_s}{H_s} = \Phi\left[\frac{q}{n}, \Delta, \frac{H_s}{\Delta D}, \frac{a_1}{H_s}\right] \tag{3.28}$$

Neglecting the influence of viscosity for fully turbulent flows and assuming that the relative submerged density of the sediment is constant, Eq. (3.28) has been simplified as follows:

$$\frac{y_s}{H_s} = \Phi\left[\frac{a_1}{H_s}, \frac{H_s}{\Delta D}\right] \tag{3.29}$$

It can be observed that the first parameter represents the ratio between the energy loss associated with the drop and the flow energy on the sill, whilst the second is the ratio between the flow energy on the sill and a term proportional to the mobility of the bed particles.

Marion et al. (1998) – also in Gaudio et al. (2000) – and Gaudio and Marion (2003) tested different slopes ranging from 0.0062 to 0.0160, distances between the sills L from 2 to 6.5 m, two uniform gravel gradings (D_{50} = 4.1 mm and 8.5 mm) and a uniform coarse sand distribution (D_{50}=1.8 mm). The formation of a small step (named a_2, not shown in Fig. 3.24) in front of each sill was also observed. It was related to the subcritical regime through the Froude number Fr, as follows:

$$a_2 = h_u - h_c = h_u(1 - Fr^{2/3}) \tag{3.30}$$

The step a_2 was shown to be a quantity dependent from the variables listed in Eq. (3.20), and therefore it was not added to that equation.

It appeared that in all low-gradient tests the parameter product of the two groups in Eq.(3.29) affected the results only. The overall regression formulae presented by Gaudio and Marion (2003) is the following:

$$\frac{y_s}{H_s} = 0.180\frac{a_1}{\Delta D_{50}} + 0.369 \tag{3.31},$$

which covers the range $1.3 \leq a_1/(\Delta D_{50}) \leq 9.1$, with a correlation coefficient R=0.94.

Similarly, adopting the same dimensional analysis for the scour length l_s, the authors obtained the following empirical relation (valid only for the gravel sediment tests, Gaudio et al., 2000):

$$\frac{l_s}{H_s} = 1.87\frac{a_1}{\Delta D_{50}} + 4.02 \tag{3.32}$$

As in other studies (e.g. Whittaker, 1987_a), scour holes' dimensionless profiles were found to be self-affine, with the maximum scour depth occurring at a distance of 0.3 to 0.4 times the scour length l_s from the sill. In all these tests the scour length was never long enough to be constrained by the following sill, and uniform flow conditions along the equilibrium slope were always present downstream of scour holes.

Ferro (2002) published a different formulation starting from the following functional relationship:

$$y_s = f(H_s, Q, g, r_w, r_s, L, B, D_{50}, a_1) \tag{3.33}$$

where, as new symbols, Q = water discharge and B = channel width.

Using a_1, Q and ρ_w as independent variables, he obtained the following dimensionless relationship:

$$\frac{y_s}{a_1} = \Phi\left(\frac{H_s}{B}, A_{50}, \frac{L}{a_1}\right) \tag{3.34}$$

with the non-dimensional group A_{50} given by:

$$A_{50} = \frac{Q}{Ba_1\left[gD_{50}\left(\frac{r_s - r}{r}\right)\right]^{1/2}} \tag{3.35}.$$

After a regression analysis with flume data found in the literature, the equation for the maximum scour depth becomes:

$$\frac{y_s}{a_1} = 0.3298\left(\frac{H_s}{B}\right)^{0.3247} A_{50}^{\;0.3684}\left(\frac{L}{a_1}\right)^{0.2491} \tag{3.36}.$$

4. FLUME EXPERIMENTS

Dynamics and dimensions of local scouring in step pool systems can be studied in a flume inserting vertical channel-wide boards into a granular bed at the desired spacings and allow a certain water discharge and a given sediment rate to flow onto the bed. If the initial slope is too high for being in equilibrium with the water-sediment rates, soon the upper part of the boards will protrude from the bed because the bed profile will rotate pivoting at the downstream boundary constrain, which is the downstream sill (i.e. board) elevation (Fig. 3.24). A difference in elevation – a drop – will be therefore established between the sill and the downstream bed, thus making the flow accelerating for the increased local energy gradient at the sill lip and eventually causing the flow to become supercritical ($Fr>1$).

This falling nappe behaves as a turbulent jet which has more energy than the flow elsewhere along the bed slope, and this power excess leads to the formation of a scour hole shaped by jet diffusion turbulent stresses. In the pool so formed, jet excess energy can be dissipated by the hydraulic jump there present, and downstream of it the bed slope becomes affected only by the shear stress of the "linear" flow – which in the flume can be regarded as practically uniform – provided that enough distance from the next sill is available. If it is not the case, the hydraulic jump region stretches over the entire span between two baffles, causing the formation of the peculiar tumbling flow regime featured most commonly by natural step pool sequences.

This kind of experiments represents both a model of bed adjustments occurring in a sequence of grade-control structures and a simulation of what happens when some steps are immobile on an otherwise mobile bed. This latter situation can be found either when steps are immobile under all flow conditions (i.e. very large boulders fallen into the stream from the hillslopes, bedrock outcrops, very resistant large woody debris jams) or only below a certain stage, for example when an high-magnitude, low-frequency flood flow is no longer able to transport coarse elements but still has the competence to erode sediment from the bed, as during the falling limb of the hydrograph, or during small events whose peak discharge cannot mobilize steps but can cause scouring in the pools.

As mentioned in section 3.3.2, the fact that tests' initial configuration is a plane bed does not limit the applicability of the results only to a sequence of bed sills or to a plane bed state in a natural stream: check-dams and an already-present natural stepped profile can be modeled in such a way, if the ultimate bed profile is to be investigated. In fact, given a certain set of the independent variables (i.e. gradient between the baffles, water discharge, sediment

discharge, sediment characteristics) the equilibrium (i.e. long-term) state of the system should be independent of the initial one, at least to a remarkable extent acknowledging that random disturbances might alter local bed elevation. In particular, the equilibrium slope between two steps must be the same both for protruding (i.e. check-dams) and non-protruding (i.e. bed sills) structures. Consequently, according to Eq. 3.1, the same drop height will be achieved, and therefore the same scour hole dimensions will be reached at the equilibrium, so that the system will have lost "memory" of its origin. However, if the development over time of the scouring process is to be analyzed, then major differences would be encountered starting from different initial states such as different check-dam heights, since in this case the whole "history" of the system matters.

The rationale behind the analysis of equilibrium profiles only is twofold: first, it was noted that local scouring processes in coarse beds occur at a fast rate (Comiti, 1999), much faster than that observed for fine sediments (i.e. sand and cohesive material), thus making a given discharge in a natural setting likely scour up to its equilibrium dimensions. Secondly, from an engineering standpoint, a safety-oriented design of foundations' depth for grade-control structures cannot rely on flood duration assumptions, hence the use of the maximum, long-term scour dimensions.

Towards safety is also the performing of clear-water runs, where no recirculation or supplemental sediment feeding from upstream is provided to the system: compared to live-bed tests, scour dimensions are larger (Whittaker, 1987_a; Comiti, 1999) both because equilibrium slopes are higher and for the absence of sedimentation of jet-carried particles into the scour hole (see section 3.3.3). In addition, the effect of sediment feeding seems also to bring about inherent bed spatial instability, making equilibrium scour depth harder to determine (Whittaker and Davies, 1982, Whittaker, 1987_a; Comiti, 1999). At the prototype level actual clear-water scouring is likely to take place only downstream from reservoirs or other natural sediment-trapping obstacles. However, the actual inability to accurately predict the sediment transport rate for a given water discharge, particularly for mountain rivers (Knighton, 1998; Wohl, 2000_a) makes any predictive formulation which included such a variable useless as far as its practical application is concerned. On the other hand, the evaluation of its effect on scouring does have important meaning from a geomorphological perspective.

Two clear-water flume data sets are used herein: the first comprises 26 tests carried out in 1999 (Comiti, 1999) using a mobile-bed physical model set up in the *Sloping Sediment Duct* at HR Wallingford Ltd (United Kingdom), the second set (28 runs) was obtained in 2002

at the Hydraulic Labs of the Department of Hydraulic, Maritime and Geotechnical Engineering, University of Padova, Italy.

4.1 Experimental set-ups

4.1.1 Wallingford tests

26 tests (Tab 4.1) had been carried out in 1999 using the *Sloping Sediment Duct* at HR Wallingford Ltd (United Kingdom). The flume was 5.57 m long, 0.6 m wide, 0.245 m deep, with a metal bottom and alternate glass and metal side walls (Damgaard et al., 1996). The grain size distribution of bed sediment material used in the tests is shown in Fig. 4.1, with the characteristic diameters too. The bed material was a very heterogeneous mixture of natural particles, ranging from coarse sand to small cobbles. The geometric standard deviation $\sigma_g=\sqrt{D_{84}/D_{16}}$ =5.38 was much greater than the threshold proposed by Breusers and Raudkivi (1991) for the definition of nonuniform gradings (σ_g=1.35). The relative submerged density was Δ=1.63.

The size grading reproduces the sediment distribution of a reach of the Maso di Spinelle River, a major tributary of the Brenta River, in Valsugana (Trentino Region, Italy). Along this stream several boulder check-dams have recently been built, adopting a geomorphologic criterion (Lenzi, 2002). Scour dimensions have been subsequently surveyed in this river (section 5.1.1).

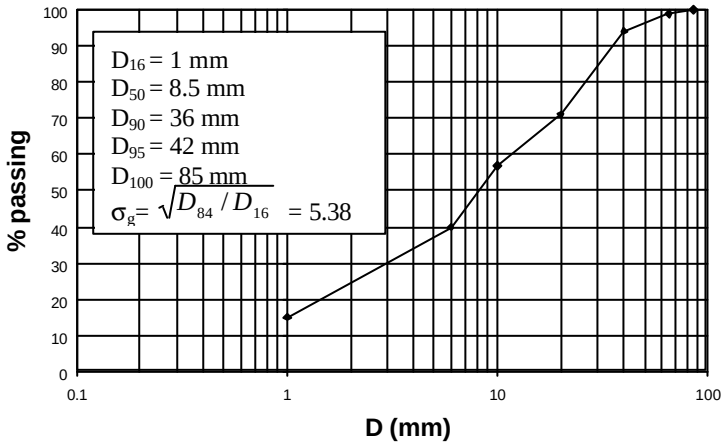

Figure 4.1 – Wallingford tests: grain size distribution of the sediment mixture and characteristic diameters.

The experiments represent actually a 1:40 scale model of the Maso River's control works based upon an undistorted Froude similitude (Giacometti, 2000). For all tests, the

initial bed was set at a constant slope, achieved by tilting the flume. The slope was determined from the difference in elevation from a horizontal water surface. Three slopes were tested: 0.078, 0.114 and 0.148. The distance between the sills was 1.050 m for Series 1 tests (labelled T1-T13) and 0.525 m for Series 2 (T14-T26). Wooden boards (1 cm-thick, and 0.6 m wide) were inserted into the granular fill of the flume.

In order to guarantee long-term equilibrium conditions the test duration was set at 18 hours for all tests. The duration was selected on the basis of direct observation and by using a video-camera to record the local scouring zone. These provided the evidence that equilibrium conditions (i.e. when scouring no longer increased and sediment transport became zero) were achieved after few hours (generally less than 5), rendering the 18-hours duration definitely reliable for obtaining the ultimate scouring dimensions.

An electrical point gauge with an acoustic device was used to measure the bed profile (error ±0.1 mm) and the water surface elevation (error ±1-2 mm according to the magnitude of the temporal fluctuations): for the former the longitudinal interval was 2.5 cm in the scour hole and 5 cm elsewhere, for the latter it was 10 cm. Elevations were also taken at each sill edge. The profiles (Fig. 4.2) were taken along the centre-line only when the scour holes were two-dimensional, otherwise two other longitudinal bed profiles were measured at a distance of 0.15 m from the flume walls. The maximum depth in the cross-section was also measured. The scour length was determined visually and measured by a tape (error ±4 mm).

The maximum scour depth was calculated identifying the cross-section where the maximum depth occurred and computing the cross-section average depth (on 13 values). For Series 1 tests, an equilibrium slope S_{eq} was attained downstream the scour hole and this was evaluated from the bed profiles. Once the equilibrium slope was obtained, the morphological jump a_1 was calculated by Eq. 3.1 (section 3.1). For Series 2, the distance between the sills was too short to permit the development of an uniform reach and the morphological jump was calculated from the bed profiles, following the graphic definition given in Fig. 4.12. When the bed in proximity of the downstream sill presented a flat or even a reversed slope, the jump equalled the head difference between two sills. Therefore in these cases it was assigned $a_1 = Z$ (section 3.1, Eq. 3.2).

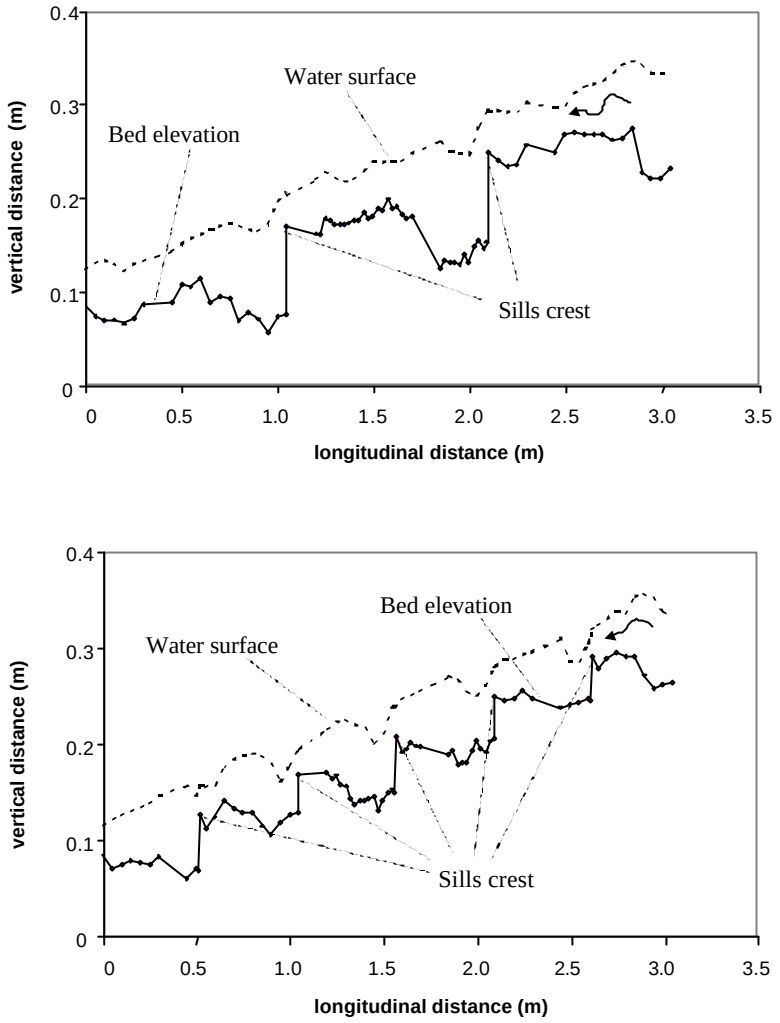

Figure 4.2 – Longitudinal profiles: above, T4 - Series 1; below, T15 - Series 2.

Cross-section averaged Froude numbers were calculated from the flow depth – data available every 10 cm – as $Fr = q / h\sqrt{gh}$, where q is the water discharge per unit width, h is the flow depth measured as difference between water and bed elevation and g is the acceleration due to gravity. In Series 1 runs, for the steepest (S_{eq}= 0.10 to 0.07) tests the flow regime along the span downstream of the scour hole was at most critical ($Fr \approx 1$). For the lowest equilibrium slopes (S_{eq}=0.07 to 0.04) the flow regime was subcritical (Fr = 0.7 to 0.9). For Series 2 the longitudinal Froude pattern exhibited a regular oscillation between subcritical flow in the scour hole and supercritical flow at the sill edge. Such peculiar regime is called tumbling flow and is characteristic of natural step-pool streams (section 2.2). For all the tests the measured flow depth just upstream of the sill edge was ascertained to correspond to the critical depth $h_c = \sqrt[3]{q^2 / g}$. In Fig. 4.3 two photos from the experiments are shown.

Tab. 4.1 – Main characteristics of the Wallingford tests. For symbols see Fig. 4.12.

Runs		Q (m^3/s)	q (m^2/s)	S	S_{eq}	L (m)	y_s (m)	l_s (m)	a_1 (m)	l_s/y_s
Series 1	T 1	0.0111	0.0185	0.078	0.068	1.050	0.050	0.21	0.011	4.20
	T 2	0.0125	0.0208	0.078	0.065	1.050	0.066	0.30	0.014	2.83
	T 3	0.0143	0.0238	0.078	0.053	1.050	0.082	0.38	0.027	4.55
	T 4	0.0165	0.0275	0.078	0.046	1.050	0.095	0.42	0.034	2.87
	T 5	0.0175	0.0292	0.078	0.044	1.050	0.106	0.42	0.036	4.63
	T 6	0.0044	0.0073	0.114	0.096	1.050	0.035	0.15	0.019	4.29
	T 7	0.0075	0.0125	0.114	0.088	1.050	0.064	0.19	0.028	2.11
	T 8	0.0098	0.0163	0.114	0.076	1.050	0.075	0.25	0.040	2.89
	T 9	0.0125	0.0208	0.114	0.062	1.050	0.106	0.30	0.055	2.26
	T 10	0.0143	0.0238	0.114	0.053	1.050	0.122	0.35	0.065	3.33
	T 11	0.0040	0.0067	0.148	0.104	1.050	0.071	0.18	0.046	2.46
	T 12	0.0060	0.0100	0.148	0.090	1.050	0.095	0.20	0.061	4.29
	T 13	0.0090	0.0150	0.148	0.073	1.050	0.133	0.30	0.079	2.11
Series 2	T 14	0.0120	0.0200	0.0785	-	0.525	0.031	0.20	0.030	6.45
	T 15	0.0160	0.0267	0.0785	-	0.525	0.052	0.25	0.041	3.33
	T 16	0.0200	0.0333	0.0785	-	0.525	0.058	0.26	0.041	2.29
	T 17	0.0240	0.0400	0.0785	-	0.525	0.061	0.30	0.041	4.81
	T 18	0.0290	0.0483	0.0785	-	0.525	0.070	0.34	0.041	3.09
	T 19	0.0075	0.0125	0.1145	-	0.525	0.032	0.14	0.030	4.38
	T 20	0.0125	0.0208	0.1145	-	0.525	0.060	0.20	0.050	2.68
	T 21	0.0175	0.0292	0.1145	-	0.525	0.081	0.25	0.060	2.63
	T 22	0.0240	0.0400	0.1145	-	0.525	0.092	0.35	0.060	6.45
	T 23	0.0065	0.0108	0.1480	-	0.525	0.064	0.19	0.047	2.97
	T 24	0.0090	0.0150	0.1480	-	0.525	0.082	0.22	0.055	4.38
	T 25	0.0110	0.0183	0.1480	-	0.525	0.095	0.25	0.065	2.68
	T 26	0.0145	0.0242	0.1480	-	0.525	0.118	0.27	0.077	2.63

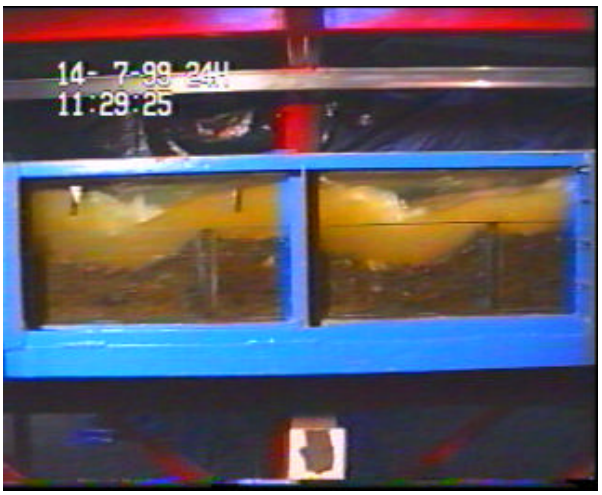

Figure 4.3 – Pictures from Wallingford runs: above, a side view during a Series 2 test; below, the bed downstream of a sill at the end of a Series 1 experiment.

4.1.2 Padova tests

28 tests were performed on a tilting flume at the Hydraulic Laboratories of the University of Padova. The steel flume is 10m-long, 0.5m-wide, 0.5m-deep, with glass windows along the whole length (Fig 4.4). Four initial slopes were tested: 0.03, 0.045, 0.062 and 0.08.

The sediment used in the tests was a slightly non-uniform gravel (s_g=1.48), with the following characteristic diameters: D_{16}=5.9 mm, D_{30}=7.3 mm, D_{50}=8.7 mm, D_{84}=13 mm, D_{90}=13.4 mm (Fig. 4.5). Fig. 4.6 shows the granular bed at the end of a test.

Figure 4.4 – The flume at the Hydraulic Laboratories of Padova. The inlet is just on the right, outside of the picture. The first scour hole from upstream was not considered in the analysis.

.

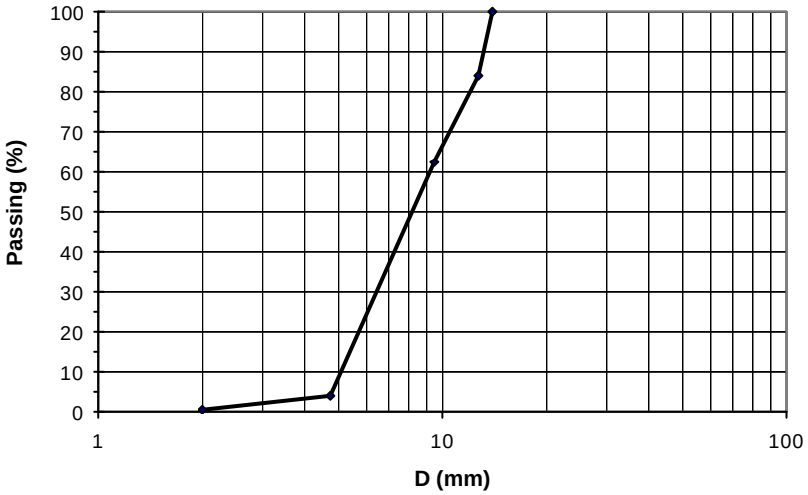

Figure 4.5 – Padova tests: grain size distribution of the sediment mixture.

Figure 4.6 – View from upstream of the Padova flume after a run was completed. Note the sediment sorting inside the scour hole in the foreground.

On the bottom of the flume two longitudinal bars supported 10mm-thick, rectangular plastic plates. The plates played the role of bed sills and were therefore fully inserted into the original gravel bed and extended over the whole flume width. The plates could be positioned at defined distances to represent a sequences of structures. The water level was measured with a point gauge placed on a gantry. Measurements of water profile were made at 5 cm intervals in the region of the scour hole and at 10 cm intervals elsewhere. Bed profile was measured with a laser profiler set on the same gantry. The bed elevations were taken at 2.5 cm intervals within the scour holes and at 5 cm intervals elsewhere. Water discharge was measured by an electromagnetic flow-meter. The measurements showed oscillations of the discharge around the mean of about half liter per second.

Two different sills' longitudinal configurations were tested, as shown in Fig. 4.7, in order to experiment different spacings and to detect possible effects due to upstream disturbances. No bed and water profiles were measured upstream of the first sill, i.e. in the transition flow.

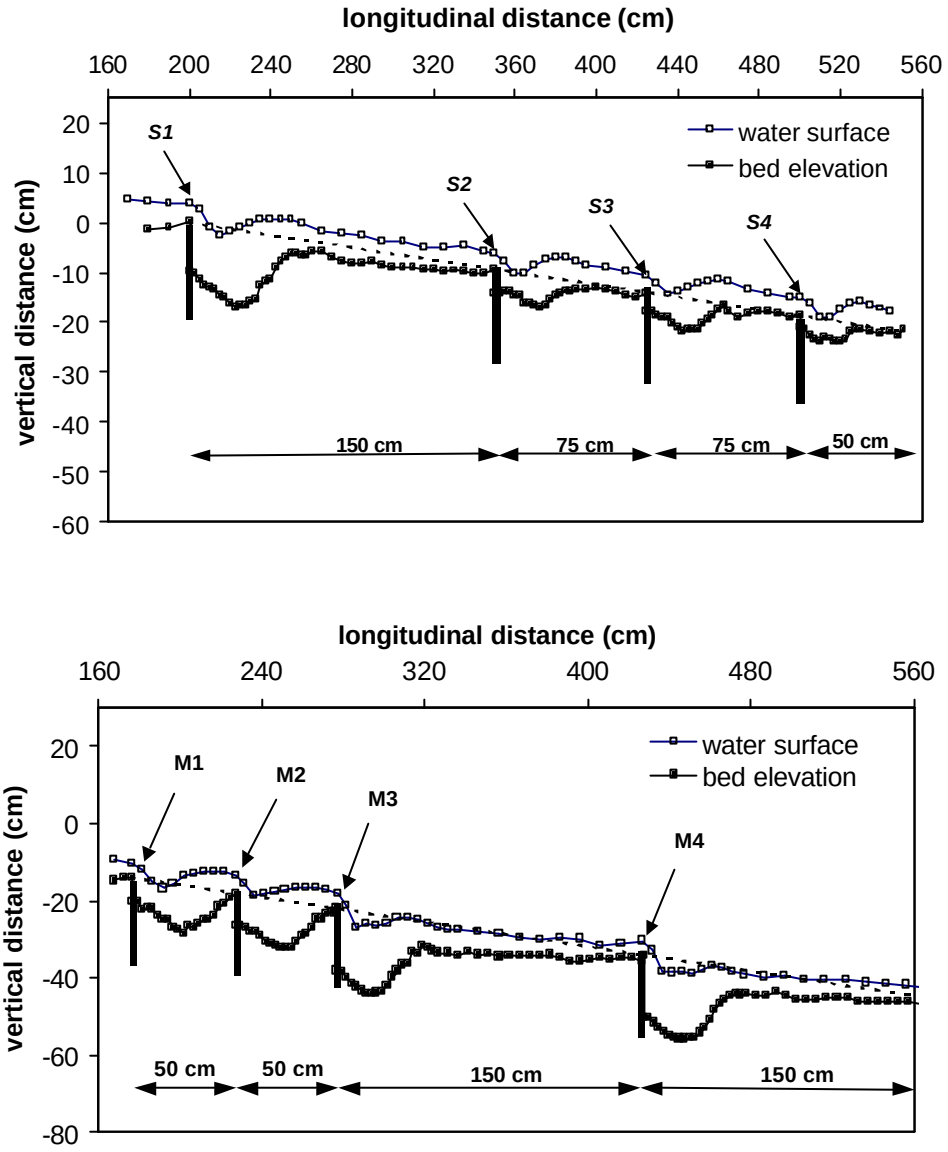

Figure 4.7 – Above, set-up for tests 1¸22 (profiles refer to test 9, Q=0.0152 m^3s^{-1}, S=0.062); below, set-up for tests 23¸28 (profiles refer to test 27, Q=0.0175 m^3s^{-1}, S=0.08).

Figs 4.8-4.9 show the look of an "unconstrained" scour hole, such as S1, M3 or M4, where the spacing to the downstream baffle was long enough to allow an equilibrium slope to form (Fig. 4.7). The flow pattern features an expanding, decelerating jet and the two horizontal counter-flowing rollers (see also Fig. 3.14), whose shear stresses shape the upstream and downstream sides of the scour hole. Instead, for short spacings (i.e. S2, S3, S4, M1, M2) and high flow rates, the scour profile appears smoother probably due a different jet geometry and/or flow pattern (Fig. 4.10).

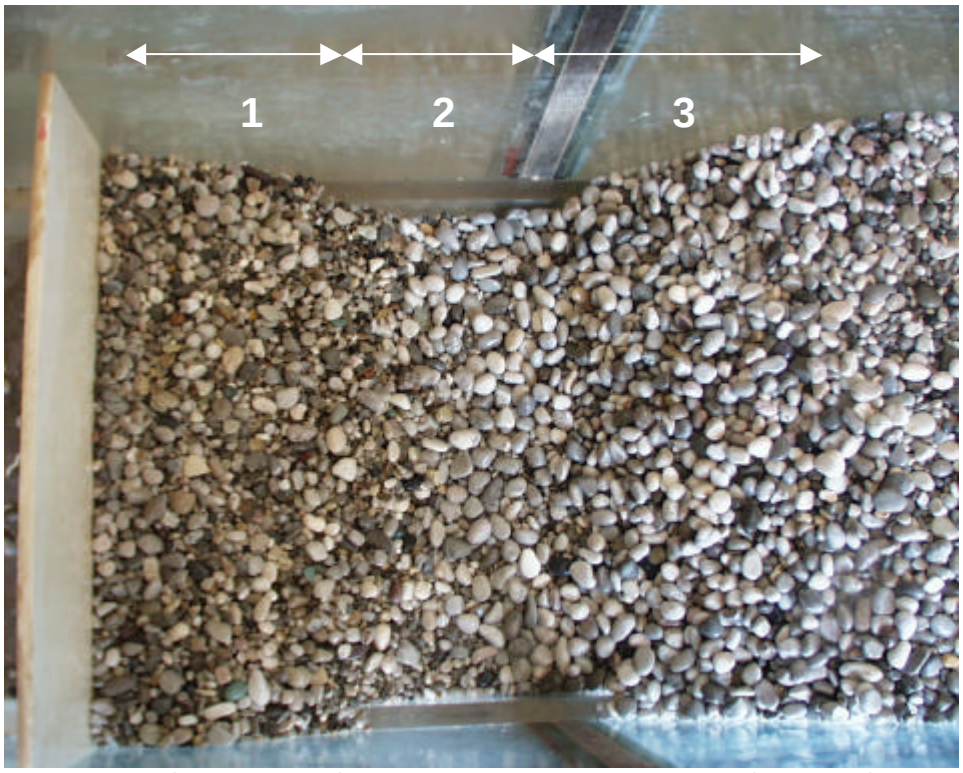

Figure 4.8 – View from above of an "unconstrained" scour hole, flow was from the left. A clear sediment sorting is visible, even though the initial sediment mixture is rather sorted. Three different zones are highlighted: 1) upstream side of the scour hole; 2) maximum depth zone; 3) downstream side of the scour hole.

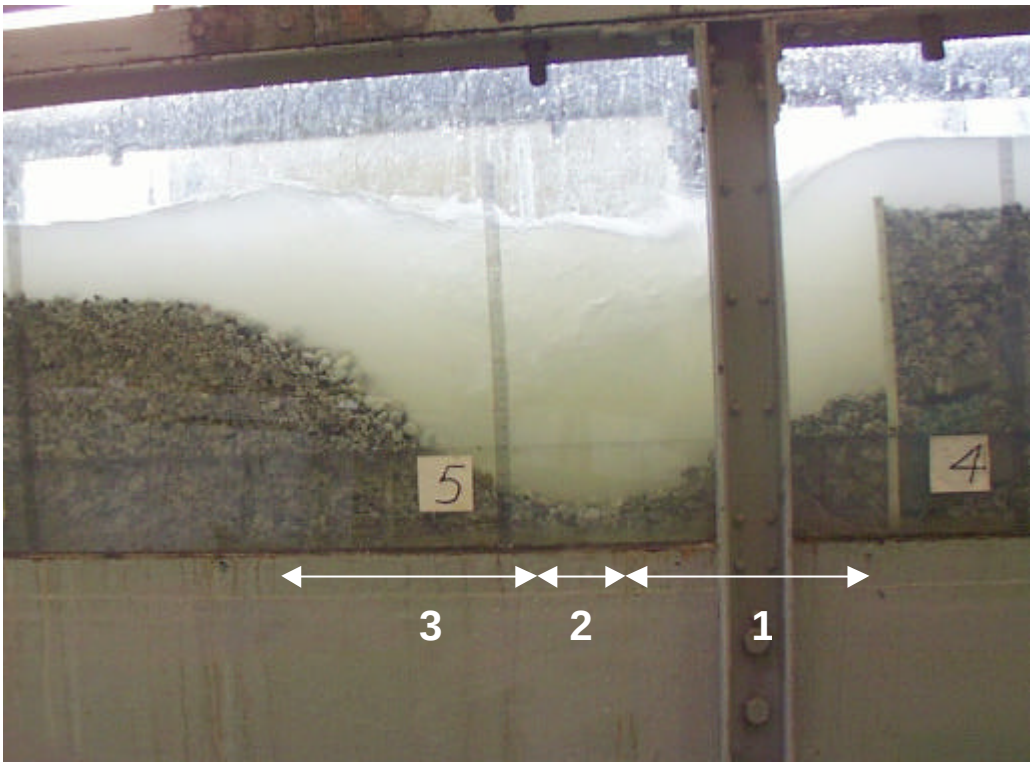

Figure 4.9 – Lateral view of an "unconstrained" scour hole. The three different zones shown in Fig. 4.7 are reported.

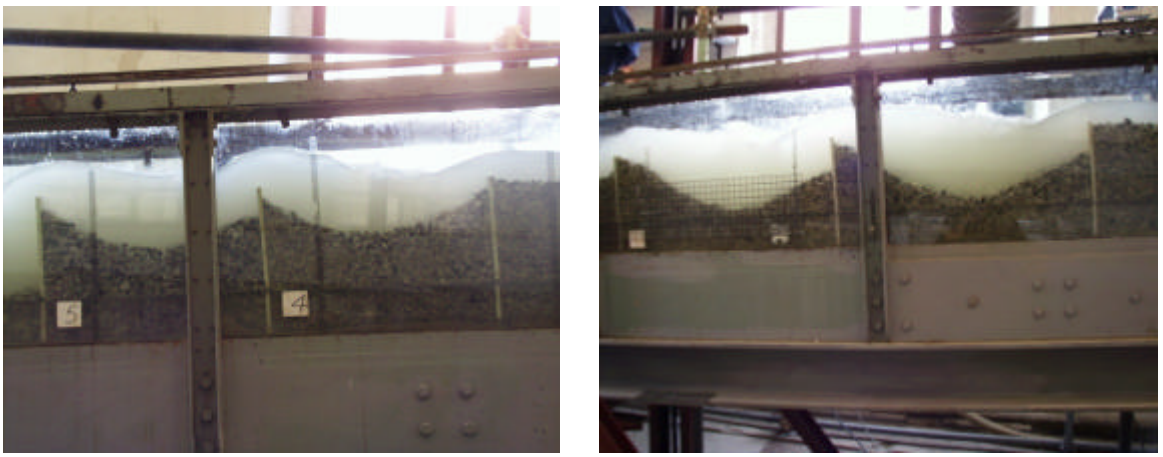

Figure 4.10 – "Constrained" scour holes at a high flow rate: left, M1-M2; right, S2-S3.

The tests were performed at constant discharge for a duration of 4 to 5 hours. Such duration was conservative, as the scour development always took place within the first two hours. Bed preparation before each tests required care in order to avoid clustering of large particles on either side of the flume that would produce non-uniform erosion across the flume width, particularly in the initial stage of the scouring process. All the scour holes obtained were two-dimensional, with minor occasional wall effects. Reduction of flow width through the developments of lateral bars occurred only in the upper part of the flume, probably generated by non-uniform inflow conditions. A length of 2.25 m upstream of the analysed reach of the flume showed to be sufficient to obtain uniform conditions over the first bed sill.

Before a new test, the bed was reconstructed so that the sills would be fully inserted into the gravel. The sediment was carefully mixed over the whole depth, to avoid grain size selection and compaction of the gravel at different depth which may have resulted in biased scouring processes.

The first six runs, having an initial slope of 0.03, showed a peculiar behavior: the initial stage of standing waves generated by the sills (section 3.3.2) did not cease to give way to the typical scour formation driven by a considerable drop, and even at the equilibrium the bed presented undulations, i.e. in-phase bedforms (Fig. 4.11). Therefore the equilibrium slope could not be determined, as well as the morphological jump. In this case, scour holes below sills can be assimilated to troughs in antidunes. The experimental conditions of these six tests are reported in Table 4.2. In Table 4.3 data from the "unconstrained" scour holes (i.e. S1, M3, M4) are shown, whereas potentially "constrained" ones (i.e. S2, S3, S4, M1, M2) are in Table 4.4.

Figure 4.11 – In the tests 1-6 the low initial slope led to an equilibrium regime dominated by standing waves shaping the bed with troughs and crests: above, view from upstream; below, side view.

Table 4.2 - Experimental conditions and measured dimensions for tests 1-6 (initial slope S=0.03). See Fig. 4.7 for the different scour hole labels. For symbols, see sections 4.2.5 and 4.2.6.

	Scour hole	Q (m^3/s)	S	h_s (m)	y_s (m)	L_1 (m)	L_{b1} (m)
Test 1	S1	0.0165	0.03	0.036	0.050	0.300	0.350
	S2	0.0165	0.03	0.033	0.034	0.250	0.275
	S3	0.0165	0.03	0.038	0.040	0.245	0.275
	S4	0.0165	0.03	0.036	0.037	0.240	0.275
Test 2	S1	0.0193	0.03	0.029	0.061	0.325	-
	S2	0.0193	0.03	0.049	0.048	0.300	0.325
	S3	0.0193	0.03	0.033	0.019	0.300	0.325
	S4	0.0193	0.03	0.025	0.027	0.300	0.325
Test 3	S1	0.0210	0.03	0.044	0.065	0.300	0.375
	S2	0.0210	0.03	0.050	-	-	-
	S3	0.0210	0.03	0.032	0.059	0.300	0.350
	S4	0.0210	0.03	0.035	0.025	0.300	-
Test 4	S1	0.0250	0.03	0.047	0.050	0.350	0.375
	S2	0.0250	0.03	0.043	0.060	0.350	0.425
	S3	0.0250	0.03	0.064	0.033	0.400	0.400
	S4	0.0250	0.03	0.058	0.047	0.350	-
Test 5	S1	0.0275	0.03	0.051	0.061	0.400	0.550
	S2	0.0275	0.03	0.048	0.058	0.350	0.500
	S3	0.0275	0.03	0.061	0.022	0.350	0.450
	S4	0.0275	0.03	0.048	0.058	0.400	-
Test 6	S1	0.0303	0.03	0.053	0.053	0.400	0.400
	S2	0.0303	0.03	0.049	0.056	0.350	0.450
	S3	0.0303	0.03	0.062	0.051	0.350	0.400
	S4	0.0303	0.03	0.077	0.059	0.350	-

Table 4.3 - Experimental conditions and measured dimensions for unconstrained scour holes. See Fig. 4.7 for scour hole labels and Fig. 4.12 for symbols.

	Scour hole	Q (m^3/s)	S	S_{eq}	a_1 (m)	y_s (m)	l_s (m)
Test 7	S1	0.0303	0.062	0.0185	0.065	0.298	0.9
Test 8	S1	0.025	0.062	0.024	0.057	0.2354	0.725
Test 9	S1	0.0152	0.062	0.0446	0.026	0.1587	0.5
Test 10	S1	0.012	0.062	0.0524	0.015	0.0958	0.35
Test 11	S1	0.0202	0.062	0.0387	0.035	0.1814	0.6
Test 12	S1	0.02	0.08	0.0252	0.082	0.2316	0.5
Test 13	S1	0.0152	0.08	0.0377	0.063	0.1907	0.45
Test 14	S1	0.025	0.08	0.0205	0.089	0.2562	0.6
Test 15	S1	0.0303	0.08	0.0161	0.096	0.2751	0.7
Test 16	S1	0.0175	0.08	0.0287	0.077	0.2085	0.46
Test 17	S1	0.0087	0.08	0.056	0.036	0.1077	0.26
Test 18	S1	0.0167	0.045	0.036	0.014	0.0776	0.4
Test 19	S1	0.0236	0.045	0.0315	0.020	0.126	0.625
Test 20	S1	0.027	0.045	0.0222	0.034	0.1631	0.7
Test 21	S1	0.02	0.045	0.0339	0.017	0.1256	0.575
Test 22	S1	0.0306	0.045	0.018	0.041	0.1674	0.775
Test 23	M3	0.028	0.062	0.0265	0.053	0.2402	0.675
“	M4	0.028	0.062	0.0185	0.066	0.2365	0.695

Test 24	M3	0.018	0.062	0.0397	0.034	0.1687	0.51
"	M4	0.018	0.062	0.0293	0.050	0.1699	0.525
Test 25	M3	0.018	0.062	0.0237	0.058	0.2065	0.6
"	M4	0.018	0.062	0.0149	0.072	0.2007	0.6
Test 26	M3	0.0225	0.08	0.0223	0.087	0.2433	0.505
"	M4	0.0225	0.08	0.0183	0.093	0.25	0.525
Test 27	M3	0.0175	0.08	0.02	0.091	0.207	0.425
"	M4	0.0175	0.08	0.0301	0.076	0.202	0.45
Test 28	M3	0.0275	0.08	0.004	0.115	0.276	0.65
"	M4	0.0275	0.08	0.0096	0.107	0.2633	0.65

Table 4.4 - Experimental conditions and measured dimensions for constrained scour holes. See Fig. 4.7 for scour hole labels and Fig. 4.12 for symbols.

	Scourhole	Q m^3/s	S	S_{eq}	a_1 m	y_s m	l_s m
Test 7	*S2*	0.0303	0.062	-	0.047	0.172	0.75
Test 8	*S2*	0.025	0.062	-	0.047	0.138	0.7
Test 9	*S2*	0.0152	0.062	0.0387	0.017	0.063	0.35
Test 10	*S2*	0.012	0.062	-	0.047	0.037	0.25
Test 11	*S2*	0.0202	0.062	-	0.047	0.121	0.55
Test 12	*S2*	0.02	0.08	-	0.060	0.156	0.575
Test 13	*S2*	0.0152	0.08	-	0.060	0.147	0.475
Test 14	*S2*	0.025	0.08	-	0.060	0.165	0.675
Test 15	*S2*	0.0303	0.08	-	0.060	0.173	0.75
Test 16	*S2*	0.0175	0.08	-	0.060	0.139	0.525
Test 17	*S2*	0.0087	0.08	0.056	0.018	0.061	0.275
Test 18	*S2*	0.0167	0.045	0.036	0.007	0.047	0.3
Test 19	*S2*	0.0236	0.045	0.0315	0.010	0.061	0.35
Test 20	*S2*	0.027	0.045	0.0099	0.026	0.063	0.375
Test 21	*S2*	0.02	0.045	0.0273	0.013	0.051	0.325
Test 22	*S2*	0.0306	0.045	-	0.034	0.077	0.55
Test 7	*S3*	0.0303	0.062	-	0.047	0.16	0.75
Test 8	*S3*	0.025	0.062	-	0.047	0.126	0.6
Test 9	*S3*	0.0152	0.062	0.0363	0.019	0.064	0.35
Test 10	*S3*	0.012	0.062	0.05	0.009	0.047	0.3
Test 11	*S3*	0.0202	0.062	-	0.047	0.115	0.5
Test 12	*S3*	0.02	0.08	-	0.060	0.152	0.55
Test 13	*S3*	0.0152	0.08	-	0.060	0.117	0.425
Test 14	*S3*	0.025	0.08	-	0.060	0.165	0.65
Test 15	*S3*	0.0303	0.08	-	0.060	0.202	0.75
Test 16	*S3*	0.0175	0.08	-	0.060	0.123	0.45
Test 17	*S3*	0.0087	0.08	0.056	0.018	0.059	0.3
Test 18	*S3*	0.0167	0.045	0.036	0.007	0.045	0.275
Test 19	*S3*	0.0236	0.045	0.0315	0.010	0.051	0.325
Test 20	*S3*	0.027	0.045	0.0099	0.026	0.057	0.325
Test 21	*S3*	0.02	0.045	0.0244	0.015	0.049	0.325
Test 22	*S3*	0.0306	0.045	-	0.034	0.067	0.475
Test 7	*S4*	0.0303	0.062	-	0.031	0.07	0.5
Test 8	*S4*	0.025	0.062	-	0.031	0.072	0.475
Test 9	*S4*	0.0152	0.062	0.0373	0.012	0.046	0.3
Test 10	*S4*	0.012	0.062	0.0211	0.020	0.041	0.25
Test 11	*S4*	0.0202	0.0621	-	0.031	0.055	0.375
Test 12	*S4*	0.02	0.08	-	0.040	0.114	0.5

Test 13	*S4*	0.0152	0.08	-	0.040	0.102	0.425
Test 14	*S4*	0.025	0.08	-	0.040	0.113	0.5
Test 15	*S4*	0.0303	0.08	-	0.040	0.107	0.5
Test 16	*S4*	0.0175	0.08	-	0.040	0.096	0.42
Test 17	*S4*	0.0087	0.08	0.056	0.012	0.05	0.2
Test 18	*S4*	0.0167	0.045	-	0.023	0.046	0.26
Test 19	*S4*	0.0236	0.045	-	0.023	0.024	0.325
Test 20	*S4*	0.027	0.045	-	0.023	0.046	0.35
Test 21	*S4*	0.02	0.045	-	0.023	0.051	0.325
Test 22	*S4*	0.0306	0.045	-	0.023	0.053	0.4
Test 23	*M1*	0.028	0.062	-	0.031	0.079	0.51
“	*M2*	0.028	0.062	-	0.031	0.08	0.49
Test 24	*M1*	0.018	0.062	-	0.031	0.105	0.51
“	*M2*	0.018	0.062	-	0.031	0.053	0.38
Test 25	*M1*	0.0225	0.062	-	0.031	0.082	0.475
“	*M2*	0.0225	0.062	-	0.031	0.069	0.425
Test 26	*M1*	0.0225	0.08	-	0.040	0.095	0.51
“	*M2*	0.0225	0.08	-	0.040	0.133	0.49
Test 27	*M1*	0.0175	0.08	-	0.040	0.124	0.51
“	*M2*	0.0175	0.08	-	0.040	0.121	0.425
Test 28	*M1*	0.0275	0.08	-	0.040	0.104	0.51
“	*M2*	0.0275	0.08	-	0.040	0.125	0.49

4.2 Results

Fig. 4.12 shows the reference sketch for the variables used hereafter in the analysis of laboratory results.

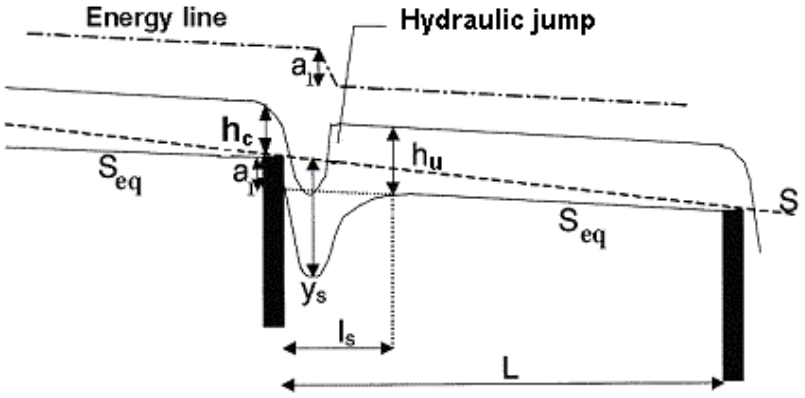

Figure 4.12 – Definition sketch of the variables.

4.2.1 Putting together low and high gradient data

Following Gaudio et al. (2000, see section 3.3.3) and considering the system sketch in Fig. 4.12, the function for the maximum clear-water, long-term scour depth can be written as (Eq. 3.20):

$$y_s = f(g, n, r_w, r_s', q, h_u, D, a_1)$$

with the morphological jump a_1 given by (Eq. 3.21):

$$a_1 = (S - S_{eq})L$$

Differently from Eq. 3.29, the following dimensionless function – still valid – will be used as a basis for the regression (Lenzi et al., 2002):

$$\frac{y_s}{H_s} = \Phi\left[\frac{a_1}{H_s}, \frac{a_1}{\Delta D}\right] \qquad (4.1)$$

In order to determine the form and the coefficients of the Equation 4.1, the high-gradient tests from Wallingford Series 1 (L=1 m) will be here considered together with previous data on mild slopes from Marion et al. (1998) and (Gaudio and Marion, 2003).

Maximum scour depth

In Fig. 4.13 the scour depths are plotted along with data reported by Marion et al. (1998) and Gaudio and Marion (2003), in accordance to their original single parameter formulation.

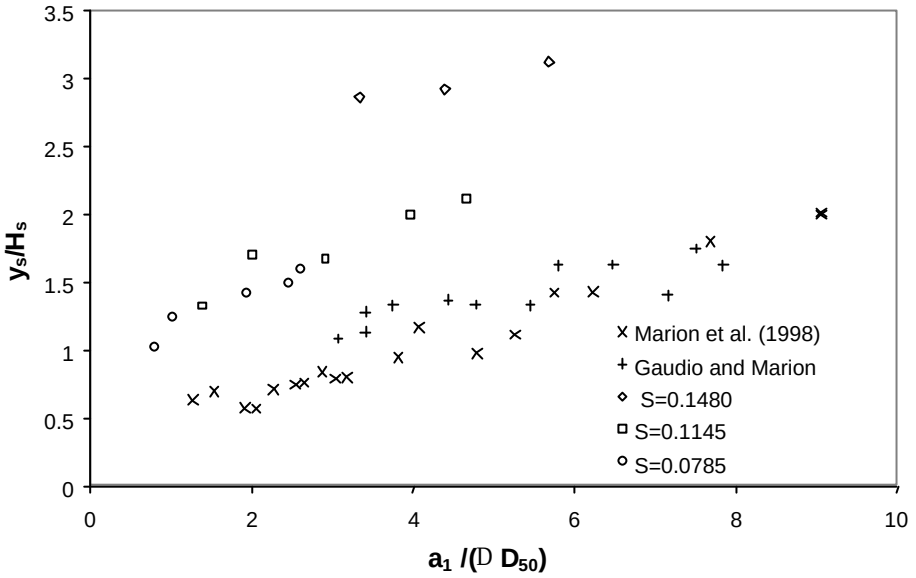

Fig. 4.13 – Non-dimensional maximum scour depths as a function of $a_1/(\Delta D_{50})$.

In their work, the grain size was uniform and the choice of a representative size was straightforward (D_{50}). It is evident that the new points do not match with the previous results and, therefore, the formulae obtained with mild slopes and uniform sediments cannot be generalized to high slopes and graded material. The choice of different representative diameter (e.g. D_{90}) did not produce any better agreement. It was hypothesised, therefore, that the adoption of a single parameter formula like Eq.(3.31), although applicable to mild slopes, is not appropriate when analysing scour at high slopes.

A multiple regression analysis was then performed using the statistical software package 'Statistica 6.1" (Statsoft, 1995). The best fit to the experimental data was obtained with the following non-linear equation:

$$\frac{y_s}{H_s} = 0.4359 + 1.4525\left(\frac{a_1}{H_s}\right)^{0.8626} + 0.0599\left(\frac{a_1}{\Delta D_{95}}\right)^{1.4908} \qquad (4.2)$$

which has a correlation coefficient R=0.951 and explains 90.5% of the variance (Figs. 4.14 and 4.15).

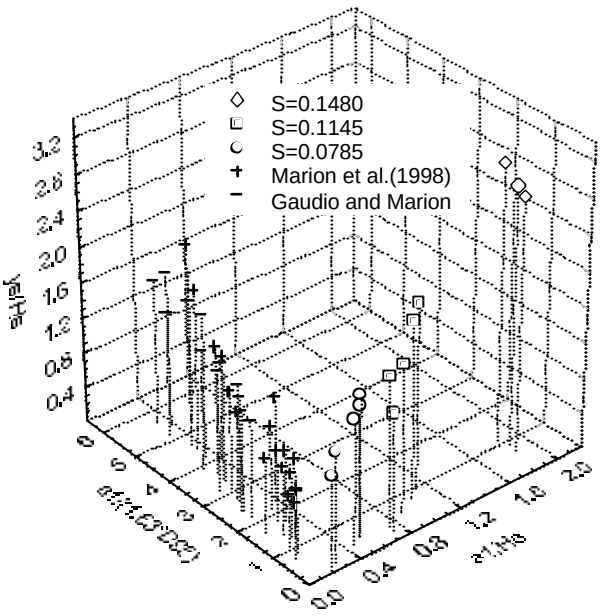

Figure 4.14 – Non-dimensional maximum scour depths as a function of $a_1/(\Delta D_{95})$ and a_1/H_s

The use of the D_{95} produced the best correlation, nevertheless this turned out to be almost insensitive to the choice of the representative grain size. In Tab. 4.5 the experimental ranges of the two parameters a_1/H_s and $a_1/(DD_{95})$ for the previous low-gradient tests and the new steep runs are reported.

Tab. 4.5 – Experimental range of the non-dimensional parameters in the low and in the high gradient tests.

	a_1/H_s	$a_1/\Delta D_{95}$
Wallingford Series 1 tests	0.225 - 1.872	0.161 - 1.150
Marion et al. 1998	0.101 - 0.512	0.720 - 5.31
Gaudio and Marion 2003	0.155 – 0.377	2.208 – 5.644

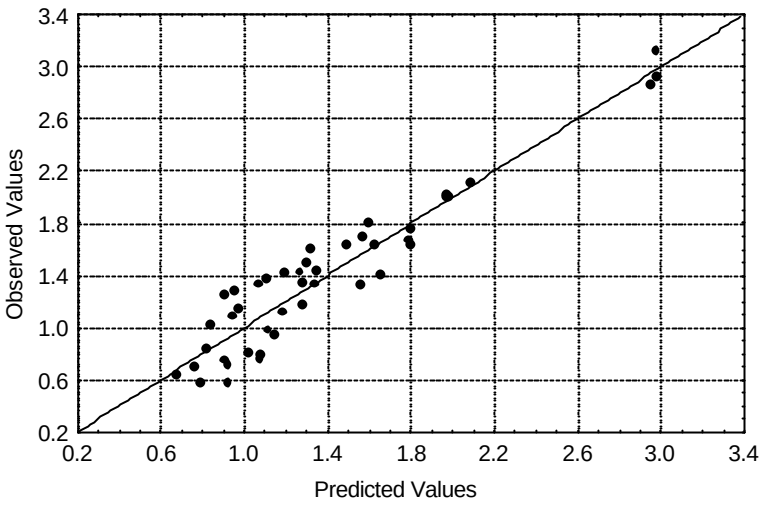

Figure 4.15 – Comparison between predicted (Eq. 4.2) and observed values of the dimensionless maximum scour depth (data from the Wallingford Series 1, from Marion et al., 1998, and from Gaudio and Marion, 2003).

Scour length

In Figs. 4.16a and 4.16b the non-dimensional lengths of the scour hole are plotted, adopting the D_{50} and D_{90} respectively; they are compared with the results obtained for uniform gravel and low-gradient tests.

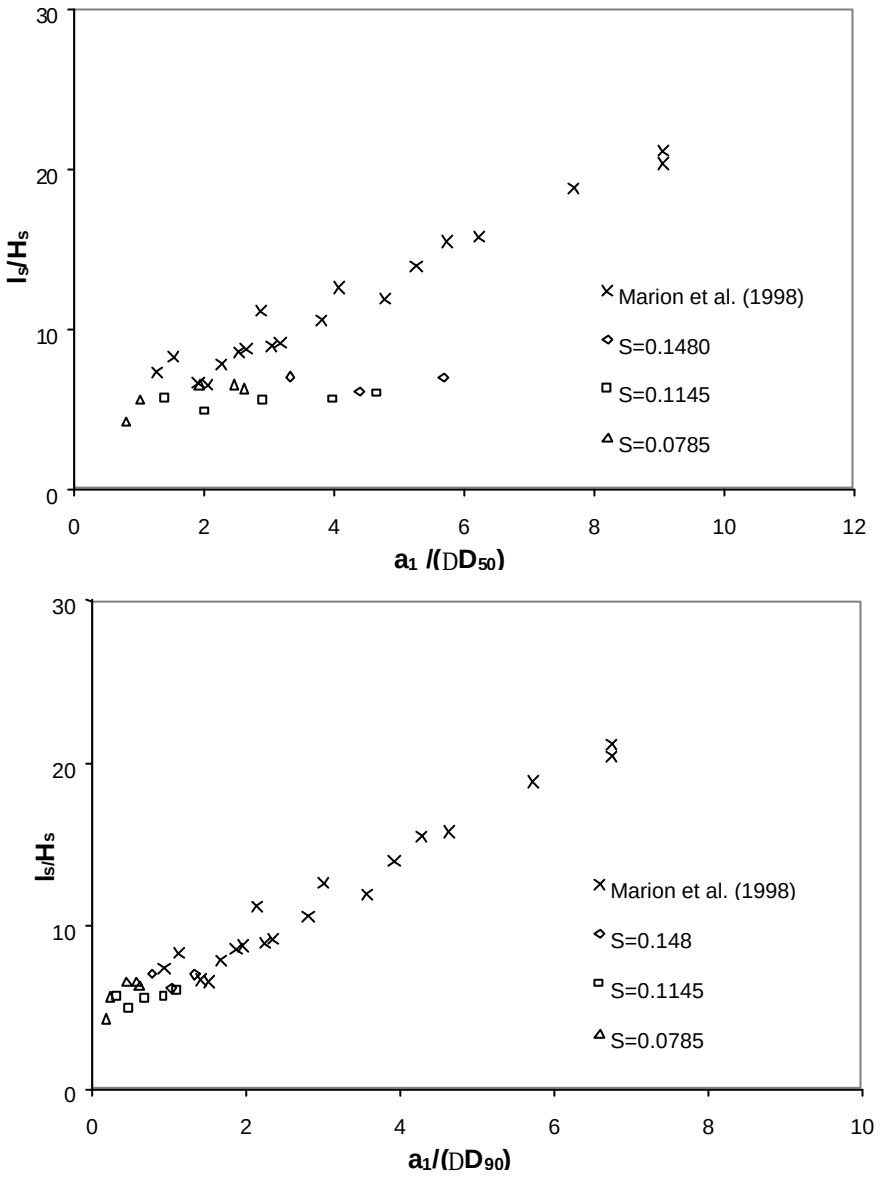

Fig. 4.16 – Non-dimensional scour lengths as a function of $a_1/(\Delta D_{90})$ (a, above) and as a function of $a_1/(\Delta D_{50})$ (b, below).

The suggestion that the choice of D_{90} provides a good fit to the data might be misleading, as the points displaced in Fig.4.16b fall into limited ranges of $a_1/(\Delta D_{90})$ without overlapping. Thus, as for the scour depths, an analysis considering the two parameters a_1/H_s

and $a_1/(DD)$ has been carried out (Fig. 4.17), leading to the following best-fit, multiple regression formula:

$$\frac{l_s}{H_s} = 4.479 + 0.023\left(\frac{a_1}{H_s}\right)^{-1.808} + 2.524\left(\frac{a_1}{\Delta D_{95}}\right)^{1.129} \qquad (4.3),$$

with R=0.986 and an explained variance of 97.3% (Fig. 4.18).

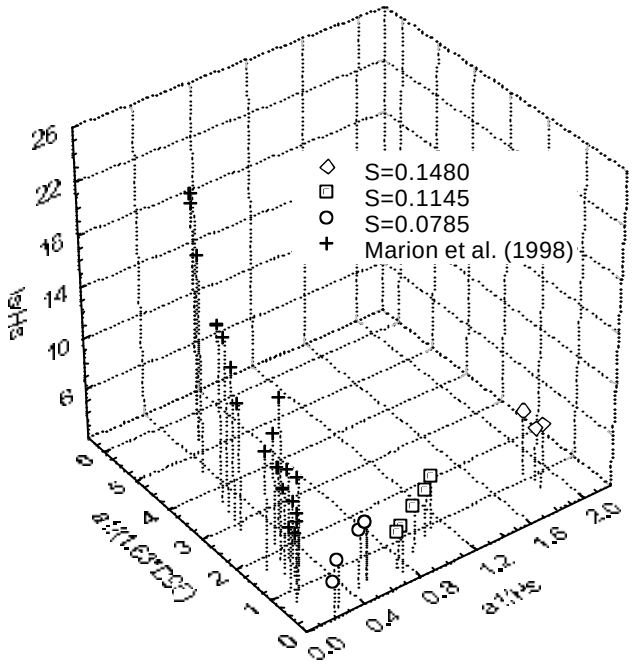

Figure 4.17 – Non-dimensional scour lengths as function of $a_1/(DD_{95})$ and a_1/H_s.

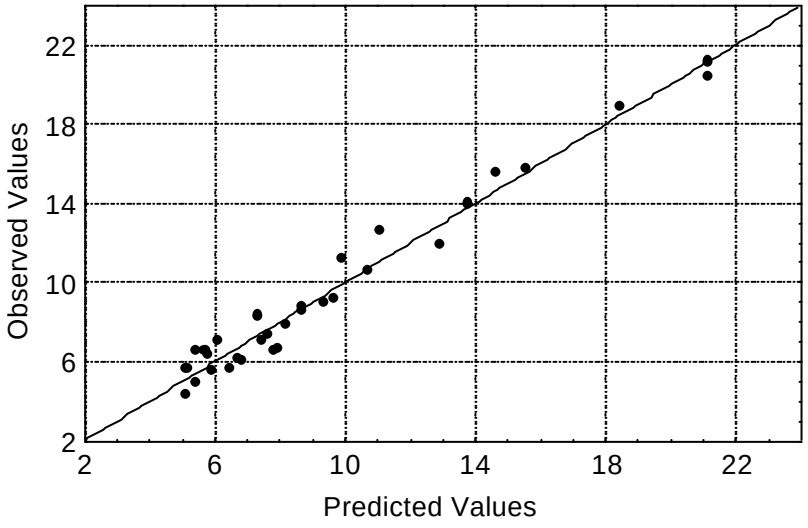

Fig. 4.18 – Comparison between predicted (Eq. 4.3) and observed values of the dimensionless scour lengths (data from the Wallingford Series 1 and from Marion et al., 1998).

For the same pair of variables but using D_{90}, the goodness of the fit did not change, whereas using D_{50} it decreased to R=0.964. Hence it seems that the length of the scour hole is affected by the coarsest grains more than the depth of the scour.

Affinity and similarity of the scour holes

Following Gaudio et al. (2000), the degree of self-affinity among the scour holes is shown in Fig. 4.19. This methodology allows the comparison of different scour holes by scaling the longitudinal distance measured starting from the sill to the scour length (x_1/l_s) and the depth to the maximum scour depth (y/y_s). Since it was not possible to quickly raise the water level by blocking the downstream end of the flume, the upstream part of the scour profile (made up of the finest particles and almost reaching the top of the sill) was always eroded by the decreasing flow rates when the pump was being closed; therefore that part of the profile ($0< x/l_s < 0.2$) should not be taken into account.

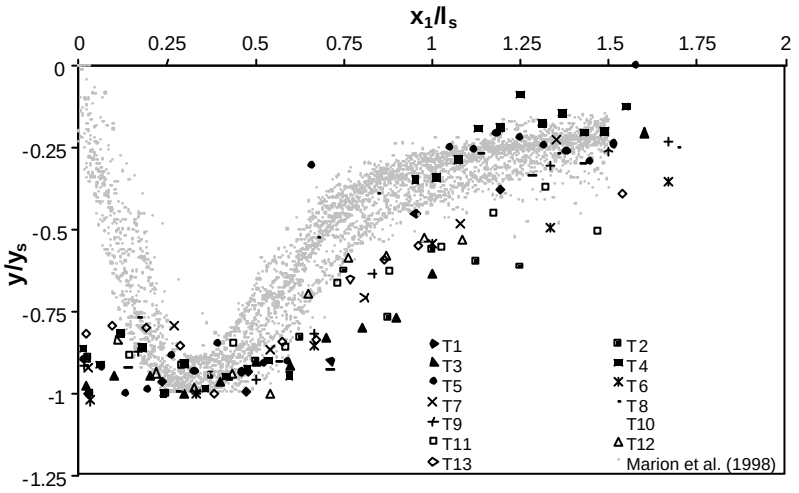

Fig. 4.19 – Affinity of the scour holes.

New test profiles show to be somewhat self-affine (with the exception of test T5, which consists of the highest flow rate experimented). However they only partly overlie with those from the low-gradient tests. The approximately affine nature of the scour hole would enable the assessment of the scour hole volume using the prediction equations for the maximum scour depth (Eq. 4.2) and the scour length (Eq. 4.3). In order to establish whether self-similarity of scour holes is present or not, it is required that both longitudinal and vertical dimensions of the scour hole are scaled to the same factor (e.g. the scour length, Fig. 4.20). New tests scour holes do not show similarity and the downstream side of the pool clearly

correlates with the initial slope values: the steeper the initial condition, the steeper this side. This is consistent with the fact that the jet angle was found to be roughly equal to the inclination of the downstream part of the scour hole (see section 3.2.2). The large difference in jet trajectory can therefore explain to some extent the larger scatter shown by the affinity graph in Fig. 4.19.

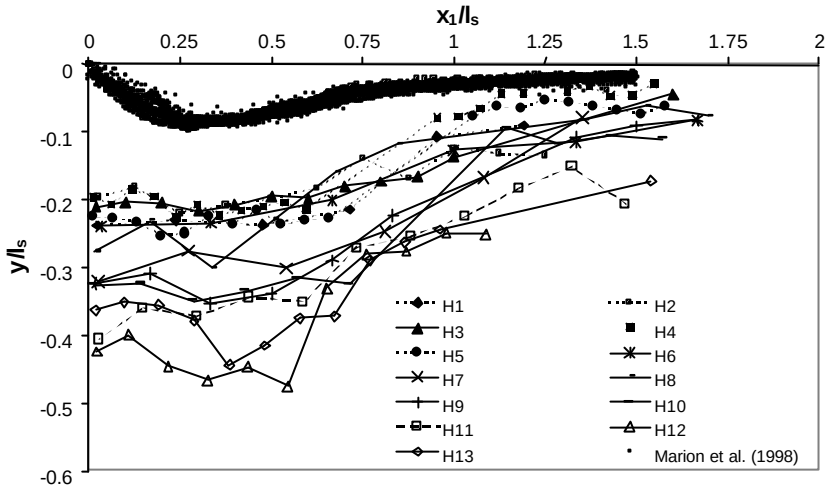

Fig. 4.20 – Similarity of the scour holes.

Application of the scour predictive formulae

In order to use Eqs. (4.2) and (4.3), estimation of the following parameters is required: the critical specific energy H_s, which can be derived from Eq. (3.27) once the design discharge is determined; the relative submerged particle density, Δ, which can be assumed in the range 1.6-1.7; the grain diameter D_{95} of the bed alluvium; the morphological jump, a_1, which is given by Eq. (3.21). The evaluation of the equilibrium slope, required for the jump a_1, is a critical point.

Marion et al. (1998), whose experiments were characterised by high relative submergence ratios, $S_r = h_u/D_{84}>10$, found good agreement between the measured equilibrium slope and the one calculated through Eq.(3.26) with $q_c=0.040$ and $D=D_{50}$, assuming that the Manning's coefficient could be determined using the expression:

$$n = \frac{D_{90}^{1/6}}{26} \tag{4.4}$$

On the contrary, the present tests feature very low submergence ratios S_r, roughly ranging from 0.7 to 1.7, as found in natural mountain torrents. Therefore Manning's coefficient has been evaluated through the Keulegan's equation developed for macro-roughness conditions:

$$n = \frac{D_{90}^{1/6}}{15.1} \tag{4.5}$$

which gives n=0.038. The critical Shields' mobility parameter, q_c, was set equal to 0.076, following the indications found in the scientific literature for coarse grain size distributions (Krey, 1925). Finally, the most appropriate diameter to be used in Eq. (3.26) was assessed by searching for different diameters the best fit between the experimental points and the theoretical curve assuming for n and q_c the above values. This calibration process led to the identification of the D_{65} (equal to 0.016 m) as the "characteristic" grain size for the equilibrium slope.

Fig. 4.21 shows the measured equilibrium slope and the curve expressed by Eq. (3.26) versus the unit discharge q: it can be observed that the agreement is fairly good except for the three runs with the smallest discharges, which have submergence ratios S_r less than 1.

The evidence that for these tests the equilibrium slope is lower than predicted might be due to the larger flow resistance induced by surface effects (i.e. small hydraulic jumps in correspondence with protruding cobbles) when the submergence drop below the unity, as found by Bathurst (1985).

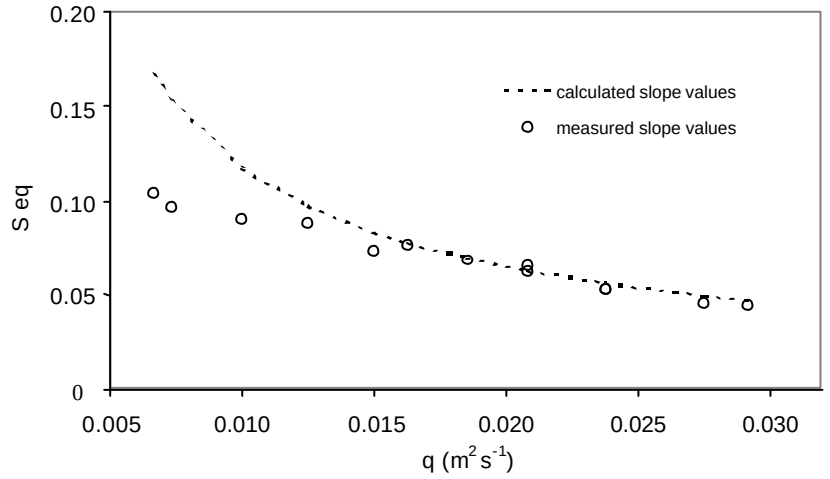

Figure 4.21 – Measured and calculated equilibrium slope values as a function of the unit discharge.

Better results in predicting the equilibrium slope might presumably be achieved using other roughness formulations (Jarrett, 1984; Bathurst, 1985; Ferro and Giordano, 1991; Baiamonte and Ferro, 1997; Ferro, 2002) which are not discussed in this study. However, in practical applications the design discharge adopted is large (return period of 50-100 years), and therefore the submergence ratio S_r, is expected to be above unity.

4.2 Geometrical interference due to short spacings: first evidences

Equilibrium bed profiles

Fig. 4.2 shows examples of Wallingford Series 1 and 2 runs, T4 and T15. The discharge in roughly the same (see Tab. 4.1) and the only difference is represented the spacing L between the sills, 1.05 m for Series 1 and 0.525 m in Series 2. The configuration depicted represents the long-term equilibrium, when sediment transport was zero. The heavily reduced scour depth is clearly observable. The upper photo in Fig. 4.3 shows the run T16 (Series 2). Other important characteristics of Series 2 tests are the following: i) no uniform flow reach was present downstream of the scour hole, where bed slope was generally zero or even negative; ii) the water surface at the scour holes presented marked superelevations accompanied by strong "boiling" phenomena (i.e. temporal fluctuations of the water level) whereas in Series 1 tests these were absent or small. This last evidence suggests that in Series 2 the flow up rise at the downstream end of the scour hole is somewhat "forced" by the closeness of the next sill (Comiti et al, 2001; Lenzi et al., 2003_a).

Maximum scour depth and scour length

In Table 4.1 the large reduction of maximum scour depth and length encountered in Series 2 runs can be observed, comparing tests with similar flow rate and initial slope (e.g. T2-T14, T4-T15, T9-T20, T13-T24). However, shallower scours for Series 2 were to be expected because morphological jumps a_1 are smaller for similar conditions, being the spacing L halved with respect to Series 1 scours (Eq. 3.1). Therefore a normalisation of the variables is needed to analyze scour holes dimensions. The plot of y_s/a_1 against h_c/a_1 is shown in Fig. 4.22.

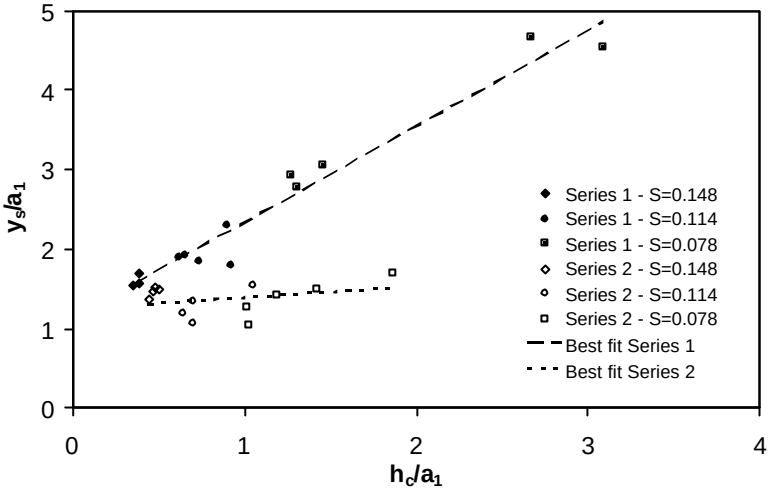

Figure 4.22 - Non-dimensional maximum scour depths y_s/a_1 against parameter h_c/a_1.

Such a normalization allows to infer the response of maximum scour depth to different flow rates, univocally represented by their critical flow depth h_c. Series 1 data plot on a positive linear trend, with no appreciable difference due to their initial slope value S. A much flatter trend, almost horizontal, is depicted by Series 2 points. This makes evident that in Series 2 runs the influence of water discharge upon the normalised scour depth is considerably weaker than in Series 1 tests. Furthermore, Series 2 points plot well below, showing that also when these scour holes are normalised they present a strong reduction compared to Series 1 data, heavier for higher h_c/a_1 values. For $h_c/a_1 \tilde{}$ 1.5, Series 1 data features ratios y_s/a_1 around 3, whereas in Series 2 they are around 1.5.

The relationship between the maximum scour depth normalized to the critical flow depth, y_s/h_c, and the ratio a_1/h_c is shown in Fig. 4.23 in order to analyze the role of the morphological jump a_1. Both Series present a linear trend, but their gradient is different, Series 2 being a little steeper. Again, normalised scour depths of Series 2 are smaller than in comparable Series 1 tests.

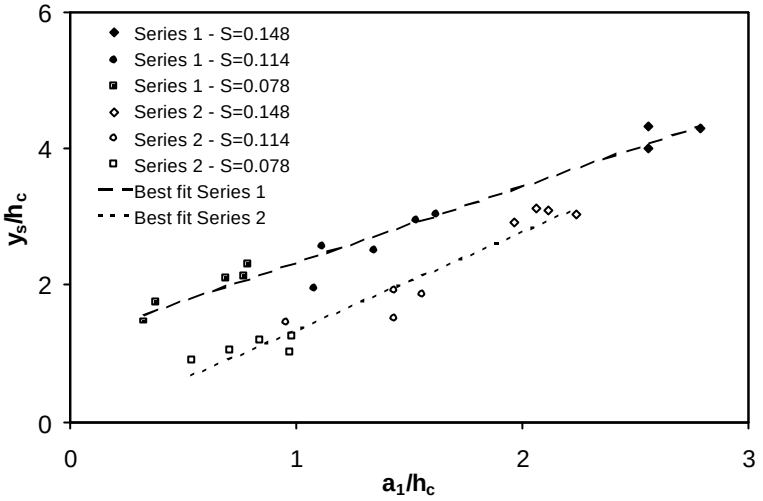

Figure 4.23 - Non-dimensional maximum scour depths y_s/h_c against parameter a_1/h_c.

Fig. 4.24 shows that normalised scour lengths l_s/a_1 of Series 1 markedly increase with the ratio h_c/a_1. D'Agostino (1996), investigating the optimal spacing of subsidiary dams obtained an equation for the scour length below isolated check-dams by regression of laboratory data (Eq. 3.6).

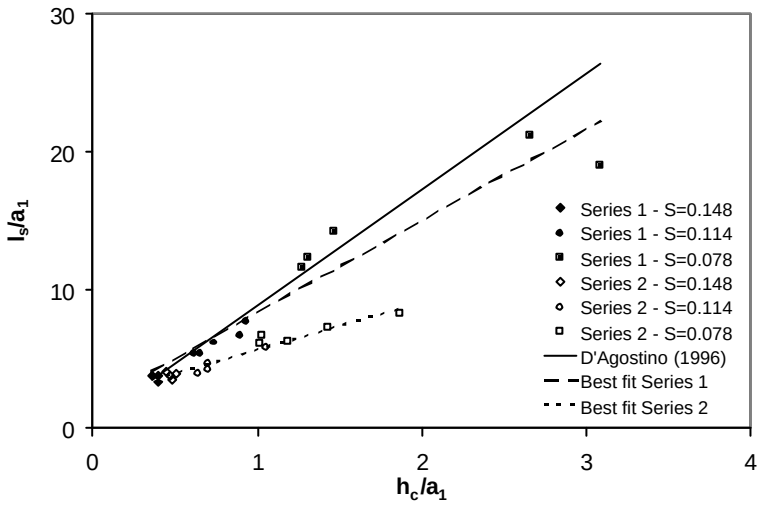

Figure 4.24 - Non-dimensional scour lengths l_s/a_1 against parameter h_c/a_1, along with D'Agostino's (1996) prediction.

The agreement between Series 1 data and Equation 3.6 is fairly good. On the contrary, Series 2 scours exhibit highly reduced lengths with much weaker dependence upon the critical flow depth as depicted by the flatter trend, similarly to the maximum scour depth (Fig. 4.22).

As to the influence of the jump a_1, Fig. 4.25 illustrates again a similar pattern to the respective normalized scour depth (Fig. 4.23), with Series 2 data falling below and showing a steeper trend compared to Series 1 points.

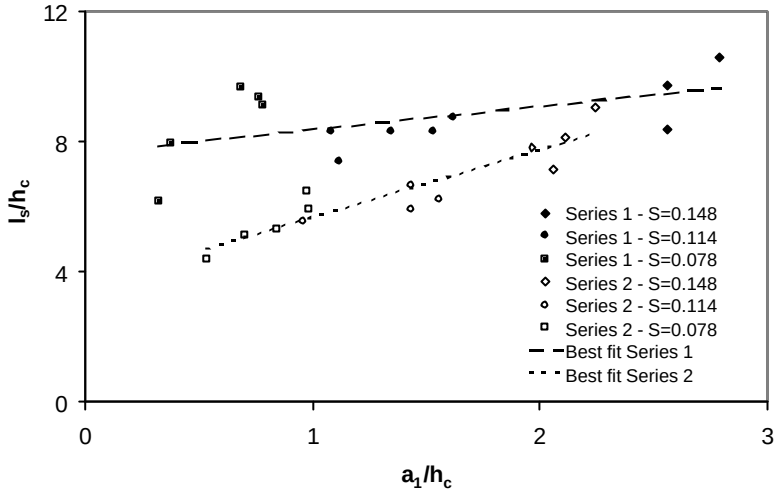

Figure 4.25 - Non-dimensional scour lengths l_s/h_c against parameter a_1/h_c.

Scour hole geometry

Comparing the non-dimensional profile – scaled to the scour length – of all scour holes, they do not exhibit similarity (graph not shown), since the inclination of the downstream side of the hole is variable and is correlated to the jet impact angle as demonstrated by several authors (see section 3.2.2). However, when the scour dimensions are scaled differently – the longitudinal distance x to the scour length and vertical depth y to the maximum scour depth – Series 1 and 2 data form a definite unique profile, even if with some scatter (Fig. 4.26). Therefore these scour holes seem to be self-affine.

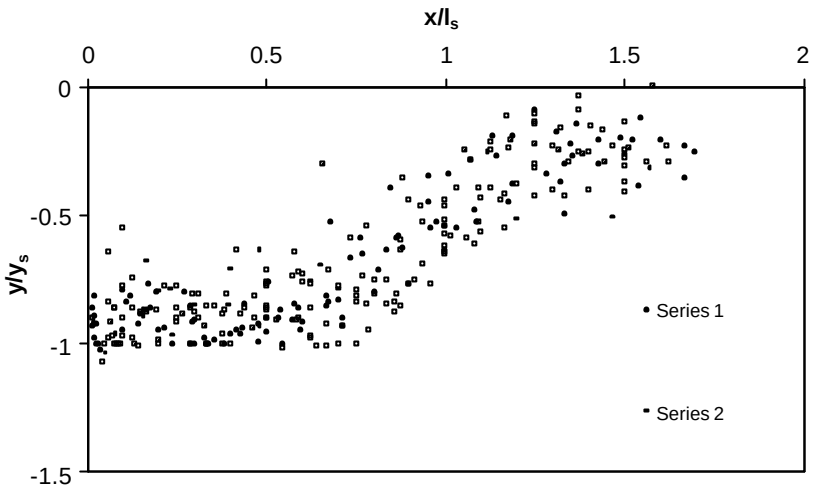

Figure 4.26 - Non-dimensional profiles of the scour hole: the longitudinal distance *x* is scaled to the scour length whereas the vertical dimension *y* is scaled to the maximum scour depth.

Franke (1968), analysing the experiments carried out by Eggenberger and Müller (1944), proposed a relationship between the scour length l_s and the scour depth s with respect to the original horizontal bed level which included the tailwater depth h:

$$\frac{l_s}{(h+s)} = 1.8 \qquad (4.6).$$

For the present experiments, it can be assumed $s = y_s - a_1$ ("residual depth") whilst h to correspond to the measured flow depth downstream from the scour hole, h_v . The plot reported in Fig. 4.27 shows a remarkable agreement between Series 1 and 2 runs. In spite of the scour length reduction in Series 2, the result suggests that the overall geometry of the scour hole is roughly constant. From the best fit line in Fig. 4.27, it results:

$$\frac{l_s}{(h_v+s)} = 2.9 \qquad (4.7)$$

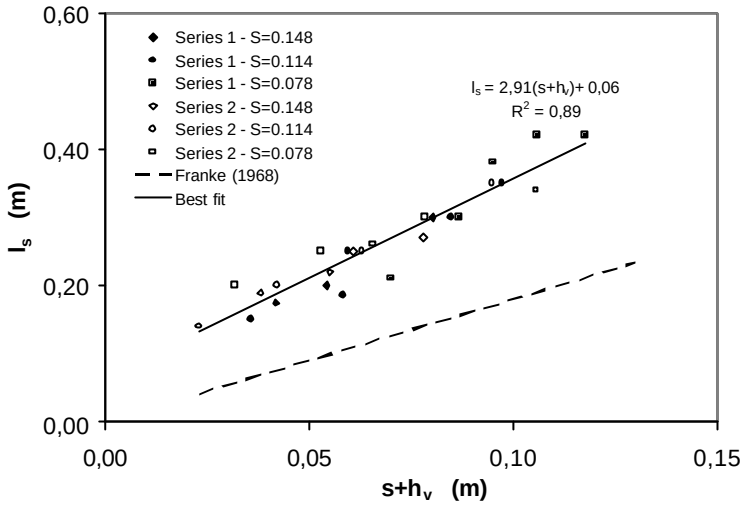

Figure 4.27 - Dimensional relationship between scour length and the residual scour depth added to the tailwater depth.

The difference with Equation 4.6 might be due to the definition of the tailwater level, i.e. at what distance from the roller it has to be evaluated. The same "consistency" between scour length and depth is illustrated in Fig. 4.28. Despite run *T*14 displaces far above the other points, there is a clear trend that indicates a decrease of l_s/y_s with the ratio a_1/h_c.

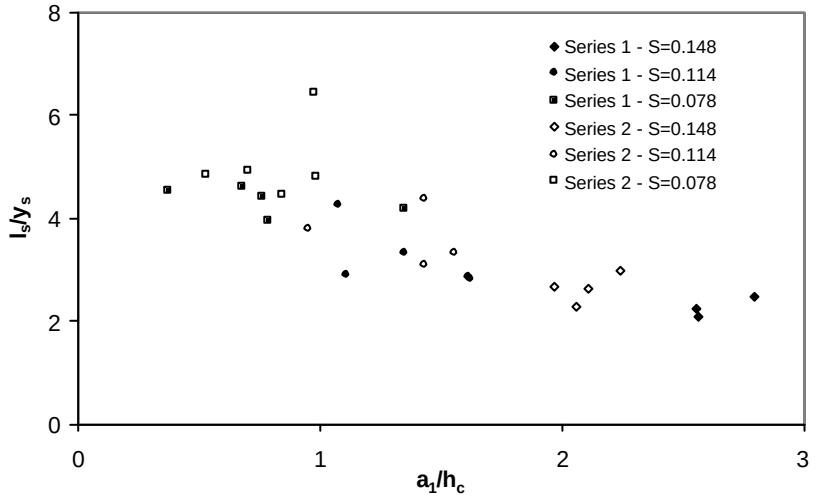

Figure 4.28 - Scour length-to-depth ratio l_s/y_s as a function of the parameter a_1/h_c.

A unique relationship between y_s and l_s seems to exist, shown in Fig. 4.28, regardless of the distance between the sills. This suggests that the difference in scour hole dimensions between Series 1 and 2 does respect a geometric constraint. It is therefore hypothesised that

scour length controls the maximum scour depth. When both the scour length l_s and the flow critical depth h_c are scaled by the spacing L, a fairly consistent relationship (R^2=0.92) is found between the two data sets (Fig. 4.29):

$$\frac{l_s}{L} = 1.10 + 0.24 Ln\left(\frac{h_c}{L}\right) \qquad (4.8).$$

The ratio h_c/L is also used in fixed-bed, stepped-channel hydraulics for the determination of the flow regime, i.e. the onset of skimming flow from nappe flow (section 3.3.1). The ratio h_c/L might also enable the prediction of scour length as a proportion of the distance L. Obviously, the role of the grain size is neglected, and it may be expected that different curves can be obtained for other grain size distributions.

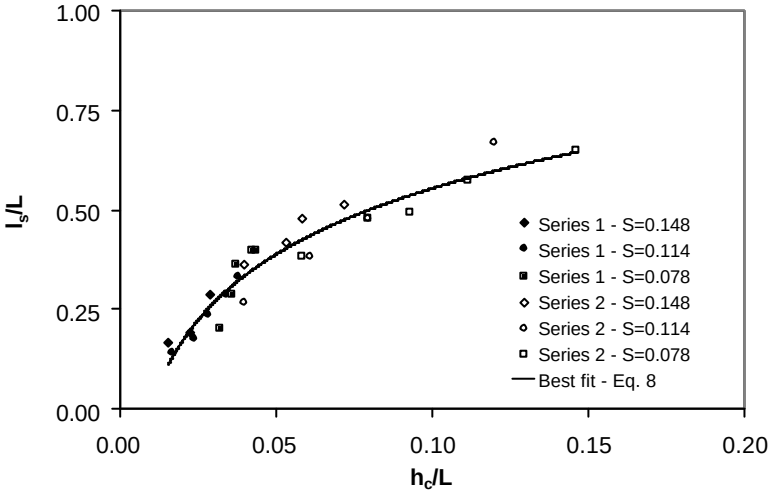

Figure 4.29 - The proportion of scour length to sill spacing as a function of the critical depth-sill spacing ratio.

The fact that scour lengths for different spacing can be brought together by a simple parameter is reckoned to be an important achievement. The unique log-like relationship (Eq. 4.8) implies that, beyond a certain value of h_c/L (in this case 0.06-0.07), the relative scour length can be increased only by much larger flow rates than below that point: a physical upper limit may exist to the ratio l_s/L. And the scour length would not be related to the channel slope. From all the non-dimensional plots shown above, it is apparent that bed slopes – initial and at the equilibrium – affect scour dimensions acting together to the creation of the morphological jump a_1 (Eq. 3.1). In fact no other influence can be inferred from the graphs.

Such a result may be explained by the fact that the flow was never supercritical (see section 4.1.1); this renders the equilibrium flow energy at sills equal to the critical (Fr=1) condition notwithstanding what the bed slope is. On the other hand, the initial slope affects the temporal evolution of the bed: at higher slopes the shear stress at the beginning of the test is larger and bed degradation occurs at a faster rate.

The part of scour length downstream of the point of jet impact is likely to be determined primarily by the length of the turbulent roller associated to the hydraulic jump: closely-spaced sills would then constrain the roller. In fixed bed channels, a threshold exists where hydraulic jumps disappear and skimming flow onsets (see section 3.3.1). In erodible bed channels, the phenomenon called "unstable tumbling flow" reported by Whittaker (1987_a) is likely to be analogous. In fact, by observing his photographs (p. 557), water flows without jumps in a smooth undular pattern. In these conditions, the scour depths no longer increased with discharge, but even decreased (see section 3.3.2).

The large reduction of the scour dimensions caused by close-spaced sills, here called “interference”, seems to be a “smooth” passage from an unconstrained condition to a limited one where the boundaries heavily affect the hydrodynamics of the system, rather than a discontinuity. The altered flow pattern would no longer be able to degrade the bed as much as without the forcing sill.

Taking into account that the maximum scour depth seems to follow roughly a same proportionality with the scour length for both Series 1 and 2 (Tab. 4.1 and Fig. 4.28), the hypothesis that the maximum scour depth might be directly linked to the ratio l_s/L is also tested (Fig. 4.30). Here the maximum scour depth y_s is scaled to the total elevation drop Z (eq. 3.2) for each step. A general trend is apparent, even if the points of Series 2 displace below the others in the common range of the l_s/L ratio. The graph provides an interesting yet partial “unification” between the two scour dimensions (i.e. depth and length) for both Series. However, further studies are needed to confirm such a result.

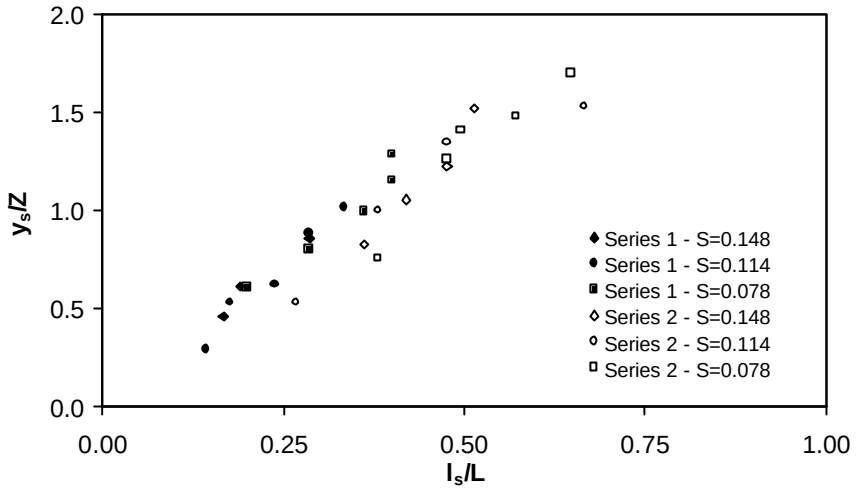

Figure 4.30 - Maximum scour depths normalised to the stream energy loss plotted versus the ratio between the scour length and the sill spacing.

4.2.3 Modeling the effect of geometrical interference and sediment gradation in steep channels

As shown in the previous section, if the downstream boundary condition – i.e. the next sill position – is closer than a certain distance, the size of the scour hole can be significantly smaller compared to the potential scour that may form in an unrestricted geometry. This effect, named 'geometrical interference' would make scour formulae over-predictive in these cases.

In order to take into account the effect of structure spacings, the length L should be added to the list in (3.20), leading to the introduction of a new dimensionless group. In addition, the effect of sediment gradation could be accounted for using an appropriate parameter. Here, the gradation coefficient s_g (Bunte and Abt, 2001) will be used, it being defined as:

$$s_g = \frac{\frac{D_{84}}{D_{50}} + \frac{D_{50}}{D_{16}}}{2} \tag{4.9}$$

With those assumptions, Eq. (4.1) becomes:

$$\frac{y_s}{H_s} = f_2\left[\frac{a_1}{\Delta D}, \frac{a_1}{H_s}, \frac{L}{H_s}, s_g\right] \tag{4.10}.$$

The new formula for interfering scour should include the one for 'free' scour as a particular case when L/H_S becomes sufficiently large. It was decided to adopt the following structure for equation 4.10:

$$\frac{y_s}{H_s} = f_1\left[\frac{a_1}{\Delta D}, \frac{a_1}{H_s}\right] f_3\left[s_g\right] f_4\left[\frac{L}{H_s}\right] \tag{4.11},$$

with:

$$f_3\left[s_g\right] = 1 \qquad \text{for} \quad s_g = 1 \text{ (uniform sediment size)} \tag{4.12},$$

$$f_4\left[\frac{L}{H_s}\right]=\begin{cases}1 & as \quad L/H_S \to \infty \\ 0 & as \quad L/H_S \to 0\end{cases} \qquad (4.13).$$

A power law is adopted for f_3, while an exponential formula is chosen for f_4, as described later. In order to find out equation (4.11), first equations f_1 and f_3 will be derived using data from non-interfering scour holes on high slopes: Wallingford Series 1 tests (s_g=5.95, section 4.1.1), Padova "unconstrained" scour holes (s_g= 1.48, excluded the runs with S=0.03 as explained in section 4.1.2), and 13 scour measurements from the Cordevole River (Italy, Lunardi, 2002) in order to have some data with intermediate values of sediment gradation (s_g=3.95, mean channel slope S=0.06). Once expressions for f_1 and f_3 are obtained, f_4 will be derived using results of 60 "constrained" scour holes from Padova and Wallingford Series 2 tests, the runs which exhibited geometric interference as described above. Overall, 108 scour holes have been used for the regression analysis (Zanini, 2002).

Prediction of scour depth with non-interfering geometry for steep gradients

In the original work on non-interfering scour holes on mild slopes, Gaudio et al.(2000) starting from the non-dimensional equation (3.29), found that the dimensionless scour depth could be expressed as a function of only one parameter, a_1/DD.

For the high-gradient data considered here, instead, it was found that the other dimensionless parameter in (3.29), a_1/H_s, is sufficient to account for equilibrium scour depth. It was obtained:

$$f_1\left[\frac{a_1}{\Delta D},\frac{a_1}{H_s}\right]=2.68\left(\frac{a_1}{H_s}\right)^{0.43} \qquad (4.14)$$

$$f_3[s_g]=s_g^{-0.19} \qquad (4.15)$$

applicable in the ranges $0.188<a_1/H_s<1.872$ and $1.48<s_g<5.95$, with a correlation coefficient R^2=0.798.

The addition of a_1/DD does not increase the capability of the formula to fit the data, indicating that sediment size plays a minor role in the scouring dynamics if sediment gradation is accounted for. However, sediment size does affect scouring by determining the

equilibrium slope and therefore the morphological jump a_1. Equation (4.14) shows that the scour depth scales with approximately the square root of the morphological jump, whereas equation (4.15) indicates that the dependency from the gradation coefficient – the more heterogeneous the sediment, the shallower the scour holes – is smaller but still relevant, being the exponent close to 0.2.

Prediction of scour depth with interfering geometry

The plot of the deviation (Fig. 4.31) of the data relevant to interfering scour holes using the product of Eqs. 4.14 and 4.15 showed that the correction formula f_4 (Eq. 4.13) could be written as follows:

$$f_3\left[\frac{L}{H_s}\right] = \left(1 - e^{-b\frac{L}{H_s}}\right) \qquad (4.16),$$

where β is a calibration exponent. The data on interference led to $b = 0.14$, so that:

$$\frac{y_s}{H_s} = 2.68\left(\frac{a_1}{H_s}\right)^{0.43} s_g^{-0.19}\left(1 - e^{-0.14\frac{L}{H_s}}\right) \qquad (4.17),$$

which fits the 108 measured data rather well (Fig. 4.32), with a correlation coefficient R^2 = 0.872. Equation (4.17) shows that the effect of geometrical interference is within 10% apart from the potential scour for sill spacing larger than 16 times the critical specific energy of the flow, and within 1% for sill spacing larger than 32 times the critical specific energy of the flow. This implies that some sequences may act as non interfering at relatively low flow stages, but may act as interfering at high flow stages.

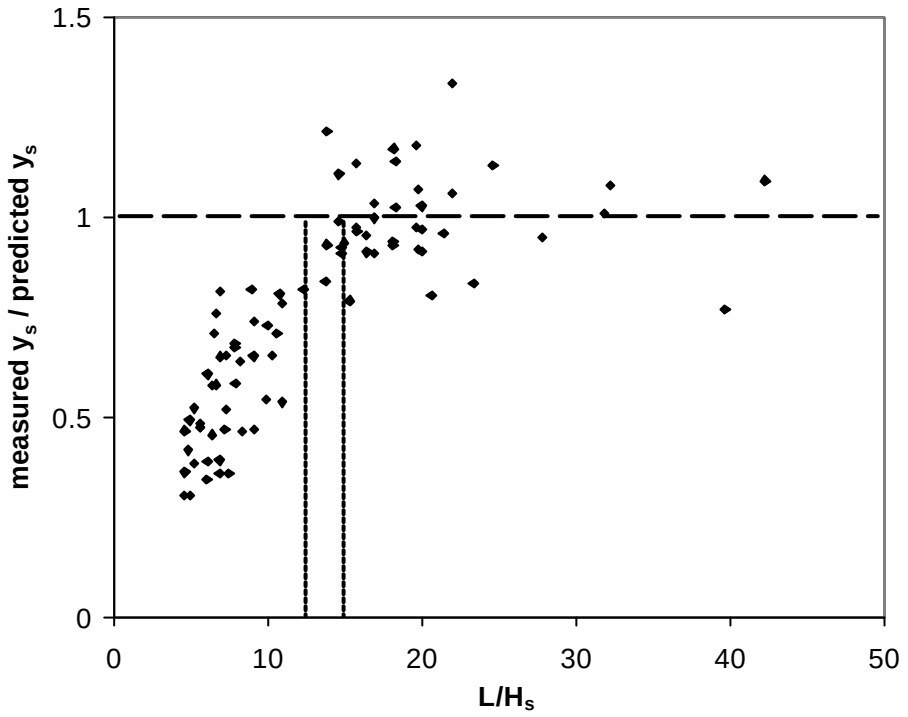

Figure 4.31 - The effect of the geometrical interference expressed as the reduction of the ratio actual-to-potential scour depth, the latter evaluated predicting depths by non-interference predictive eqs. 4.14 – 4.15. The vertical dotted lines delimitate the range $12<L/H_s<15$ below which interference is clearly present.

From Figure 4.31, it appears that interference onsets when the ratio L/H_s is smaller than 12-15, no matter sediment size and grading. Typically, natural step pool sequences present step spacing in accordance with the above range during high flows when the parameter L/H_s in such a natural tumbling flow pattern becomes very small (see section 6), as long as steps are not destroyed. Equation 4.16 might in part explain the great stability of these step pool sequences, at least with reference to the toe scouring at pools which has been observed to be a primary responsible for steps destruction, both in the field (Lenzi, 2001) and in the laboratory, where 76.6 % of all step break-ups were due to pool scouring (Crowe, 2002, see section 2.5)

Finally, Equation 4.17 could be tentatively used – with a_1 equal to the difference in height between successive steps – to evaluate what water discharge is needed to cause step undermining and thus removal by toe scouring, if the average number and diameter of step-forming clasts are known in a vertical section. Step destruction can be assumed to occur when the maximum scour depth becomes larger than the total vertical height of step-forming clasts.

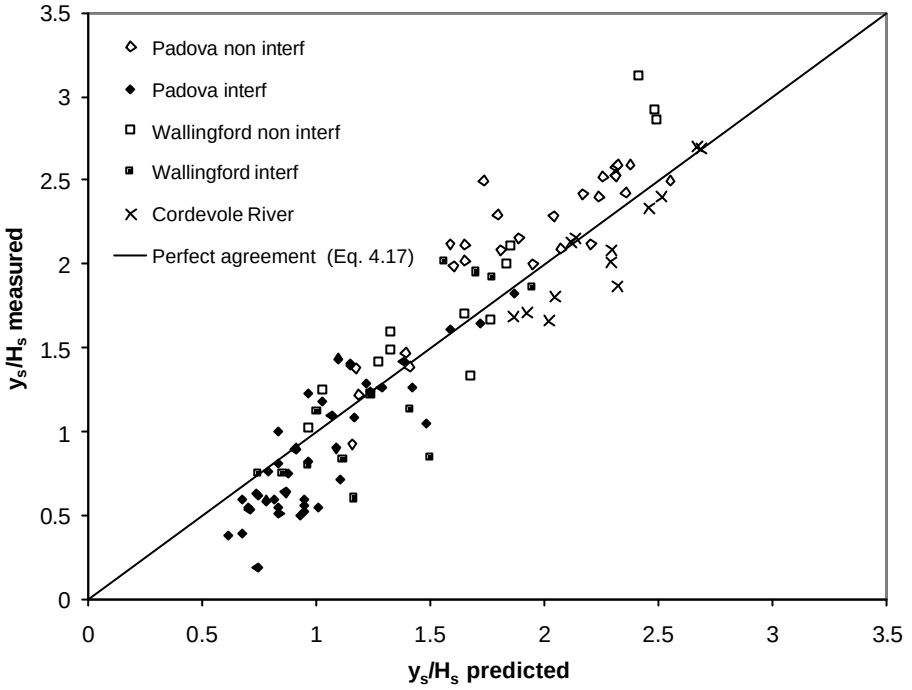

Figure 4.32 - Comparison of scour depths estimated with equation 10 and the experimental data for both non-interfering and interfering scours, plus field data from the Cordevole River.

4.2.4 Scour length, shape and volume

Turning now to the scour length l_s, for non-interfering conditions a simple relationship with the specific critical energy H_s is shown in Fig. 4.33, where data from Padova tests and Wallingford Series 1 seem to follow the same trend, notwithstanding their relevant differences about grain size distributions. Furthermore, it appears that no control is exerted on scour length by other variables, such as the morphological jump a_1 and jet geometry: the flow energy dominates the determination of the longitudinal dimension of scour holes. The best fit equation turns out (imposing the intercept at 0):

$$l_s = 6.56 H_s \qquad (4.18).$$

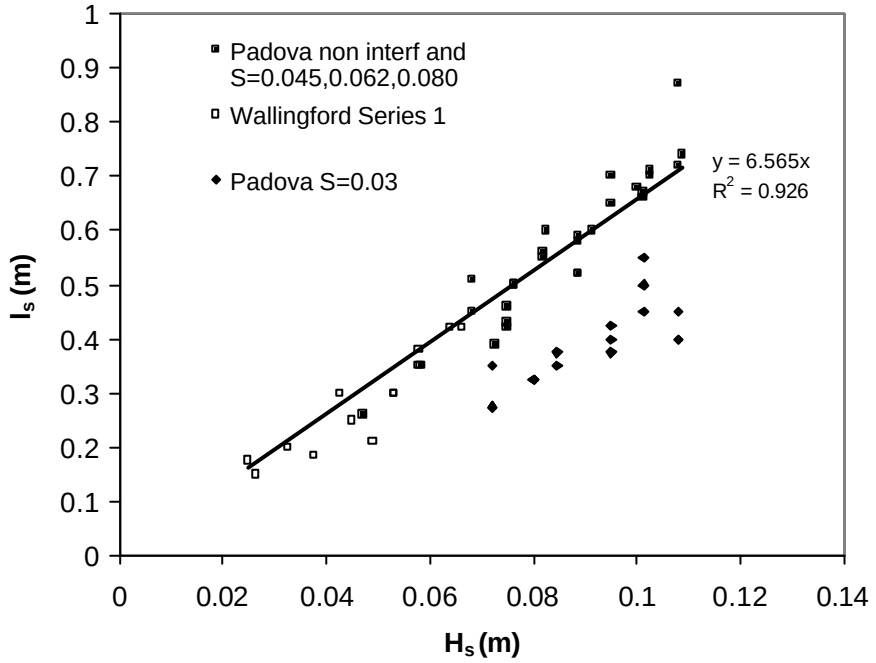

Figure 4.33 – Scour length vs specific critical energy. The trend line does not consider Padova S=0.03 scour holes.

Padova interfering scour holes are not analyzed here, because in most of them scour length has no longer meaning as a variable, being represented by the downstream sill location when the hole extended up to the next baffle (Zanini, 2002).

In Fig. 4.33, points from Padova $S = 0.03$ – those displaying the peculiar standing wave pattern as described in section 4.1.2 – are also plotted, where the first crest distance L_{b1} (see

4.2.5) is considered as scour length. They fall well below the trend line. Hydraulic phenomena controlling scour longitudinal extension are therefore different in the lowest gradient runs, and they will deserve a closer look in the next sections.

Let's analyze now the shape of scour holes. In order to do this, a normalization is required to put together different dimensional profiles. The experimental runs from the Padova set (expect those having S=0.03) will be used. The dimensionless scour hole profiles where both longitudinal and vertical dimensions are scaled to the scour length – thus allowing to seek possible self-similarities – are shown in Fig. 4.34, 4.35 and 4.65, which refer respectively to spacing L=1.5 m (S1-M3-M4, non-interefering conditions), to L=0.75 m (S2-S3, interfering) and to L=0.5 m (S4-M1-M2, interfering).

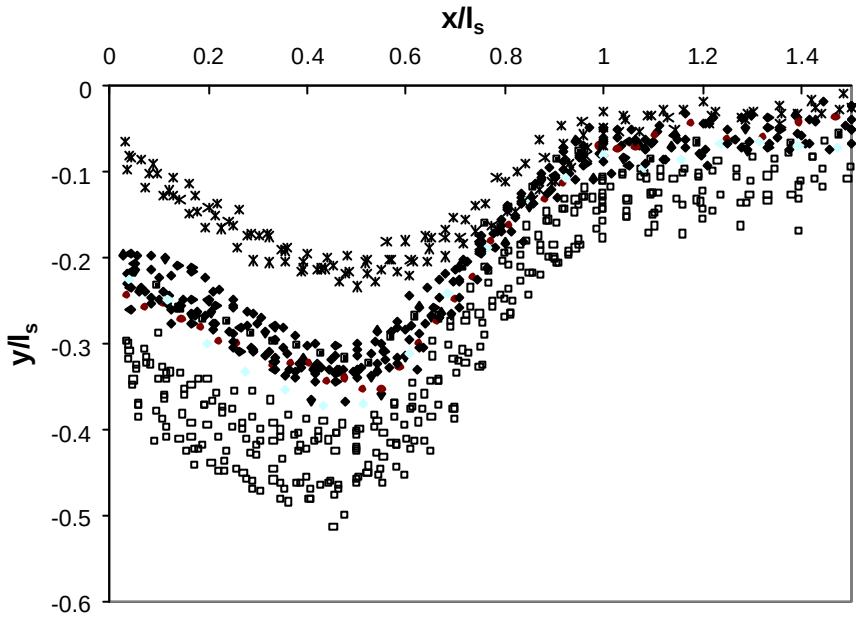

Figure 4.34 – Self-similarity in Padova non-interfering scour holes, grouped according to their initial slope: 0.045 (crosses), 0.062 (black squares) and 0.080 (white squares).

First, it is evident that self-similarity can be assumed to be valid only for a same initial slope, due to the general lowering of the profiles caused by higher morphological jumps occurring for higher slopes (Eq. 3.1). Such an effect is more apparent in Fig 4.34, where the largest spacing brings about the largest variation of the jump a_1. Instead, for the shortest spacing (Fig. 4.36), the various profiles are less distinct, especially for S = 0.08. It must be pointed out, however, that the upstream side of the scour hole presents large scatter because in many tests this part happened to be altered when closing the pump of the flume, whereas the remaining profile was not affected. Approximately, the maximum scour location lies always around $0.5l_s$, and the lower the initial slope, the more symmetric the scour hole.

Besides, self-similarity does not hold because the larger the initial slope, the more inclined the downstream side of the scour hole, probably because of the larger drop heights causing the jet to impinge more vertically (see section 3.2.2). The same result was also inferred in section 4.2.1.

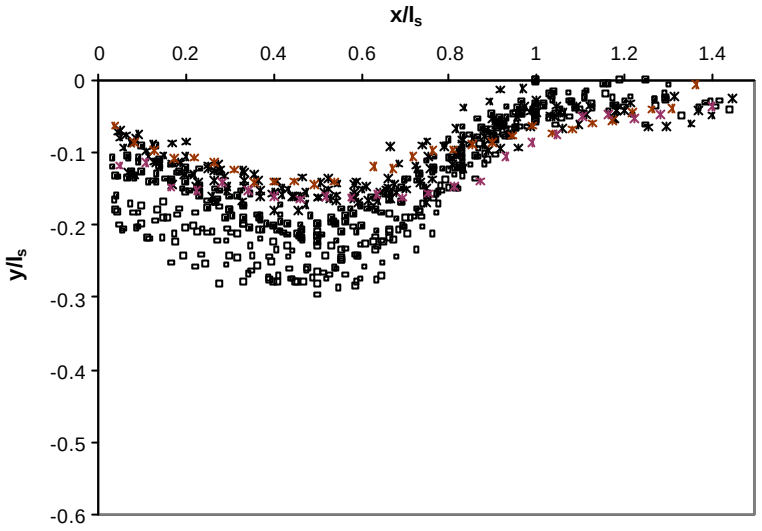

Figure 4.35 – Self-similarity in Padova interfering scour holes S2-S3 (L=0.75 m), grouped according to their initial slope: 0.045 (crosses), 0.062 (black squares) and 0.080 (white squares).

Therefore, no self-similarity can be ascribed to the entire set of scour holes. Nevertheless, as obtained for Wallingford tests (section 4.2.2), scour profiles exhibit a well defined self-affinity (Fig.4.37).

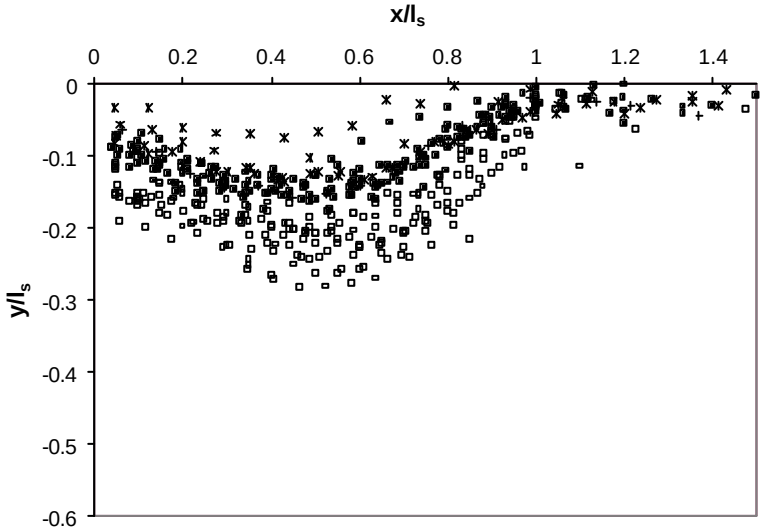

Figure 4.37 – Similarity in Padova interfering scour holes S4-M1-M2 (L=0.5 m), grouped according to their initial slope: 0.045 (crosses), 0.062 (black squares) and 0.080 (white squares).

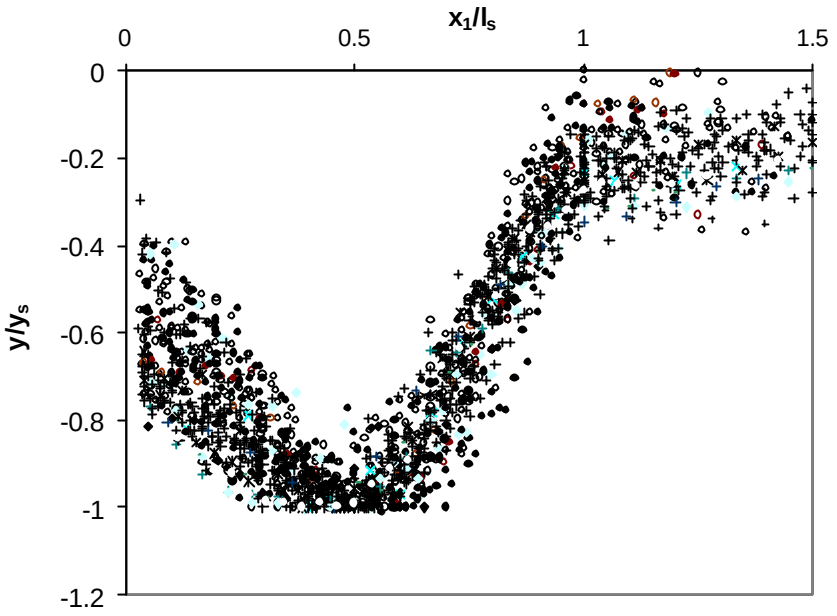

Figure 4.37 – Affinity in Padova scour holes: black circles refer to S4-M1-M2 (L=0.5m); white circles to S2-S3 (L=0.75 m), and crosses to S1-M3-M4 (L=1.5 m).

This finding implies that only two scale parameters, y_s and l_s, determine the scour hole area and its volume – if holes are two-dimensional – given the underlining geometric invariance. This hypothesis has been tested evaluating the scour area for each scour hole by using the software AUTOCAD 2000, as defined in Fig. 4.38. From an initial level bed, the eroded sediment within two sills can derive from a triangular wedge W produced by the bed slope decrease, whose specific (i.e. per unit width) volume can be approximated as $0.5a_1L$, and from the residual scour hole V volume due to the localized erosion. Plotting $A=V/b$ (scour area or volume per unit width) against the product of the two scale parameter y_s*l_s, a well-defined linear trend appears with a high correlation $R^2=0.954$ (Fig. 4.39). The best fit equation – imposing the intercept at 0 for sake of rationality – turns out:

$$A = 0.564\, y_s l_s \qquad (4.19),$$

where the value 0.564 represents a sort of shape coefficient for scour holes.

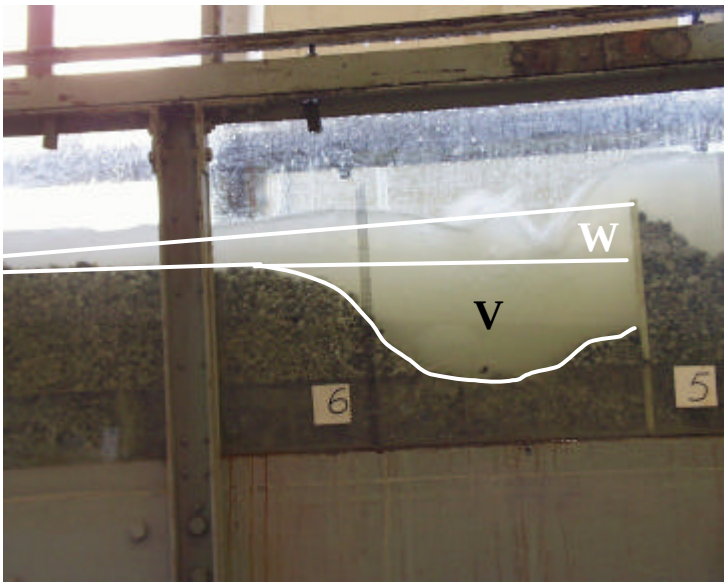

Figure 4.38 – Graphic definition of the scour hole volume considered in the analysis.

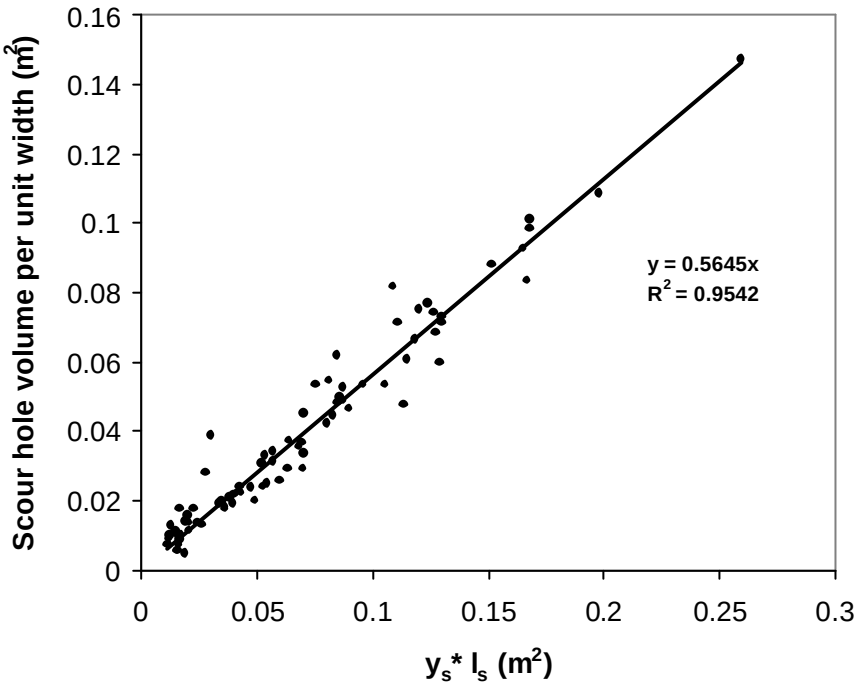

Figure 4.39 – Scour hole volume per unit width versus the product $y_s * l_s$ for all Padova scour holes (tests with S=0.03 are not included).

4.2.5 Morphodynamic interference

Padova tests with an initial slope S = 0.03 showed a rather different behavior compared to the other experiments, both about flow hydrodynamics and bed deformation. In fact, the combination of the experimented flow rates and sediment properties together with the initial slope value did not lead to a substantial general degradation of the bed, on the contrary of what occurred at higher slopes. There, the morphological jump a_1 could develop after some minutes because the equilibrium slope determined by the flow-sediment rates was much lower than the initial channel slope, i.e. bed stability was far from equilibrium at the beginning of each run. Standing waves were observed only during the very first minutes of the runs, when the flow was slightly supercritical.

The conceptual approach adopted so far and the dimensional analysis assuming critical conditions on the sills requiring the evaluation of the morphological jump are no longer valid if the flow is even slightly supercritical. These are the conditions that occurred in the six tests described here. Standing waves prevented the bed from reaching a regular equilibrium slope. The absence of a proper equilibrium slope makes unfeasible to calculate and to use the morphological jump to quantify jet's drop energy.

In all the tests, at each drop a train of standing waves was generated which shaped the bed with in-phase undulations, similar to fixed antidunes (Fig. 4.40). After few hours (2-3), the bed would achieve its equilibrium state, i.e. no more sediment transport.

Let's first analyze local scouring at the uppermost sill S1, which was not altered by oncoming wave trains (Zanini et al., 2003). In Figure 4.41a the crude representation of the relationship between maximum scour depth y_s and specific water discharge q is shown. Looking at S1 data, they do not exhibit any clear positive or negative trend and the deepest hole is associated to an intermediate flow rate. However, scour holes' small dimensions compared to sediment grain size and their fewness make more detailed data analysis poorly significant. In Fig. 4.41b, the maximum scour depth is normalized to the critical flow depth h_c=2/3 H_s and then plotted against the Froude number at its sill, given by:

$$Fr_{sill} = \frac{q}{h_s (gh)^{0.5}} \qquad (4.20),$$

where h_s is the flow depth measured at the center of the sill (i.e. 5 mm before the lip). It can be noted that S1 ratios y_s/h_c range between 0.73 and 1.15 for Froude numbers almost constant, varying from 1.44 to 1.56.

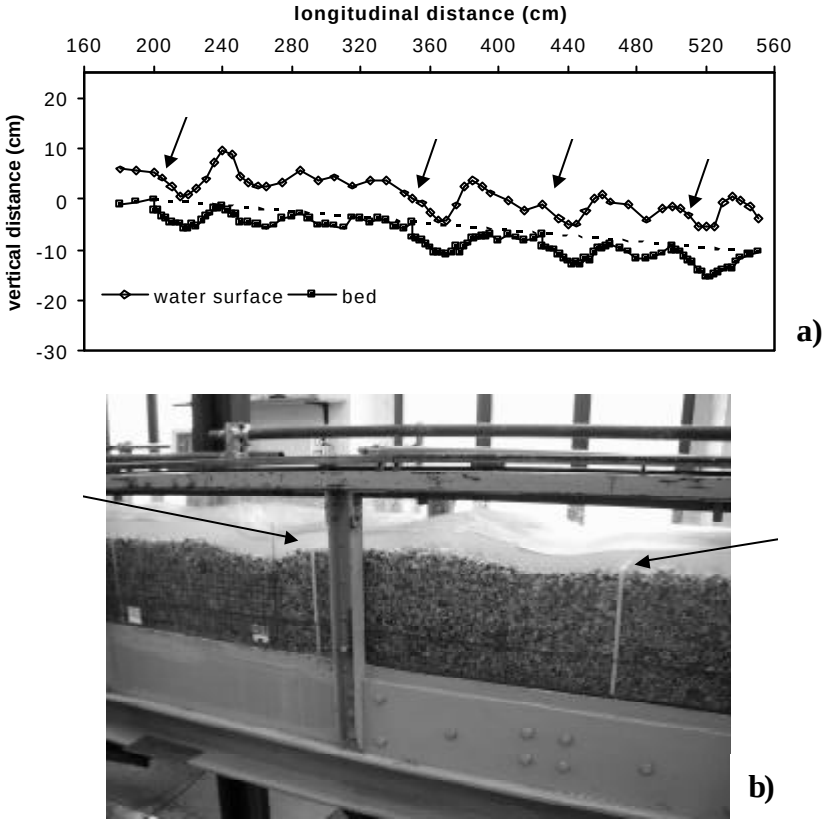

Figure 4.40 – PadovaTest 3 (q=0.0606 m^2s^{-1}), arrows indicate sills.
a) water and bed profile (from the left, S1-S4); b) side view of the reach S2-S4 from upstream.

Considering now the downstream scour holes (i.e. S2-S4), they plot generally below S1 data (Fig. 4.41a) without any evident systematic order among the six tests. Only a small improvement is made analyzing the data as in Fig. 4.41b: Froude number does seem to play a role in determining the scour depth – the higher the Froude, the deeper the holes – yet a large scatter still remains.

In one run (Test 5, q = 0.042 m^2s^{-1}) the bed sill S2 did not even produce any local scouring at the equilibrium, whereas the others caused well-defined scour holes. The variability of Fr_{sill} partly depends on the upstream flow disturbances, in fact for S1 – no bed sills upstream – the range is rather small, whereas for S2-S3-S4 it becomes much wider (Fig. 4.41b). Nevertheless a complex interaction involving also the downstream control (i.e. the next sill) might be responsible for the quasi-random dimensions of the scour holes, since Fig.

4.41b which includes only the upstream forcing does not provide an exhaustive analysis of the phenomenon.

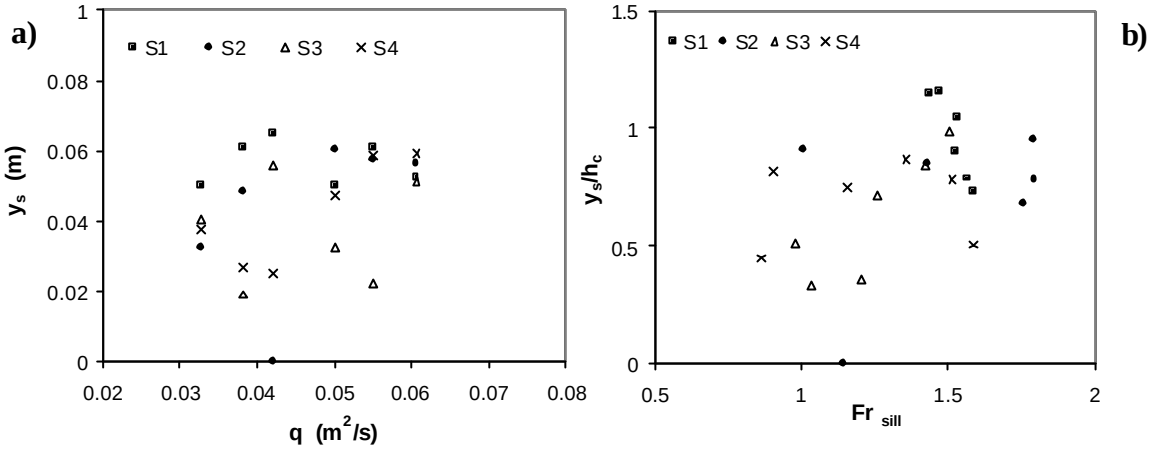

Figure 4.41 – Maximum scour depth of the scour holes: a) against the specific water discharge; b) in non-dimensional terms versus the flow Froude number on the sill.

In Figure 4.42 the reach from S2 to almost S4 is shown at the beginning of the Test 5, before S2's scour hole was filled because of upstream altered conditions. The standing wave generated by S2 is depicted with its associated in-phase bed form, a crest which resembles for curvature the scour hole (i.e. the trough). The effects of the standing wave upon the next sill are clearly visible: just upstream of S3 a trough is present which "masks" the presence of the sill, making the flow "skipping" the potential drop structure. The same kind of phenomena took place also at the bed sill S4, mostly forced by the presence of the S3.

Figure 4.42 – Test 5 (q=0.0420 m^2s^{-1}): side view of S2 (right arrow) and S3 (left arrow); the flow is from the right. This water surface and bed configuration was different at the end of the run.

In these runs, therefore, a morphodynamic interference occurred, in the sense that the existence of trains of standing waves with their spatial pattern of acceleration and deceleration (Chanson, 2000) superimposing on the bed sill configuration interfered with local scouring dynamics making scour hole dimensions rather unpredictable. This kind of interference, mainly due to upstream conditions, appears to be different from that described in section 4.2.2 arising from closely-spaced sills at steep slopes. In fact in that case: a) the flow was always subcritical, b) the control was by downstream boundary conditions, and c) the scour reduction turned out to follow a fairly predictable trend (section 4.2.3).

4.2.6 Wavelength of standing waves at drops

Near-critical flow conditions (i.e. flow energy close to its minimum and $Fr \tilde{} 1$) are common in channels with gradient around 0.01-0.03. Flow instabilities (i.e. water surface undulations) are inherent of such a condition (Henderson, 1970), and standing waves may establish over a part or across the whole section (Grant, 1997; Tinkler, 1997). The undulated water surface profile tends to shape the bed creating in-phase bedforms (Chanson, 2000) traditionally called antidunes because their tendency to travel upstream (Kennedy, 1963). Step pool architecture in steep mountain streams has been hypothesized to derive – under certain circumstances – from antidune trains (see section 2.4).

Standing wave trains are also generated by river structures that make an undular hydraulic jump to occur. This kind of jump forms at low supercritical inflow Froude numbers (Fr_1): traditional textbooks (e.g. Chow, 1959) report its occurrence for $Fr_1<1.7$. However, a certain experimental disagreement is present as to the upper Fr_1 value for its persistency before a direct jump (i.e. a jump with a surface roller) onsets: 1.6 was found by Reinauer and Hager (1995), around 1.7 by Ohtsu et al. (2001) for fully developed flow and by Bradley and Peterka (1957), between 1.5 - 2.9 by Chanson and Montes (1995), and as high as 3.6 by Montes (1986). Such a large range has been demonstrated to be at least partly determined by the influence of the aspect ratio B/h_1 (B=channel width and h_1=inflow depth; Chanson and Montes, 1995), of the turbulent boundary layer development d/h_1 (d=boundary layer thickness at the toe of the jump; Ohtsu et al., 2001), and of the Reynolds number (Ohtsu et al., 1995).

Wavelength and amplitude of standing waves and undular jumps have been studied both theoretically and experimentally. Kennedy (1963) derived the well-known equation for antidunes associated to standing waves:

$$\frac{L}{h} = 2pFr^2 \qquad (4.21),$$

where L is the antidune wavelength, h is mean undular flow depth, and Fr is the undular Froude number.

Andersen (1978) analyzed theoretically the problem of the wavelength of undular jumps through the linearization of the Boussinesq equation when the wave amplitude is small compared to the flow depth. The solution expressed in terms of Froude number is (Chanson, 2000):

$$\frac{L}{h_2} = \frac{1.79}{(1 - Fr_2)^{0.614}} \tag{4.22}$$

valid in the range $0.7 \leq Fr_2 < 0.9$, where h_2 is the conjugate flow depth and Fr_2 is the conjugate (subcritical) Froude number.

Chanson (1995) analysing free-surface profile data obtained (for $0.7 \leq Fr_2 < 0.9$):

$$\frac{L}{h_2} = 11.1 Fr_2^{3.5} \tag{4.23}$$

Reinauer and Hager (1995) found – for approaching supercritical flow $h_1 > 65$ mm in order to avoid scale effects – a linear influence of the inflow Froude number Fr_1, such that:

$$\frac{L_1}{h_1} = 6.5[1 + 0.5(Fr_1 - 1)] \tag{4.24}$$

where L_1 is the wavelength between the first and second crest.

Few studies have concerned characteristics of undular jumps generated by drops (Rajaratnam and Ortiz, 1977; Little and Murphey, 1982) as in the case of low grade-control structures. Little and Murphey (1982) derived experimentally an expression for the distance of the first crest from the drop:

$$\frac{L}{h_c} = 3.54 + 4.26\left(\frac{H}{h_c}\right) \tag{4.25}$$

with h_c being the critical flow depth and H corresponding to the drop height.

To date, no specific investigations have been published about standing waves at drops in mobile-bed channels. Direct field observations have nevertheless shown to the writer the formation of standing wavetrains at bed sills during a flood event in a channel with a slope around 0.02 (see Fig. 4.43). Padova tests with S=0.03 presented the opportunity to analyze standing waves wavelength (Comiti et al., 2003).

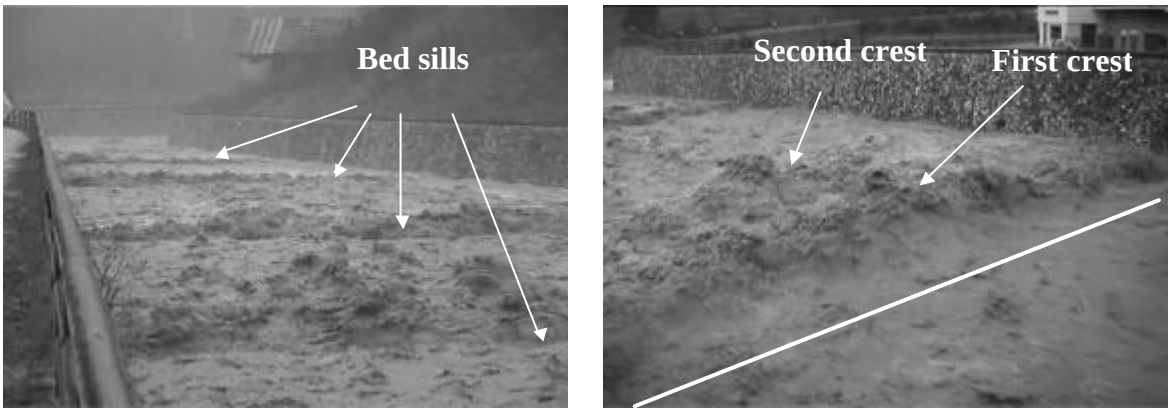

Figure 4.43 – Standing waves at bed sills in the Maè River (Eastern Italian Alps).

From the measured profiles the wavelengths of both free-surface and bed waves were calculated (Fig. 4.44). For each of the 6 tests, at every sill (except a S2 in one test) the first free-surface wavelength (i.e. the first after the sill, L_1) could be reliably determined, for a total of 23 values. As to the bedforms, only 18 first wavelengths (L_{b1}) were clearly detectable. 11 second wavelengths (L_2) were calculated from the water profiles, whereas only two were taken from the bed elevations (L_{b2}). Finally, 4 third wavelengths were measured from the free-surface (L_3) and again only two for the bed (L_{b3}).

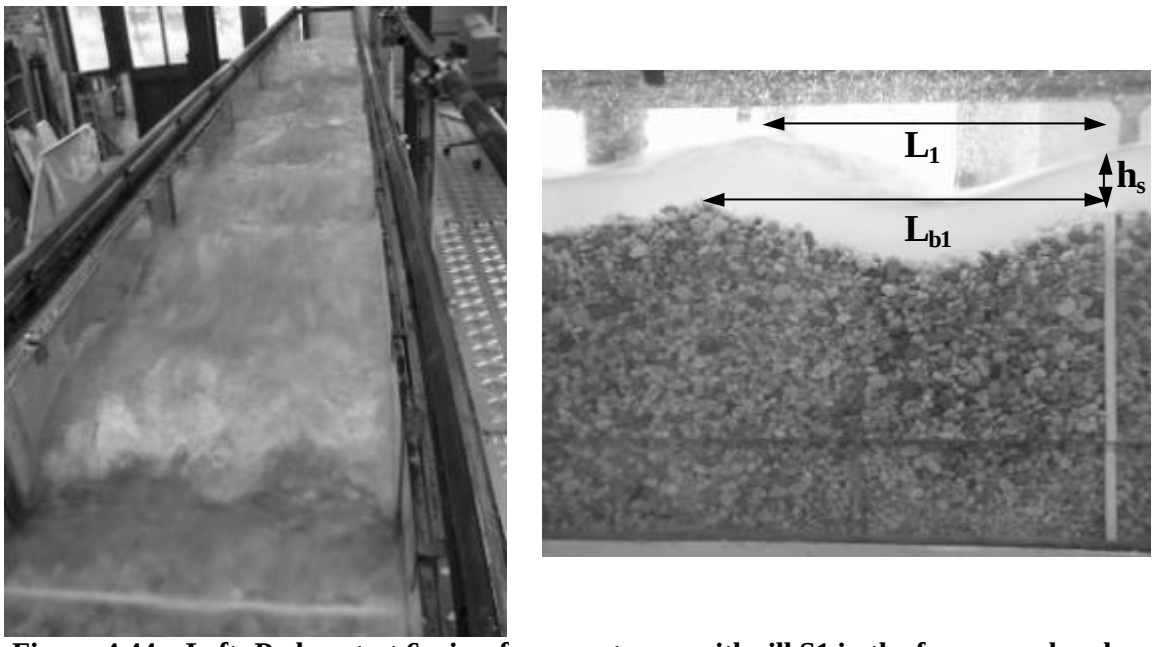

Figure 4.44 – Left: Padova test 6, view from upstream with sill S1 in the foreground and its associated first (breaking) standing wave; the two successive waves are not breaking; Right: Test 3: side view of sill S1 with superimposed the definition of the measured variables used in the analysis: L_1 free-surface first wavelength, L_b bed first wavelength, and h_s flow depth at the sill.

Sill Froude numbers ranged overall between 0.9 and 3.11, whereas considering S1 sills 5 out of 6 values are around 1.4-1.5. As discussed in the previous section, the variability of Fr_s seemingly depends mostly on upstream flow disturbances, in fact for S1 – no bed sills upstream – the range is rather small, whereas for S2-S3-S4 it becomes much wider for the presence of oncoming wavetrains generated upstream. However, cross-section uneven flow depths might be partly involved too, as measurements were taken along the centre-line only. Three-dimensional characteristics of standing waves will be therefore not addressed here.

Froude numbers were calculated also upstream of the first sill S1, in order to give an indication of the "undisturbed" flow regime: they ranged between 1.06 and 1.18, with no clear correlation with water discharge. The approaching flow was therefore very slightly supercritical, but no bedforms such as antidunes were observed or detected upstream of S1. Free-surface standing waves and associated bedforms occurred only because of the acceleration given by the developing drop at each sill, which raised the flow energy as high as to scour a trough followed by a deposition mound, i.e. the first standing wave crest, as described by Bateman et al. (2000, see section 3.3.2).

This disturbance propagated downstream generating a standing wavetrain in the reach S1-S2; this resulted well-defined until the first-order wave broke down forming a surface roller, then subsequent waves tended to become less steep and, in some cases, eventually flattened down. In such cases the bed profile kept a "reminiscence" of the former undular flow characteristics, exhibiting at the end of the run a slight undulated pattern not fully coupled with the equilibrium free-surface profile.

In Fig. 4.45 measured first wavelengths L_1 normalized to flow depth at sills h_s are plotted against the corresponding sill Froude numbers as calculated through Eq. (4.20). Data have been subdivided among the different sills in order to discern if spacing and location could be involved in determining the wavelengths.

The dependence of Fr_s variability upon sill location – already mentioned above – is evident; however, non-dimensional first-order wavelengths seem not to be influenced by such variable, following a consistent trend driven by the sill Froude number only. It must be pointed out that two points (S3 and S4) present Fr_s even slightly below the unity, because flow at these sills was affected by the deceleration occurring at the crest of waves generated upstream. A positive linear trend is shown, with the following best-fit equation (R^2=0.90):

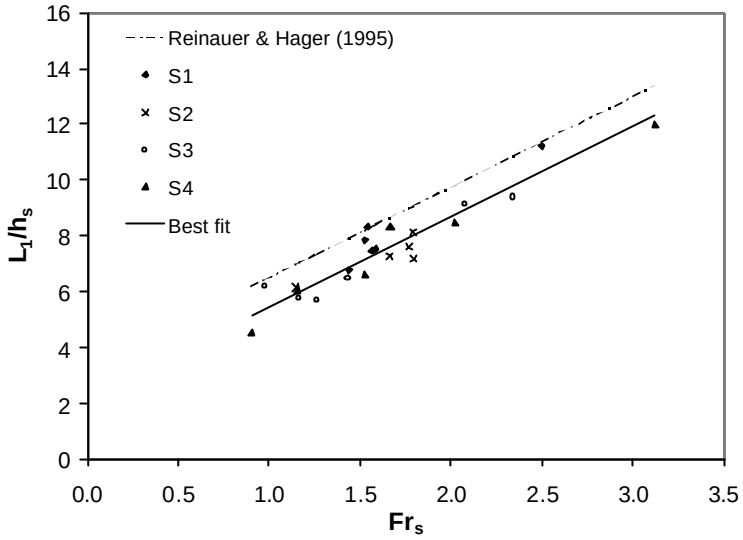

Figure 4.45 – Non-dimensional first-order wavelengths against sill Froude numbers.

$$\frac{L_1}{h_s} = 2.26 + 3.22 Fr_s \qquad (4.26).$$

In Fig. 4.45, equation 4.24 obtained by Reinauer and Hager (1995) for classical undular jumps in horizontal smooth channel is plotted too. The inclination of the two lines is definitely similar; equation 4.44's displacement above present data could suggest that the basic difference existing between these and Reinauer and Hager's experiments is due to the presence of a deformable sediment bottom. The larger roughness leads to higher energy dissipation that in turn causes a reduction of wavelengths.

For the comparison with equations 4.21 to 4.23, wavelengths have been normalized by the conjugate flow depth h_2 – as in Chanson and Montes (1995) – calculated with respect to sill flow depth h_s - and plotted against the calculated conjugate Froude number Fr_2 (Fig. 4.46).

Figure 4.46 shows that, in contrast to Equation 4.44, both Andersen (1978) and Chanson (1995) relationships derived for undular jumps consider a non-linear influence of the Froude number. However, Andersen's theoretical equation performs reasonably well in the range $0.5<Fr_2<0.7$ – i.e. roughly $1.4<Fr_s<2$ – but underestimates wavelengths; nonetheless, this interval falls outside of the validity range for such a relationship. On the other hand, for very low supercritical flows (i.e. for conjugate values $0.8<Fr_2<1$) Kennedy's equation for antidune wavelength seems more appropriate, nicely fitting five experimental points.

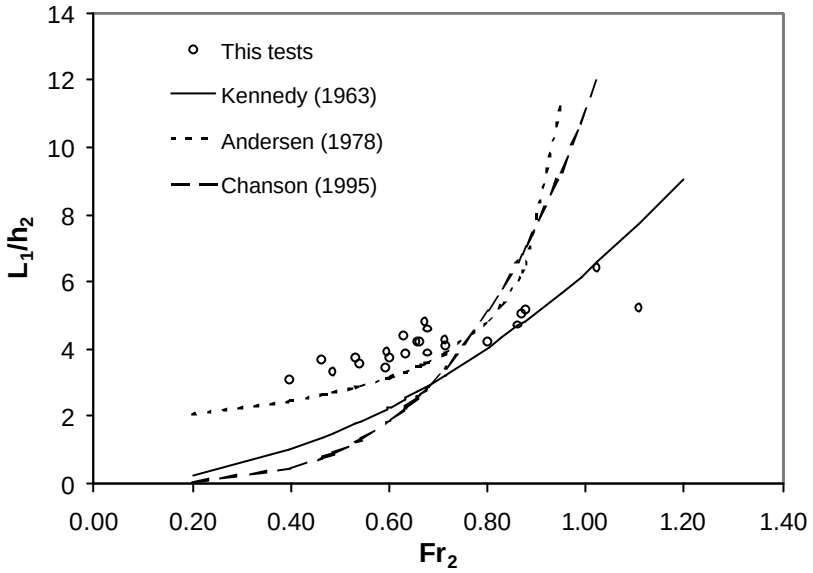

Figure 4.46 - Non-dimensional first-order wavelengths against conjugate sill Froude numbers.

In Table 4.6 higher-order (i.e. subsequent) free-surface wavelengths are considered, expressed as the ratio to their corresponding first-order ones, L_2/L_1 and L_3/L_1. Unfortunately, very few data are available for the latter. In the same table bedform first wavelengths are shown too, in terms of ratio to the associated free-surface wave, L_{b1}/L_1.

Table 4.6 – Free-surface and bedform wavelengths normalized to first-order free-surface wavelengths.

	Sample dimension	Mean value	Range
L_2/L_1	11	1.07	0.87-1.33
L_3/L_1	4	1.27	1.07-1.43
L_{b1}/L_1	18	1.16	1.00-1.43

No downstream reduction in free-surface wavelength is shown, as commonly observed for classical experiments on undular jumps (Chanson and Montes, 1995). On the opposite, mean values are slightly higher than 1 and L_3/L_1 is even greater than L_2/L_1, but only 4 third wavelengths were detectable. This seems to be more in accordance with the observed wavelength invariance in antidune wavetrains (Kennedy, 1963).

As to bed undulations, on average first crests are slightly shifted downstream from water surface crests. This is probably due to the fact that a surface roller formed on the first waves in most of the runs after the sediment mounds were deposited up to their final height. Wave breaking caused free-surface at crests to be pushed a bit upstream, thus somewhat shortening water surface wavelength, without affecting the bedform previously molded.

Finally, first free-surface wavelengths L_1 have been normalized to the critical flow depth h_c calculated from each specific water discharge q (g being the acceleration due to gravity) as:

$$h_c = \sqrt[3]{\frac{q^2}{g}}$$

A rather unexpected invariance is shown in Figure 4.47, where on the x-axis the sill Froude numbers Fr_s is present as in Figure 4.45. The positive correlation with Fr_s is no longer present. L_1/h_c mean value is 5.46, the range is between 4.85 and 6.30 with a standard deviation of 0.42. No previous similar findings have been traced in the literature.

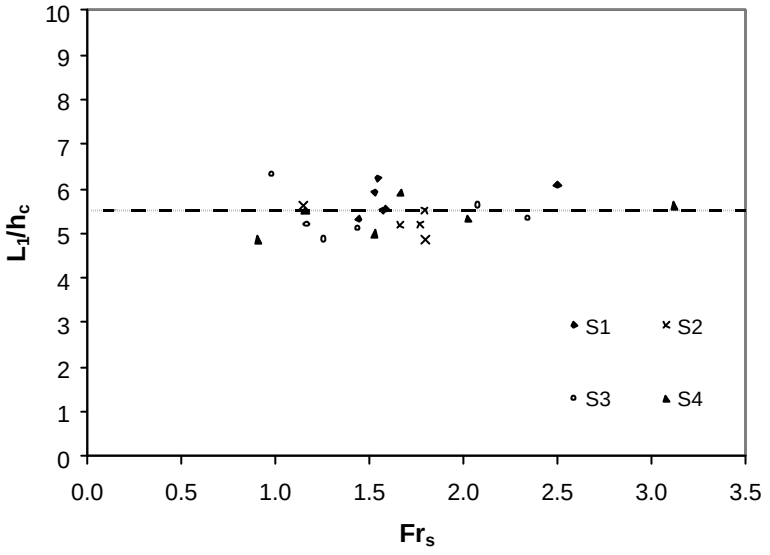

Figure 4.47 - Non-dimensional first-order wavelengths against sill Froude numbers. Wavelengths are normalized to the calculated critical flow depth h_c instead of the measured sill flow depth h_s as in Figure 4.45. The horizontal line represents the mean value.

5. FIELD MEASUREMENTS

5.1 Scour dimensions at grade-control structures

Study sites

Several characteristics of local scouring below grade-control structures in six mountain rivers in the Eastern Italian Alps (Fig. 5.1) were measured in summer 2001 (Comiti et al., 2002; Lenzi et al., 2003$_b$). All the streams are perennial and present a typical Alpine hydrologic regime, with two periods of high stages: in autumn (rainfall floods) and spring (snowmelt runoff). Their mean longitudinal gradients range between 0.02 and 0.16 (Table 5.1). The watersheds are geologically different and very complex. Sediment gradings are, however, highly non-uniform with streambeds characterised by an armour layer of coarse clasts.

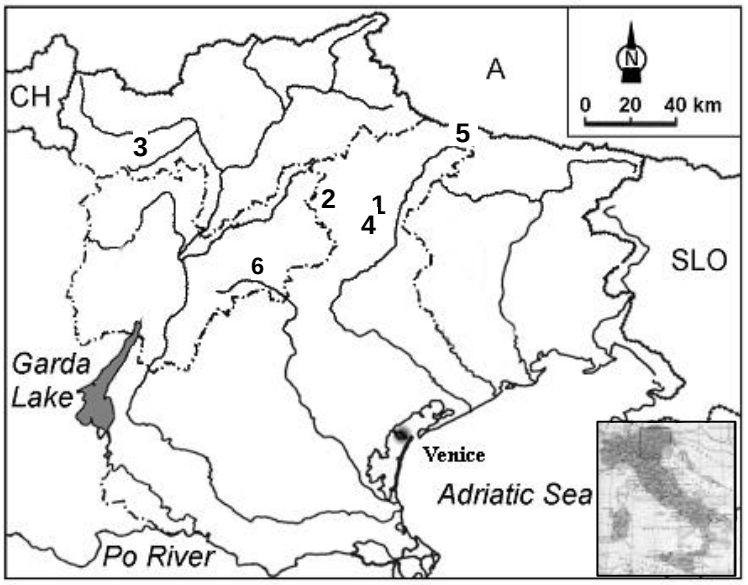

Figure 5.1 – Location map of the six mountain rivers object of the study in North Eastern Italy: 1=Maè, 2=Biois, 3=Plima, 4=Pramper, 5=(Cordevole di) Visdende, 6=Maso (di Spinelle).

Table 5.1. Some characteristics of the surveyed rivers.

River	Channel slope S[a]	Discharge Q[b] (m^3s^{-1})	Geology[c]	No. scour holes
Mae'	0.02	30	D, L, S	10
Biois	0.05	11	D, L, S, I	3
Plima	0.04-0.09	20	Gr, Me	22
Pramper	0.14	10	D, L	4
Visdende	0.10-0.15	30	Me, S, L	5
Maso	0.12-0.16	52	Gr, Me	29

[a] Mean gradient between work's crests (see Fig. 5.2);
[b] Peak discharge used for scouring data analysis;
[c] D=dolomites, L= limestones, S=other sedimentary rocks, I=igneous rocks, Gr=Granites, Me=metamorphic rocks.

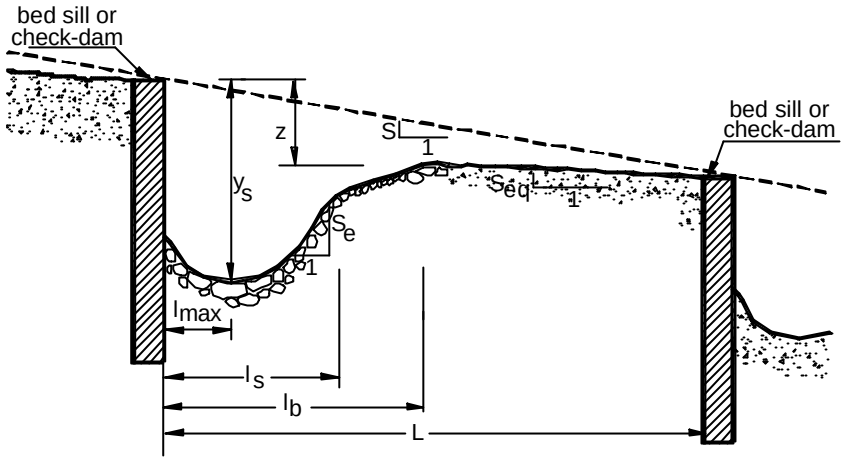

Figure 5.2 – Definition sketch of the geometric variables surveyed in the field activity; the berm is highlighted by the presence of coarser bed particles and the armoring of the scour hole bottom is shown too.

In the past these mountain streams, like most Italian mountain rivers, have been subject to the construction of sequences of bed sills and check-dams to prevent erosion and to reduce the channel bed slope. Equilibrium bed slopes S_{eq} (Fig. 5.2) between two grade-control structures in the six surveyed rivers ranged overall between 0.01 and 0.05.

The structures are made of concrete, except in the Plima and in the Maso River (Lenzi, 2002) where they were built using large boulders strengthened with concrete to blend in with the surrounding landscape.

Structure heights differ considerably among the six rivers and in some cases even within a single stream, for an overall range between 0.15 m and 5 m (Table 5.2). Only bed sills were built in the Maè and Plima rivers, whereas in the others mainly check-dams were constructed. Figs. 5.3-5.8 show images from the six surveyed rivers: In Fig. 5.3 the lowest bed sills are depicted, whereas Fig. 5.8 exhibits the highest surveyed check-dam.

The six surveyed rivers were chosen either for the availability of gauging stations (rivers Maè, Biois, Visdende, Plima, Maso) or for the possibility of using estimated discharge by highly-detailed distributed models (Pramper River). The rivers Biois, Maè, Pramper and Visdende have been affected in November 2000 – the autumn preceding the summer survey – by flood events with return periods of at least 3-5 years. In the Plima River, whose hydrologic regime is controlled by a reservoir dam, a water discharge equal to the highest since the bed sills were constructed was released just before field measurements. In 1998 the Maso River

was subject to an important flood event characterized by a recurrence interval of around 20-25 years (Lenzi, 2002).

Figure 5.3 – Maè River (Forno di Zoldo, Belluno, Italy).

Figure 5.4 – The writer while measuring into the Biois River (Cenceniche Agordino, Belluno, Italy)

Figure 5.5 – Pramper River (Forno di Zoldo, Belluno, Italy).

Figure 5.6 - The writer surveying the Maso River (Borgo Valsugana, Trento, Italy)

Figure 5.7 – Plima River (Val Martello, Bolzano, Italy).

Figure 5.8 – The highest check-dam is left fot the assistants…
(Visdende River, S.Stefano di Cadore, Belluno, Italy).

Table 5.2. Range of effective crest width *B*, representative grain size at pool bottom *D*, drop height *z* and spacing *L*.

River	B (m)	D (m)	z (m)	L (m)
Mae'	14.5-27.0	0.3	0.20-1.15	33.0-130.0
Biois	12.6-18.0	0.5	0.65-3.45	10.2-45.0
Plima	7.0-15.0	0.5	0.15-2.80	18.5-28.0
Pramper	8	0.4	2.10-2.60	13.5-26.0
Visdende	13.5-19.5	0.7	1.45-5.00	12.7-50.0
Maso	23.2	1.0	0.47-2.56	5.3-23.8

Local scour dimensions measured in summer 2001 can be tentatively correlated with the peak flow rates of such events, which have probably shaped the scour holes as they now appear. In support of such a hypothesis it was observed that almost all pool bottoms were armoured by coarse particles, about the largest clasts found in the each stream, ranging between 0.3 m (Maè) and 1 m (Maso). Cobbles and boulders present at pools bottom were tightly adjoined to each other, and no clasts lay on the surface as deposited by successive flows. Fine sediment (gravel and sand) was present only at the pool sides. This may suggest that the last flood events did not cause deposition in the scour holes, and that equilibrium between water-sediment discharges and scour dimensions was achieved.

Field Methods and measured variables

The measured features (Fig. 5.2) are maximum scour depth y_s and the corresponding distance from the crest l_{max}, scour length l_s, pool width B_p, drop height z, berm distance l_b, pool exit gradient S_e and particle size at the pool bottom D. Additionally, the work's crest effective width B was also measured in order to calculate water discharge per unit width at the crest. In turn this allowed the estimation of the thickness of issued jets.

Tailwater levels at pools could not be reliably determined in the field and no hydraulic modelling has been performed to estimate its value; such a variable will be therefore neglected in the present study.

The maximum scour depth y_s was taken with respect to the elevation of the structure crest, whereas the drop height z was measured as the difference in level between the crest and the control section downstream of the pool: this could either be determined by the next artificial grade-control structure or represented by the point at which the river bed was no longer prevalently affected by local scouring dynamics, thus showing the onset of a positive gradient representing the equilibrium slope. In this way the drop height z should correspond

roughly to the morphological jump a_1 described in the introduction. In most cases such a "borderline" between local and general scouring was marked by a naturally-formed berm made up of 0.20-0.50 m clasts. Only downstream of it the bed achieved a positive gradient, i.e. the "equilibrium" slope. This sedimentary structure has been commonly observed in other rivers downstream of grade-control works with large spacings and probably represents a hydraulic jump separation berm as described by Carling (1995). Furthermore, all experimental studies of overfall scouring report the formation of a sediment mound made up by the eroded material downstream of the scour hole. Such a mound is thought to correspond to the observed berm. The longitudinal distance between each structure and its berm was measured (l_b).

It was inferred from a preliminary analysis that scour lengths measured by the authors in the flume runs described in section 4 actually refer to the berm distance. This in accordance with Gaudio et al. (2000) who originally defined scour length referring to the point where the equilibrium slope became established. However, since in some cases such a transition point (i.e. berm) was not reliably determinable, scour length in this study refers to the longitudinal distance between the crest and the point corresponding to a sharp change in pool profile at the end of the downstream slope (Fig. 5.2). Therefore this scour length does not correspond to the berm position – this being located downstream of the former – or to measured lengths in the flume.

Scour hole dimensions and structure heights were measured directly by 5m-long telescopic stadia. Effective crest width was measured using a meter tape. River bed gradients S and S_{eq} were taken by a total station survey. Due to practical problems, for some pools not all the dimensions listed above could be collected, i.e. in some cases the determining points for l_{max}, l_b or S_e could not be reliably detected.

Sediments size at the location of scour holes' maximum depth was measured only at the surface layer; no subsurface sampling was performed due to practical problems arising from large clast dimensions and deep water in the pools. Indeed, in the Maso River most of the scour holes were too deep to collect surface sample, and therefore only a rough estimate was possible; the same problems were also encountered for the deepest pools in the other rivers. Because of the paucity of clasts within a single scour hole and for their rather approximate measurement, only one representative size D of grain dimension at pool bottom has been assigned to each river by averaging values taken within each scour holes. Table 5.3 reports the measured geometric variables for the surveyed 73 scour holes.

Table 5.3 - Measured variables in the 73 scour holes (see text and Fig. 5.2 for symbols).

	B (m)	L (m)	D (m)	z (m)	y_s (m)	l_s (m)	l_{max} (m)	l_b (m)	S_e (-)
Maè	20.0	100.0	0.3	1.00	2.35	5.0	1.7	10.0	0.35
	20.0	110.0	0.3	0.85	2.40	5.0	1.7	7.5	0.29
	19.2	130.0	0.3	1.15	2.50	4.0	1.6	6.0	0.25
	25.0	70.0	0.3	0.60	1.70	3.0	0.9	5.0	0.30
	14.5	33.0	0.3	0.40	1.10	2.6	0.8	4.6	0.33
	27.0	36.0	0.3	0.40	1.30	2.8	1.0	4.0	0.30
	26.0	44.0	0.3	0.40	1.10	3.0	0.8	4.5	0.36
	26.0	34.0	0.3	0.20	0.80	2.5	0.8	4.0	0.31
	26.0	35.0	0.3	0.40	1.20	3.2	0.9	4.7	0.36
	20.0	34.0	0.3	0.25	0.80	2.5	0.7	4.0	0.27
Biois	18.0	10.2	0.5	3.45	4.65	6.0	1.6	-	0.20
	17.0	45.0	0.5	0.65	1.35	2.6	1.0	4.5	0.27
	12.6	45.0	0.5	2.10	3.20	6.0	2.0	9.0	0.28
Plima	13.0	20.0	0.5	0.75	1.50	3.0	0.9	-	0.38
	12.0	22.0	0.5	0.20	0.75	3.6	1.3	-	0.31
	10.0	23.5	0.5	0.20	0.75	5.0	1.3	-	-
	13.0	22.3	0.5	0.20	0.80	4.3	1.0	-	-
	13.0	25.0	0.5	0.15	0.60	3.5	2.3	-	0.20
	13.0	28.0	0.5	0.70	1.60	2.4	1.0	-	-
	10.0	20.0	0.5	0.60	1.55	3.0	1.2	-	0.33
	10.0	18.5	0.5	0.50	1.25	4.0	1.5	-	0.27
	11.0	25.0	0.5	0.45	1.15	2.0	-	-	-
	11.0	24.0	0.5	0.40	1.00	2.2	-	-	0.25
	10.0	-	0.5	0.80	2.00	5.8	1.7	7.5	0.64
	7.5	25.0	0.5	0.55	1.20	2.5	1.2	6.0	0.33
	8.2	26.5	0.5	0.50	1.50	2.2	1.0	4.3	0.40
	7.0	24.0	0.5	1.00	2.00	4.3	1.3	7.0	0.34
	10.6	24.0	0.5	1.10	2.10	3.0	1.5	6.5	0.40
	9.0	20.0	0.5	0.90	1.90	-	1.3	-	-
	8.0	19.0	0.5	1.90	2.70	4.4	1.0	6.0	0.45
	9.0	24.0	0.5	0.65	1.20	3.2	1.0	-	-
	9.6	24.0	0.5	0.50	1.25	3.5	0.8	-	0.23
	8.4	22.0	0.5	0.80	1.30	3.0	1.1	4.5	0.33
	9.0	21.0	0.5	0.40	1.20	3.3	1.1	5.0	0.30
	15.0	-	0.5	2.80	4.10	5.5	2.6	-	-
Pramper	8.0	26.0	0.4	2.20	2.90	3.4	2.0	5.7	0.27
	8.0	26.0	0.4	2.60	3.70	4.0	1.8	6.5	0.25
	8.0	26.0	0.4	2.40	3.90	5.0	1.8	7.0	0.20
	8.0	13.5	0.4	2.10	3.00	4.5	-	-	-
Visdende	17.0	12.7	0.7	2.80	4.00	4.2	-	-	0.39
	17.0	21.0	0.7	2.30	4.20	8.3	2.5	12.0	0.43
	19.0	29.0	0.7	5.00	6.10	6.5	2.8	-	0.27
	19.5	50.0	0.7	1.45	2.35	4.4	2.0	6.0	0.24
	13.5	34.5	0.7	2.40	3.70	4.2	-	6.7	0.73
Maso	23.2	10.1	1.0	1.86	2.53	4.8	-	6.2	-
	23.2	14.3	1.0	1.41	2.09	3.9	-	5.9	-
	23.2	11.6	1.0	1.20	1.57	2.7	-	5.0	-
	23.2	20.9	1.0	1.30	2.43	6.0	-	7.2	-
	23.2	9.7	1.0	1.84	3.10	5.1	-	6.8	-
	23.2	18.0	1.0	1.10	2.35	6.3	-	8.0	-
	23.2	12.3	1.0	1.16	2.05	4.3	-	5.5	-
	23.2	20.5	1.0	1.09	2.47	4.5	-	6.2	-
	23.2	9.6	1.0	2.14	2.66	-	-	-	-
	23.2	13.2	1.0	2.50	3.17	5.9	-	7.3	-
	23.2	16.5	1.0	1.38	2.17	-	-	-	-
	23.2	10.8	1.0	1.81	2.80	3.5	-	6.6	-
	23.2	15.1	1.0	1.49	2.48	3.8	-	5.4	-

Maso	23.2	13.0	1.0	0.79	1.72	3.1	-	4.0	-
	23.2	12.9	1.0	1.20	2.08	3.2	-	4.6	-
	23.2	23.8	1.0	0.86	2.05	4.6	-	5.8	-
	23.2	11.6	1.0	1.42	2.20	5.5	-	6.5	-
	23.2	21.8	1.0	1.46	2.90	4.6	-	7.3	-
	23.2	12.3	1.0	1.85	2.73	5.2	-	7.4	-
	23.2	11.4	1.0	2.32	3.80	6.6	-	7.8	-
	23.2	9.2	1.0	2.46	3.46	5.2	-	6.2	-
	23.2	8.0	1.0	2.56	3.60	3.8	-	5.0	-
	23.2	18.9	1.0	2.13	3.61	5.0	-	7.4	-
	23.2	8.6	1.0	2.12	2.99	5.4	-	5.4	-
	23.2	8.0	1.0	0.97	2.25	3.5	-	4.6	-
	23.2	13.2	1.0	2.12	2.44	-	-	-	-
	23.2	9.1	1.0	1.10	2.05	3.3	-	5.5	-
	23.2	7.3	1.0	1.38	2.14	4.4	-	5.7	-
	23.2	5.3	1.0	0.47	1.01	3.1	-	3.1	-

5.1.1 Case-study A: The Maso River

In 1996 and 1997, the Torrent Control Agency (TCA) of the Autonomous Province of Trento (Italy), with the scientific support of the University of Padua, carried out hydraulic control works on selected reaches of a mountain river, the Maso di Spinelle, using transverse boulder works to protect channel against incision. The Maso di Spinelle forms, along with the Maso di Calamento, the Maso River, a tributary that flows into the Brenta River (NE Italy, Fig. 5.1). For a complete description of the basin, see Lenzi et al. (2000) or Lenzi (2002).

Degraded deposits of Quaternary age dominate the channel, particularly in the lower reach. Talus often covers moraine and fluvioglacial deposits close to the banks. Moraine deposits lead to large boulders of various shapes intermixing with a high percentile of sandy and sandy-gravelly materials on stream banks. Some of these boulders, whose volumes range to hundreds of cubic metres, caused huge flow diversions during 1966 and 1993 floods, leading to bank slides.

Maso di Spinelle's bed, especially the middle-lower part, experienced considerable incision and deepening during the flood of 3-4 November 1966 with a return interval $100 < Tr < 200$ yr. The average bed width increased from 6-7 to 35-50 m after the flood, while the bed profile decreased by about 10-15 m in some reaches. Similar results, although lower in magnitude, accompanied the flood event of 2 October 1993 ($50 < Tr < 75$ yr).

After the 1993 flood, further incision was prevented by using boulder check-dams that should reproduce natural step-pool structures. TCA constructed both uncemented boulder check-dams and boulder check-dams strengthened with cement.

The stability of the interventions described above was actually tested during the final stages of their construction, in October 1996, when a flood with a maximum discharge around 43 m^3s^{-1} and a return time of ~ 10 yr occurred. On 7 October 1998, another flood with a peak discharge of 52 m^3s^{-1} and a return interval of 20-25 yr put the completed control works through more rigorous testing. The behaviour of both check-dams strengthened with concrete and uncemented boulder steps was satisfactory during both of these floods.

Detailed field surveys were carried out in September 2001 (Lenzi and Comiti, 2003) along two reaches stabilised with cemented boulder check-dams separated by a block stone ramp. The channel width in both rests between 20 and 25 m, with an average of 23.5 m.

The upstream 300 m-long reach (R1, Fig. 5.9) presents a mean gradient of about $S = 0.125$, whereas the shorter – 90 m – downstream reach (R2, Fig. 5.10) is somewhat steeper ($S = 0.159$). A total station-positioning system was used to measure thalweg points in order to

generate a longitudinal profile of both scour holes and intervening bed spans (Figs. 5.11 and 5.12).

Figure 5.9 – Reach R1 of Maso di Spinelle River;
the closest artificial step is the N°16 (see profile in Fig. 5.11).

Twenty-two cemented boulder check-dams were installed along reach R1, with spacing ranging from 9.2 to 23.8 m; 220 points were surveyed, and 21 scour holes analysed. As for the shorter reach R2, 72 points were measured; spacing between check-dams ranged from 5.3 to 18.8 m, and eight scour holes were considered.

For each scour hole, the drop height, maximum scour depth, and scour length were calculated from the profiles. Scour length is defined as the distance between the upstream step and a typical "cusp" downstream. In fact, a well-defined linear berm of coarse clasts (0.7-0.8 m in diameter) characterised the downstream end of pools below artificial steps. Such a berm likely represents the zone where roller's turbulent stress due to jet diffusion abruptly calms down and hydrodynamics tend towards a linear flow. When the distance between two check-dams was short compared to the pool length, berms were not so conspicuous.

**Fig. 5.10 – Reach R2 of the Maso di Spinelle River;
the closest artificial step in N°28 (see profile in Fig. 5.12).**

In this study, *Z* represents the difference in height between one check-dam and the one downstream, whereas *z* is the actual drop height with respect to the pool end. In some cases, *z* and *Z* are equal because the spacing *L* is so short that the bed affected by the scour hole almost extended to the downstream check-dam. Otherwise, the two vertical parameters differ because an "equilibrium" slope establishes downstream of the scour hole. The value of such a slope, calculated from the profile, appears to be rather constant in R1 (around 0.04-0.05). The actual water level difference responsible for the scour development (i.e., the air-surrounded vertical distance) is reasonably assumed to correspond to the drop height z. This neglects the fact that water depth at the pool end (i.e., the control depth downstream) might differ from the nearly critical water depth that is achieved at the step's crest. However, such an assumption was already proved in laboratory tests. Water discharge can be assumed to be equal in the two reaches, because there are no tributaries from the valley sides.

Before construction of control works, surface bed material was sampled at three sites using a systematic "grid-by-number" method (Wolman, 1954). An averaged grain size distribution was obtained to use it – appropriately scaled – in the laboratory tests described in section 4.1.2.

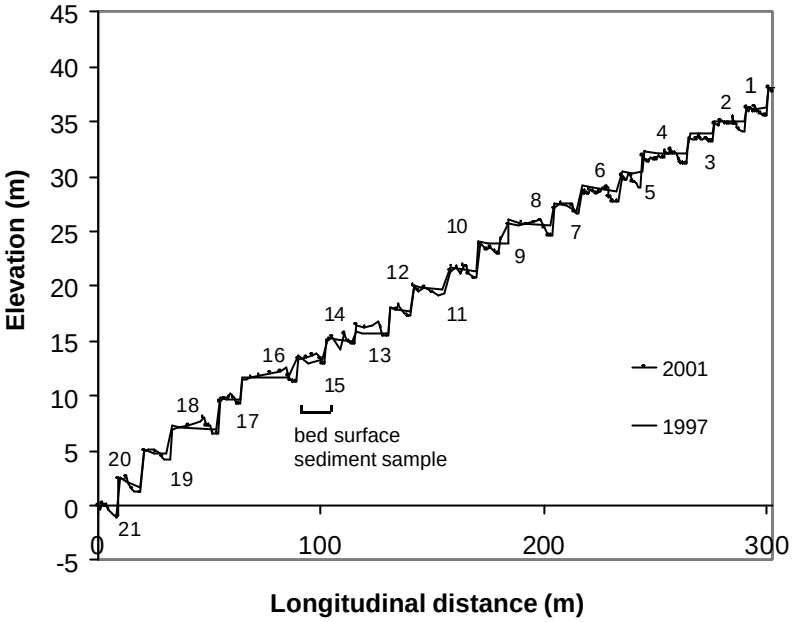

Figure 5.11 – Reach R1 after-construction (1997) and present (2001) longitudinal profiles; the numbers identify the location of the 29 analysed scour holes.

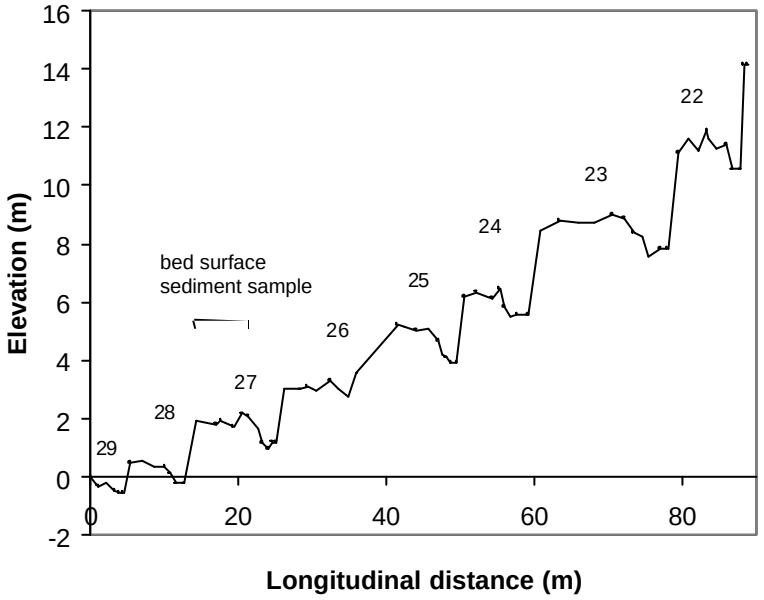

Figure 5.12 – Reach R2 present (2001) longitudinal profile; the numbers identify the location of the 29 analysed scour holes.

In September 2001, two other samplings were performed following the same methodology. The number of clasts measured was 133 in R1 and 95 in R2. The sample grid

did not cover pool sites. However, the pool bottom resulted in being mainly armored by boulders ranging from 0.8 to 1 m. All grain size distributions are shown in Fig. 5.13.

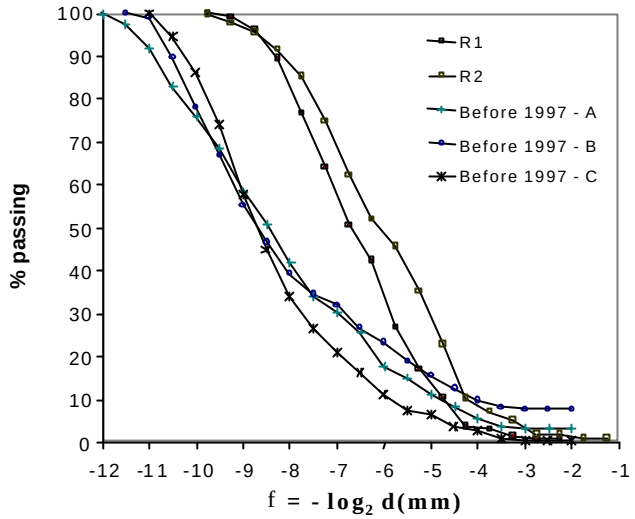

Figure 5.13 - Surface grain size distributions of the Maso di Spinelle: before control works (A, B, C) and at present (R1 and R2).

Evolution of bed morphology and surface grain size distribution

The control works were constructed implementing a $(H/L)/S$ ratio of 1.1-1.3, thus a weak reverse bed slope was assured between most boulder check-dams, as shown in Fig. 5.11 (1997 profile). First, this section compares the changes in the bed profile occurred from 1997 and 2001 in the reach R1.

Where artificial steps are long-spaced (for example N° 8, 13, 16), local scouring formed a well-defined hole, deepening the former bed level. Downstream of scour holes, prevalent depositional dynamics (favoured by the large channel width, too) raised the level and formed a sloping bed with a gradient of around 0.04-0.05. In the shorter spacings, however, erosive processes have prevailed, lowering the bed only in connection with scour hole development. At some locations, the pool depth has not increased significantly, indicating that initial geometry was already in a general equilibrium with later flow rates. Berms are clearly distinguishable in profiles as abrupt changes (a sort of “cusp”) in bed inclination at the end of pools.

Although not shown by the profiles, lateral and median bars occurred mostly in the long-spaced spans, as can be seen in Fig. 5.9. In such cases, water at low discharge flows within one or two narrower channels. Step-pool beds formed naturally along most of these; see particularly N° 4 and 14. Median bar formation was probably triggered by upstream step irregularities that caused differential jet flow concentration, in turn affecting local flow rates below the drop.

The original profile for reach R2 is not available. However, because of short distances between steps, an evolution similar to R1 short-spaced steps likely occurred. R2 reach lacked bars.

As for the surface grain size distribution, Fig. 5.13 shows a large decrease in particle size in the upper and median parts of the curve. The general reduction has not developed for the finest material (up to D_{20}, roughly), because most of the large boulders found in the Maso River bed had been used for building the artificial steps. Thus, the previous coarsest dasts with diameters up to 4 m (Tab. 5.4) are now "grouped" as boulder check-dams. In sum, the "shift" of grain size distribution cannot be seen as a natural evolution pattern.

Table 5.4 Some characteristic grain sizes of past (A, B, C) and present (R1, R2) surface bed material of the Maso di Spinelle River.

	A (1996)	**B** (1996)	**C** (1996)	**R1** (2001)	**R2** (2001)
D_{max} (mm)[a]	4050	2990	2005	800	1000
D_{90} (mm)[b]	1783	1448	1218	304	274
D_{50} (mm)[b]	338	416	430	111	68
D_{16} (mm)[b]	48.5	37	90	37	23

a D_{max} is the largest boulder size.
b D_{90}, D_{50}, and D_{16} are the diameters for which the 90%, 50%, and 16% of the particles are finer respectively.

The fining of bed material contains important consequences for enhancing sediment transport, if hydraulic conditions remain unaltered. On the other hand, lower bed slopes between steps downstream of the pools should reduce flow competence, counteracting this fining effect.

Local scouring characteristics

In Fig. 5.14, ratios y_s/z (hereafter called relative scour depths) plot against the ratio z/L between the drop height z and the spacing L. The parameter z/L roughly measures the

potential energy lost by the falling jet in the span length fixed by two check-dams. When this parameter increases, the relative scour depth is reduced, declining from values around 2.5 to about 1.3. The initial general decreasing trend up to $z/L \approx 0.1$ seems to reach an asymptote at a y_s/z value of about 1.4. The residual scatter is probably due in part to the well-graded nature of the grain size distribution. This easily leads to larger boulders occasionally being present at the pool bottom. Uneven planimetry of step crests – causing higher jet flow concentration – might be an additional source of variability.

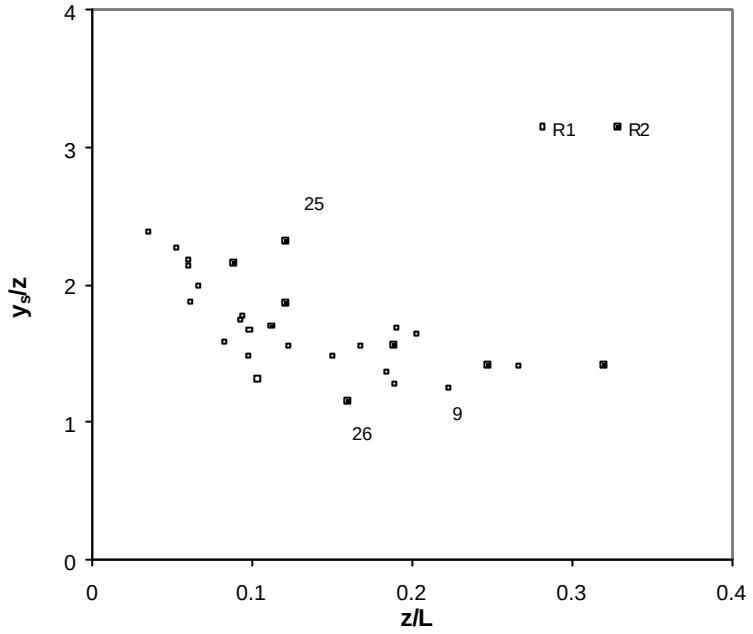

Figure 5.14 - Nondimensional maximum scour depth plotted versus the ratio *z/L*.

The same pattern is shown by relative longitudinal scour extension (i.e. the berm distance) l_b/z (Fig. 5.15). Here, the declining trend accentuates; the ratio moves from 8 to 2 without asymptotic behaviour. The scour holes that plot outside of the points' clouds in both Figs. 5.14-5.15 (N° 9, 11, 26) are noteworthy. These originated by those check-dams that resemble (because of the positioning of boulders) a short, steep ramp where flow energy dissipates and deflects more irregularly than in the other steps. In these places scour depth and berm distance are no longer determined only by the parameter *z/L*. Complex energy dissipation patterns make it difficult to analyse these local scourings. As for scour N° 25 in Fig. 5.14, no clear explanations for its far larger relative depth are available. It might, however, be due either to a somewhat different local flow field (e.g., caused by the pool's boulders) or to an upstream flow concentration that determined a thicker free jet.

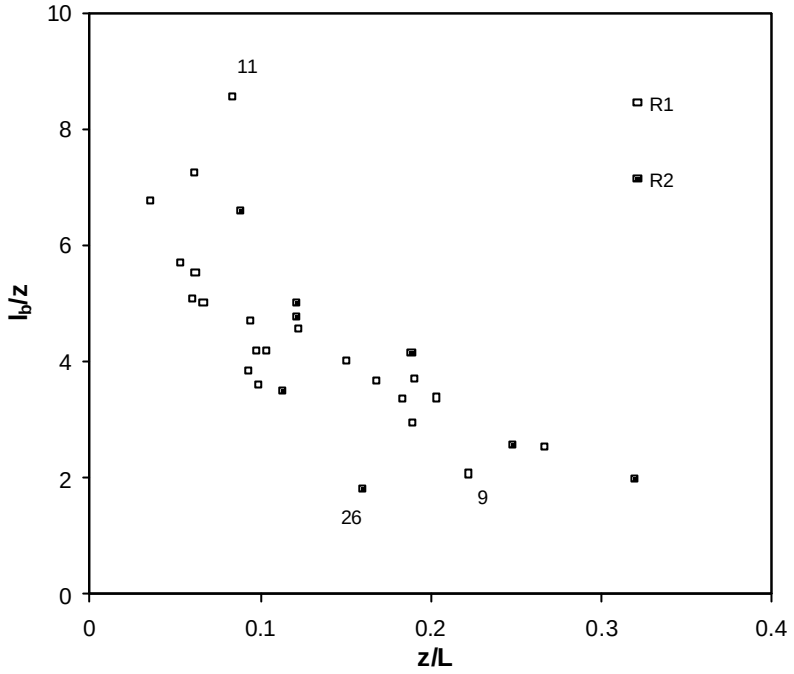

Figure 5.15 - Nondimensional berm distance plotted versus the ratio *z/L*.

In Fig. 5.16, the mutual relationship between the vertical (i.e. scour depth) and longitudinal (i.e. berm distance) dimensions is displayed where both are normalised to the drop height. A consistent, seemingly linear trend might exist; this highlights the tight relationship between them.

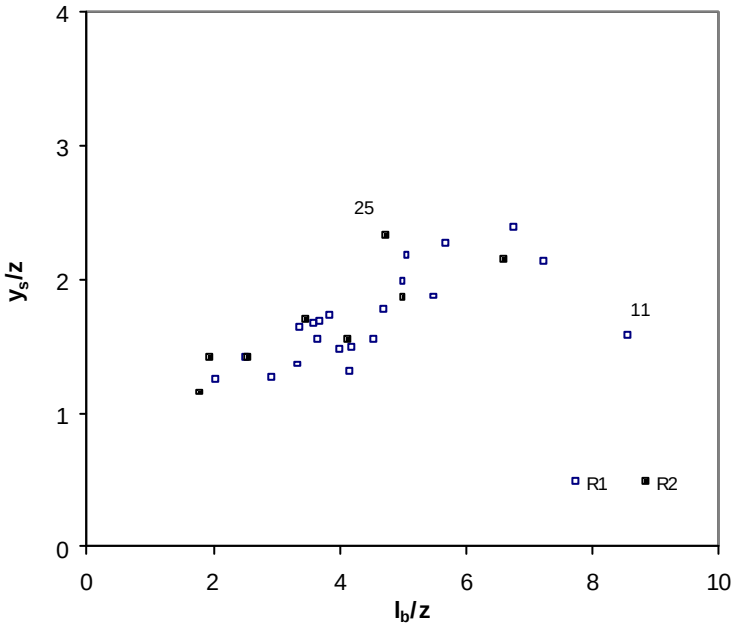

Figure 5.16 - Relationship between non-dimensional vertical and longitudinal scour dimensions; a consistent trend is apparent.

Comparison with laboratory results

Dimensionless vertical and longitudinal scour dimensions are shown in Figs. 5.17 and 5.18, respectively, where the independent parameter is the ratio h_c/z. As described in section 4.1.2, Wallingford flume tests aimed at simulating sediment and flow conditions found in the Maso River. A general overlap does exist which indicates the soundness of the non-dimensional approach. As already explained above (5.1), scour lengths in the flume runs correspond to berm distances in the field survey.

Several field points fall along the trend delineated by Wallingford Series 1 laboratory tests, which were referred to as non-interfering scours. Almost all of these points represent scour holes that are characterised by a long spacing and, therefore, by an equilibrium slope downstream. This matches the description for non-interference conditions given in section 4.2.2..

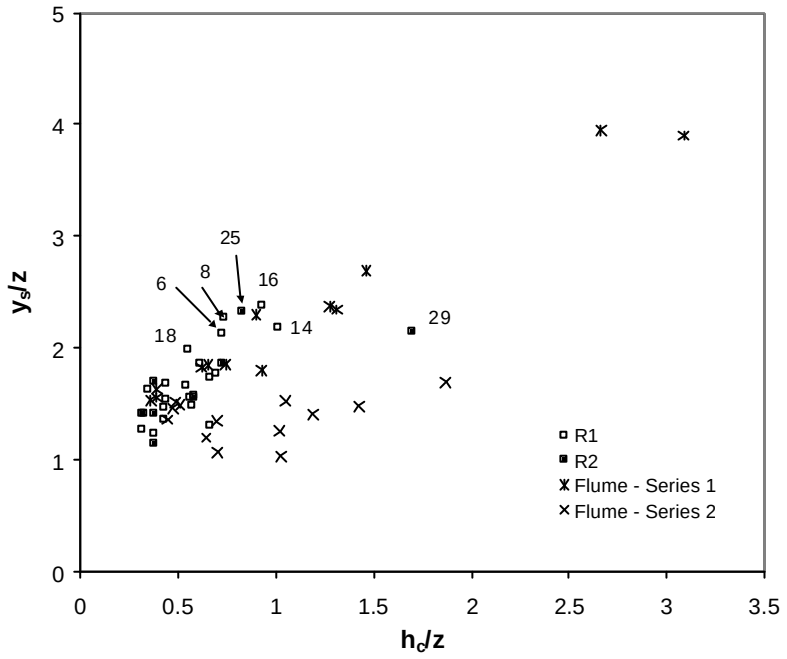

Figure 5.17 – Non-dimensional maximum scour depth of scour holes (both field and flume data) plotted versus relative critical flow depth, h_c/z.

A clear distinction between non-interfering and interfering conditions was not possible even for the flume tests for the lowest h_c/z values (< 0.5-0.6). At these small ratios falling jets tend to become more vertical with smaller scour lengths. Thus, even shorter spacings are required for the onset of interference effects. Field data having large relative depth (>1) lack because only scour hole N° 29 is available. Nevertheless, such a point apparently confirms the existence in nature of a mechanism that inhibits local scouring because of downstream control exerted by a non-erodible sill point.

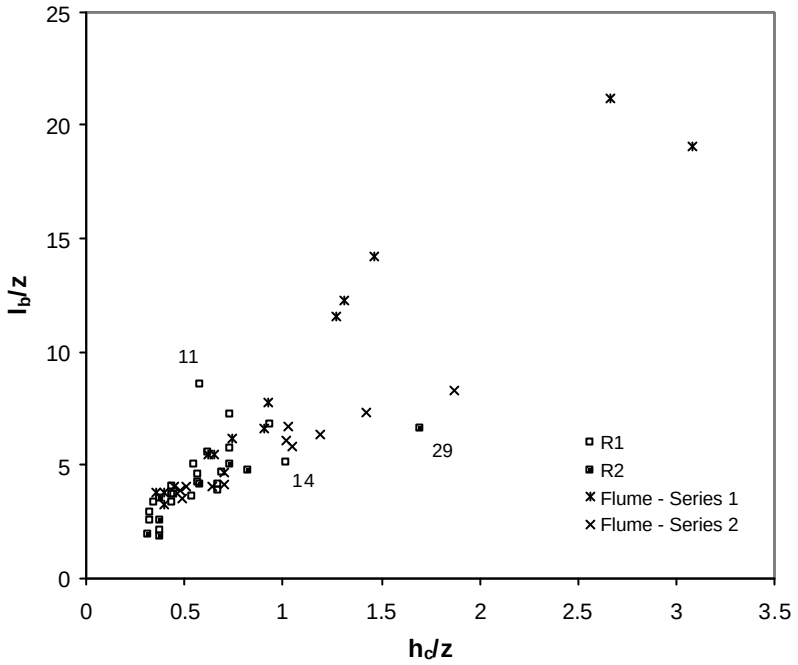

Figure 5.18 – Non-dimensional berm distance (both field and flume data) plotted versus relative critical flow depth, h_c/z.

For the flume data, a unique relationship between the parameter h_c/L and the ratio l_s/L (i.e. in this case l_b/L) was discovered to exist. Field measurements in Fig. 5.19 show a much larger scatter that may be due to the influence of drop height, perhaps negligible in the laboratory research. Moreover, field data present an upper value for l_s/L of about 0.7-0.8, whereas flume points appear to tend toward an asymptote around 0.6-0.7 (Fig. 5.19).

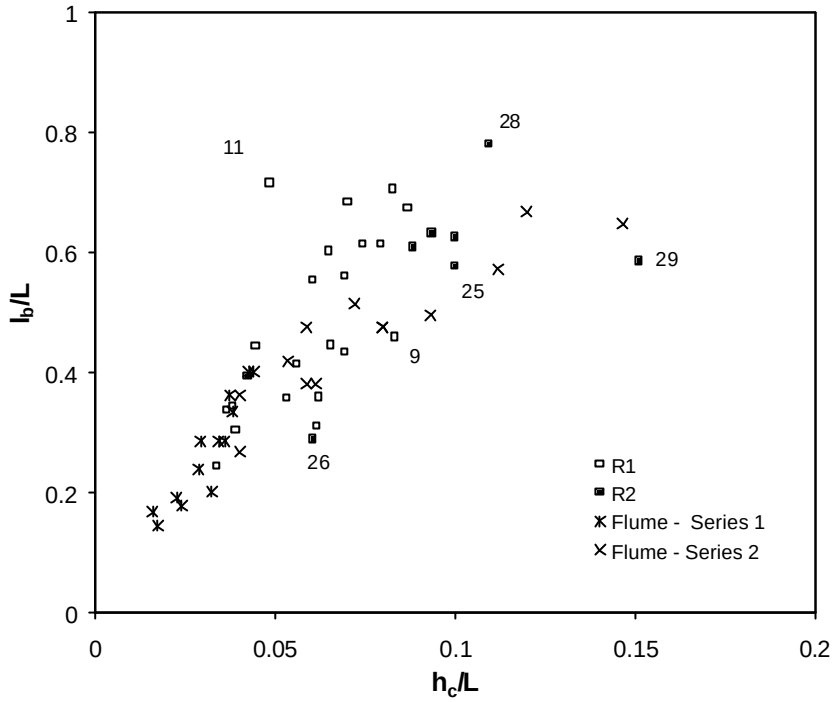

Figure 5.19 - Scour longitudinal extension (i.e. berm distance) as a proportion of the spacing *L* in relation to the ratio h_c/L; field data generally plot above flume points, and present a larger scatter.

After a certain stage, the energy available might be enough to break such upper limits of ratios l_b/L, and this could be linked to the threshold between stable and unstable tumbling flow as reported by Whittaker (1987_a). In Whittaker's flume experiments, unstable tumbling flow (i.e., no longer well-defined scour holes, flow instabilities, slug waves) takes place at a value of h_c/L between 0.11 and 0.14 depending on the gradient (from 0.098 to 0.248). Some of this paper's flume data fall within Whittaker's range without showing signs of instability. The much finer material used by Whittaker (D_{90} = 0.0049 m) might be the reason for the unstable tumbling flow he observed.

As to scour holes geometry, the laboratory tests - both interference and non-interference conditions in 4.2.2 – have showed the consistence of the ratio $l_s/(s+h)$, where s is the "residual" scour depth calculated as y_s-z and h is tailwater depth above the scour hole. A precise evaluation of tailwater depths in the field was very difficult, so the critical water depth is assumed in Fig. 5.20 as a rough estimation, just to permit a comparison between flume and Maso di Spinelle data. The agreement is rather good and indicates that most scours have ratios ranging between 3 and 4.5, with no influence from the geometry of the system summarised by the z/L parameter. The scatter may be due differences between actual tailwater and critical

depth, which is slightly variable for each scour hole depending on the downstream control. For flume data only, a ratio of ~ 3 was found using the tailwater depth.

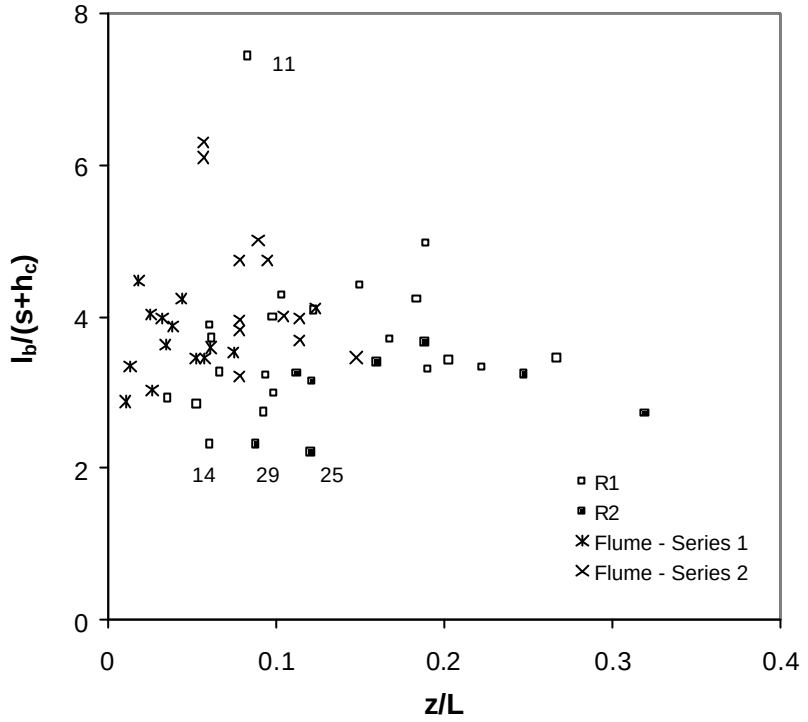

Figure 5.20 – Geometry of the scour hole (with $s = y_s - z$) as an invariant of the system; the tailwater depth (not known for field data) is approximated by the critical depth.

Therefore, the idea that an intrinsic geometry of scour holes might be a basic aspect in local scouring seems to be valuable and might prove to be important in the understanding of fluvial forms that are connected to diffusing jets such as step-pool structures.

Geomorphological implications for step-pool channels

In analysing step-pool bed forms, Abrahams et al. (1995) first introduced the parameter $c = (H/L)/S$, called relative steepness factor, where H is step height, L step wavelength, and S reach gradient (see section 2.3). They showed that parameter c ranged between 1 and 2, with an average value of 1.5, in all surveyed step-pool streams. Abrahams et al. also carried out laboratory tests with fixed weirs and found that maximum flow resistance (i.e., least mean velocity) occur for a regular configuration of steps having values of c within the same range.

They then concluded that step-pool geometry maximizes resistance to flow and therefore leads to a more stable bed morphology.

The upper limit for the relative steepness factor may be related to local scouring maximum depths. Figure 5.21 shows the ratio y_s/Z measured in the Maso di Spinelle plotted against l_b/L; the drop Z is the difference in level between two artificial steps.

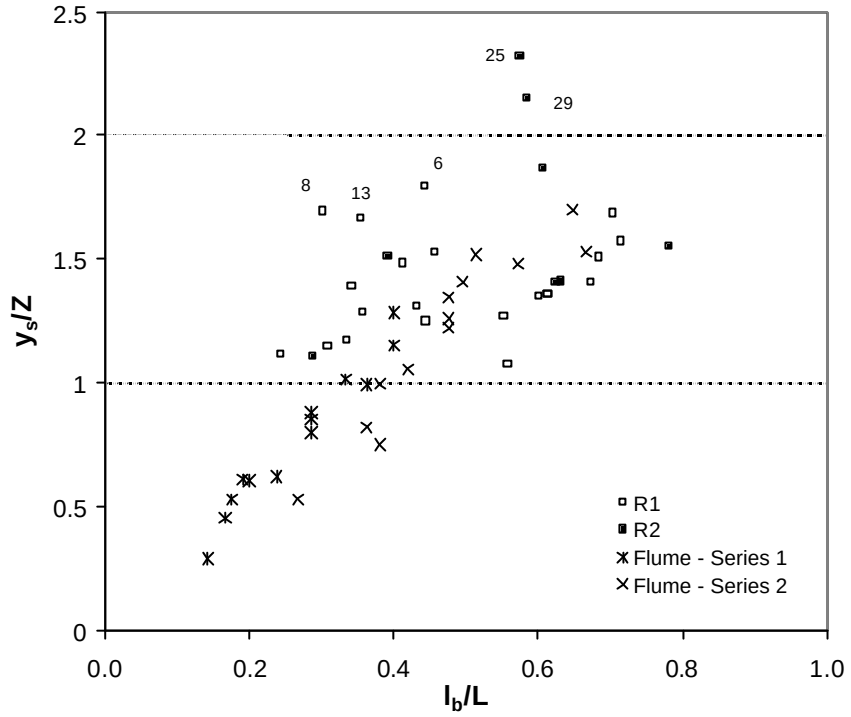

Figure 5.21 – The relative steepness $c = y_s/Z$ plotted versus the ratio l_b/L; the range ($1 < c < 2$) proposed by Abrahams et al. (1995) for natural step-pool channels is highlighted.

The ratio y_s/Z corresponds to the steepness factor when a mean channel gradient S is converted into a specific ratio between drop and length for each step. In fact,

$$c = \frac{H/L}{S} = \frac{H/L}{Z/L} = \frac{H}{Z} = \frac{y_s}{Z} \qquad (5.1).$$

The graph shows that only two scour holes present y_s/Z slightly > 2, whereas the average value is 1.47, very close to the 1.5 claimed by Abrahams et al. (1995).

The water discharge that scoured the Maso di Spinelle's pools was pretty large (estimated return period 20-25 yr), but one could wonder about the effects of a still heavier

flow rate. As long as unstable tumbling flow is not triggered, scour length maintains an upper limit fixed by the distance L, for whatever flow rate. From Fig. 5.21, scour depth can be inferred to not increase beyond a value of roughly two times the drop height $z = Z$ when $l_b/L = 1$. This is consistent with step-pool channel's steepness factor, which is rarely higher than 2 for steep channels, over about 0.07-0.08 (see section 2.3).

5.1.2 Case-study B: The Plima River

The Plima River is a major tributary of the Adige River and is located in the Eastern Italian Alps (Bolzano Province, Fig. 5.22). Its basin corresponds to the Martello Valley, which has a total area of 168 km^2 ranging in elevation between 3764 m a.s.l. (Mount Cevedale) and 650 m a.s.l. (confluence with the Adige, Val Venosta thalweg). The Plima is approximately 22 km long with an average gradient of about 14%.

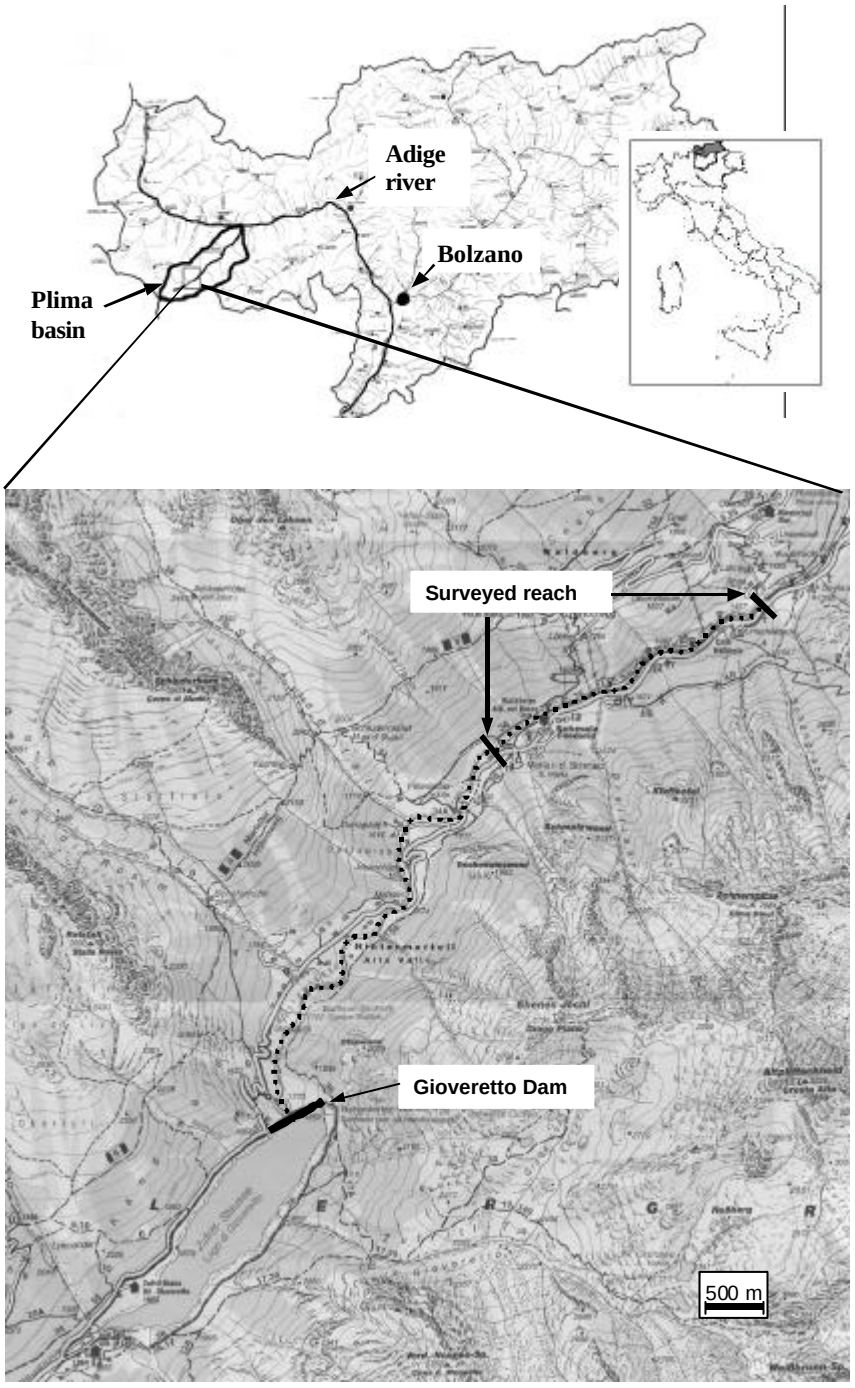

Figure 5.22 – Study area: the Plima basin.

Geologically the valley is made up of quartziferous phyllites, mica schists, marbles and granites. Moraine and talus deposits are commonly found close to the thalweg. Morphologically it was first formed by glaciers and then by the intense erosive activity of the Plima River and its tributaries. The valley sides are very steep, with a well-defined V-shaped transverse profile. The Plima originates as a proglacial river, draining meltwater from a permanently glaciated area of about 18 km^2. The 50-year flood discharge is evaluated around 60 m^3s^{-1}. Nowadays, however, flow rates in the Plima River are mostly determined by the amount of water released from a reservoir dam (Gioveretto Dam) built in the '50s for hydropower production. The dam is 81 m high and is located at 1850 m a.s.l. which corresponds to a drained area of 117.4 km^2. On August 24, 1987, a combination of heavy rainfall and dam gate operations led to the erroneous release of 400 m^3s^{-1} of water which caused dramatic flooding along the whole valley downstream. The enormous damage to private buildings and public infrastructure was due mainly to the extraordinary sediment transport, including massive boulders. Fortunately, no lives were lost. However, such a severe event triggered many instabilities along the course of the river, including channel incision, shallow and deep landslides.

After this massive flood, control works aiming to re-define the river channel and to prevent channel incision were undertaken in 1990. Such works represent one of the first examples of "naturalistic engineering" carried out in the Italian Alps. New embankments and several bed sill sequences were constructed. The surveyed reach considered here is located at 1600-1400 m a.s.l. (Fig. 5.22). Fig. 5.23 shows an aerial view of part of the reach before bed sill construction with their planned location indicated. The effective crest width of the bed sills ranges between 8 m and 15 m and their spacing L (i.e. the longitudinal distance between each) is on average 22 m; the gradient between the crests ranges between 0.04 and 0.09, whereas the bed slope downstream of the plunge pools varies from 0.03 to 0.07. The structures consist of boulders strengthened with concrete designed to fit in with the surrounding settings. The original design of the bed sills is shown in Figure 5.24.

Furthermore, other large boulders were placed in the channel to create habitat diversity for fish. Commonly 4-6 boulders were lined up along a cross-section just downstream (on average 5 m) of the bed sills (Fig. 5.25). These boulders themselves also act as grade-control works. In fact, as will be discussed later, the dimension of local scouring downstream of the bed sills is influenced by the presence of these boulders.

Figure 5.23 - Aerial photograph of part of the surveyed reach after the 1987 flood and before control works construction; the future location of the bed sills is also drawn on (by courtesy of the Province of Bolzano).

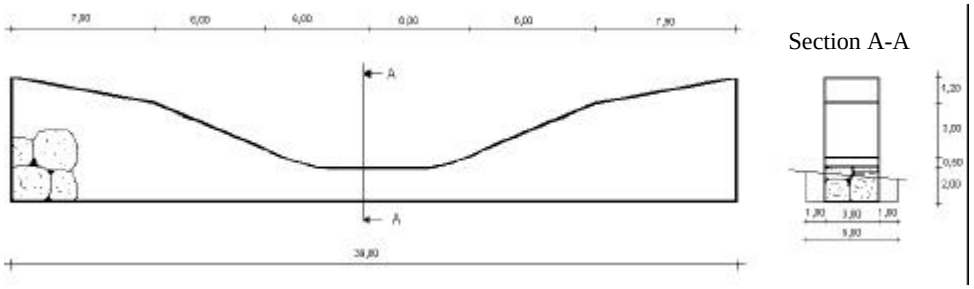

Figure 5.24 - Original bed sill design: front view and section.

Field measurements

During summer 2001, the main characteristics of local scour holes downstream of 26 bed sills were measured in the Plima River along the reach described in the previous section (Loza Lozano, 2002). The maximum scour depth y_s was taken with respect to the elevation of the sill crest, whereas the drop height z was measured as the difference in level between the sill crest and the most likely control section downstream of the pool: this could either be

determined by the artificial boulder berm described in the previous section, or represented by the point at which the river bed was no longer prevalently affected by local scouring dynamics, thus showing the onset of a positive gradient representing the equilibrium slope. In this way the drop height z should correspond to the morphological jump a_1 described in the introduction.

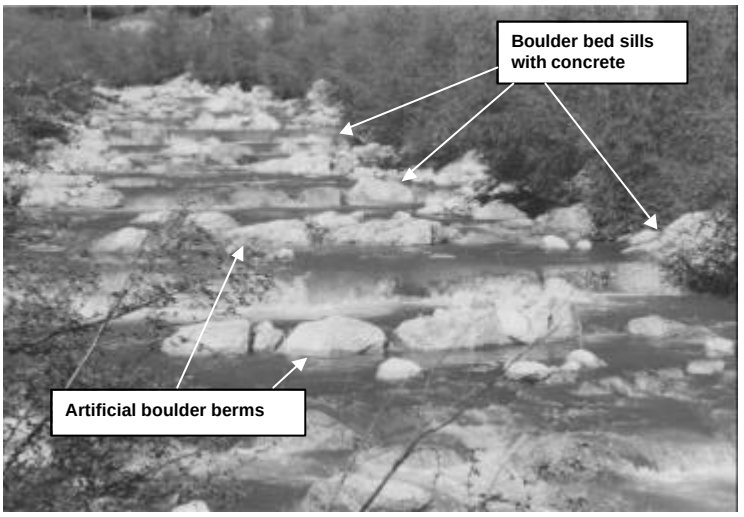

Figure 5.25 - View from downstream of the control works in the Plima River (May 2001); the site is the same of that shown in Fig. 5.22.

Measured drop heights z ranged between 0.15 and 2.80 m (on average 0.72 m); maximum scour depth y_s from 0.60 to 4.10 m with a mean value of 1.56. All the bed sills form part of a sequence, each lying within a short distance (on average 22 m) of another structure. Sills N° 17 and 26 are exceptions, being located at the end of their respective sequences, hence having no artificially-fixed bed level downstream: in fact N° 26 features the largest drop height z and scour depth y_s.

Bed sills N° 1-15 (hereafter Series 1 scours) are those where an artificial berm (a transverse row of very large boulders) was placed during the control works (section 2.1) 3 - 6.5 m from the sill edge . Sills N° 16-26 (Series 2 scours), however, are characterized by the absence of such a secondary structure.

The mean values of drop heights of Series 1 scours are half those of Series 2 scours, due to the control level represented by the boulder berm. Accordingly, maximum scour depths are also much lower in the former (i.e. 1.29 m vs 1.94 m) as are scour lengths (2.99 m vs 4.02 m).

On July 16, 2001, an almost constant water discharge of 18 m^3s^{-1} was released from the Gioveretto Dam into the Plima River, just one month before field measurements. Such a flow rate is the biggest released since the construction of the bed sill sequences. Taking into account the small portion of the basin flowing into the reach between the dam and the first bed sills, the water discharge used for the analysis was estimated as 20 m^3s^{-1}.

All local scour dimensions measured in August and September 2001 can therefore be tentatively correlated with such a discharge, which supposedly shaped the scour holes as they then appeared. Such a hypothesis is supported by the observation that almost all pool bottoms were armoured by coarse particles (D = 0.4-0.6 m), which are about the largest clasts found on the streambed apart from the large boulders placed in the channel during the control works. Finer sediments (gravel and sand) were only present at the pool sides.

Comparison with scour depth predictive equation (Eq. 4.2).

In order to evaluate the predicted values for y_s, the critical specific energy H_s has been calculated as (Eq. 3.27):

$$H_s = \frac{3}{2}h_c = 1.5\sqrt[3]{\frac{Q^2}{B^2 g}}$$

For each bed sill the critical flow depth h_c is therefore calculated from the water discharge of Q=20 m^3s^{-1} and the effective crest width B, different for each bed sill. Critical flow depth is thus assumed to occur at each bed sill crest, since supercritical conditions are most unlikely for approaching bed slopes around 0.03-0.05 characterised by very large relative roughness (Jarrett, 1984; Bathurst, 1985; Trieste, 1994; Grant, 1997). Evidence from the flume experiments also supports such an assumption.

The morphological jump a_1 should actually correspond to the measured drop height z. The relative sediment density Δ was assumed to be 1.63, while the D_{95} has been approximated to the average particle size D found at pools bottom, 0.5 m (Aderibigbe and Rajaratnam 1998).

Equation 4.2 reasonably predicts most measured maximum depths for both series, as shown in Figure 5.26. In fact, relative errors (i.e. |measured value-observed value|/measured

value) are on average 0.15. Ignoring labeled points representing somewhat "irregular" holes, the mean error becomes as low as 0.09

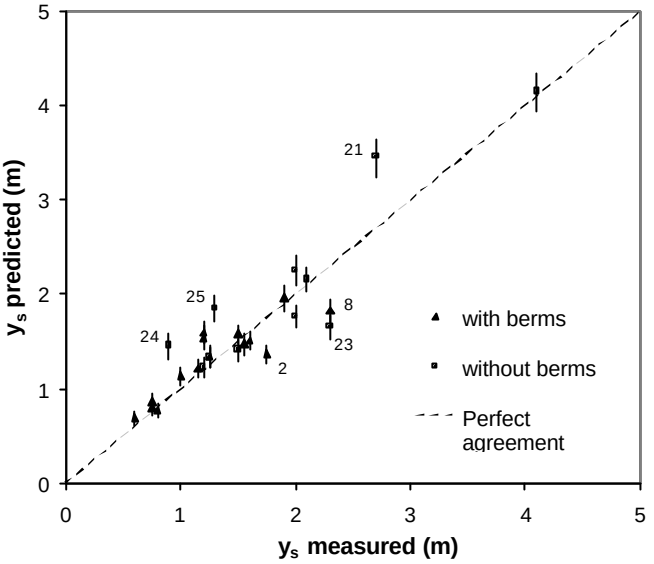

Figure 5.26 - Scatterplot relative to the maximum scour depths as predicted by Equation 4.2; "with berms" refers to Series 1 holes and "without berms" to Series 2 as discussed in the text.

The sensitivity (error bars) connected to the choice of a different water discharge for the calculation of critical specific energy is also shown in the graph. Error bars represent the variability of the scatterplot for flow rates between 15 and 25 $m^3 s^{-1}$. It appears evident both from the graph and a numerical appraisal of the relative errors that the discharge Q=20 $m^3 s^{-1}$ actually best fits the predictive equation.

Implications for grade-control structures

Boulder bed sills built in the Plima River 12 years ago have so far been effective in stabilizing the stream bed, reducing the longitudinal channel slope and fixing the bed level according to critical points along the river such as landslides and man-made structures (buildings, bridges, roads). Nevertheless, the transverse works have caused the typical morphological response in the stream bed apart from gradient reduction, i.e. the formation of deep scour pools. The project designers assigned a height of 2 m to the bed sills – including foundations – at the channel center-line (Fig. 5.24). Only the bed sills placed at the

downstream “closure” of a sequence (N° 17 and 26), were built higher in the absence of a fixed point immediately downstream.

Leaving aside these two particular cases, the measurements taken show that in 6 pools the maximum scour depth equals or exceeds the structure height of 2 m, with an extreme value of 2.7 m (bed sill N° 21). These works are therefore potentially at risk of failure. Local scouring capacity appears to be even more underestimated when considering that the scour holes were formed by a water discharge of only about 20 m^3s^{-1}.

Figure 5.26 seems to reject the hypothesis that artificial berms downstream of structures might lead to interference effects such as those observed in the laboratory (section 4.2.2 and 4.2.3), since Series 1 (presence of artificial berm) and Series 2 (absence of artificial berm) do not show any appreciable consistent difference between them. This is possibly due to the permeable nature of the downstream boulder berms, thus allowing bed material to be “swept away” downstream. However, even though they do not reduce scour depth by interference, such berms effectively diminish local scouring through the reduction of the actual spacing *L*; therefore they act as grade-control works themselves, fixing the bed level and thus determining the actual drop height for the upstream sills.

On the other hand, bed sill N° 26 is located at the lower end of the surveyed reach, and no grade-control structure is present downstream of it. Over a decade the “unconstrained” downstream bed erosion has therefore led to the formation of a 2.8 m drop height, which determines a total maximum scour depth of 4.1 m, the deepest pool measured in the Plima River. This evidence highlights the fundamental role of downstream control for the stability of control works in degrading rivers.

5.1.3 Analysis of scour dimensions

All the 73 scour holes measured in the six rivers described at the beginning of section 5.1 will be addressed here (Lenzi et al., 2003_b). In order to estimate jet thickness, one of the most important variables affecting local scouring, critical flow depth was assumed to occur at each crest, since strong supercritical conditions are most unlikely (Jarrett, 1984; Bathurst, 1985; Trieste, 1994; Grant, 1997; Tinkler, 1997; Wohl, 2000_a). For each grade-control structure the critical flow depth h_c is calculated from the peak water discharge Q (see Tab. 5.1) and the effective crest width B, through:

$$h_c = \sqrt[3]{\frac{Q^2}{B^2 g}} \qquad (5.2),$$

where g is the acceleration due to gravity.

Besides the flow depth (i.e. jet thickness), drop height at each structure is the other main variable in local scouring at grade-control works, as long as sediment size remains almost constant and interference effects due to short spacings between works do not occur. In fact, the combination of flow depth and drop height into a single parameter enabled the description of non-dimensional scour dimensions y_s and l_s obtained in flume experiments (see section 4.2.2).

Sediment size in the armoured layer at pool bottom was measured and it was observed that such clast dimension always roughly corresponded to the largest found along the channel bed. This allowed the approximation of the sediment size at pool bottom D to the D_{90}-D_{95} of the bed grain size distribution, as already found in laboratory tests by some authors (Whittaker, 1987_a; Aderibigbe and Rajaratnam, 1998). However, some others found the D_{85} to be median size of the armoured pool bottom (Hallmark, 1955; Kuroiwa, 1999) and in the next section this topic will analysed in detail. Such a strong armouring may suggest that the 73 surveyed scour holes actually achieved erosive equilibrium conditions, thus enabling us to neglect the temporal variable of the process, which otherwise would have been highly complex to deal with.

Furthermore, the three-dimensional aspect of local scouring will be not addressed, since most of the holes were consistently of the same depth along a cross-section, as also testified by the pool-to-crest width ratio B_p/B close to the unity (see section 3.2.3). Only the Maso

River, due to the slightly uneven nature of its boulder check-dams, presented some irregularly shaped scours, and this is likely to cause some additional scatter to its data.

In the following sections, local scouring characteristics will be analysed in non-dimensional terms according to critical flow depth h_c and to drop height z, by means of the drop ratio z/h_c. Points relative to the Wallingford Series 1 (i.e. non interfering) high-gradient tests described in 4.1.2 will also be plotted, with the assumption $z = a_1$, i.e. the measured drop height corresponds to the morphological jump (Figs. 5.2 and 4.12). Possible deviations due to other non-dimensional parameters (e.g. involving sediment characteristics or bed gradient) will be pointed out and discussed, since no better result was achieved by the introduction of more complex, comprehensive non-dimensional groups.

Maximum scour depth

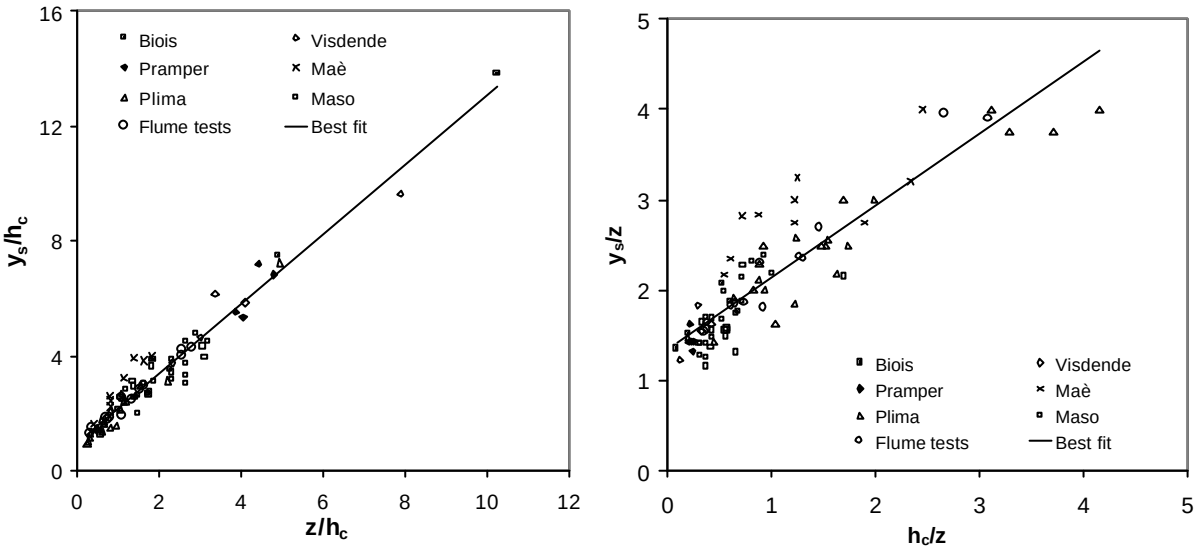

Figure 5.27 – Plot of non-dimensional maximum scour depth: (a, left) y_s/h_c versus the drop ratio z/h_c; (b, right) y_s/z against h_c/z. In the former the linear trend is much more defined. Flume points fall along with field data.

Figs. 5.27a and 5.27b show the maximum scour depth (m.s.d. hereafter) normalized to the critical flow depth (c.f.d.) and to the drop height plotted against the drop ratio z/h_c and its inverse, respectively.

The first graph displays a good linear trend. The equation, which also takes into account laboratory data is as follows:

$$\frac{y_s}{h_c} = 1.21\frac{z}{h_c} + 0.96 \qquad (5.3)$$

with R^2=0.95.

Such a linear response of the normalised m.s.d. to increasing drop ratios (i.e. to increasing drop height) "masks" the fact that y_s comprises the drop z (Fig. 5.2). A certain degree of spurious correlation is therefore present in the regression. In fact if one considers only the residual scour depth $s = y_s - z$, the plot still shows a positive trend but with a very large scatter (graph not shown). However, being y_s the variable of interest when designing bed sills, Equation 5.3 represents a valuable tool; it also suggests that when the drop ratio approaches zero (i.e. very small drops in relation to the flow depth) the m.s.d. is approximately equal to the c.f.d.

In Fig. 5.27b the effect of increasing c.f.d. on the drop-normalised m.s.d can be evaluated. Even if at a first sight the trend appears to be non-linear, the best-fit equation turns out to be:

$$\frac{y_s}{z} = 0.80\frac{h_c}{z} + 1.34 \qquad (5.4)$$

with R^2=0.81.

For h_c/z approaching zero the y_s/z tends to values close to the unity (i.e. no scouring), while for larger flow depths the points plot below the linear trend line, hinting that scouring effectiveness possibly decreases for such low-drop conditions.

In both graphs, flume points displace nicely among the field data, roughly at the baricentric line of the cloud and along the best-fit curve. If it is not a mere coincidence, this should lead one to consider laboratory experiments as well representative of the physical phenomenon occurring at a real scale. Further, in Fig. 5.27b, field data show a considerable scatter, as was predictable considering that only one simple non-dimensional parameter was adopted for the analysis. Nevertheless, in Fig. 5.27a the dispersion of the points around the trend is much less apparent. Generally, it seems that the existing differences among the six rivers (i.e. bed slope, sediment lithology and size, hydrologic characteristics of flood events) play a minor role in determining how deep scour holes can be. The reason might lie in the overlapping ranges – see Tab. 5.5 – of other non-dimensional basic parameters, like h_c/D and z/DD (Gaudio et al., 2000). In fact, the only river which points plot well apart from the others

is the Mae', which features the lowest mean channel slope and fairly high h_c/D ratios (see. Tabs. 5.2 and 5.5). The Plima River is characterised by similarly high ratios, but its mean slope is steeper. The reasons for a milder-sloping channel being more prone to local scouring are not yet clear, but presumably they might be related to downstream flow conditions, ie. tailwater depth and velocity, as will be argued later.

Table 5.5. Range of non-dimensional parameters for both field data and flume tests.

River	z/h_c	h_c/D	$z/\Delta D$	z/H_s
Mae'	0.41-1.83	1.64-2.53	0.41-2.35	0.27-1.22
Biois	1.86-10.26	0.67-0.85	0.80-4.23	1.24-6.84
Plima	0.24-4.95	1.13-3.71	0.18-3.44	0.16-3.30
Pramper	3.87-4.80	1.36	3.22-3.99	2.58-3.20
Visdende	0.66-7.89	0.89-1.14	1.55-5.26	1.27-4.38
Maso	0.59-3.20	0.8	0.29-1.57	0.39-2.13
Flume tests	0.32-2.79	0.39-1.10	0.16-1.15	0.22-1.86

Let's consider now the problem from an energetic perspective. When the m.s.d. is normalised to the flow energy available at each drop (i.e. potential z + critical specific energy H_s=1.5h_c), a weak positive trend is revealed when plotted against the drop ratio (Fig. 5.28). For drop ratios larger than 3, there seems to be a constant asymptotic value around 1.1-1.2. Non-dimensional m.s.d range between 0.55 and 1.35, with an average value of 0.92. The Mae' River data fall as usual above the others, whereas flume points plot roughly in the middle of the cloud.

Scour length and berm position

Figs. 5.29a and 5.29b show the scour length normalized to the c.f.d. and to the drop height plotted against the drop ratio z/h_c and its inverse respectively. Flume data are not available as explained at page 123. Unlike the maximum scour depth, the former normalization leads to a highly scattered graph, which nevertheless displays a positive correlation of scour length to drop height when the c.f.d. influence is taken out. A better-defined positive trend is shown in Fig. 5.29b against the c.f.d. for drop-normalized points. Likewise for the maximum scour depth, the Mae' points plot higher than the other rivers. The best-fit regressive equation for l_s/z against h_c/z takes the form of a second grade polynomial:

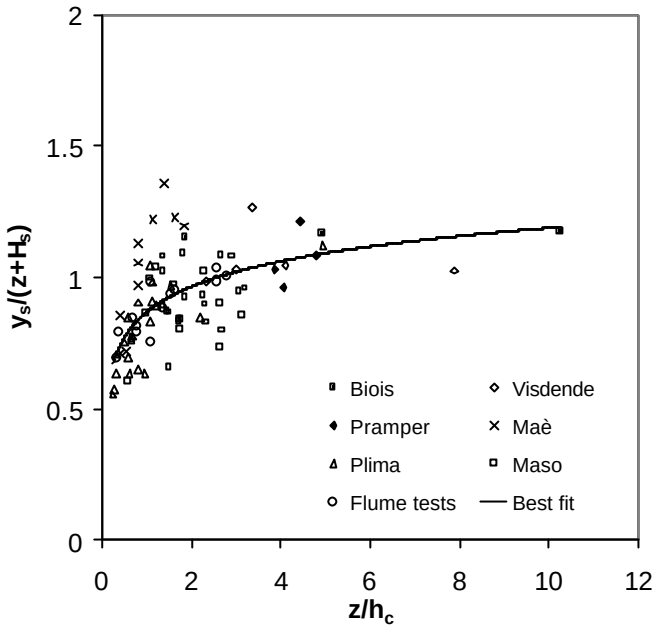

Figure 5.28 – Energy-based normalization of the maximum scour depth: the quantity $y_s/(z+H_s)$ as a function of the drop ratio z/h_c. An asymptotic trend towards a value slighly above the unity is apparent for high drop ratios.

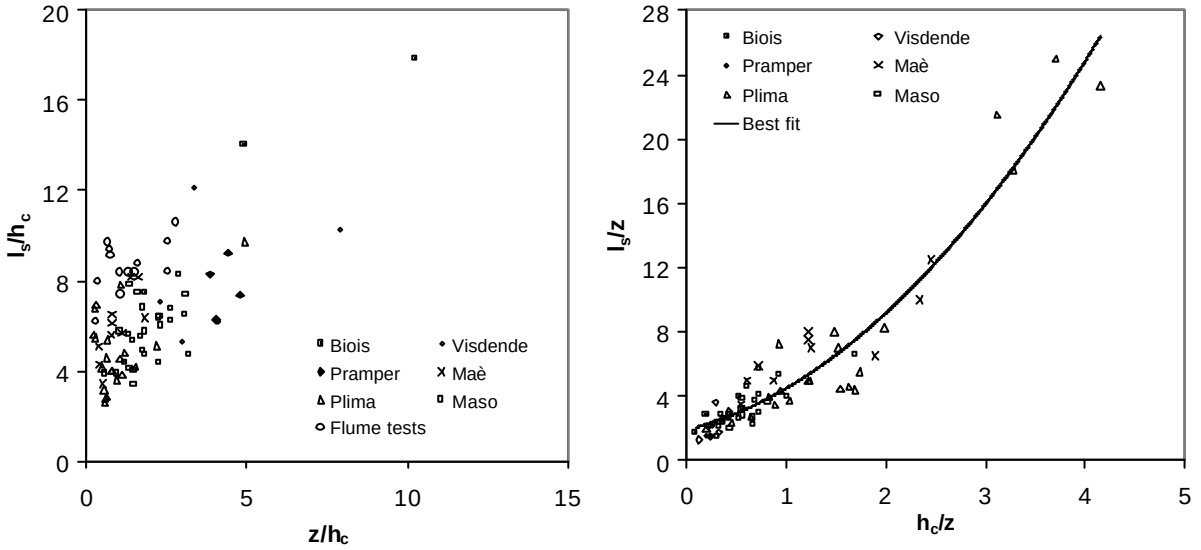

Figure 5.29 – Plot of non-dimensional scour length: (a, left) l_s/h_c versus the drop ratio z/h_c; (b, right) l_s/z against h_c/z. The latter normalization appears to be more suited, indicating the stronger influnce of the critical flow depth (i.e. jet thickness) upon the scour length than the drop height.

$$\frac{l_s}{z} = 1.05\left(\frac{h_c}{z}\right)^2 + 1.54\frac{h_c}{z} + 1.89 \qquad (5.5),$$

leading to a correlation of R^2=0.91.

Similar results are shown analysing the berm distance l_b and the same couple of non-dimensional graphs is presented (Figs. 5.30a and 5.30b).

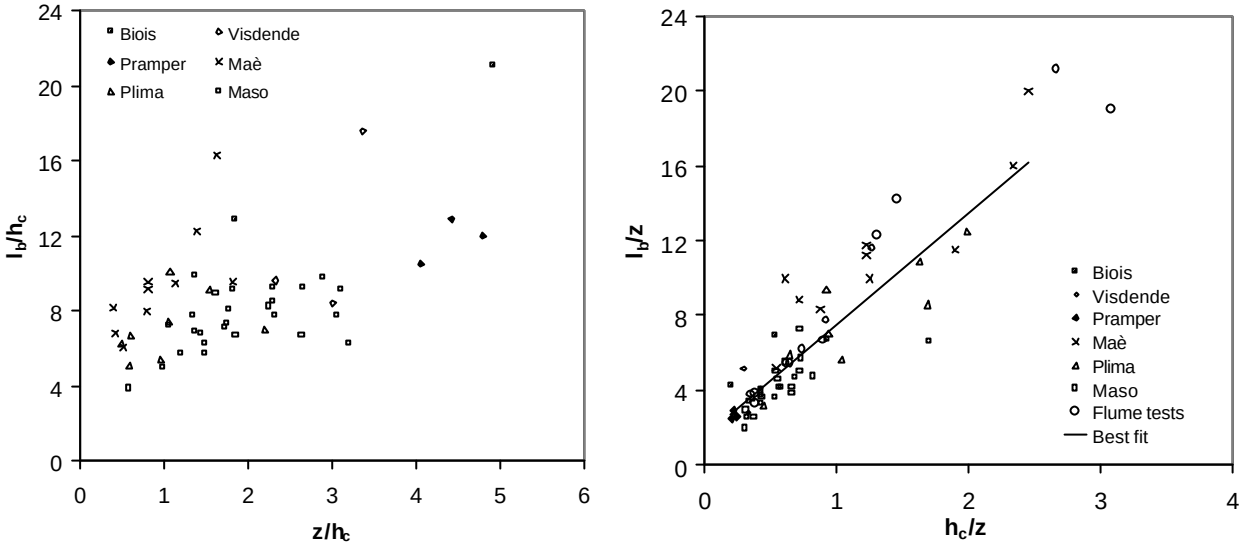

Figure 5.30 – Plot of non-dimensional berm distance: (a, left) l_b/h_c versus the drop ratio z/h_c; (b, right) l_b/z against h_c/z. As noted for the scour length, the second approach provides a better description of field data variability.

In this case field points are fewer but, on the other hand, flume data are available (p. 123). A positive yet weak correlation is apparent between c.f.d.-normalized berm position and drop height, while the drop-normalized relationship seems to be stronger. The best-fit equation (R^2=0.85) is linear:

$$\frac{l_b}{z} = 6.38\frac{h_c}{z} + 1.35 \qquad (5.6).$$

Analogously as done for the scour depth, let's now normalize scour length and berm distance by the available energy at each crest, i.e. $z + H_s$ (Figs. 5.31 and 5.32 respectively). The former shows a knee-shaped decreasing trend, steeply moving from $l_s/(z+H_s)$ around 4 for drop ratios close to zero towards values between 1.6 and 2.4 for z/h_c around 2. Thereafter, the decreasing trend is much gentler, with values around 1.1-1.5 even for very large drop ratios.

To the berm position l_b, again a negative correlation is shown but in this case it appears to be more constant, possibly because of the lack of points for both small and large drop ratios.

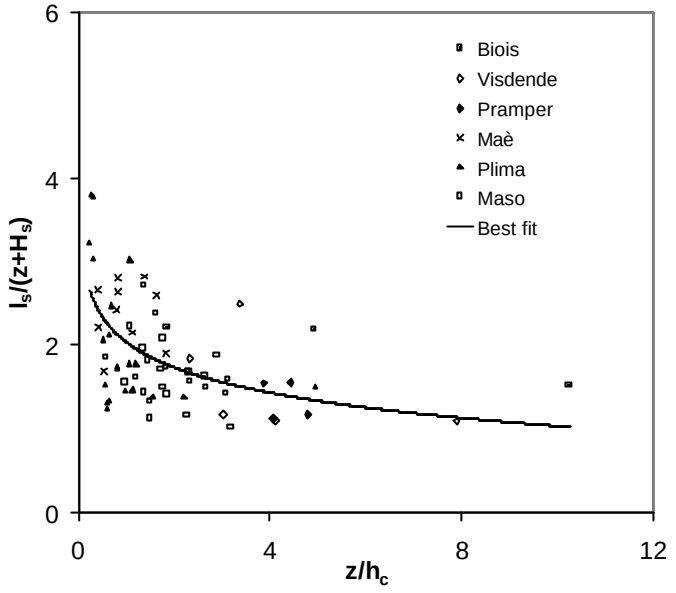

Figure 5.31 - Energy-based normalization of the scour length: the quantity $l_s/(z+H_s)$ as a function of the drop ratio z/h_c. A marked decreasing trend is shown.

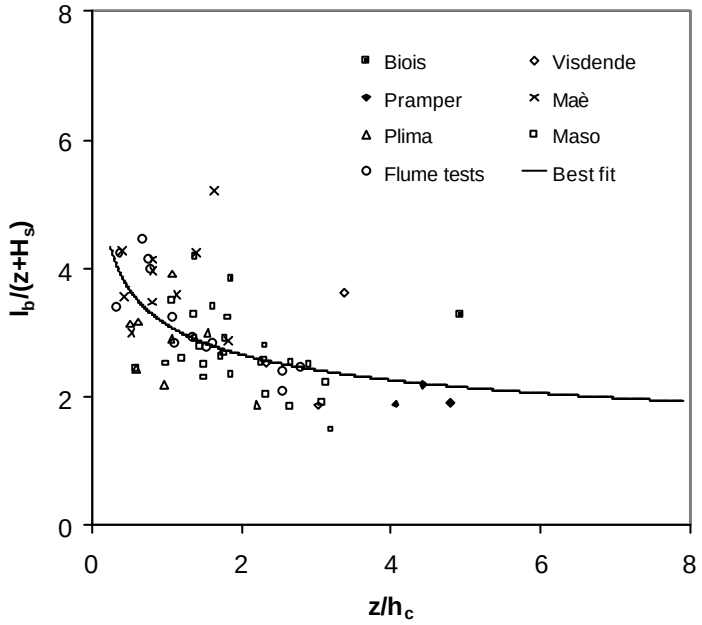

Figure 5.32 – Energy-based normalization of the scour length: the quantity $l_b/(z+H_s)$ as a function of the drop ratio z/h_c.Likewise the scour length, as the drop ratio increases the normalized distance diminishes.

Scour hole shape

Detailed profiles of the scour holes were not taken, nevertheless it is possible to outline the average shape as well as deviations from it by means of some non-dimensional geometric parameters (Tab. 5.6). First, let us consider the ratio l_{max}/l_s between the m.s.d. distance and the scour length.

Table 5.6. Some geometrical ratios of scour holes (N = number of observations).

	Range	Mean value	Standard deviation	N
l_{max}/l_s	0.22 – 0.71	0.37	0.11	39
S_e	0.11 – 0.73	0.33	0.11	36
l_b/l_s	1.18 – 2.4	1.51	0.26	50
$l_s/(s+h_c)$	1.19 – 4.01	2.50	0.65	69

The average value is 0.37, with a standard deviation of 0.11 (sample dimension N=39). Such a result is in agreement with many experimental studies which have shown that the deepest point in an impinging jet-formed scour hole occurs between 0.3 – 0.4 (Gaudio et al., 2000) and 0.5 (Whittaker, 1987_a). There seems to be a positive correlation with the drop ratio, but it is rather weak and the scatter is considerable (graph not shown). Since the drop ratio gives information about the impinging jet angle – the higher the ratio, the more vertical the jet (Stein and Julien, 1994) – the positive correlation might explain the low l_{max}/l_s ratios found by Gaudio et al. (2000), who tested low-gradient (<0.01) channels, compared to the higher ratios observed by Whittaker (1987_a), which regarded steep (>0.09) gradients.

Moving into the scour hole downstream from the maximum depth, the exit pool gradient S_e is then encountered (Fig. 5.2). The average value turns out to be 0.33, (approximately 18 degrees with respect to the horizontal) with a standard deviation of 0.11 (N=36). A large scatter is thus present again, but no trend is now apparent with the ratio h_c/z. A negative correlation was expected to be found in the light of the observations that such an exit slope is positively correlated to the jet inclination (see section 3.2.2). However, Kuroiwa (1999) found that this slope is constant for jet inclinations below 18° with respect to the vertical. More likely in this research the lack of any correlation might be due to sediment deposition in the pool exit zone occurring during subsequent lesser events, as described by Whittaker (1987_b, see next section).

Downstream of the scour length point, a subhorizontal span occurs before the berm. The mean ratio l_b/l_s between the berm distance from the structure and the scour length is 1.51,

featuring a standard deviation of 0.26 (N=50). A negative correlation to the drop ratio can be inferred for this ratio, despite the scatter. This would imply that the more vertical the jet, the closer the berm to the pool end.

Finally, considering the scour length-to-depth ratio l_s/y_s, an interesting trend is shown when plotted against the drop ratio (Fig. 5.33). As long as the drop ratio is lower than about 2, a strong negative correlation holds, with l_s/y_s ranging from 6.6 to roughly 2. At z/h_c around 2, a sharp change in the trend gradient is apparently present, since thereafter ratios l_s/y_s decline slowly from values around 2 to 1.1-1.4 at drop ratios around 4-5. The two points characterised by very high drop ratio, i.e. 7.9 and 10.3, feature length-to-depth ratios that are not smaller, suggesting an asymptotic trend might be present. More data are needed in order to establish reliable results for this extreme limb of the curve.

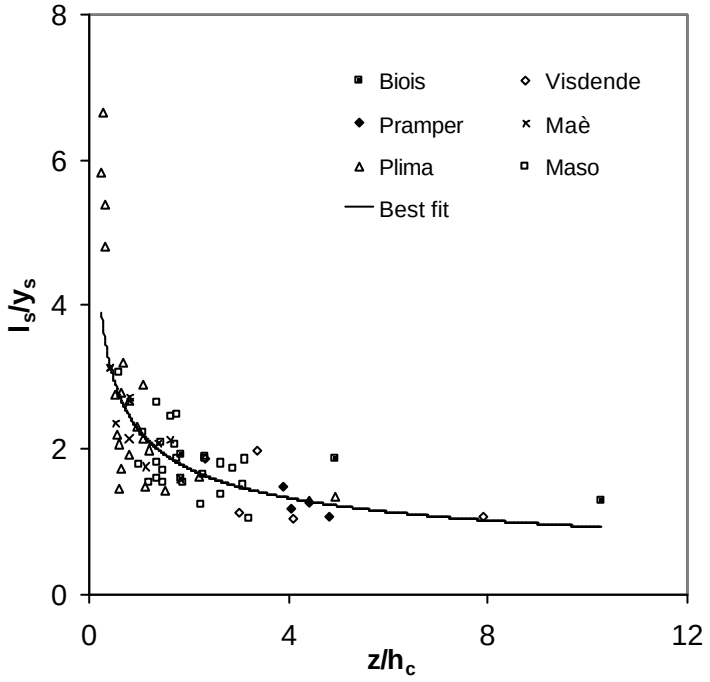

Fig. 5.33 – Relationship between the length-to-depth ratio and the drop ratio: a strong decreasing trend is evident from values up to 7 (Plima's low bed sills) towards the unity (Visdende's high check-dams).

If the ratios between the scour length l_s and the residual depth $s = y_s - z$ are computed, no trend is shown and the range is very large, between 2.2 and 9.1. Nevertheless, when the critical flow depth is added to the residual depth the ratio $l_s/(s+h_c)$ varies from approximately 1.2 to 4, with an average of 2.50 and a standard deviation of 0.65. Here the c.f.d. is used to provide a likely minimum value for the unknown tailwater depth. In fact, Franke (1968) found

that the ratio $l_s/(s+h_v)$, where h_v is the tailwater depth, was an invariant characteristic of scour holes obtained in several flume tests, averaging 1.8. Therefore the results of this research seem to support his findings, taking into account that tailwater depth must generally be somewhat larger than the c.f.d. Finally, considering the berm distance, the average ratio $l_b/(s+h_c)$ for the field data turns out to be 3.56, very close to the mean value 3.65 exhibited by the 13 high-gradient flume data.

Comparison with predictive equations (Eqs. 4.2 and 4.3)

In order to calculate predicted values for y_s and l_s, Eqs. 4.2 and 4.3 can be used, whereas Eq. 4.17 would require the gradation coefficient of the grain size distribution which is not known for most of the surveyed rivers. In fact, unfortunately, Padova tests were performed after the field activity was carried out.

As to the parameters needed in Eqs. 4.2-4.3, the critical specific energy H_s is calculated from Eq. 3.27, and the morphological jump a_1 is approximated to the measured drop height z (see 5.1). Relative sediment density Δ is assumed to be 1.63 for all the rivers, while the D_{95} is approximated to particle size D found at the pool. Field data present ratios z/H_s ranging between 0.16 and 4.38 and z/DD between 0.16 and 5.26: these intervals are wider than those of the flume tests used to obtain the empirical equations (Table 5.5).

Equation 4.2 is effective in predicting most measured maximum depths, as shown in Fig. 5.34. In fact, defining relative errors ε of the estimate as:

$$e = \frac{\left| observed\ y_s - predicted\ y_s \right|}{observed\ y_s} \qquad (5.7),$$

they present an average value of 0.13. Looking at the six rivers, it is evident how the Mae' data are all slightly underestimated, as are those of the Biois though to a lesser extent, whereas most of the Maso, Visdende and Pramper maximum depths are weakly overestimated.

In contrast to the fairly good performance of Eq. 4.2, the longitudinal extension of the local scouring is very poorly predicted by Eq. 4.3, which generally overestimates measured values (graph not shown). Predicted l_s values are in this case compared to the measured values

l_b, as previously explained, whereas measured l_s values cannot be compared to previous flume results. The reason underlying such differing accuracy between scour depth and scour length (i.e. berm distance) is not yet clear. However, one might tentatively propose the hypothesis that the low-gradient data – characterised by very long scour holes (Gaudio et al., 2000) – used to get Equations 4.2 and 4.3 led to a formula overestimating scouring dimensions in steep channels.

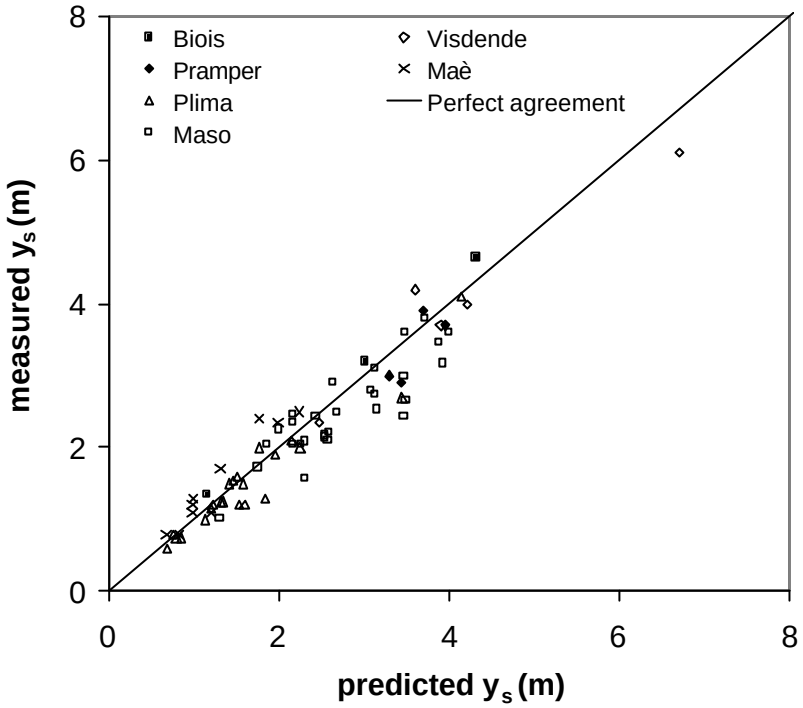

Figure 5.34 – Scatterplot referring to Equation 4.2's prediction of measured scour depths: the mean relative error is 13%.

Discussion

To date, no field studies had addressed the problem of scour hole dimensions below grade-control structures in steep rivers, apart from Falciai and Giacomin (1978) who measured local scouring at grade-control works in several rivers in the Tuscan Appenines (Central Italy). The formative discharges were assumed to be those with a 20-year return period. Working on their data set, they proposed an empirical formula similar to the classical model by Schoklitsch (1932) but with an exponent for the D_{90} equal to 0.19, lower than Schoklitsch's 0.32. Mason and Arumugam's (1985) formula obtained through both model and

prototype data features an even lower exponent for the grain size, 0.10, but in that case the mean diameter was used.

It appears, therefore, that the phenomenon of local scouring in rivers is not very sensitive to bed sediment size, at least much less than to the other independent variables acting in the system, i.e. drop height and specific discharge-critical flow depth. Further, the actual determination of an effective grain size is not straightforward, since a commonly performed pebble count survey would provide the D_{90} of the surface material, which can be much larger than the corresponding percentile for the sub-surface sediment. Since scour holes deepen into the bed material during a flood event after grade-control works are completed, the use of pebble count-derived grain sizes might be misleading. On the other hand, performing volume sampling in order to get a reliable bed grain size distribution is very expensive and also has a considerable environmental impact, because for strongly non-uniform distributions with coarse fractions typical of mountain rivers a considerably high volume is required.

Therefore it seems valuable to provide designers the following simple relationship which does not need any sediment size, which is derived from Figure 5.28 :

$$0.6 \leq \frac{y_s}{z + H_s} \leq 1.4 \tag{5.8}$$

As to scour longitudinal dimensions (i.e. l_s and l_b), given the strong influence of the drop ratio on their normalized values (Figs. 5.31 and 5.32), it does not appear appropriate to propose a similar inequality.

This relationship must be considered valid only for perennial mountain rivers with mean channel gradient larger than 0.02 and up to 0.16.

Equation 5.8 can be regarded as statements about scouring efficiency at the equilibrium given a certain amount of flow energy. A very small part of the original jet energy is dissipated before entering the tailwater, but during this stage air entrainment occurs (section 3.2.1). From the point the nappe penetrates the plunge pool, a great deal of energy becomes dissipated through momentum diffusion, causing large-scale turbulence. The amount of energy that remains available for picking up clasts and sweeping them out of the scour hole depends on many factors, e.g. jet inclination and aeration, boundary bed roughness, tailwater depth. However, for given remaining energy amount to scour the bed, boundary resistance to erosion still has to be accounted for. Nevertheless, the present research's field data seem to

indicate the minor role played by sediment resistance compared to the jet energy and jet characteristics.

If the residual depth s (i.e. y_s-z) is now considered (Fig. 5.35) – in order to take away the direct geometric "weight" of drop height upon the m.s.d. – a decreasing trend is apparent, suggesting the actual scouring efficiency does decrease with larger drop ratios.

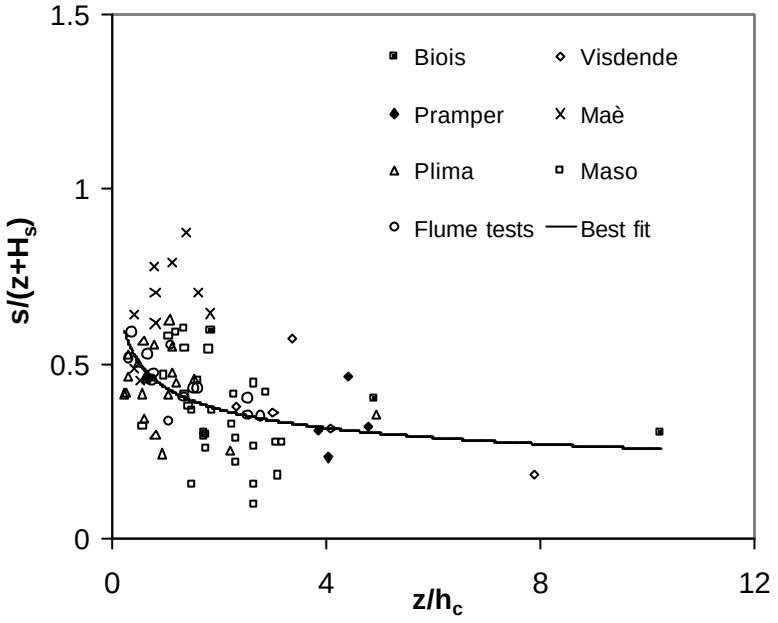

Figure 5.35 – Energy-based normalization of the residual scour depth: the quantity $s/(z+H_s)$ as a function of the drop ratio z/h_c. Unlike in Fig. 5.28 which refers to the scour depth with respect to the crest elevation, the residual depth appears to decrease for larger drop ratios.

Since previous flume studies have shown that more inclined plunging jets tend to be more effective in scouring sediment from the pool bottom, it is likely that such an opposite trend might be determined by the effect of jet aeration, which is directly proportional to the drop height (see section 3.2.1). The available energy of the water fraction of the jet does not change significantly even when the air concentration is high. However, air entrainment is relevant because the total energy of the jet is expanded into a larger area before impingement. The air concentration of the jet at the tailwater surface influences the velocity decay of the centerline of the jet after impingement (see 3.2.1).

Additionally, jet air concentration may alter the jet trajectory within the pool because of the buoyancy of air bubbles which would push upward the immerging flow (Prof. P.Y. Julien, Colorado State University, personal communication).

From Figures 5.28 and 5.35 it is again well apparent that the Mae' data – featuring a higher scouring efficiency – seem to be affected by some factors not acting in the other rivers, as reported above.

In particular, tailwater conditions (i.e. depth and velocity) are actually a variable affecting free jet local scouring dynamics but their role is not addressed in this research as well as in the previous laboratory experiments on bed sills because of the uncertainties connected to their reliable prediction. In fact, unlike the case of isolated drops with secondary structures determining such a depth, in a typical staircase-like sequence of grade-control structures this appears to be mainly controlled by the flow depth established downstream from the pool, according to the actual flow resistance encountered along that reach, plus the effect of possible altered flow pattern (i.e. convergence-divergence) due to bank constrictions or irregularities. Just taking into account the problems arising when attempting to properly quantify flow resistance in steep, large-roughness channel beds, seems to suggest any parameter involving tailwater depth should not be included in a predictive formula.

However, other possible factors leading to the deep scour holes in the Mae' River can be envisaged. First, the Mae' channel presents the least rough bed boundary, and its banks are also much smoother than the other rivers. These together might have determined the establishment of slightly supercritical conditions, despite the Mae' lowest bed slope, thus making the flow at crests more energetic (i.e. Froude numbers above the unity) than in the other channels.

Secondly, Mae' scour holes were the most two-dimensional, notwithstanding their wide cross-section, whereas in the other rivers they exhibited a more or less three-dimensional aspect which was not addressed in the present research. As found by D'Agostino (1994), the more three-dimensional the scours, the shallower their depth for otherwise similar conditions. However, flume test points also fall below the Mae' data in all the graphs, despite their overall strong two-dimensionality.

Finally, as shown in section 4.2.6, standing waves were observed to occur at Mae's bed sills during a recent (2002) flood event (Fig.4. 43). An impinging jet regime was instead either directly witnessed or presumed at the other grade-control structures analysed above. Hence it may also be hypothesised that surface jet regimes are more scouring-efficient compared to the impinging regime, where its highly turbulent characteristics dissipate more flow energy, thus leaving less of it for scouring and sweeping sediments out of the scour hole.

5.1.4 Sediment longitudinal sorting

The reason to study sediment sorting along a sequence of grade-control structures is multifold. Primarily, the evaluation of the degree of armoring of pool bottom should help identify which grain size of the original bed mixture is the limiting one in the scouring process, since field quantitative descriptions of pool armoring are still lacking, as well as validation of lab results like those by Hallmark (1955) and Kuroiwa (1999). As already reported in section 3.2.2, these two authors studied in a physical model scour holes below dams, and analyzed sediment sorting in the scour hole. Hallmark found that the material constituting the bottom surface of scour holes was approximately D_{85}; Kuroiwa reported median grain size at the bottom ranging from D_{77} to D_{85}, and selected D_{85} to be used in his maximum scour depth equation.

Beside the coarsening of pool bottom, deposition of finer material at pool exit slope has been described for riffle pools (Lisle, 1982) and step pools (Whittaker, 1987_b), and its implications for watershed management have been put forward (Lisle and Hilton, 1992, 1999; Wohl, 2000_a). Furthermore, pool-end berms are characterized by being visually coarser than the surrounding material but no studies have quantified it yet.

Two channels were chosen in order to look at surface grain size sorting occurring along an artificial step pool sequence: the Cordevole River at Arabba (Belluno, Italian Alps) – which provided the scouring data used in 4.2.3 (Lunardi, 2002) – and the Mae' River at Forno di Zoldo, in the same reach object of scour dimensions analysis in 5.1. The former is a small basin (drainage area of 12.5 km^2), with a rather steep (S=0.06) and narrow (B=10m) channel, whereas the latter – a much larger basin, 79 km^2 – features a gentler slope (S=0.02) and a wider channel (B=14.5-27 m).

Extensive grid-by-number pebble counts were carried out in both sites on the stream bed area downstream of pools, where the "equilibrium" slope was present, between l_b and L (see Fig. 5.2). The grain size distribution of this zone will serve as a reference for the other distributions referring to different pool areas such as pool bottom, pool exit slope (between l_{max} and l_s, pool end (between l_s and l_b) and finally berms.

The reference grid counts in the sloping bed length were performed using the systematic, spatially integrated methodology described in Bunte and Abt (2001), whereas for the other zones different local methods were required, and they differed between the two field sites due to their strongly dissimilar width.

On the sloping bed downstream of pools, in the Cordevole four grids – each featuring more than 200 sampling points – were set up along the reach and then all the clasts were put together and treated as a single sample (total of 951 points) to produce the reference surface grain size distribution. Also in the Mae' River four grids were performed, but with a larger overall sample size: 1614 clasts.

Figure 5.36 – Cordevole River, example of one pebble-counts grid; view from upstream, a sill crest is visible at the lower left corner.

Figure 5.37 – Maè River, example of one pebble-counts grid; view from downstream.

Figure 5.38 – Maè River, a closer view of the sampling grid; a bed sill is on the right.

In the Cordevole River, all pool bottom and berm-forming clasts were measured in the 13 pools surveyed, since they were few at every pool; some difficulties were encountered because berms did not stretch along the whole cross-section in some cases, being punctuated by spots with deeper flows and finer sediments. It was decided to measure only particles along the berm's cross-section that were clearly coarser than the surrounding ones; unfortunately this methodology introduces a certain degree of subjectivity in the sampling. At pool exit slope and pool end zone the particles to be measured were instead chosen along three stream-wise transects, selecting all adjacent clasts along each transect.

In the Mae' River, given its larger width, clasts at all pool locations except berms were selected following a similar transect procedure, but in this case the number of lines was larger (10-12).

At each pool, all the measurements referring to the four pool zones were added up and treated as a single sample, in order to come up with a single grain size distribution for each of them. Subsequently, putting together and considering as a single sample all the pools, each river could be characterized by 4 curves only for its pool locations, plus the one stemming from the equilibrium sloping span downstream.

In the Cordevole River, 162 particles were measured at pool bottoms, 431 at pool exit slopes, 264 at pool ends, and 61 at berms. As stated above, the "uniform flow" zone (i.e. the

sloping bed downstream of pools) sample is made up by 951 points. The frequency distributions are shown in Fig.5.39a , whereas in Fig. 5.39b are their cumulative curves.

In the Maè, 137 particles were sampled at pool bottoms, 494 at pool exit slopes, 416 at pool ends, and 52 at berms. The equilibrium slope area features, as already described, a sample size of 1614. In Figs. 5.40a and 5.40b the grain size distributions are reported.

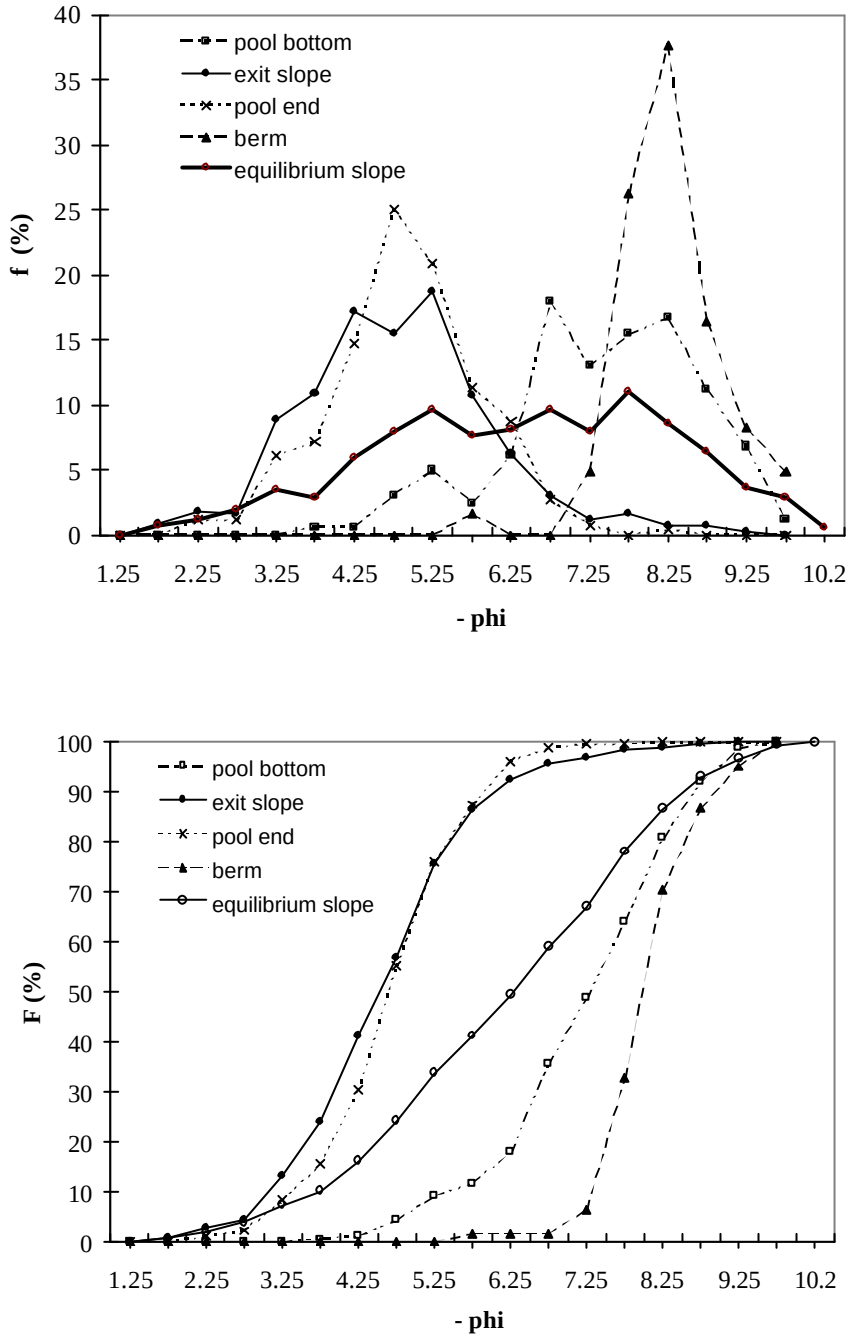

Figure 5.39 – Grain size distributions in the Cordevole River: (a, above) frequency curve; (b, below) cumulative frequency curve.

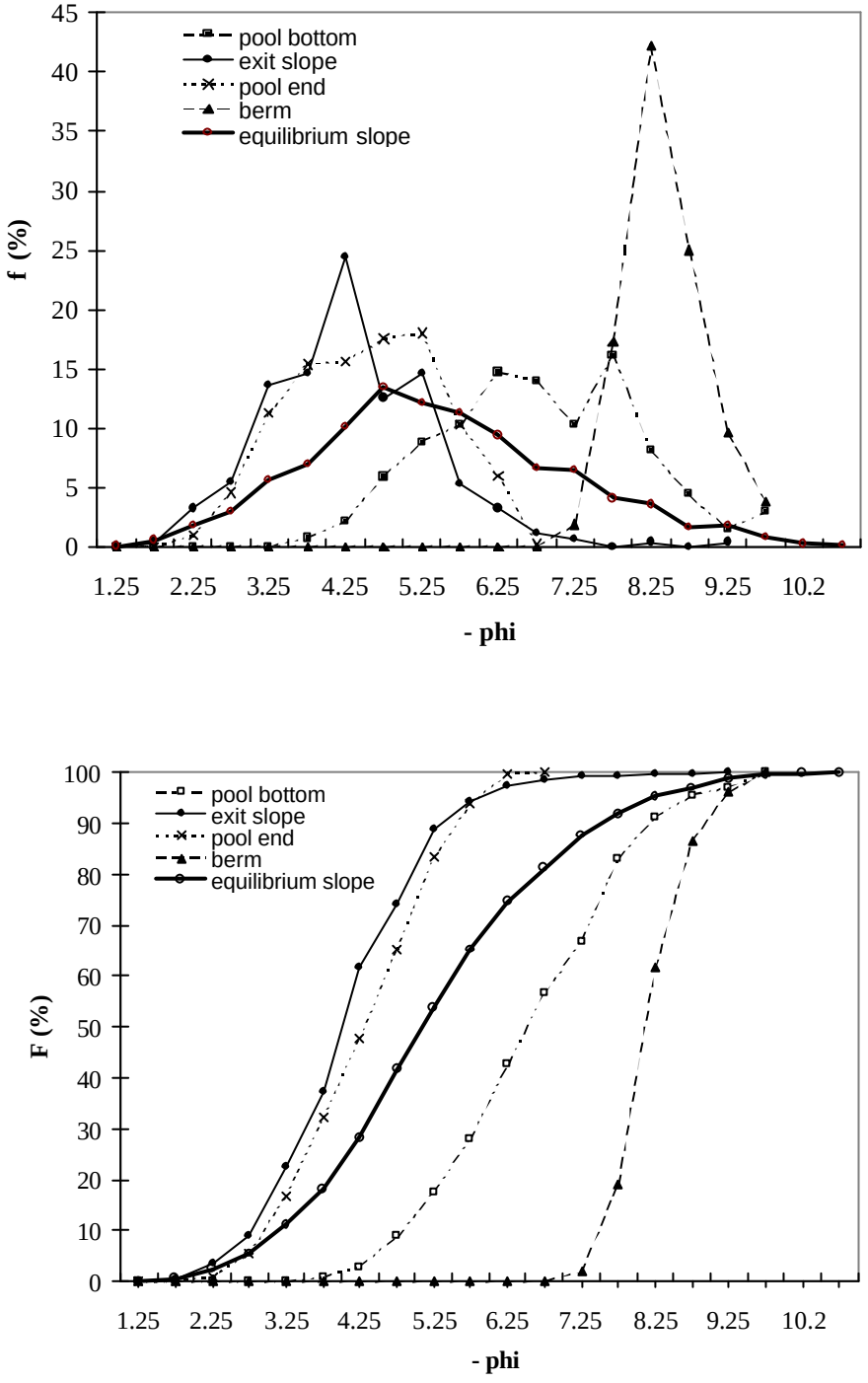

Figure 5.40 – Grain size distributions in the Maè River: (a, above) frequency curve; (b, below) cumulative frequency curve.

In the Cordevole, the mean f (=$\log_2 D$) value for particles at pool bottoms is –7.86, equal to 232 mm. This size approximately corresponds to the D_{80} of the equilibrium slope stretch. A larger degree of armoring is apparent for the Maè, where the mean f value for the pool bottom is –7.24 (152 mm), matching the D_{87} of the reference, undisturbed bed. These findings thus support Hallmark's (1955) and Kuroiwa's (1999) laboratory results about the armoring of the scour hole bottom. However, a difference exists as to how the reference grain size distribution is evaluated, here the bed surface layer having been considered in contrast to volumetric analysis of the pre-test sediment performed in the laboratory.

In both rivers, particles collected at pool ends and exit slopes show similar distributions, finer and well-sorted compared to the reference curve (D_{30}-D_{35} for the Maè, D_{33}-D_{38} in the Cordevole). Particles found at berms represent the coarsest – and more uniform too – group: in the Maè f_m= -8.2 (295 mm) equivalent to the D_{95} of the undisturbed downstream bed, for the Cordevole the f_m is - 8.42 (342 mm), corresponding to the D_{90}. These results contrast with Kuroiwa's findings about the grain size distributions of the pool downstream slope and of the mound formed immediately downstream: he described sediment at the mound as always finer than particles at pool bottom and the downstream slope to feature clasts almost as coarse as those of the bottom. As to the first disagreement, the much more heterogeneous and coarser sediments in the field situations analyzed here might be involved. For the second discrepancy, the role of subsequent deposition in the pool by waning flows can be hypothesized, as described by Whittaker (1987_b).

The fact that berms are formed by very large, well-sorted clasts (D_{90}-D_{95} of the surface distribution) suggests a sort of analogy with natural steps, which have been described as composed of a similarly coarse fraction of the streambed grain size distribution (Grant and Mizuyama, 1991; Chartrand and Whiting, 2000). This idea will be explored and tested in detail in sections 5.2 and 5.3.

5.2 Pool dimensions in natural step pool streams

Five channels were selected for the survey of "natural" pool dimensions (Fig. 5.41), all but Biois drain rather small catchments (<20 km^2, Tab. 5.7), and represent typical natural step pool sequences. Natural pools in the Biois river were instead measured in the trained reach object of the study described in the previous sections, between two check-dams. Geologically, the basins lie in the Dolomitical area and present very complex alternations of sedimentary and igneous rocks. An exception is the Digon catchment, which features a prevalent metamorphic substrate.

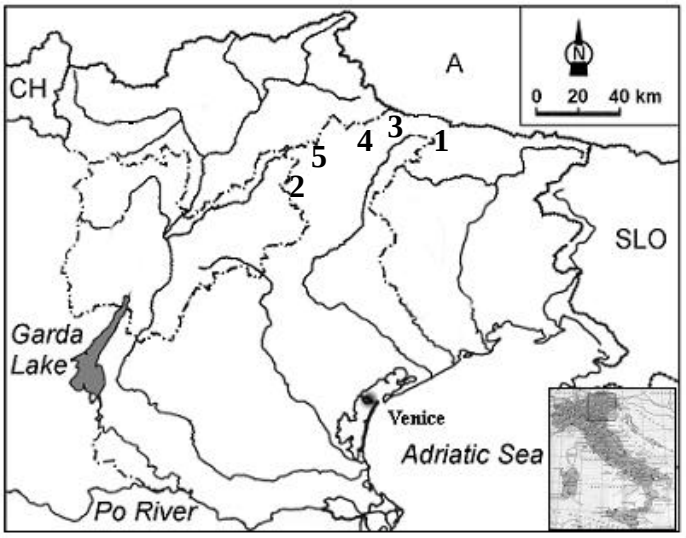

Figure 5.41 – Location of the study basins for natural pools; numbers refer to Tab. 5.7.

Table 5.7 – Main characteristics of the five basins, with the number of pool measured for each channel.

	Basin	Area (Km^2)	Max elevation (m a.s.l.)	Min elevation (m a.s.l.)	Channel length (km)	Mean gradient (m/m)	N° Pools
1	Piave	1.18	2639	1675	2	0.15	10
2	Biois	134	3192	780	14.5	0.07	5
3	Digon	16	2678	1630	5.4	0.10	5
4	Giralba	12	3046	1180	4.87	0.13	6
5	Cordon	5	2748	1763	3	0.16	11

A total of 37 natural pools has been measured (Andreoli, 2002). The surveyed dimensions are shown in Fig. 5.42. Bankfull width at steps, at pools and, most importantly,

bankfull flow depth at steps were also surveyed. The latter, in fact, will be hypothesized to correspond to the critical flow depth, in order to allow a comparison with pools below artificial steps, adopting similar dimensionless approaches. Discharge data are available only for the Rio Cordon creek, where a recording station for flow and sediment rates is located just downstream of the surveyed reach (Lenzi, 2001). Hence jet thickness, in contrast to the case of grade-control structures where it was mostly evaluated from flood discharge data, here is more roughly estimated from bankfull marks at steps, which present difficulties as to their interpretation. However, Rio Cordon discharge data furnished a means to test this methodology, and proved its validity. For this torrent, the flow depth at crest will be the one calculated by the November 2000 peak discharge and bankfull widths at each step, as given by Eq. 5.2.

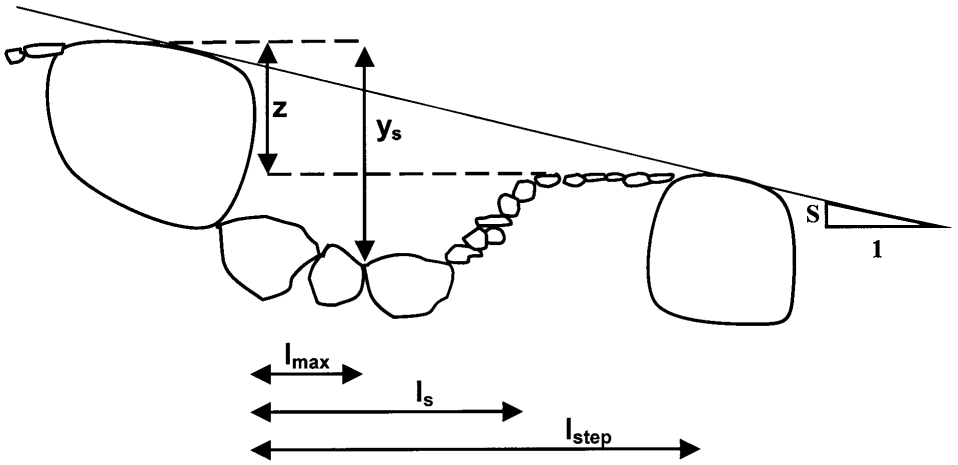

Figure 5.42 – Sketch of the measured pools' geometrical dimension.

Scour length l_s and berm distance l_b characterize the longitudinal extension of artificial pools, with the latter representing the downstream border of the pool region, because just after the berm the bed typically shows a positive slope. For natural step pools, instead, the longitudinal dimension L_{step} is the distance to next step downstream, since no similar berms were found in natural systems between the scour length location and the next step, and a positive bed slope was generally absent. Figs. 5.43 to 5.48 report images of the five natural step pool channels. Table 5.8 lists the main measured variables.

Figure 5.43 – Rio Cordon's step pools.

Figure 5.44 – Giralba's step pools.

Figure 5. 45 – Piave's step pools.

Figure 5.47 – Digon's step pools.

Figure 5.48 – Biois' step pools.

Table 5.8 - Measured variables in the 37 pools. D is the average sediment size at pool bottom, h_c is the measured bankfull flow depth at step crest (except for the Cordon where is the calculated from discharge data), S_e is the pool exit gradient measured only where a well defined slope was present. For the other symbols, see Fig. 5.42.

	D (m)	z (m)	y_s (m)	l_s (m)	l_{max} (m)	L_{step} (m)	h_c (m)	S_e (-)
Piave	0.17	0.40	0.90	3.00	1.40	3.00	0.35	0.49
	0.50	0.40	0.75	2.50	0.80	3.30	0.20	0.33
	0.5	0.50	0.75	3.50	1.00	3.50	0.25	0.13
	0.30	0.50	1.15	2.40	1.25	4.50	0.18	0.50
	0.40	0.30	0.65	1.70	1.10	2.50	0.20	0.29
	-	0.70	0.90	2.80	1.70	3.70	0.30	0.60
	-	1.25	2.00	1.60	1.50	3.20	0.25	0.26
	-	0.35	0.90	2.00	0.65	3.80	0.20	-
	0.15	0.45	0.80	1.90	0.50	3.70	0.25	-
	0.15	0.35	0.85	3.30	1.50	4.00	0.20	0.31
Biois	-	0.40	0.40	-	-	2.80	0.40	-
	-	0.50	0.50	-	-	2.20	0.40	-
	0.50	0.25	0.85	3.00	1.90	4.60	0.40	-
	0.40	1.00	1.10	-	0.80	3.20	0.40	-
	0.50	0.35	1.40	-	1.10	4.70	0.40	-
Digon	0.10	0.93	1.50	3.30	1.50	4.60	0.30	0.37
	0.05	0.55	1.15	2.40	1.20	4.00	-	0.44
	0.13	0.75	1.05	1.50	0.75	2.25	0.20	0.76
	0.40	0.55	1.00	2.00	0.90	3.00	0.40	1.14
	0.50	0.45	0.90	1.90	1.20	2.90	0.30	-
Giralba	0.40	0.40	1.25	2.00	1.30	3.20	0.75	0.36
	0.20	0.50	0.90	1.50	0.90	1.50	0.30	-
	0.27	0.65	1.45	1.80	1.05	3.60	0.45	0.69
	0.15	0.45	0.70	1.20	0.90	2.00	0.40	0.86
	-	0.75	1.60	1.20	1.10	3.30	0.40	1.00
	0.17	0.60	1.15	1.50	0.90	2.60	0.20	0.36
Cordon	0.40	0.40	0.84	1.00	-	3.20	0.68	-
	0.40	0.40	0.85	2.50	-	2.50	0.41	-
	0.40	0.50	0.70	1.50	0.70	2.80	0.41	-
	0.40	0.70	1.50	2.00	1.50	3.20	0.47	-
	0.40	0.85	1.20	1.20	0.70	2.00	0.34	-
	0.40	0.40	0.90	3.30	1.40	3.80	0.61	-
	0.40	1.00	1.50	2.20	0.80	2.90	0.20	0.30
	0.30	0.55	1.00	2.20	1.15	2.20	0.61	-
	0.50	1.00	1.50	0.00	1.00	2.20	0.74	-
	0.50	1.00	-	2.40	1.10	3.50	0.86	-
	0.40	0.65	1.30	3.00	1.10	3.00	0.54	-

The same dimensionless parameters used to analyze scour holes below artificial steps (i.e. grade-control structures) have been adopted to plot natural pool dimensions (see section 5.1.3). Fig. 5.49 shows the relationship between maximum scour depth normalized to critical flow depth and the drop ratio z/h_c. Natural and artificial pools are displayed together: their points delineate a similar linear trend, overlying considerably in the range having more measurements, i.e. for $z/h_c<4$. For larger drop ratios, natural pool data are totally lacking, whereas the two high check-dams points seem to follow the same trend. It is remarkable that such an accordance is achieved with one parameter only, and no sediment properties are taken into account.

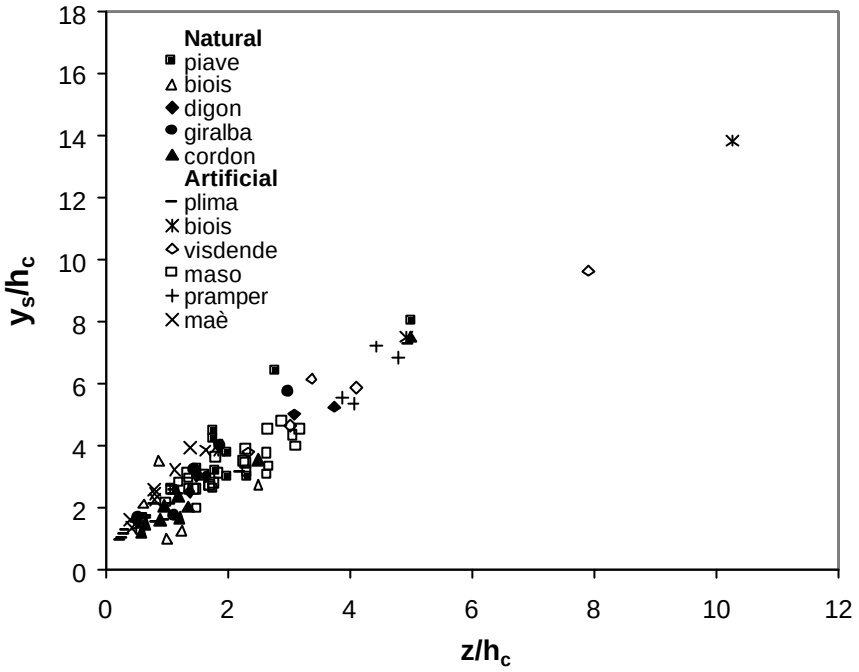

Fig. 5.49 – Dimensionless plot of maximum scour depth versus the drop ratio for both grade-control structures' pools (i.e. artificial) and natural step pool.

As done in section 5.1.1, the parameter z/L is now introduced to analyze scour dimensions. It indicates the potential energy lost by the falling jet in the span length between two fixed points, i.e. represents a sort of local gradient relevant to each pool. If berm distance l_b for artificial pools and step spacing L_{step} for natural ones are used, with the ratio y_s/z – analogous to the relative steepness factor c (eq. 5.1) – considered as the dependent variable, the following graph (Fig. 5.50) turns out:

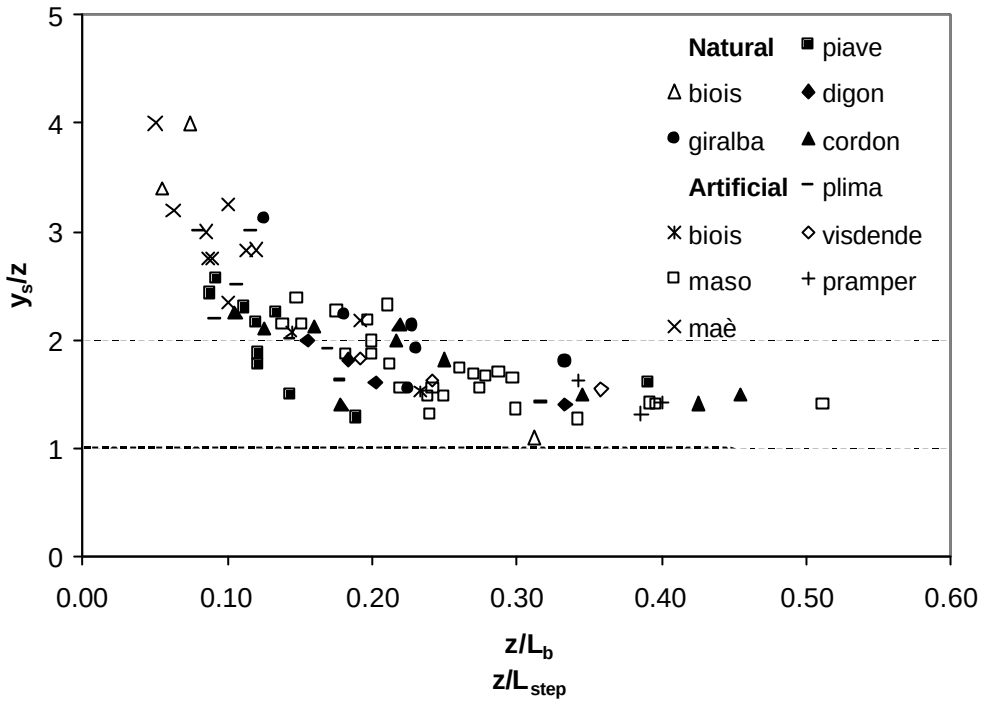

Fig. 5.50 – Dimensionless plot of maximum scour depth versus the "local gradient" factor; for artificial pools the berm distance l_b is the reference L, whereas L_{step} is used for natural pools. The range $1<c<2$ for the steepness factor proposed by Abrahams et al. (1995) is marked too.

If the parameter in abscissa is regarded as a slope and the y-axis as the relative steepness factor, both referring to berms in the case of artificial pools, Fig. 5.50 becomes analogous to Fig. 2.9, and a similar decreasing trend is shown. Compared to that graph where the mean channel slope is the independent variable, here the "slope" values are much higher because they derive from local measurements of drop heights and step/berm distances. However, the tendency towards a c or y_s/z of approximately 1.5 is exhibited in both figures, as well as the "rise" up to values around 4 for the lower gradients.

Figs. 5.49 and 5.50 suggest strong similarities between natural pools and scour holes below grade-control structures; furthermore, a strong link seems to exists between natural steps and depositional berms found downstream of artificial pools. The next section deals with the statistical evaluation of these analogies. Finally, Fig. 5.50 can be interpreted also in terms of geometric invariance between the vertical and the longitudinal dimensions of pools; in section 5.4 a simple analytical explanation for the observed trend occurring between channel slope and steepness factor will be put forward.

5.3 Statistical comparison between artificial and natural systems

As shown in section 5.1.3, jet virtual energy $E=z+H_s$ appears to be the physical variable which best normalizes pool dimensions in both natural and artificial systems, in the sense that it narrows the variability range of the dependent geometrical variables, leaving only a certain amount of variance due to the system geometry summarized by the drop ratio z/h_c. Therefore if some analogies exist between natural and artificial pools, these are best sought comparing the geometrical variables scaled to this jet energy.

The problem is to test statistically whether two independent groups, in this case natural (*N*) and artificial (*A*) pools, are significantly similar with respect to some of their features – namely maximum depth and its longitudinal location, length, berm distance/step spacing – when these are made non-dimensional through the jet energy E. Furthermore, pools' two-dimensional shape in the longitudinal direction can be summarized by some non-dimensional ratios. The underlying assumption is that similarities in shape reflect similarities in the formative process, even though this might not be always the case, as pointed out by Knighton (1998, p. 225) for meanders.

Given the fairly large sample size available, the commonly-used Student's *t*-test could be performed. However, this test requires the variances of the two groups to be similar, since their difference may alter test's significance. Here, it was chosen first to verify if variance homogeneity was respected by applying the standard Fischer's F test and the more powerful Levene's test too (Statsoft, 2002). In the case it was not, non-parametric statistics were adopted instead of the *t*-test in order to decide whether to reject the null hypothesis H_0 "the two sample (groups) belong to the same population". The non-parametric tests analogous to Student's *t* performed for this analysis are the Mann-Whitney *U*, the Kolmogorov-Smirnov and the Wald-Wolfowitz. All the calculations were carried out using the software "Statistica 6.1" (Statsoft, 2002). Table 5.9 reports the main values of interest for the comparison of all pool non-dimensional geometrical variables.

Table 5.9 – Pool dimensions normalized to jet energy: descriptive statistics and significance level *p* for the three non-parametric tests used to compare natural (N) and artificial (A) pools. *p*-values smaller than 0.05 are highlighted, indicating a probable difference between the two groups.

	Mean		**Stand. Dev.**		**Mann-Whitney *p***	**Wald-Wolfowitz *p***	**Kolmogorov-Smirnov *p***
	N	A	N	A			
y_s/E	0.95	0.92	0.27	0.18	>0.10	>0.10	>0.10
s/E	0.47	0.43	0.22	0.16	>0.10	>0.10	>0.10
l_s/E	2.11	1.88	1.05	0.63	>0.10	>0.10	>0.10
l_b/E **L_{step}/E**	3.00	2.90	1.37	0.78	>0.10	**<0.05**	>0.10

Vertical dimensions

Maximum scour depth y_s and residual depth s (= y_s-z) are the main vertical dimensional characteristics of pools. Their normalization by the jet energy E led to the box-and-whisker graphs reported in Figs. 5.51a and 5.51b respectively, where the median value is shown along with the 25-75 percentile range and the overall variation range. The median value is used instead of the mean value because the Student's *t* test was not reliable for non-homogeneity of groups' variance, thus non-parametric tests – which refer to the median value – were needed. All the three tests (see above) did not allow reject the null hypothesis of extraction from the same population, being $p>>0.10$. The *t*-test would give the same result too (not shown in the table).

These results indicate that the vertical extent of natural pool does not significantly differ from that characterizing pools created by grade-control structures, when the forcing – i.e. upstream – energy conditions are taken into account.

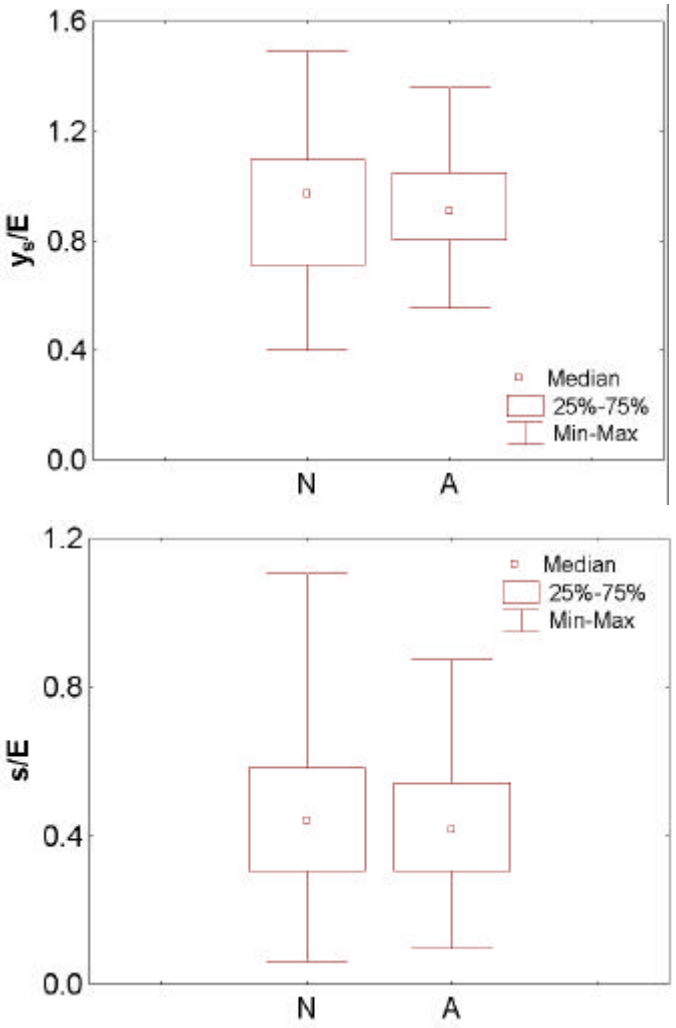

Figure 5.51 – Pool maximum scour depth y_s (a, above) and residual depth s (b, below) normalized to jet energy E, below natural steps (N) and grade-control structures (A).

Longitudinal dimensions

Scour length l_s and berm distance l_b characterize the longitudinal extension of artificial pools, with the latter representing the downstream border of pool region, because just downstream of the berm the streambed shows a positive slope. For pools below natural steps, instead, the downstream step distance L_{step} is the pools' final point, since no similar berms were found in natural systems between the scour length location and the next step, and a positive bed slope was generally absent either. The normalization through the nominal jet energy for scour length produced l_s/E frequency distributions which turned out to be non significantly different between natural and artificial pools, both using the t-test – but with non-homogenous variance – and the three non-parametric tests (see Table 5.9). In Figure 5.52

the graphical comparison is shown, where it can be seen a fairly wider range for the 25-75 percentile region occurring for natural pools, as well as for the overall variation range.

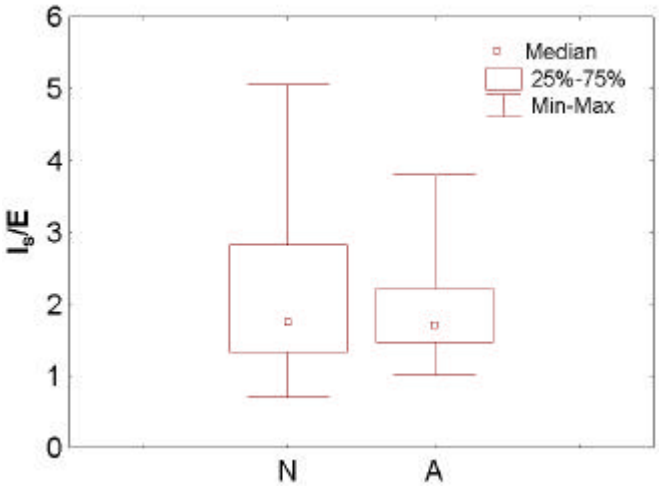

Figure 5.52 – Scour length normalized to jet energy *E* below natural steps (N) and grade-control structures (A).

As regards the berm distance and downstream step distance, they were made non-dimensional in the same way, and the two distributions of l_b/E for artificial pools and L_{step}/E for natural pools were obtained. Their statistical comparison gave as result the non-rejection of the null hypothesis by two tests out of three, in fact the Wald-Wolfowitz's led to $p<0.05$ (Tab. 5.9). Graphically (Fig. 5.53, see the median point) it is apparent that their similarity is less strong than that found for the previous geometrical variables. The fact that normalized berm and step distances on the whole probably belong to the same population prompts to theorize a similar formative process.

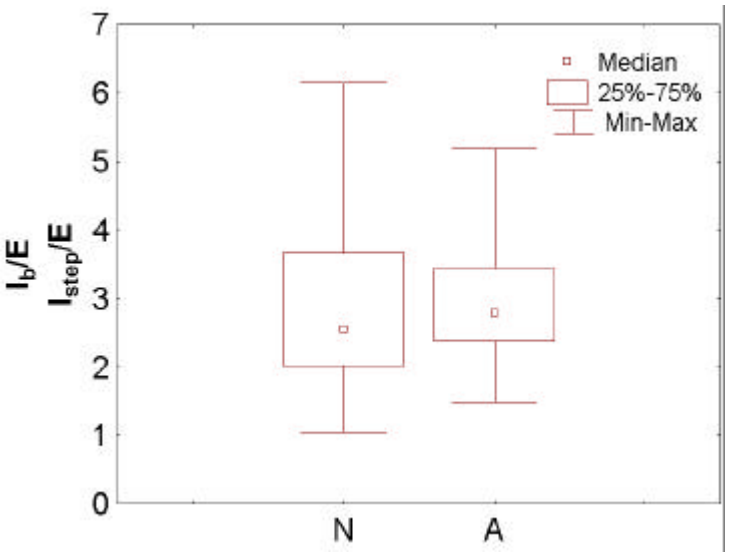

Figure 5.53 – Step and berm distance normalized to jet energy *E* below natural steps (N) and grade-control structures (A), respectively.

Pool shape

Unfortunately, no detailed profiles were available for pools' field data to establish a common pool shape as done for flume scour holes (see section 4.2.4). In addition, since the third dimension (i.e. pool width) was not considered here, pool geometry can only be expressed in terms of ratios among longitudinal dimensions themselves and with vertical ones too, plus the gradient of the pool exit slope which was directly measured.

The longitudinal dimensions are location of maximum scour depth l_{max}, scour length l_s, berm/step distance l_b and L_{step}; maximum scour depth y_s and residual depth s were adopted as vertical dimensions. Table 5.10 provides a summary of all the ratios that were statistically compared along with the tests' results.

Table 5.10 – Pool geometric ratios: descriptive statistics and significance level *p* for the three non-parametric tests used to compare natural (N) and artificial (A) pools. *p*-values smaller than 0.05 are highlighted, indicating a probable difference between the two groups. For symbols see Figs. 5.2 and 5.42.

	Mean		**Stand. Dev.**		**Mann-Whitney**	**Wald-Wolfowitz**	**Kolmogorov-Smirnov**
	N	A	N	A			
l_{max}/l_s	0.53	0.37	0.17	0.11	**<0.001**	**<0.05**	**<0.001**
l_b/y_s L_{step}/y_s	3.28	2.86	1.23	0.87	>0.10	>0.10	>0.10
L_{step}/l_s l_b/l_s	1.57	1.51	0.49	0.26	>0.10	>0.10	>0.10
l_b/s L_{step}/s	7.02	6.50	3.27	1.83	>0.10	>0.10	>0.10
S_e	0.51	0.33	0.29	0.11	**<0.05**	>0.10	**<0.05**

It turns out that the only significant (p<0.05) dissimilarities regard the exit slope gradient S_e (Fig. 5.54) and the ratio l_{max}/l_s (Fig. 5.55) All the other parameters have similar distributions and median values in both natural and artificial system, thus reinforcing the idea that similar formative processes underlie the creation of these pools.

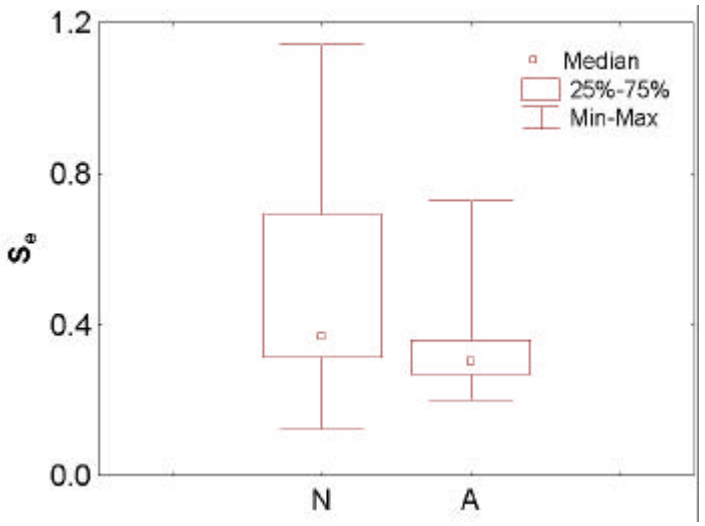

Figure 5.54 – Exit slope S_e for pools below natural steps (N) and grade-control structures (A).

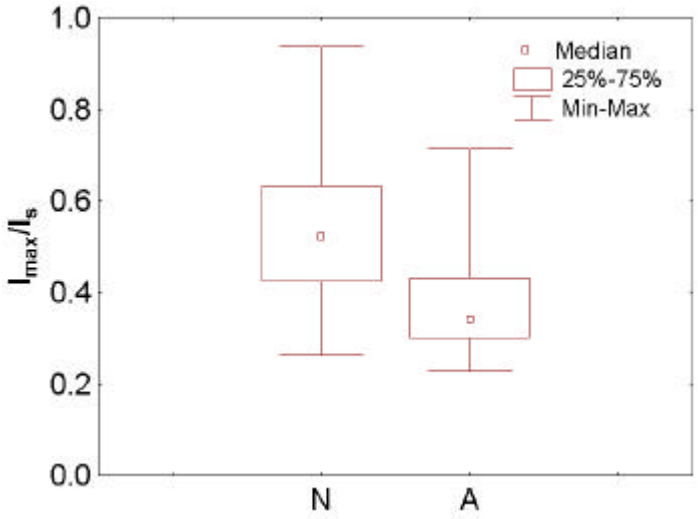

Figure 5.55 – The ratio l_{max}/l_s for pools below natural steps (N) and grade-control structures (A).

The pool exit slope is the location where sedimentation of finer cobbles and gravel occurs during the receding limb of a flood or however during successive lower yet sediment-transporting flows (Whittaker, 1987_b). A very large variation range of such a parameter is present especially for natural pools, and artificial step pool systems present statistically lower exit slope gradient. This is probably due a smaller critical angle of repose possessed by finer particles forming this negative slope in artificial pools. Pools formed at grade-control works are in fact generally bigger with respect to the average transported sediment size than natural pools are, because they are "artificial" in sense that drop height is set without any consideration of bed sediment size, whereas in natural systems the largest boulders command the maximum vertical drops, and their dimension is generally connected to the rest of the

grain size distribution. Larger drop heights mean longer longitudinal shift between flood and post-flood impinging location given an equal jet thickness variation, thus leaving a larger pool zone where hydrodynamic forces are weak enough to cause particle deposition.

Therefore artificial pools might be more effective in trapping sediment at lower discharges when pool dimensions are too large to permit the diffusing jet to sweep away particles from the plunge pool. Besides, the significantly lower l_{max}/l_s ratios found in artificial pools bring more support to the idea that post-peak flows – whose jets impinge closer to the structure – are in these systems more effective than in natural step pools, causing a readjustment of the pool shape probably disrupting the upstream pool side moving its material onward to the exit slope region.

As already reported, when the exit slope is formed by a definite patch of fine (from small cobbles to possibly some coarse sand) sediment, as it was the case for most of the artificial pools measured, this is made up mostly by particles transported either at the receding limb of the flood hydrograph or at successive smaller events. Therefore a certain flow range within which bed load transport occurs along the channel is needed, and this range positively correlates with channel size (i.e. with basin area, Wohl, 2000_a). The larger the range, the bigger is the quantity of sediment that can be deposited inside pools. The natural step pool creeks here analyzed drain all small basins (area < 10 km^2), whereas the artificial systems present areas larger than 45 and up to 160 km^2. Further, more extended catchments have more chances to include numerous sediment source areas, thus being generally less sediment-starved than small creeks, so becoming transport-limited instead of supply-limited.

As regards this aspect of pool shape related to successive adjustments, it is clear that a problem of scale arises due to the difference in sediment routing dynamics between small creeks and larger streams. On the contrary, as shown by the significant similarities regarding l_b/y_s and l_b/s, the overall geometry – presumably created during flood peaks – does not suffer from such a scale problem, with the jet erosive pattern molding (i.e. scouring up to the maximum depth and depositing berm/step elements) the pools.

5.4 Why is step pool geometry function of channel slope ? A new hypothesis

Pool shape expressed as the ratio L/s (where L represents both berm distance and step spacing) appears to be rather constant, ranging mostly between 6 and 8 both in the field data and in flume experiments with well-graded sediments (i.e. Wallingford tests). Padova laboratory data, characterized by a well-sorted mixture, present lower L/s ratios, with a mean value of 4.66.

This approximate invariance let us assume a relationship such as:

$$s = \frac{1}{k} L \qquad (5.9).$$

Therefore the elevation drop z between steps can be expressed as (with $H = y_s$):

$$z = H - s = H - \frac{1}{k} L \qquad (5.10).$$

For one ideally regular (i.e. no down-sloping treads) step pool architecture, the following equation (Eq. 3.2) holds:

$$z = S \cdot L .$$

Combining equations (5.10) and (3.2), one obtains:

$$S \cdot L = H - \frac{L}{k} \qquad (5.11),$$

which can be rearranged to give:

$$\frac{L}{H} = \frac{k}{k \cdot S + 1} \qquad (5.12),$$

and, inverting the relationship and dividing both terms by S:

$$\frac{H/L}{S} = \frac{k \cdot S + 1}{k \cdot S} \qquad (5.13).$$

The left term in Equation 5.13 is the relative steepness *c* introduced by Abrahams et al. (1995). When this equation is plotted for different *k* values, the following graph turns out (Fig. 5.56):

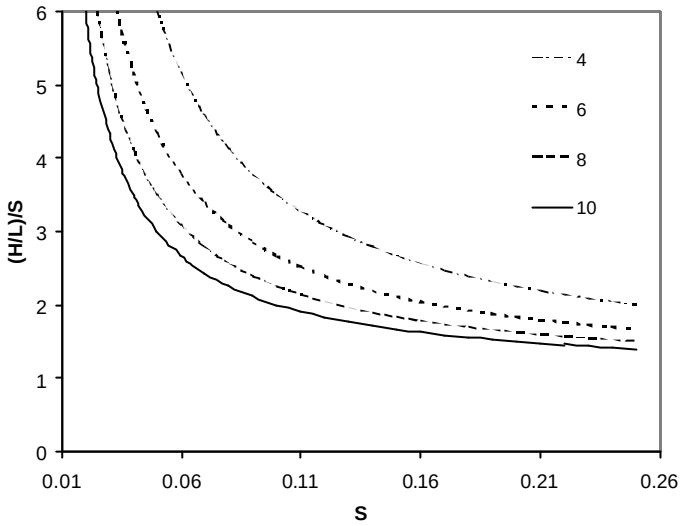

Figure 5.56 – Plot of Equation 5.13 for different values of the parameter *k*.

Previous field data about natural step pool geometry plot below the curves (compare Fig. 5.56 to Fig. 2.9), but a remarkable similar trend is apparent anyway. A large *k* value would fit these points, but – as reported at the beginning of this section – both lab and field results suggest the parameter to be no much greater than 8. Other reasons can be surmised for the discrepancy. In fact, the shift might be due to the assumption of an ideal step pool structure, i.e. to the validity of Eq. 5.11, whereas in actual field situations the relationship between drop height, step spacing and channel slope is more variable because of bed irregularities which make the profile depart from the ideal staircase model.

However, if equation 5.13 is plotted with the field data gathered in this research on natural and artificial pools organized as in Fig. 5.50, a very good agreement is shown (Fig. 5.57):

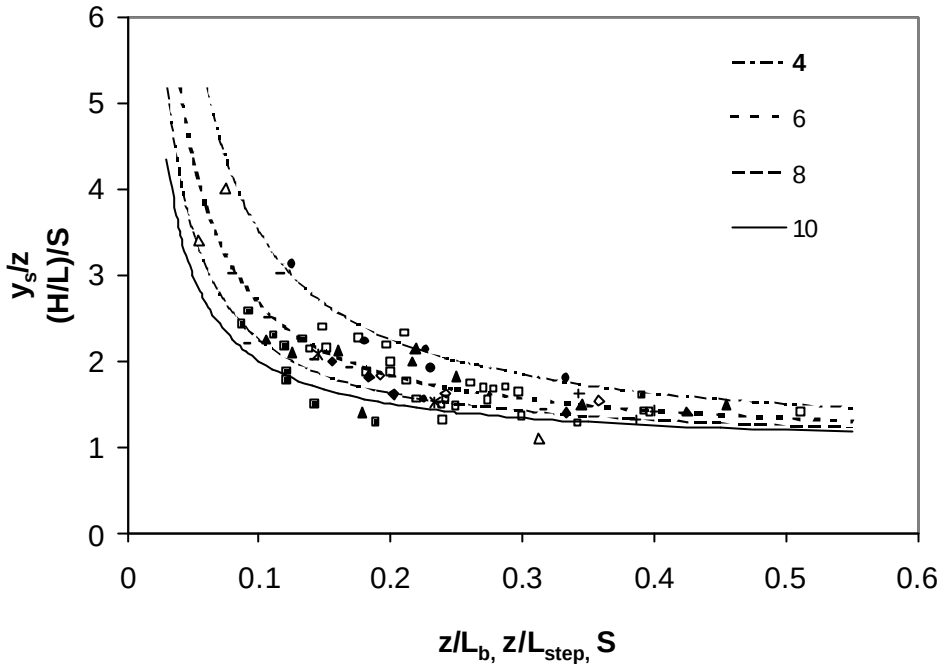

Figure 5.57 – Plot of Equation 5.13 and field data from natural and artificial pools (see Fig. 5.50).

As previously stated based on observed L/s values, Fig. 5.57 as well suggests for the geometrical parameter k a value ranging from 6 to 8 to be adopted in equation 5.13. The graphs show that even though an invariant pool shape (i.e. approximated by $L/s=k$) is assumed, step pool geometry expressed as L/H or $(H/L)/S$ manifests a definite trend related to the mean channel slope. And this is due to the fact that slope determines drop height z; at higher slopes, z increases in turn making H larger. As S increases, L/H decreases because only the denominator increases, whereas for the ratio $(H/L)/S$ the numerator increases at a slower rate than the denominator does, leading again to the a decreasing trend.

Summarizing, since $L/s \tilde{} k$, $H = s + z$ and $z = f(S)$:

$$\frac{L}{H} = \frac{L}{s+z} = f(S)$$

and thus also:

$$c = \frac{H/L}{S} = f(S).$$

Therefore the hypothesis by Abrahams et al. (1995) about the uniqueness of the ratio c is proved to be theoretically not possible – or at least not likely – for different channel slopes, as already suggested by some authors (Chartrand and Whiting, 2000; Zimmermann and Church, 2001) on the basis of field data. And the reason for it seems to be solely geometrical, without any hydraulic control. Water discharge do affect both step distance L and depth s by determining jet thickness at steps for a given channel width., but the overall geometry (i.e. their ratio) is approximately constant as long as external disturbances are negligible.

6. CLOSURE DISCUSSION

Applicability of local scouring equations to grade-control structures

The collected field data on scour holes below grade-control structures showed the validity of Equation 4.2 for the prediction of maximum scour depth in high-gradient channels. This formulation nevertheless represents an extension of previous results (Gaudio et al., 2000; Gaudio and Marion, 2003) for mild slopes and long spacings between bed sills. On the contrary, Equation 4.17 embodies the identification of the newly-described geometrical interference phenomena occurring when structures are placed close to each other, so that the downstream sill exerts a control which adds to the simple determination of the morphological jump a_1, as in the case of non-interfering sequences.

This control appears to be mainly acting by fixing the scour length, and because of the inherent scour hole invariance (i.e. self-affinity in general but as strong as self-similarity if similar jet geometries are concerned) the maximum scour depth is constrained not to go under a certain level, physically depending on scour hole's sides stability. In turn, this stability depends on sediment characteristics, with sediment gradation apparently the most important factor, as long as sediment general size is similar (e.g. gravel, cobbles).

In fact, Equation 4.17 does not incorporate any characteristic diameter, as well as field-derived Equations 5.3, 5.4 and 5.8 for scour depth, and the others about scour length and berm distance (eqs 5.5 – 5.6). A preliminary testing (not shown in the dissertation) of Equation 4.17 against the available field data has showed its validity at least for non-interference conditions, in fact the sample lacks enough closely-spaced structures. In the case of control works in streams where the equilibrium slope is expected not to differ substantially from the initial one, a morphological jump close to zero can be assumed. In this case Equation 5.3 can still be considered valid, predicting a maximum scour depth approximately equal to the critical flow depth, a value confirmed by flume tests (section 4.2.5) apart from possible effects due to morphodynamic interference.

The field conditions examined here probably present a narrow range of sediment grading which did not lead to identify it as variable for scour dimensions. Coarse (e.g. D_{84} - D_{95}) sediment size in both laboratory tests and real streams were not much different either, much less than an order of magnitude, hence suggesting to use the field-derive equations mentioned above in natural channels featuring similar conditions only, which can be exemplified as steep (>1%), perennial streams flowing on rather resistant sedimentary (e.g.

limestone, dolomites), magmatic and metamorphic alluvial substrates. For all the other situations, Equation 4.2 is probably more suited because it features a parameter taking into account sediment size (D_{95}) as well, even if results from section 5.1.4 indicate that a somewhat finer percentile (e.g.. D_{84}-D_{90}) of the streambed surface grain size distribution actually better represents the average particle size found at pools bottom.

Implications for natural step pool streams

As illustrated in section 2.4, Judd (1963) and Judd and Peterson (1969) proposed for natural step pool formation an upstream-forced model where a large immobile clast promotes the formation of a particle cluster around it, up to create a channel spanning step, the initial one. This bed irregularity would generate a train of standing waves downstream of it, with large particles settling down in correspondence with wave crests, thereby building up a series of steps. Pools then originate from local scouring below each step. This model hypothesizes that step wavelength is set by standing waves characteristics, and requires the random formation of an initial step.

A similar cascade model was developed by Allen (1982, 1983), which also invokes a self-repeating process of deposition with an upstream commencement. As in the particle cluster model by Judd (1963), it is stressed the importance of random large elements to start the formation of a sequence. The difference between Judd's and Allen's models lies in the actual hydraulic phenomena taking place downstream of each step. The former assumes standing waves to occur, whereas the latter suggests that hydraulic jumps are responsible for the deposition of large particles which will become the next step.

However, Crowe (2002) noted in the laboratory that as much as 75 % of step locations were obtained without any influence of the water surface, because only for the "mound" process (see section 2.4) there is a direct influence of the hydraulic conditions, i.e. wavelength of standing waves. The influence of step formation mechanism on step wavelength is then limited to the extent of the exclusion zone downstream of a step where deposition is less likely because of higher stresses due to jet diffusion. Previously, Hayward (1980) described major and minor steps, where the former – composed of bedrock outcrops, immobile rocks and large boulders – control the large-scale channel morphology. In between these control points, minor steps are present with their unstable pattern superimposed.

The results of the statistical comparison between pools at grade-control structure and below natural steps presented in section 5.3 lends support to an upstream-forced cascade model, i.e. where falling jet characteristics – virtual energy E given by the specific critical flow energy H_s plus the potential drop energy z – control the geometry of the system, hence representing the most important scaling independent variable. Berms formed at the end of the pools downstream of grade-control structures have been found to be probably analogous (sedimentologically and geometrically) to steps in natural systems, and pool geometry to be statistically similar in the two cases. Field data (Tab. 5.9) indicate that step spacing L_{step} and berm distance l_b are multiple of the jet energy E, with on average:

$$l_{step}, l_b \cong 3E \cong 3(z + H_s) \tag{6.1}.$$

A similar value – 3.2 – derives from Wallingford non-interfering tests, which were characterized by a well-graded sediment mixture and large relative roughness, conditions very similar to those encountered in the field. On the contrary, Padova "unconstrained" tests present a larger mean value, 4.1, and an even greater factor – 4.59 – is shown by Padova "standing wave" runs (tests 1-6, see section 4.1.2) assuming the energy to be given by H_s only. However, as discussed in 5.1.3 (Fig. 5.32), the drop ratio z/h_c or a_1/h_c affects the ratio l_b/E; Fig. 6.1 shows too a clear decreasing trend for increasing drop ratios taking into account laboratory data only.

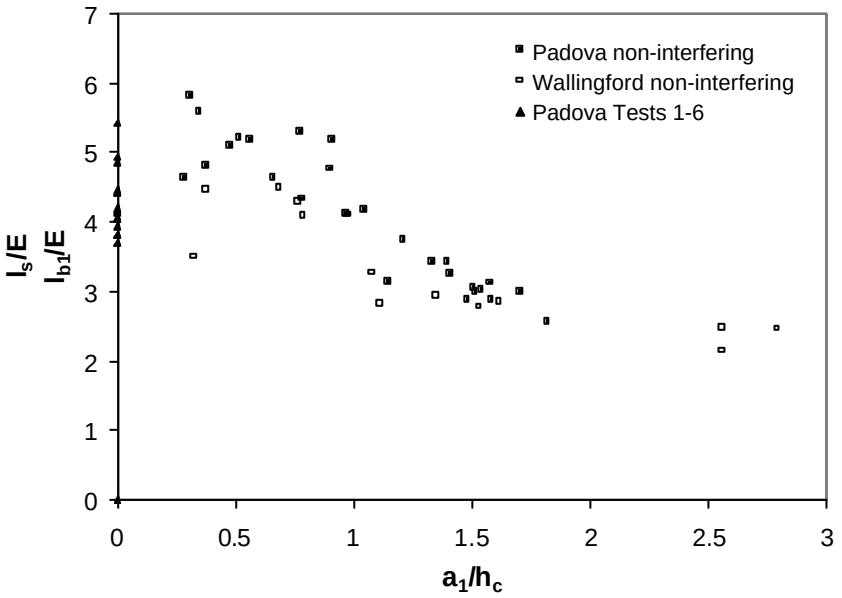

Figure 6.1 – The influence of the drop ratio a_1/h_c on the energy-normalized scour length l_s for non-interfering scour holes and first crest distance l_{b1} for Padova S=0.03 tests.

As it is evident from the graph, the higher average value characterizing Padova tests is not due entirely to smaller drop ratios, since Wallingford points plot below Padova's at corresponding values of a_1/h_c as well. The reason is probably the finer and better sorted sediment mixture used in Padova tests. Padova standing waves runs (slope S=0.03, sections 4.2.5 - 4.2.6) are plotted assigning $a_1 = 0$ because of the absence of clear equilibrium slopes downstream of the first crest. However, such an equality actually intends to represent "close to zero" drop heights (i.e. where the gravity acceleration on the jet is negligible compared to the critical flow energy) because it was impossible to determine any more accurate value.

Bearing in mind this approximation, an interesting pattern is depicted in Fig. 6.1. In fact, normalized bed crests l_{b1}/E show smaller values compared to depositional berms (here corresponding to scour length l_s in Wallingford and in the other Padova runs) occurring for steeper gradients, where the scour hole features a direct jump, i.e. an impinging jet regime with recirculation vortexes. In other words, for a same jet energy E, the depositional distance – where a step will be most probably created – is shorter in a surface wave regime compared to the case of impinging jet regime as long as the drop ratio does not exceed approximately the unity. Furthermore, within the impinging regime the strong negative correlation with the drop ratio makes the average value of L_{step}/E = 3 (Eq. 6.1) valid only for the range $1<a_1/h_c<1.5$.

Natural step pools measured in this research present an average drop ratio z/h_c = 1.82, with $a_1 \tilde{} z$, thus very close to the range specified above. For more submerged steps (i.e. smaller drop ratios), spacings up to 5-6 the jet energy would be expected. This variation is caused by the influence of jet geometry upon scour hole shape, as described in section 4.2.4. For $a_1/h_c<0.5$, the change towards the standing wave characteristics can be inferred from Fig. 6.1. On the contrary, for "high" steps (i.e. large drop ratios), shorter (<2E) dimensionless spacings more likely occur.

The drop ratio should correlate rather well with mean channel slope in natural streams, since at lower gradients step-forming particles size – i.e. the determining factor for the drop height z – are smaller (Chin, 1999_a, see section 2.3), and flow depth generally larger, because of the increase in water discharge and given the typical weak dependency of stream width on discharge (Lee and Ferguson, 2002). Therefore the steeper the channel, the larger the drop ratio, and in turn the shorter the dimensionless step spacings. Step spacing variations are included in such a model too, being linked to the actual step-forming clast size (i.e. step height) and step width (i.e. critical flow depth at the step lip). This evidences regarding step spacings as a function of hydraulic forces integrate from a different perspective the analysis

presented in section 5.4 where the relationship between channel slope and step pool geometry – i.e. relative steepness factor c – was carried out in terms of pool geometric invariance ($L_{step}/s=k$) only.

The present model for step pool formation is valid for all flows which energy E is large enough to cause pool erosion and berm (step) deposition. In steep boulder-bed streams, the availability of a wide range of large clasts – relative to flow depths – allows the existence of different sizes of steps, as described by Hayward (1980) and Chin (1998), having different permanence times (section 2.5). An extreme event with very low-recurrence interval will be able to form high steps ("major steps") by scouring and depositing downstream the largest mobile boulders present in the stream bed, with a spacing in accordance to the flood energy E. More frequent flood events but still with enough competence to mobilize large clasts will build-up other – less stable – step pool sequences featuring smaller step heights and shorter spacings ("minor steps"), each superimposed on previous – more stable – patterns determined by major steps. Therefore for a given mean channel slope, more than one step wavelength can be encountered depending on the channel's floods history. To complicate even further the bed configuration, sediment transport occurring as propagating waves filling-up pools may alter local flow condition altering the regularity of the formative process, as well as non-hydraulic factors such as bank and/or bed obstacles. Hence it is not surprising that many investigators (see section 2) argued that a single, averaged step wavelength poorly represent step pool morphology in the field and even in the laboratory with live-bed conditions (Crowe, 2002).

In addition, this research suggests that interference processes described in sections 4.2.2-4.2.3 might be involved in enhancing step stability against toe erosion, which Crowe (2002) found in her laboratory tests to account for 76.6% of all step break-ups. In fact, the average ratio L_{step}/H_s of the 37 step pool measured during the field activity is 6.55, well below the threshold L/H_s=12-15 for the onset of interference (section 4.2.3). Furthermore, plotting the energy-normalized scour depth versus the dimensionless step spacing, a clear trend becomes apparent (Fig. 6.2).

As long as steps are not destructed, the degree of interference depends on the flow rate, i.e. on the critical energy H_s. The higher the discharge, the greater is the scour-reducing effect by the vicinity of the next step, thereby increasing relative step stability against pool undermining. However, after a certain flow rate is passed, steps will be eventually mobilized, no longer able to withstand the combination of more direct jet stresses and anyway deeper pools.

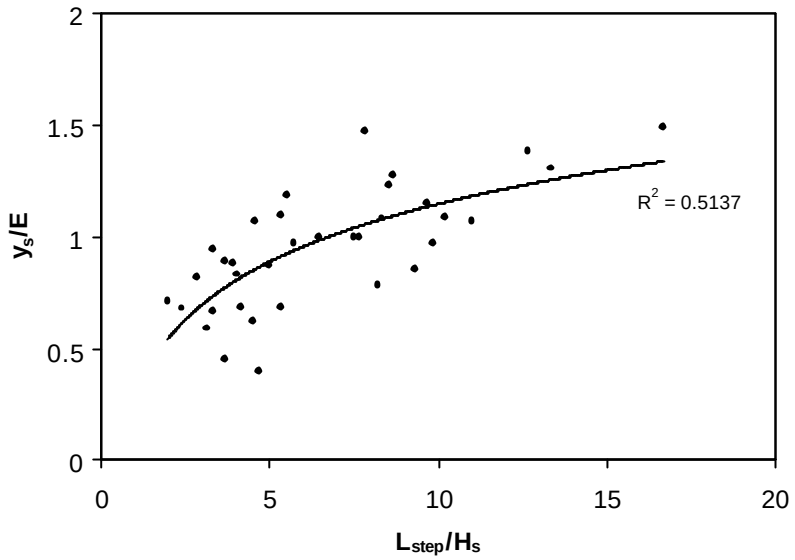

Figure 6.2 – The dimensionless maximum scour depth in pools below natural pools results affected by the ratio L_{step}/H_s. The best fit line is a logarithmic curve.

7. CONCLUSIONS

In order to synthesize the results presented in this thesis, the main achievements can be summarized as follows:

- A semi-empirical equation from laboratory data for maximum scour depth below grade-control structures (Eq. 4.2) applicable for low and high gradient channels ($0.006<S<0.148$), validated with field data;
- The first description of the "geometric interference" phenomenon, causing reduction of scour dimensions, and their modeling by:
- A semi-empirical equation (Eq. 4.17) from laboratory and field data for maximum scour depth valid for steep streams ($0.04<S<0.148$) only, accounting for possible interference conditions and different degrees of sorting of the sediment mixture: the poorer the sorting, the smaller the scour depth;
- The verification of the existence of scour holes self-affinity, and of the absence of self-similarity;
- A formula for calculating scour hole volume (Eq. 4.19);
- The first description of the "morphodynamic interference" caused by standing waves, along with a quantitative analysis of their wavelength;
- Four empirical equations (Eqs. 5.3-5.6) from field data for maximum scour depth, scour length and berm distance at pools below grade-control structures in steep ($S>0.02$) mountain rivers; no sediment characteristics are included in the formulae.
- The introduction of jet energy as the best scaling factor for scour dimensions, allowing to highlight a decreasing scouring efficiency – both longitudinal and vertical – for increasing relative drop heights;
- The first quantitative evaluation in the field of the longitudinal grain size sorting occurring in a sequence of grade-control structures, showing that the mean diameter at pool bottom ranges between the D_{80} and D_{87} of the surface grain size distribution found on the equilibrium slope bed, the berm-forming clasts to be on average the D_{90}-D_{95} and finally particles at exit slope and pool end to correspond to the D_{30}-D_{38};
- The presence of statistically significant similarities between dimensionless characteristics and geometry of pools formed downstream of grade-control structures

and below natural steps; however, exit pool gradients and ratios l_{max}/l_s turned out to be statistically different;

- The explanation of step formation in terms of depositional berms, whose distance is function of jet energy (Eq. 6.1) but varies with drop geometry as well; shorter spacings are to be expected if a surface wave regime (i.e. an undular jump) characterizes drop hydraulics instead of an impinging jet regime (i.e. a direct jump).
- The analytical derivation of the relationship between relative steepness factor c and mean channel slope from the evidence that the ratio L_{step}/s is roughly constant.

In spite of the advances attained by the present study, a great deal of research is still required. In fact, most of the results exposed above need confirmation from a more conspicuous data set, in particular for natural pools. Scour dimensions at grade-control structures in channels having finer and less graded sediment are also lacking. Furthermore, more investigations both in the laboratory and in the field are needed for channel slopes in the range 1-4%, where standing waves triggered by drops and steps may dominate the flow pattern and as a consequence the bed deformation. Live-bed experiments with sediment feeding are also much needed to quantify the role of sediment transport, testing in particular unsteady conditions typical of real streams. Measurements of jet and jump aeration would permit to assess its supposed influence on scour dimensions. Field data from closely-spaced structures likely producing geometrical interfering conditions are also needed to validate the model obtained by laboratory runs only. Finally, the role of pools' three-dimensional characteristics have also to be included in a more refined scour model, especially if intended to provide insights into natural step pool systems.

8. REFERENCES

Abrahams, A.D., Li, G., and Atkinson, J.F., 1995. Step-pool streams: Adjustment to maximum flow resistance. *Water Resourc. Res.*, 31(10), 2593-2602.

Aderibigbe, O., Rajaratnam, N., 1998. Effect of sediment gradation on erosion by plane turbulent wall jets, *J. Hydr. Engrg.*, ASCE, 124(10), 1034-1042.

Allen, J.R.L., 1982. Sedimentary Structures: Their Character and Physical Basis, Vol. 1, *Development in Sedimentology*, 30A. Elsevier, Amsterdam.

Allen, J.R.L, 1983. A simplified cascade model for transverse stone-ribs in gravelly streams. *Proc. Royal Society of London*, A385, 253-266.

Andersen, V.M., 1978. Undular hydraulic jump, *J. Hydr. Engrg*., 104(HY8), 1185-1188.

Andreoli, A., 2002. Analisi sperimentale sull'influenza dell'erosione localizzata nella dinamica dei torrenti montani. *MSc thesis*, University of Padova, pp. 153 (in Italian).

Ashida, K., Egashira, S., and Ando, N., 1984. Generation and geometric features of step-pool bed forms. *Annals 27*, Disaster Prevention Research Institute, Kyoto University, 341-353.

Baiamonte, G., and Ferro, V., 1997. The influence of roughness geometry and Shields' parameter on flow resistance in gravel-bed channels, *Earth Surface Processes and Landforms*, 22(8), 759-772.

Balachandar, R., and Kells, J.A., 1997. Local channel scour in uniformly graded sediments: the time-scale problem, *Can. J. Civ. Eng.*, 24, 799-807.

Balachandar, R., Kells, J.A., and Thiessen, R.J., 2000. The effect of tailwater depth on the dynamics of local scour, *Can. J. Civ. Eng.*, 27, 138-150.

Bateman, A., Andreatta, A., Muñoz, N., Estudio experimental de la erosión local producida por la presencia de umbrales de fondo en lecho vivo, *Proc. XIX Congreso Latinoamericano de Hidráulica*, Córdoba, Argentina, 2000 (in Spanish).

Bathurst, J. C., 1985. Flow resistance estimation in mountain rivers. *J. Hydr. Engrg.*, ASCE, (111), 625-643.

Beltaos, S., and Rajaratnam, N., 1974. Impinging circular turbulent jets, *J. Hydr. Div., ASCE*, 100(10),1313-1328.

Benini, G., 1990. Sistemazioni idraulico-forestali. Ed. UTET, Torino, Italy, pp. 283 (in Italian).

Biedenharn, D.S., and Smith, J.B., 1997. Design considerations for grade control siting. *Proc. Conf. on Management of Landscapes Disturbed by Channel Incision*, Wang, S.S.Y, Langendoen, E.J., Shields F.D. Jr (eds.), 229-234.

Bisaz, E., and Tschopp, J., 1972. Profundidad de erosion al pie de un vertedero para la aplicacion de correction de arroyos en quebradas empinados. *Proc. V Congreso Latinoamericano de Hidraulica*, Lima, Perù, D2-1 - D2-13.

Bohrer, J. G., and Abt, S.R., 1996. Plung pool velocity prediction of rectangular free falling jets, *Report*, Dept. Civil Engineering, Colorado State University, Fort Collins, Colorado.

Bormann, N, and Julien, P.Y., 1991. Scour downstream of grade-control structures. *Journal of Hydraulic Engineering*, 117(5), 579-594.

Bradley, J.N., and Peterka, A.J., 1957. The hydraulic design of stilling basins: hydraulic jumps on a horizontal apron (Basin I), *J. Hydr. Div., ASCE*, 83(HY5), 1-24.

Breusers, H.N.C, and Raudkivi, AJ., 1991. Scouring. *Hydraulic Structures Design Manual*, IAHR, A.A. Balkema, Rotterdam, The Netherlands.

Bowman, D., 1977. Stepped-bed morphology in arid gravelly channels. *Geo.l Soc. America Bull.*, 88, 291-298.

Bunte, K., and Abt, S.R., 2001. Sampling surface and subsurface particle-size distributions in wadable gravel- and cobble-bed streams for analysis in sediment transport, hydraulics, and streambed monitoring. *Report RMRS-GTR-74*, USDA Forest Service, , 409 pp.

Carling, P.A., 1995. Flow-separation berms downstream of a hydraulic jump in a bedrock channel. *Geomorphology*, 11, 245-253.

Chamani, M.R., and Rajaratnam, N., 1994. Jet flow on stepped spillways. *J. Hydr. Engrg.*, ASCE, 120(2), 254-259.

Chanson, H., 1994. Hydraulics of skimming flows over stepped channels and spillways. *J. Hydr. Res.*, IAHR, 32(3), 445-460.

Chanson, H., 1995_a. Hydraulic design of stepped channels cascades, channels, weirs and spillways, Pergamon Press, Oxford, UK, 292 pp.

Chanson, H., 1995_b. Flow characteristics of undular hydraulic jumps: comparison with near-critical flows, *Rep. CH45/95*, 202 pp., Dep. of Civ. Eng., Univ. of Queensland, Brisbane, Australia.

Chanson, H., and Montes, J.S., 1995. Characteristics of undular hydraulic jumps: experimental apparatus and flow patterns, *J. Hydr. Engrg.*, 121(2), 129-144.

Chanson, H., 1996. Comment on Step-pool streams: Adjustment to maximum flow resistance by Athol D. Abrahams, Gang Li, and Joseph F. Atkinson, *Water Resour. Res.*, 32(11), p. 3401.

Chanson, H., 2000. Boundary shear stress measurements in undular flows: application to standing wave bed forms, *Water Res. Res.*, 36 (10), p. 3063.

Chartrand, S.M. and Whiting, P.J., 2000. Alluvial architecture in headwater streams with special emphasis on step-pool topography. *Earth Surf. Process. Landforms*, 25, 583-600.

Chen, J.Y., and Hong, Y. M., 2001. Characteristics of check dam scour hole by free over-fall flow, *J. Chin. Inst. Eng., 24(6)*, 673-680.

Chin, A., 1989. Step-pools in stream channels, *Progr. Phys. Geog*., 13, 391-408.

Chin, A., 1998. On the stability of step-pool mountain stream, *Journal of Geology*, 106, 59-69.

Chin, A., 1999_a. The morphologic structure of step-pools in mountain streams. *Geomorphology*, 27, 191-204.

Chin, A., 1999_b. On the origin of step-pool sequences in mountain streams, *Geophysical Research Letters*, 26 (2), 231-234.

Chow, V.T., 1959. Open channel hydraulics, McGraw-Hill International, New York.

Comiti, F., 1999. Studio sperimentale dei processi di scavo a valle di soglie di fondo." *MSc thesis*, University of Padova, Italy, pp. 99. (in Italian).

Comiti, F., Lenzi, M.A., and Marion, A., 2001. Interference of erosion-control structure in mountain streams, *Proc. 3rd Int. Symp. Environmental Hydraulics*, ISEH, 5-8 December, Tempe, AZ, USA.

Comiti, F., Lenzi, M.A., and Marion, A., 2002. Local scouring at grade-control structures in mountain rivers: laboratory and field data, *Proc. Int. Conf. River Flow 2002*, 4-7 October, Louvain-La-Neuve, Belgium, A.A. Balkema Pub, The Netherlands.

Comiti, F., Zanini, S., Lenzi M.A., and Marion, A., 2003. Wavelength of standing waves caused by bed sills, *Proc. 3rd IAHR Symposium on River, Coastal and Estuarine Morphodynamics*, 1-5 September, Barcelona, Spain.

Costa, J.E., 1983. Paleohydraulic reconstruction of flash-flood peaks from boulder deposits in the Colorado Front Range. *Geol. Soc. America Bull.*, 94, 986-1004.

Crowe, J.C., 2002. An experimental study of the step pool bed form. *PhD Dissertation*, The Johns Hopkins University, Baltimore, USA, 147 pp.

Curran, JH., and Wohl, E.E., 2003. Large woody debris and flow resistance in step-pool channels, Cascade Range, Washington. *Geomorphology*, 51, (1-3), 141-157.

D'Agostino, V., 1994. Indagine sullo scavo a valle di opere trasversali tramite modello fisico a fondo mobile. *L'Energia Elettrica*, 71(2), 37-51 (in Italian).

D'Agostino, V., 1996. La progettazione delle controbriglie. *Proc. XXV Convegno di Idraulica e Costruzioni Idrauliche*, Turin, 16-18th September 1996, 107-118, (in Italian).

Damgaard, J.S., Whitehouse, R.J.S., and Soulsby, R.L., 1996. A sloping sediment duct for the study of sediment transport, *Proc. 25th International Conference on Coastal Engineering*, Orlando, Florida, 3913-3920.

Davies, T.R., and Sutherland, A.J., 1980. Resistance to flow past deformable boundaries. *Earth Surface Processes*, 5, 175-179.

Della Lucia, D., and Fattorelli, S., 1981. Nuovo metodo per la stima della pendenza dopo la sistemazione dei torrenti del Trentino. *Proc. Conv. Inter. "Problemi idraulici nell'assetto territoriale della montagna"*, Vol. F, 1-13 (in Italian).

Duckson, D.W., and Duckson L.J., 1995. Morphology of bedrock step-pool systems, *Water Resources Bullettin*, 31, 43-51.

Duckson, D.W., and Duckson L.J., 2001. Channel bed steps and pool shapes along Soda Creek, Three Sisters Wilderness, Oregon. *Geomorphology*, 38, 267-279.

Egashira, S., and Ashida, K., 1991. Flow resistance and sediment transportation in streams with step-pool bed morphology. In: *Fluvial hydraulics of mountain regions*, edited by A. Armanini and G. Di Silvio, Springer-Verlag, 45-58.

Eggenberger, W., and Müller, R., 1944. Experimentelle und theoretische Untersuchungen über das Kolkproblem, *Mitteilung aus der Versuchsanstalt für Wasserbau*, 5, Verlag A.G. Gebr. Leemann & Co., Zürich, 59-79 (in German).

Ergenzinger, P., 1992. Riverbed adjustments in a step pool system: Lainbach, Upper Bavaria. In: Billi, P., Hey, R.D., Thorne, C.R., Tacconi, P. (Eds), *Dynamics of gravel-bed rivers*, Wiley, Chichester, 415-430.

Ervine, D. A., Falvey, H.T., and Withers, W.A., 1997. Pressure fluctuations on plunge pool floors, *J. Hydr. Res.*, IAHR, 35(2), 257-279.

Falciai, M., and Giacomin, A., 1978. Indagine sui gorghi che si formano a valle delle traverse torrentizie, *L'Italia Forestale e Montana*, 33, 111-123 (in Italian).

Falciai, M., Giacomin, A., Silvagni, G., and Tonetti, G., 1977. Sul pendio di stabilimento di alcuni alvei torrentizi. *Annali Acc. It. Scienze Forestali*, Vol. XXVI, 107-130 (in Italian).

Faustini, J. M., and Jones, J.A., 2003. Influence of large woody debris on channel morphology and dynamics in steep, boulder-rich mountain streams, western Cascades, Oregon. *Geomorphology*, 51, (1-3), 187-205.

Ferrell, W. R., 1958. Report on channel stabilization feasibility, *Unpubl. Report*, Los Angeles County Flood Control District, Dams and Conservation Branch.

Ferreri, G.B., and Nasello, C., 2002. Hydraulic jumps at drop and abrupt enlargement in rectangular channel. *J. Hydr. Res.*, IAHR, 40(4), 494-505.

Ferro, V., 2002. La sistemazione dei bacini idrografici, McGraw-Hill, 700 pp.

Ferro, V., and Giordano, G., 1988. Formulazioni e campi di applicazione del criterio del moto incipiente per la deduzione della penzenza di equilibrio di un corso d'acqua. *Idrotecnica*, 3, 253-262 (in Italian).

Ferro, V., and Giordano, G., 1991. Experimental study of flow resistance in gravel-bed rivers, *J. Hydr. Engrg.*, ASCE, 117(10), 1239-1246.

Fiorotto, V., and Rinaldo, A., 1992. Turbulent pressure-fluctuations under hydraulic jumps, *J. Hydr. Res.*, 30 (4), 499-520.

Franke, P.G., 1968. Erosione a valle di traverse fluviali. *L'Energia elettrica*, 6, 445-446 (in Italian).

Ganz, T.F., 2003. Development of Flow Instabilities in Steep Stepped Channels - Experimental Analysis of the Influence of Channel Geometry, Bottom Roughness and Suspension Concentration. *PhD thesis*, Water Resources Institute, University of Innsbruck, Austria (in German).

Ganz, T., Schöberl, F., 2003. Limits of flow instability in steep stepped channels. *Proc. XXX IAHR Congress*, Thessaloniki, Greece, 24-29 August, 141-148.

Gaudio, R., and Marion, A., 2000. Time evolution of local scouring at bed sills. *Report TR69*, HR Wallingford Ltd., UK.

Gaudio, R, and Marion, A., 2003. Time evolution of scouring downstream of bed sills. *J. Hydr. Res.*, IAHR, 41(3), 271-284.

Gaudio, R, Marion, A., and Bovolin, V., 2000. Morphological effects of bed sills in degrading rivers, *J. Hydr. Res.*, IAHR, 38(2), 89-96.

Gessler, J. 1970. Self stabilization tendencies of alluvial channels. *J. Wtrwy. Harb. And Coast. Eng. Div*., ASCE, 99, 235-249.

Ghodsian, M., and Faradonbeh, A.A., 2001. Effect of sediment gradation on scour below free over fall spillway. *Proc., 3rd Int. Symp. Environmental Hydraulics*, ISEH, Tempe, USA.

Ghodsian, M., and Najafi, J., 2003. Maximum depth of scour by impinging circular turbulent jet. *Proc. XXX IAHR Congress*, Thessaloniki, Greece, 24-29 August, 353-359.

Giacometti, G., 2000. Indagine sperimentale sullo scavo a valle di opere trasversali in alvei a media ed alta pendenza. *PhD dissertation*, University of Padova, Padova, Italy, 190 pp. (in Italian).

Goitom, T.G., and Zeller, M.E., 1989. Design procedures for soil-cement grade control structures. *Proc. Nat. Conf. Hydr. Eng*., ASCE, New Orleans, LA.

Grant, G. E., 1994. Hydraulics and sediment transport dynamics controlling step-pool formation in high gradient streams: a flume experiment. In: Ergenzinger P. and Schmidt

K.H. (eds.), *Dynamics and Geomorphology of Mountain Rivers*, Lect. Notes in Earth Sc., Springer Verlag, 52, 241-250

Grant, G.E., 1997. Critical flow constrains flow hydraulics in mobile-bed streams: a new hypothesis, *Water Resourc. Res.*, 33 (2), 349-358.

Grant, G. E., Swanson, F. J., and Wolman, M.G., 1990. Pattern and origin of stepped-bed morphology in high-gradient streams, Western Cascades, Oregon. *Geol. Soc. America Bull.*, 102, 340-352.

Grant, G. E., and Mizuyama, T., 1991. Origin of step-pool sequences in high-gradient streams: a flume experiments. *Proc. Japan-USA Workshop on snow avalanche, landslides and debris flow prediction and control*, Japan Science and Technology Agency, National Research Institute for Earth Science and Disaster Prevention, Tsubuka, Japan, 523-532.

Hallmark, D. E., 1955. Influence of particle size gradation on scour at base of free overfall, *MSc thesis*, Colorado State University, Fort Collins, USA.

Hayward, J.A., Hydrology and stream sediments from Torlesse stream catchment, , *Spec. Publ. 17*, Tussock Grassland and Mountain Lands Inst, Lincoln College, New Zealand, 236 pp.

Heede, B.H., A study of early gully-control structures in the Colorado Front Range, *U.S. Department of Agriculture, Forest Service Rocky Mountain Forest and Range Experiment Station Paper No. 55*, Fort Collins, Colorado, December 1960.

Henderson, F.M., 1970. Open Channel Flow, MacMillian, New York, 522 pp.

Hoffman, G., 1998. Jet scour in equilibrium phase, *J. Hydr. Engrg.*, ASCE, 124(4), 430-437.

Hoffmans, G.J.C.M., and Verheij, H.J., 1997. Scour manual. A.A. Balkema, Rotterdam, The Netherlands.

Hom-ma, M., 1953. An experimental study on water fall. *Proc. Minnesota Intl. Hydraulics Convention*, Minneapolis, 477-481.

Jaeger, C., 1939. Über die Ähnalichkeit bei flussbaulichen Modellversuchen. *Wasserwirtschaft und Wassertechnik*, 34, N° 23/27 (in German).

Jarrett, R.D., 1984. Hydraulics of high-gradient streams. *J. Hydr. Engrg.*, ASCE, 110(11), 1519-1539.

Jia, Y., Kitamura, T., and Wang, S.S.Y., 2001. Simulation of scour process in plunging pool of loose bed-material. *J. Hydr. Engrg.*, ASCE, 127 (3), 219-229.

Julien, P.Y, Wargadalam, J., 1995. Alluvial channel geometry: theory and applications. *J. Hydr. Engrg.*, ASCE, 121(4): 312-325.

Judd, H.E., 1963. A study of bed characteristics in relation to flow in rough, high-gradient natural channels. *PhD dissertation*, Utah State University, 115 pp.

Judd, H.E., and Peterson, D.F., 1969. Hydraulics of large bed element channels. *Report PRWG 17-6*, Utah Water Research Laboratory, 85 pp.

Kaetz, G.A., and L. R. Rich, Report of surveys made to determine grade of deposition above silt and gravel barriers, *Unpublished Report*, Soil Conservation Service, Albuquerque, New Mexico, 1939.

Keller, E.A., and Swanson, F.J., 1979. Effects of large organic material on channel form and fluvial processes. *Earth Surface Process. Landforms*, 4, 361-380.

Kennedy, J.F., 1963. The mechanics of dunes and antidunes in erodible-bed channels, *J. Fluid Mech.*, 16(4), 521-544.

Knighton, A. D, 1981.Channel form and flow characteristics of supraglacial stream, Austre Okstindbreen, Norway. *Arctic and Alpine Research*, 13, 295-306.

Knighton, D., 1998. Fluvial forms and processes: a new perspective, Arnold, London, 383 pp.

Krey, H., 1925. Grenzen der Übertragbarkeit der Versuchsergebnisse, *Z. angew. Math. Mech.*, 5(6).

Kuroiwa, J.M., 1999. Scour caused by rectangular impinging jets in cohesionless bed. *PhD thesis*, Colorado State University, Fort Collins, USA, 365 pp..

Lee, A.J., and Ferguson, R.I., 2002. Velocity and flow resistance in step-pool streams. G*eomorphology*, 46 (1-2), 59-71.

Lencastre, A., 1961. Descarregadores de lamina livre, bases para o seu estudo e dimensionamento, *Memoria No. 174*, National Laboratory of Civil Enginnering, Ministry of Public Works, Lisboa, Portugal.

Lenzi, MA., 2001. Step-pool evolution in the Rio Cordon, Northeastern Italy, *Earth Surf. Process. Landforms*, 26, 991-1008.

Lenzi, M.A., 2002. Stream bed stabilization using boulder check dams that mimic step-pool morphology features in Northern Italy. *Geomorphology*, 45, 243-260.

Lenzi, M.A. and D'Agostino, V., 1998. Dinamica dei torrenti con morfologia a gradinata e interventi di sistemazione dell'alveo. *Quaderni di Idronomia Montana*, 17, 37-56 (in Italian).

Lenzi, M.A, and D'Agostino, V., 2000. Pattern, origin and dynamics of step pool structures of alpine torrents, *Excerpta*, 14, 21-53, Ed. CUEN, Italy.

Lenzi, M.A, and Comiti, F., 2003. Local scouring and morphological adjustments in steep channels with check-dam sequences, *Geomorphology*, 55, Special Issue, 97-109.

Lenzi, M.A, D'Agostino, V. and Sonda, D., 2000. Ricostruzione Morfologica e Recupero Ambientale dei Torrenti, Ed. Bios, Cosenza, Italy (in Italian).

Lenzi, M.A., Marion, A, Comiti, F., and Gaudio, R., 2002. Local scouring in low and high gradient streams at bed sills, *J. Hydr. Res*., IAHR, 40(6), 731-739.

Lenzi, M.A., Marion, A., and Comiti, F., 2003_a. Interference processes on scouring at bed sills, *Earth Surf. Process. Landforms*, 28(1), 99-110.

Lenzi, M.A., Marion, A., and Comiti, F., 2003_b Local scouring at grade-control structures in mountain rivers, *Water Resourc. Res.*, 39(7), 1176-1188.

Leutheusser, H.J., and Birk, W.M., 1991. Downproofing of low overflow structures. *J. Hydr. Engrg*., ASCE, 117(2), 205-213.

Lisle, T. E., 1982. Effects of aggradation and degradation on riffle-pool morphology in natural gravel channels, northwestern California, *Water Resourc. Res.*, 18, 1643-1651.

Lisle, T. E., and Hilton, S., 1992. The volume of fine sediment in pools: an index of sediment supply in gravel-bed streams. *Water Resourc. Bullettin*., 28, 371-383.

Lisle, T. E., and Hilton, S., 1999. Fine bed material in pools of natural gravel bed channels. *Water Resourc. Res., 35(4),*1291-1304.

Little, W.C., and Murphey, J. B., 1982. Model study of low drop grade control structures, *J. Hydr. Eng.*, ASCE, 108(10), 1132-1146.

Loza Lozano, J., 2002. Análisis experimental sobre la excavación agues abajo de obras transversales de corrección de torrentes (umbrales de fondo y diques de corrrección). *Thesis*, Escuela Técnica Superior de Ingenieros de Montes, Universidad Politécnica de Madrid, Spain, 166 pp.

Lunardi, S., 2002. Indagine sperimentale presso il torrente Cordevole (Arabba, BL) sullo scavo a valle di soglie di fondo: aspetti sedimentologici e geometrici. *MSc thesis*, University of Padova, Italy, 117 pp. (in Italian).

Marion, A, Gaudio, R., Bovolin, V., 1998. Scour downstream of bed sills. *HR Wallingford Research Report TR70*, Wallingford, United Kingdom, 50 pp.

Martin Vide, J.P., J. Del Agua Razquin, 1995. Erosion local en traviesas de proteccion en cauces, *Ingenieria Civil*, 58-64, (in Spanish).

Martin Vide, J.P, and Bateman, A., 1999. Experiments on steep-stream stabilization. *Proc. Intl. Water Resources Engineering Conf*., Seattle, USA.

Martin Vide, J. P., and Andreatta, A., 2003. Bed sill disturbance on the slope of steep streams. *Proc. XXX IAHR Congress*, Thessaloniki, Greece, 24-29 August, 149-157.

Martin Vide, J.P, Bateman, A., Garcia Revilla, C., Lopez Garcia, E., and Solans, D., 1998. Estudio experimental en lecho vivo de la estabilizacion del perfil longitudinal de un cauce de gran pendiente, *Proc. XVIII Congresso LatinoAmericano de Hidraulica, IAHR*, Oaxaca, Mexico.

Mason, P.J, and Arumugam, K., 1985. Free jet scour below dams and flip buckets. *J. Hydr. Engrg.*, 111(2), ASCE: 220-235.

McDonald, T.J., and Day, B.C., 1978. An experimental flume study on the formation of transverse ribs: current research, part A., *paper 78-1A*, Geological Survey of Canada, 441-451.

McKeogh, E. J., and Elsawy, E. M., 1980. Air retained in pool by plunging water jets, *J. Hydr. Div*., ASCE, 106(10), 1577-1593.

Mendrop, K.B., and Little, C.D., 1997. Grade stabilization requirements for incised channels. *Proc. Conf. on Management of Landscapes Disturbed by Channel Incision*, Wang, S.S.Y, Langendoen, E.J., Shields F.D. Jr (eds.), 229-234

Mirtskhulava, E., Dolidze, I.V., and Magomedova, A.V., 1967. Mechanism and computation of local and general scour in non-cohesive, cohesive soils and rock beds. *Proc. Twelfth Congress of Intl. Ass. Hydr. Res.*, Colorado State University, Fort Collins, USA, C20 (1-8).

Montes, J.S., 1986. A study of the undular jump profile, *Proc. 9th Australasian Fluid Mech. Conf., AFMC*, Auckland, New Zealand, 148-151.

Montgomery, R. D., and Buffington, J. M., 1997. Channel-reach morphology in mountain drainage basin, *Geol. Soc. Am. Bull.*, 109 (5), 596-611, 1997.

Moore, W.L., 1943. Energy loss at the base of free overfall. *Transaction*, ASCE, 108, 1343-1360.

Mossa, M., 1998. Experimental study on the scour downstream of grade-control structures. *Proc. of XXVI Convegno di Idraulica e Costruzioni Idrauliche*, Catania, Italy, 581-594.

Mossa, M., 1999. On the oscillating characteristics of hydraulic jumps. *J. Hydr. Res.*, IAHR, 37(4), 541-558.

Mossa, M., Petrillo, A., and Chanson, H., 2002. Tailwater level effects on flow conditions at an abrupt drop. *J. Hydr. Res.*, IAHR, 40(4), 1-13.

Mussetter, R. A., 1982. Equilibrium slopes above channel control structures, *MSc. thesis*, Colorado State University, Fort Collins, 90 pp.

Naden, P.S., and Brayshaw, A.C., 1987. Small- and medium-scale bedforms in gravel bed rivers. In: Richards, K.S. (ed.), *River channels: environment and process*. Blackwell, Oxford, UK, 249-271.

O'Connor, M.D, 1994_a. Sediment transport in steep tributary streams and the influence of large organic debris. *PhD dissertation*, University of Washington, Seattle, WA.

O'Connor, M.D., 1994_b. Energy losses in steep tributary streams at flows near the threshold of bedload entrainment. In: G.V. Cotroneo and R.R. Rumer, Editors, *Hydraulic*

Engineering '94, Proceedings of the 1994 Conference vol. 1, American Society of Civil Engineers, Buffalo, NY, p. 778.

Ohtsu, I., and Yasuda, Y., 1997. Characteristics of flow passing over drop-structures. *Proc. Conf. on Management of Landscapes Disturbed by Channel Incision*, Wang, S.S.Y, Langendoen, E.J., Shields F.D. Jr (eds.), 217-222.

Ohtsu, I., Yasuda, Y., Gotoh, H., 1995. Characteristics of undular hydraulic jumps in rectangular channels, *Proc. 26th IAHR Congress*, 1C14, London.

Ohtsu, I., Yasuda, Y., Gotoh, H., 2001. Hydraulic condition for undular jump formations, *J. Hydr. Res, IAHR, 39(2)*, 203-209.

Peterson, D. F., and Mohanty, P. K., 1960. Flume studies of flow in steep, rough channels, *J. Hydr. Div*, 86, *ASCE*, 55-76.

Porto P, Gessler J. 1999. Ultimate bed slope in calabrian streams upstream of check dams: field study. *J. Hydr. Engrg.*, ASCE, 125(12), 1231-1242.

Rajaratnam, N., 1981. Erosion by plane turbulent jets. *J. Hydr. Res.*, IAHR, 19(4), 339-358.

Rajaratnam, N., 1990. Skimming flow in stepped spillways. *J. Hydr. Engrg*., ASCE, 116(4), 587-591.

Rajaratnam, N., and Ortiz, N.V., 1977. Hydraulic jumps and waves at abrupt drops, *J. Hydr. Div.*, ASCE, 103 (HY4), 381-394.

Rajaratnam, N., and Chamani, M.R., 1995. Energy loss at drops. *J. Hydr. Res.*, IAHR, 33(3), 373-384.

Rand, W., 1955. Flow geometry at straight drop spillways. paper 791, *Proceedings* ASCE, 81, 1-13.

Reinauer, R., and Hager, W.H., 1995. Non-breaking undular hydraulic jumps, *J. Hydr. Res*, IAHR, 33(5), 1-16.

Rickenmann, D., and Dupasquier, P., 1995. EROSLOPE Project Final Report WSL. Swiss Federal Institute for Forest, Snow and Landscape Research, Birmensdorf, Switzerland.

Rosport, M., and Dittrich, A., 1995. Step-pool formation and stability – a flume study. *Proc. Sixth Intl. Symp. on River Sedimentation*. New Delhi, India, 525-532.

Schleiss, A.J., and Bollaert, E. (eds.), 2002. Rock scour, Balkema Pub., Rotterdam, The Netherlands.

Schoklitsch, A., 1932. Kolkbildung unter Überfallstrahlen. *Die Wasserwirtschaft*, 341 pp. (in German).

StatSoft Italia srl, 2002. STATISTICA, version 6, www.statsoft.it.

Stein, O.R, and Julien, P.Y., 1994. Sediment concentration below free overfall. *J. Hydr. Engrg.*, ASCE, 120(9), 1044-1053.

Stüve, P.E., 1990. Spatial and temporal varation of flow resistance in an Alpine river. In: *Hydrology in mountainous regions I. Hydrological measurements: the water cycle*, edited by H. Lang and A. Musy, IAHS Publ. No. 193, Wallingford, UK, 307-314.

Thomas, R., 1953. Scour in a gravel bed at the base of a free overfall. *MSc thesis*, Colorado State University, Fort Collins, CO, USA.

Thomas, D.B., 1999. A hydraulic and geomorphic analysis of step pool structures, *MSc thesis*, Colorado State University, Fort Collins, USA, 171 pp.

Thompson, S.M., and Campbell, P.L., 1979. Hydraulics of a large channel paved with boulders. *J. Hydraul. Res.*, 17, 341-354.

Thorne, C.R., and L.W. Zevenbergen, 1985. Estimating mean velocity in mountain rivers. *J. Hydr. Engrg.*, 111(4), pp. 612–624.

Tinkler, K.J., 1997. Critical flow in rockbed streams with estimated values for Manning's *n*, *Geomorphology*, 20, 147-164.

Trieste, D.J., 1994. Supercritical flows vs subcritical flows in natural channels, In: *Hydraulic Engineering '94*, G.V. Cotroneo and R.R. Rumer (eds.), ASCE, 732-736.

Ursino, N., Salandin, P., and Da Deppo, L., 2003. Fluctuating pressures at the bottom of a plunge pool, *Proc. XXX IAHR Congress*, Thessaloniki, Greece, 24-29 August, 191-198.

Vallé, B., and Pasternak, G.B., 2002. TDR measurements of hydraulic jump aeration in the South Fork of the American River, California. *Geomorphology*, 42, (1-2), 153-165.

Veronese, A., 1937. Erosioni di fondo a valle di uno scarico. *Annali dei Lavori Pubblici*, vol. LXXV, 9, 717-726.

Vischer, D., and Hager, W.H (eds), 1995. Energy dissipators, *IAHR Hydraulic Structures Design Manual 9,* A.A. Balkema, Rotterdam, 206 pp.

Volkart, P., 1972. Die Stabilisierung von Flussläufen mittels einer Folge von Querschwellen. *Mitteilungen der Versuchsanstalt für Wasserbau, Hydrologie und Glaziologie*, No. 6, Zürich, Switzerland, 59 pp.

Volkart, P., Tshopp, J., and Bisaz, E., 1973. The effect of sills on river bed. *Proc. of International Symposium on River Mechanics*, IAHR, 1, Bangkok: 167-178.

Weichert, R., Bezzola, G.R., and Minor, H.E., 2003. Bed morphology, flow resistance and stability of mountain torrents. *Proc. XXX IAHR Congress*, Thessaloniki, Greece, 24-29 August, 159-166.

Whittaker, JG., 1987_a. Sediment transport in step-pool streams. In: *Sediment Transport in Gravel Bed Rivers*, Thorne CR, Bathurst JC, Hey RD (eds.). Wiley & Sons; 545-570.

Whittaker, J.G., 1987_b. Modelling bed-load transport in steep mountain streams, *Erosion and Sedimentation in the Pacific Rim*, IAHS Publ. No. 165, 319-332.

Whittaker, J.G., and Jaeggi, M.N.R., 1982. Origin of step pool system in mountain streams, *J. Hydr. Div.*, ASCE, 108, 758-773.

Whittaker, J.G., and Davies, T.R.H., 1982. Erosion and sediment transport processes in step-pool torrents. In: *Recent developments in the Explanation and Prediction of Erosion and Sediment Yield*, IAHS Publ. No. 137, 99-104.

Wilcox, A., Wohl, E., Kray, J., and Vallance, G., 2002. Controls on hydraulic resistance in step-pool channels. *Abstracts with Programs - Geological Society of America*, 87-14.

Wilcox, A., and Wohl., E., 2003. Spatial and temporal patterns of velocity and turbulence in a step-pool channel. *Abstracts with Programs* - Geological Society of America.

Wohl, E.E., and Grodek, T., 1994. Channel bed-steps along the Nahal Yael, Negev desert, Israel, *Geomorphology*, 9, 117-226.

Wohl, E.E., Madsen, S., and MacDonald, L., 1997. Characteristics of log and clast bed-steps in step pool streams of northwestern Montana, USA. *Geomorphology*, 20, 1-10.

Wohl, E.E., 2000_a. Mountain Rivers. *Water Resource Monograph* 14, Washington DC, USA., p. 320.

Wohl, E.E., 2000_b, Substrate influences on step-pool sequences in the Cristopher Creek Drainage, Arizona, *Journal of Geology*, 108, 121-129.

Wohl, E.E., and Thompson, D.M., 2000. Velocity characteristics along a small step-pool channel. *Earth Surf. Process. Landforms*, 25, 353-367.

Wolman, M.G., 1954. A method of sampling coarse river-bed material. *Am. Geophys. Union Trans*. 35, 951-956.

Woolhiser DA, Lenz AT. 1965. Channel gradient above gully-control structures. *J. Hydr. Engrg.*, ASCE, 91(3), 165-187.

Wu, S., and Rajaratnam, N., 1996. Submerged flow regimes of rectangular sharp-crested weirs, *J. Hydr. Eng*, ASCE, 122 (7), 412-414.

Wu, S., and Rajaratnam, N., 1998. Impinging jet and surface flow regimes at drops. *J. Hydr. Res.*, IAHR, 36(1), 69-74.

Wu, C.C., Hou, C.H., Chen, C.N., and Shih, C.Y., 2002. Determination of groundsills interval for stream training, *Proc. River Flow 2002 Conf*., 4-7 Sept., Louvain-La-Neuve, Belgium, Balkema Pub., 1109-1115.

Yang, C.T., 1971. Formation of riffles and pools, *Water Resourc. Res.*, 7, 1567-1574.

Yang, C.T., and Song, C.S.S., 1979. Theory of minimum rate of energy dissipation. *J. Hydr. Div*., ASCE, 105, HY7, 769-784..

Yang, C.T., 1987. Energy dissipation rate approach in river mechanics. In: *Sediment Transport in Gravel Bed Rivers*, Thorne, C,R., Bathurst, J.C., Hey, R.D. (eds.). Wiley & Sons; 735-766.

Zanini, S., 2002. Studio sperimentale sulla risposta morfologica delle sistemazioni a soglie di fondo nei corsi d'acqua ad alta pendenza, *MSc thesis*, University of Padova, Italy, pp. 107, (in Italian).

Zanini,. S., Comiti, F., Lenzi M.A., and Marion, A., 2003. Morphodynamic interference on scour holes generated by bed sills in mountain rivers, *Proc. XXX IAHR Congress*, 24-29 August, Thessaloniki, Greece.

Zimmermann, A., and Church, M., 2001. Channel morphology, gradient profiles and bed stresses during flood in a step-pool channel, *Geomorphology*, 40 (3-4), 311-327.

ACKNOWLEDGEMENTS

First, the technical ones…I'm grateful to:

- *Azienda speciale per la regolazione dei corsi d'acqua e la difesa del suolo of the Province of Bolzano, particularly to Rudolph Pollinger and Diego Mantovani for original designs, photographs and reports about the Plima River.*

- *Edison S.p.A for making the Gioveretto Dam data available.*

- *ARPAV – Centro Meteorologico di Teolo for hydrometric and discharge data of rivers Cordevole di Visdende, Maè and Biois.*

- *ARPAV – Centro Valanghe di Arabba for Rio Cordon data.*

- *Antonio Lana for the help at the Dept. IMAGE, University of Padova Hydraulic Laboratory.*

And then…to Prof. Mario A. Lenzi, for his guidance over these years and for having made my graduate student's life rich of terrific opportunities; to Dr. Andrea Marion, for hosting me at the Hydraulic Laboratory of the Dept. IMAGE, and for his suggestions, discussion and friendly support; to all the collaborators who became friends, as Andrea Andreoli, Javier Loza Lozano, Simone Zanini, Stefano Lunardi, Andrea Pepato; to my friends Gionata Asti and Luca Mao for their help in the field; to Prof. Ellen Wohl, for having me at the CSU in Fort Collins, and to Prof. Greg Pasternak, for the hospitality at UC Davis, and to Andrew Wilcox and Brett Vallé: with all of them I had the pleasure to work and exchange impressions on hydraulics and life; to all the colleagues of my department, for the enjoyable time and real fun over these three years; to my old friends in Venezia and my new ones all over the world, because anything else is less important.

Grazie a mio padre, a mia nonna e a mia madre, per tutto.